Immune cell infiltration and interaction with stellate cells in pancreatic ductal adenocarcinoma

Ene-Obong, Abasi E

PhD thesis

Abasi E Ene-Obong

Supervisors

Hemant M Kocher

John F Marshall

Centre for Tumour Biology

Barts Cancer Institute

Barts and the London School of Medicine and Dentistry, Queen Mary University of London

Table of contents

List of figures

List of Tables

Acknowledgement

As I reflect on the years I spent researching and studying for my PhD degree, there are many people I wish to thank for their support in one form or another. Firstly, my thanks go to Mr Hemant Kocher for the opportunity given to me to study under him; his guidance and tutelage have been excellent and I can only describe working with him as a privilege. Dr John Marshall, for the understanding and perspective he always brought to the table. My regret; I wish we had worked together for longer. Prof Kairbaan “Kebs” Hodivala-Dilke, for being a friend; I will really like to keep in touch.

Upstairs at haemato-oncology which became my second home at Charterhouse square, my thanks go out to Dr Alan Ramsay; who kept giving me blood cells (I must have depleted your resources) and who was also a friend, no more meeting at the gym. Mr Andrew “Foggy” Clear: what an amazing fellow! I am not wrong when I say you made my project a reality. Thanks a lot! And to Prof John Gribben, many thanks for allowing me the resources of your amazing department and for the much needed scientific advice and guidance.

There are many of my colleagues to mention but for space. My regards go out to you all in Tumour Biology, Molecular Oncology, Haemato-oncology and Cancer and inflammation. From the Pancreas group, a huge thanks to Stacey Coleman who gave me one of my very first lessons in human cell culture. Thanks also to Dr Sabari “Sab” Vallath, a good friend indeed, and my onetime desk mates: Drs Bernado Tavora and Silvia Batista, and of course Dr Tony “ping pong” Wong. To my group members past and present not already mentioned: Jen, Mo, Prabs, Francesco, Elisabete, Leonardo, Raghu, Fieke and Erdinc, a huge thank you.

Now to my family who have been my bedrock; my father and mother, Prof and Prof (Mrs) Ene-Obong there are no words to express my gratitude. My wife, Jay, who allowed me the late nights using the dreaded Casy counter and supported me through all my lows, and there were a few, I love you and baby it's done! I've handed in my thesis! And to my newly born baby girl, Eliora, you are my greatest achievement and not even this PhD comes close to you. Daddy loves you.

Conferences attended

2011 Postgraduate student day

Abstract presentation: Stromal entrapment of immune cells in pancreatic ductal adenocarcinoma

2011 NCRI Cancer conference

Poster presentation: Stromal entrapment of immune cells in pancreatic ductal adenocarcinoma

2012 London Pancreas meeting

Attended

2012 Postgraduate student day

Oral presentation: Stromal entrapment of immune cells in pancreatic cancers

2012 Pancreatic Society of Great Britain and Ireland (PSGBI) annual meeting

Poster presentation: Activated pancreatic stellate cells inhibit $CD8^+$ infiltrate in pancreatic ductal adenocarcinoma via CXCL12

Immune cell infiltration and interaction with stellate cells in pancreatic ductal adenocarcinoma

Abstract

Pancreatic ductal adenocarcinoma (PDAC) is a disease with very poor prognosis amongst all pancreatico-biliary cancers. PDAC is characterised by a pronounced desmoplastic stroma which upon depletion has been associated with immune cell mediated tumour clearance. *In situ* analyses of various immune cell markers in the stromal compartments may provide a lucid picture of immune cell migration to the tumour epithelia.

Automated, unbiased, high throughput imaging and analysis of specifically designed tissue microarrays, from surgically resected tissue samples of PDAC, advanced PDAC, and other pancreatico-biliary diseases; stained for distinct immune cell markers was carried out in the juxtatumoural stroma and the panstromal compartments. Prognostic significance was determined with X-Tile software. *In vitro* and *in vivo* assays were undertaken to outline the possible mechanisms.

Immune cell infiltration to PDAC was higher than infiltration to other pancreatico-biliary diseases with the exception of $CD8^+$ T cells. While $CD4^+$, $CD68^+$ and myeloperoxidase$^+$ cells could infiltrate the juxtatumoural stroma of PDAC; $CD3^+$, $CD8^+$, $Foxp3^+$ and $CD20^+$ cells could not in the early stage PDAC patients tissue analysed and also in an independent validation cohort of advanced stage PDAC patients. Survival analyses demonstrated pro-survival effects of having high $CD8^+$ densities. $CD8^+$ T cells could only infiltrate the juxtatumoural compartment of KPC mice after stromal collapse resulting from targeting stellate cells with All-trans Retinoic Acid.

In vitro migration assays demonstrated increased $CD8^+$ T cell migration towards activated pancreatic stellate cells compared to quiescent pancreatic stellate cells and appeared to be dependent on CXCL12.

T cells are hindered from migrating to the juxtatumoural compartment by activated pancreatic stellate cells as a result of an increase in CXCL12 secretion. Rendering activated pancreatic stellate cells quiescent results in a reduction of CXCL12 secretion which may allow $CD8^+$ T cells to migrate to the tumours and perform cytotoxic functions.

1.0 Introduction

Pancreatic cancer

a. Pancreatic ductal adenocarcinoma

Pancreatic ductal adenocarcinoma (PDAC) even with its low incidence is a leading cause of mortality in the world and the fourth cause of death in the Western world. Less than 4% of patients diagnosed with the disease survive longer than 5 years, even though there are advances in imaging protocols and improved surgical outcomes (Mazur and Siveke 2011). The high mortality of PDAC may be because patients often present with metastatic disease at diagnosis (Mazur and Siveke 2011). Also pancreatic cancer is notoriously resistant to systemic chemotherapy (Maitra and Hruban 2008). A recent study showed that in a transgenic mouse model of PDAC the chemotherapy is not delivered to the tumour as a result of vascular deficiency (Olive, Jacobetz et al. 2009) which correlates with the dense stromal matrix that makes up the bulk of PDAC tumours (Neesse, Michl et al. 2011).

PDAC is believed to undergo a stepwise process wherein genetic alterations are accumulated from inception of disease to malignant disease with corresponding histopathological and morphological changes. This stepwise process model originates with a genetic alteration resulting in activating oncogenic K-*ras* gene and telomerase shortening among others and is followed by silencing somatic mutations in tumour suppressor genes *p16, DPC4* and *p53* (Hruban 2000) (Figure 1.1A). The origins of PDAC may be hereditary in about 10% of patients, and often involves genes such as *BRCA2, STK11, P16* and *PRSS1* (Neesse, Michl et al. 2011) (Hruban 2005). A validated risk factor believed to cause pancreatic cancer is cigarette smoking (Bosetti, Lucenteforte et al. 2012). Others including diet rich in meats and

fats, obesity, low serum folate levels, chronic pancreatitis and diabetes mellitus; these have not been validated definitely (Maitra and Hruban 2008).

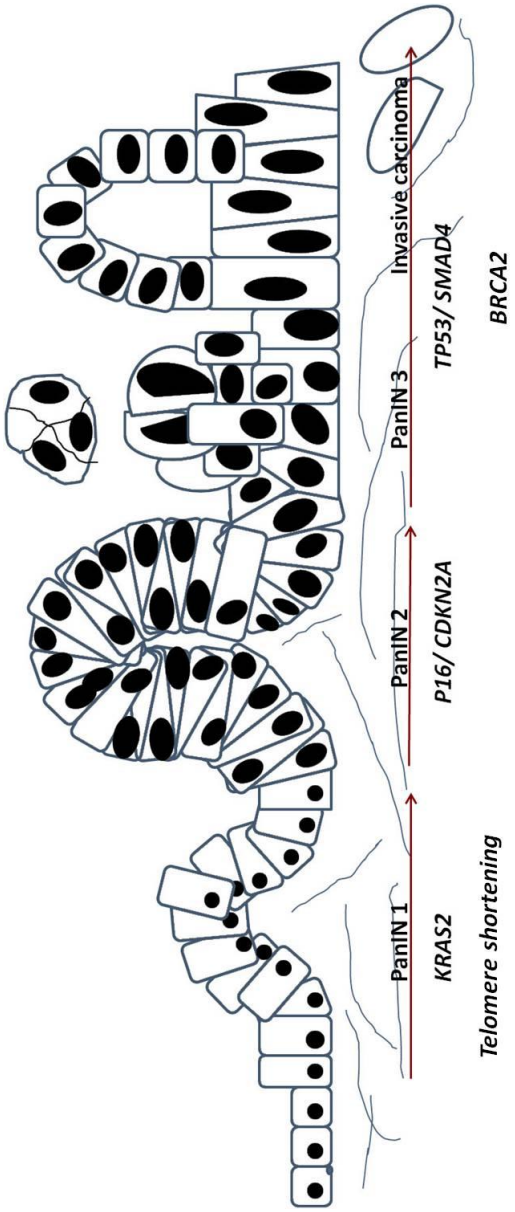

Figure 1.1 Genetic alterations accompanying progressive stages in a putative model of pancreatic ductal adenocarcinoma progression *Modified (Maitra and Hruban 2008).*

Representation of genetic changes during PDAC progression from normal to the PanIN stages and to invasive disease

1.1 b. Stromal microenvironment in PDAC

The stroma in PDAC (Figure 1.2) is conspicuous histologically and is composed of extracellular matrix (ECM), activated fibroblasts, myofibroblasts, inflammatory cells, hypertrophic nerve fibres and blood and lymphatic vessels resulting a distorted pancreatic tissue architecture which is distinct from the normal (Figure 1.2) (Neesse, Michl et al. 2011). Production of stroma is induced by the activation of cancer driven pathways such as: hepatocyte growth factor (HGF/Met), fibroblast growth factor (FGF), transforming growth factor beta (TGFβ), epidermal growth factor (EGF) and insulin-like growth factor 1 (IGF-1) (Ide T 2006; Mahadevan D 2007), and their autocrine and paracrine signalling leading to production of ECM components such as proteases, proteoglycans, collagen and fibronectin amongst others (Neesse, Michl et al. 2011).

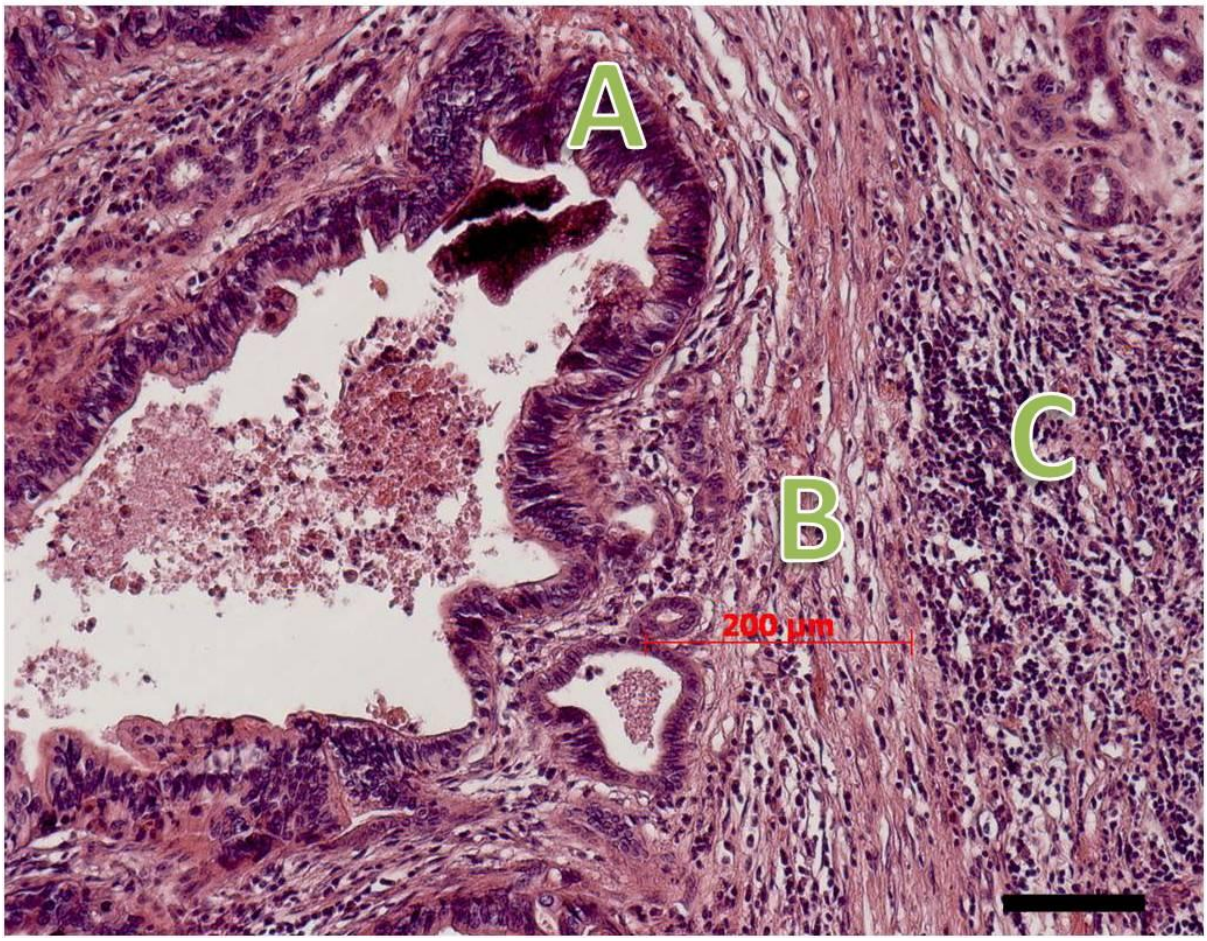

Figure 1.2 Hematoxylin and Eosin of pancreatic ductal adenocarcinoma (PDAC)

A representative picture of PDAC, “A” shows the glandular pattern and duct-like structure of an infiltrating neoplasm; “B” shows the intense desmoplastic stroma that is a characteristic feature of this disease; and “C” shows an infiltration to tissue of inflammatory cells.

Scale bar: 100µm

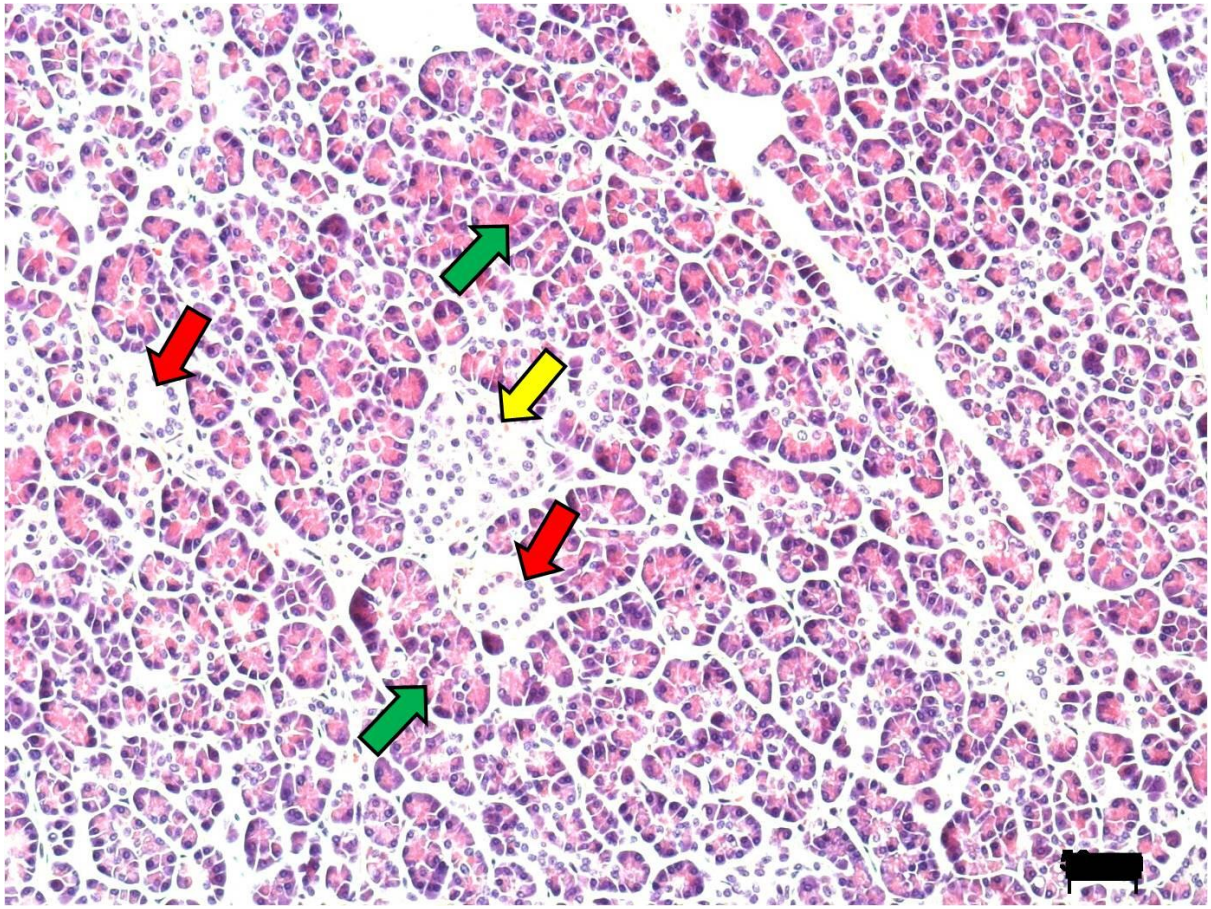

Figure 1.3 Normal pancreas

A representative picture of a normal pancreas, “green arrows” point to the acinar cells which with the help of ducT-cells (“red arrows”) make up the exocrine pancreas responsible for secretion of digestive enzymes. Islets of Langerhans (“yellow arrows”) make up the endocrine pancreas that regulates metabolism and homeostasis of glucose by secreting various hormones such as insulin, glucagon and somatostatin, into the blood stream (Hezel, Kimmelman et al. 2006). Scale bar 50µm.

1.1 c. Characteristics of PDAC

PDAC can be distinguished by the following characteristics (Sharma and Green 2004):

1. Nuclear size variation of greater than 4:1 in a single duct
2. Incomplete lumina
3. Luminal necrosis
4. Invasion into surrounding vasculature
5. Perineural invasion
6. A haphazard growth pattern

Precursor lesions

There are three possible precursor lesions leading to PDAC; pancreatic intraepithelial neoplasia (PanIN), mucinous cystic neoplasm (MCN) and intraductal papillary mucinous neoplasm (IPMN). All of these precursor lesions undergo similar genetic alterations from early carcinogenesis to invasive disease beginning with telomere shortening (Ottenhof, de Wilde et al. 2011).

Telomeres are made up of simple tandem DNA repeats that are found at the ends of human chromosomes (Jiang, Ju et al. 2007). They do not encode any gene products and shorten with each round of cell division ensuring cells do not proliferate indiscriminately, and by so doing, may act as tumour suppressor (Jiang, Ju et al. 2007). “Pathologically” short telomerase form “dicentric and ring” chromosomes that result in “anaphase bridges” during mitosis; when these bridges break, DNA repair

processes occur which may inadvertently lead to chromosomal rearrangements (Ottenhof, de Wilde et al. 2011). Telomerase, the gene responsible for telomere shortening, has reduced expression in the earliest stages of PDAC carcinogenesis and is re-expressed in invasive disease (Ottenhof, de Wilde et al. 2011).

PDAC precursors are discussed below:

1.2 a. Pancreatic intraepithelial neoplasia (PanIN)

PanINs are “non-invasive microscopic epithelial neoplasms, located in the smaller pancreatic ducts, characterised by cytologic and architectural atypia” (Hruban, Maitra et al. 2007). PanINs are classified into 3 main stages, PanINs 1 – 3 (Figure 1.4- 1.6), and represent progressive states of pancreatic carcinogenesis characterised by varying nuclear and architectural atypia with increasing rates of genetic aberrations (Maitra, Fukushima et al. 2005). Genetic aberrations are similar to PDAC and begin with telomere shortening and activation of the K-*ras* oncogene in early PanIN and progresses with loss-of-function mutations in tumour suppressor genes *CDNK2A, p53*, *SMAD4* and *BRCA1,* as well as alterations in Ki-67 (Maitra, Fukushima et al. 2005).

PanIN lesions are common and they increase with age and are found in all regions of pancreas (Tanaka, Chari et al. 2006): however, their value as a therapeutic target has not been established as the rate and frequency with which they progress to PDAC is unknown (Hruban, Maitra et al. 2007). While PanINs can mimic PDAC, they can be distinguished by their histology characteristics (Table 1) (Maitra, Fukushima et al. 2005).

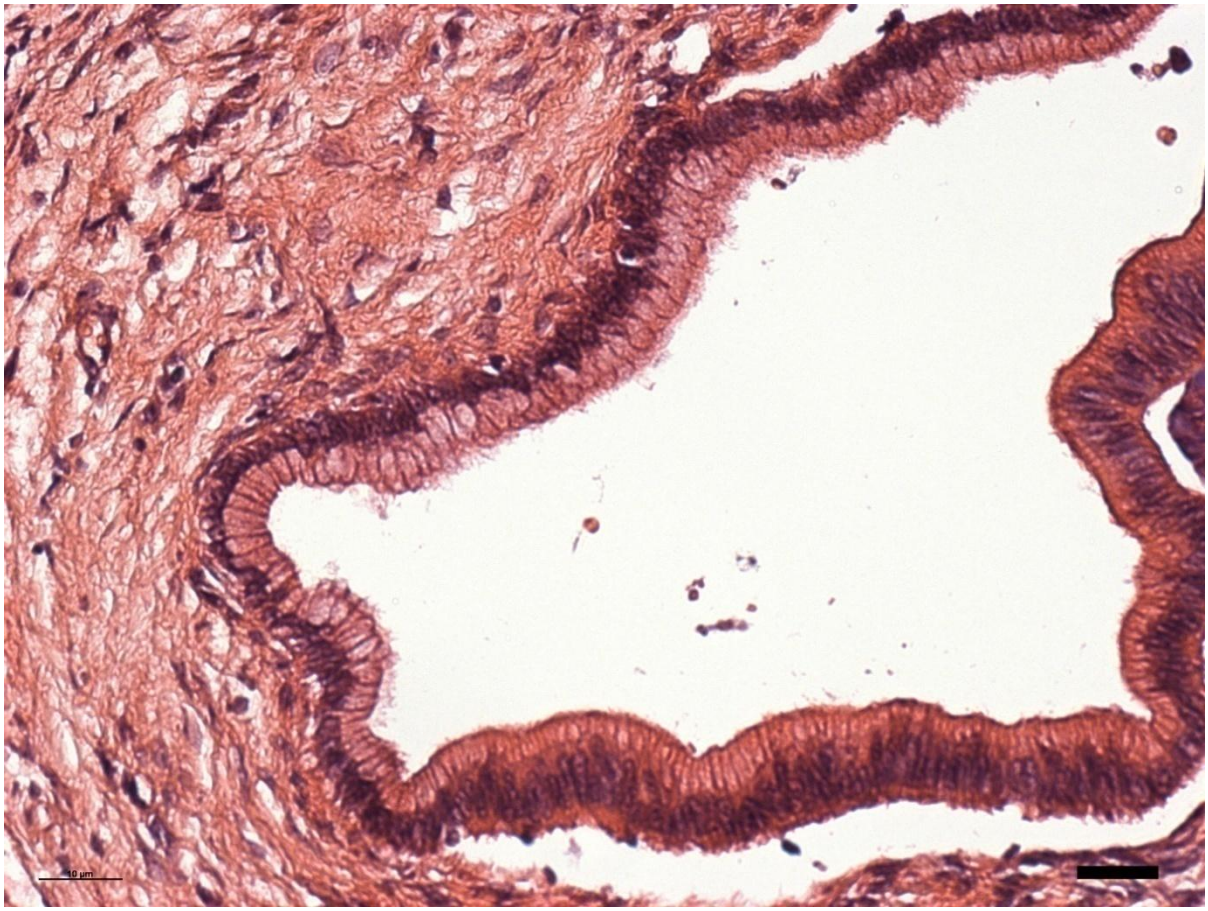

Figure 1.4 Representation of a PANcreatic Intra-epithelial Neoplasia 1 (PanIN1)

A representation of a PanIN1 lesion characterized by tall columnar cells with nucleus basally located. Nuclei are small and may be oval or round in shape.

Scale bar: 10µm

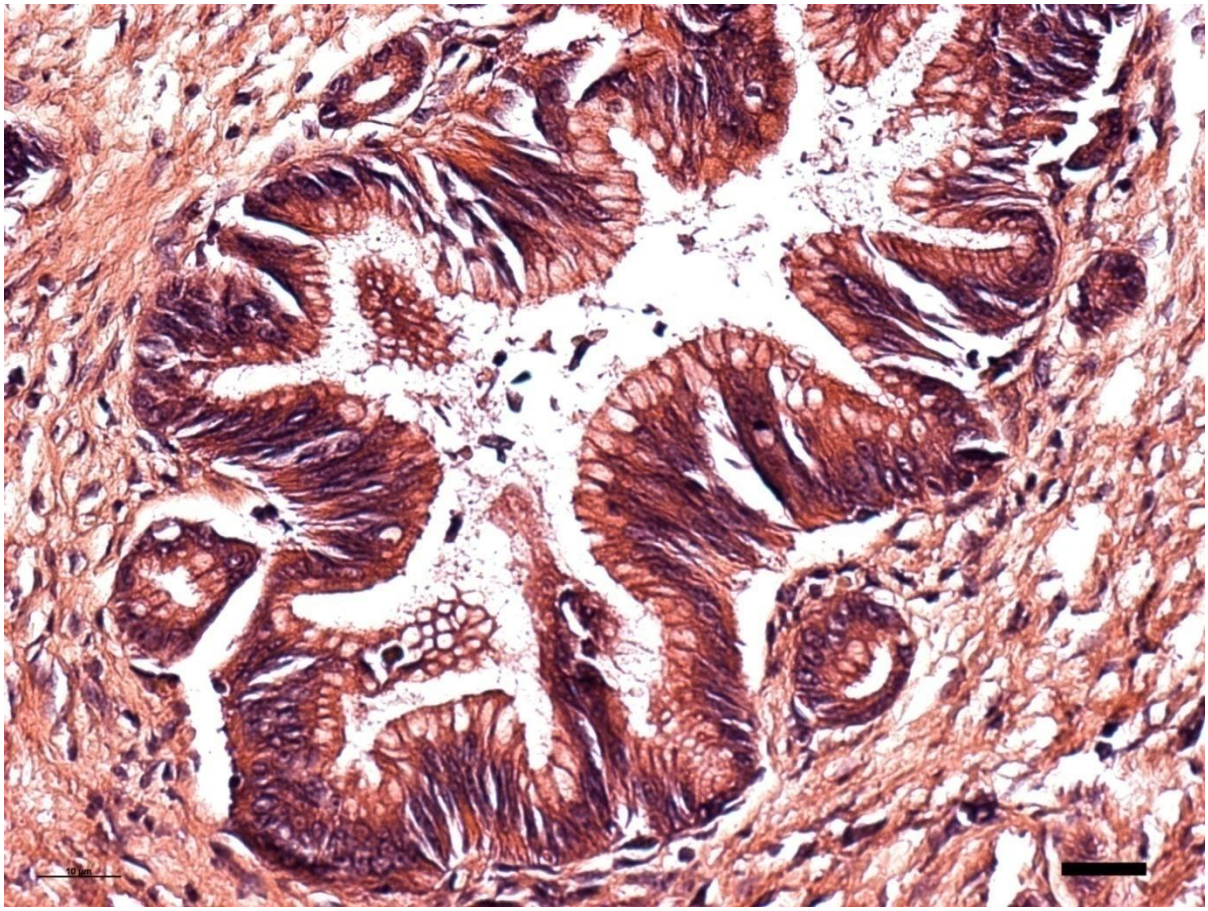

Figure 1.5 Representation of a pancreatic epithelial neoplasia 2 (PanIN2)

A representation of a PanIN2 lesion which is architecturally papillary; cytological changes such as loss of polarity by nucleus, enlarged nuclei, nuclear crowding, hyperchromatism and pseudo-stratification are present.

Scale bar 10μm.

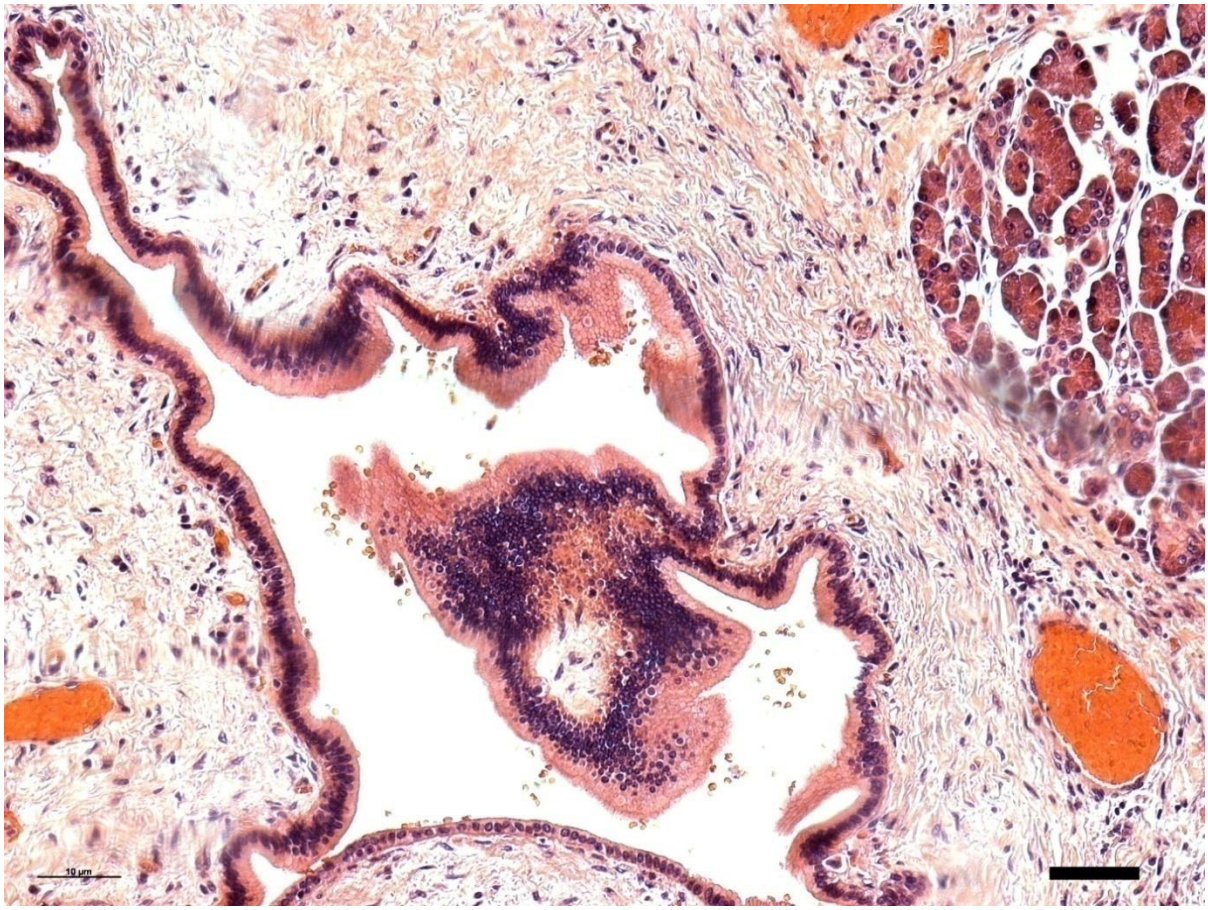

Figure 1.6 Representation of a pancreatic epithelial neoplasia 3 (PanIN3)

A representative picture of a PanIN3 lesion; characterized by its papillary architecture, luminal necrosis, loss of nuclear polarity, and prominent nuclear irregularities.

Scale bar 10µm.

1.2 b. Mucinous cystic neoplasms (MCN)

MCNs (Figure 1.7) are mucin producing, cyst forming epithelial neoplasms with a characteristic ovarian type stroma. This ovarian type stroma differentiates MCNs from IPMNs and is essential in the definition of MCN. 90% of MCNs occur in females with an average age of 50 years (range 14-95 years) (Maitra, Fukushima et al. 2005; Hruban, Maitra et al. 2007). Patients mostly present with symptoms such as abdominal pain, anorexia or a sense of fullness while other patients are asymptomatic (Maitra, Fukushima et al. 2005). MCNs form large multilocular cystic masses in the tail of the pancreas (Albores-Saavedra, Angeles-Angeles et al. 1987). The average size of an MCN is about 10cm and the external surface is usually smooth. Cut sections show a number of well-defined cysts which may be separated by fibrous septa. Some of the cysts contain thick mucin while others contain watery hemorrhagic material (Maitra, Fukushima et al. 2005). Diagnosis is arrived at by a combination of different diagnostic imaging modalities; computed tomography, magnetic resonance and endoscopic ultrasonography, that help to differentiate MCNs from the other neoplastic cysts such as intraductal papillary mucinous neoplasm, serous cystadenomas and solid and pseudopapillary tumours; and pseudocysts of the pancreas (Sahani, Kadavigere et al. 2005; Khalid and Brugge 2007). Because pseudocysts are benign and resection may be considered unjustifiable, initial patient evaluation of pancreatic cysts should exclude pseudocysts (Martin, Hammond et al. 1998; Sahani, Kadavigere et al. 2005). Pseudocysts have the following radiographic characteristics that differentiate them from cystic neoplasms: a lack of septae, cyst wall calcifications, loculation, communication between the pancreatic duct and cyst and hypovascularity (Holzheimer and Mannick 2001; Holzheimer, Mannick et al. 2001)

Activating mutation for the oncogene K-*ras* is observed early in MCN development. SMAD4 and p53 mutations have also been observed in later stages of the disease (Bartsch D, Bastian D 1998; Flejou JF, Boulange B 1996).

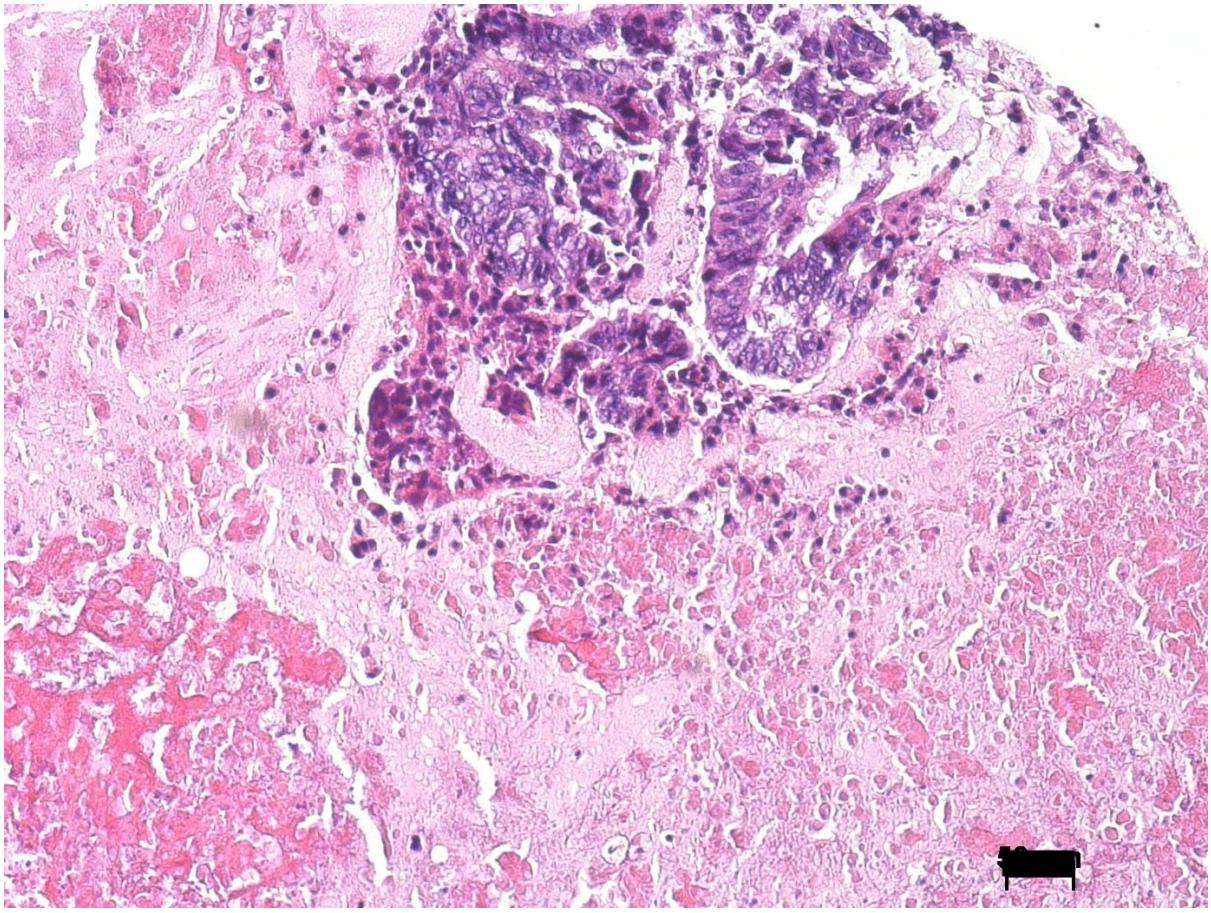

Figure 1.7 Mucinous cystic neoplasm (MCN)

A representative picture of MCN stained with haematoxylin and eosin, characteristically showing mucin secretion and ovarian type of stroma.

Scale bar 10µm.

1.2 c. Intraductal papillary mucinous neoplasm

IPMNs (Figure 1.8) are large, non-invasive and mucin producing neoplasia of the epithelia that form finger-like papillae that arise from the main duct or branch ducts. A characteristic and diagnostic feature of main-duct IPMNs is the oozing of mucin from a patulous ampulla of Vater observed during endoscopy (Maitra, Fukushima et al. 2005; Hruban, Maitra et al. 2007). Unlike MCN, IPMN lacks an ovarian type stroma, occurs more frequently in men than women (60: 40 ratio) and the cystic ducts of an IPMN typically involve the larger pancreatic ducts (Fukushima, Mukai et al. 1997; Maitra, Fukushima et al. 2005; Hruban, Maitra et al. 2007). The symptoms of IPMN include abdominal pain, weight loss, nausea and vomiting, steatorrhea, diabetes mellitus, back pain, jaundice and pancreatitis (Maitra, Fukushima et al. 2005; Hruban, Maitra et al. 2007). IPMNs mostly arise in the head of the pancreas, they may also arise in the body, tail or diffusely across the entire length of the pancreas (Maitra, Fukushima et al. 2005).

Non-invasive IPMNs may be divided into 2 main groups: main-duct type and branch-duct type. The main duct type involves the main pancreatic duct and has higher probability of dysplasia and is associated with invasive carcinoma more often than the branch-duct type. Non-invasive IPMNs are histologically graded by their degree of architectural and cytological atypia into IPMNs with mild dysplasia (IPMN adenoma), IPMNs with moderate dysplasia and IPMNs with severe dysplasia (carcinoma *in situ*) (Hruban, Maitra et al. 2007).

Similar to PDAC, IPMNs have an initiating oncogenic K-*ras* mutation with increases in frequency correlating with increasing dysplasia (Hruban, Maitra et al. 2007) and tumour suppressor gene mutations such as *p53* and *CDNK2A* occur at

later stages. But unlike PDAC, *LKB1*/ *STK11,* the Peutz-Jeghers gene, is inactivated in about 30% of IPMN patients (Sato N, Rosty C, 2001).

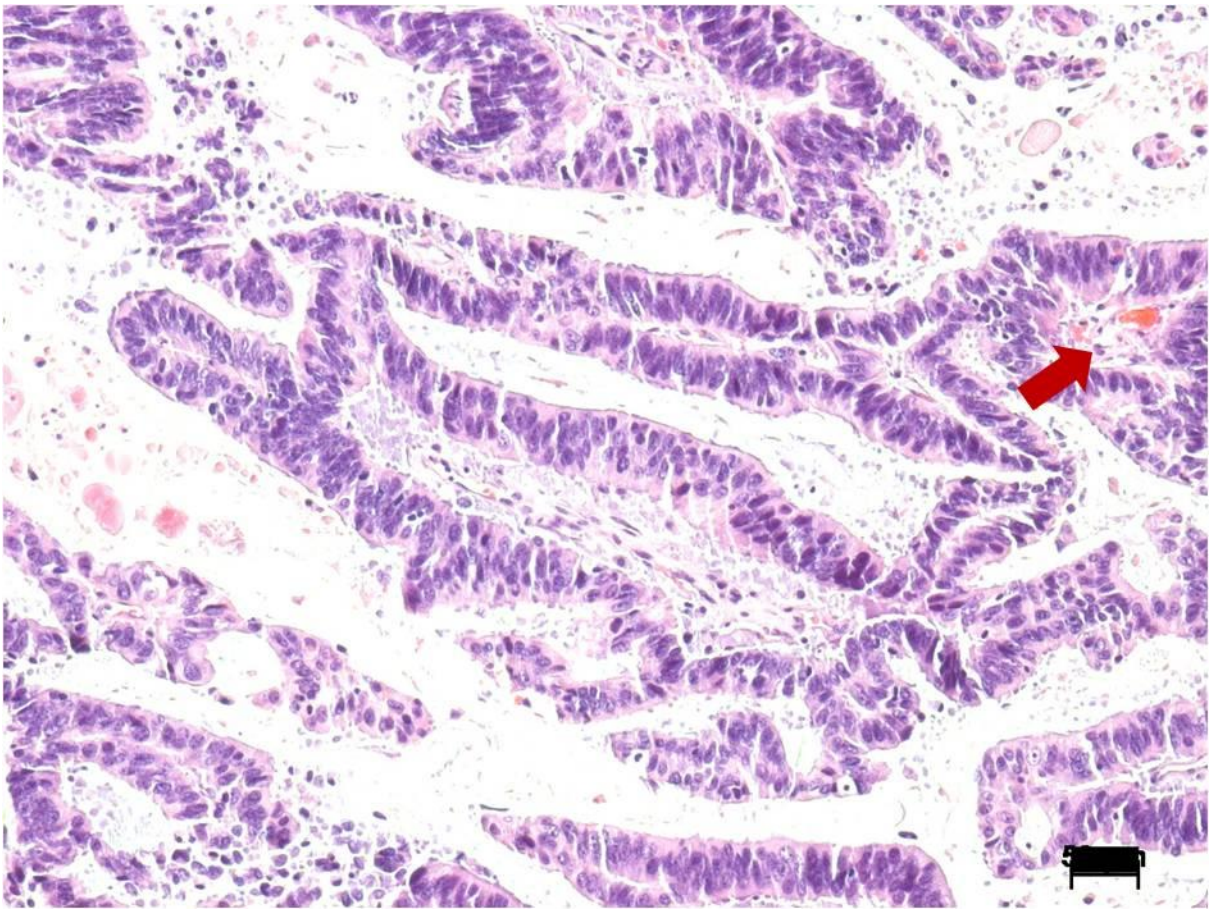

Figure 1.8 Intraductal papillary neoplasm (IPMN)

A representative picture of IPMN stained with haematoxylin and eosin, characteristically showing mucin production (red arrow) and papillae.

Scale bar 50µm.

	PanIN	IPMN (Non invasive)	MCN
Often clinically detected	No	Yes	Yes
Often grossly visible	No	Yes	Yes
Often grossly visible mucin	No`	Yes	Yes
Well formed papillae	No	Yes	Minimal
Muc2 expression	No	Sometimes	Yes (gobleT-cells only)
Associated with invasive colloid carcinoma	No	Yes	No (rarely)
Ovarian type stroma	No	No	Yes
Communication with ducts	Yes	Yes	No

Table 1.1 Features distinguishing PanINs from IPMNs and MCN. Adapted (Levi, Klimstra et al. 2004; Hruban, Maitra et al. 2007; Baker, Seeley et al. 2012)

Pancreatico-bilary diseases mimicking PDAC

1.3 a. Chronic pancreatitis

Pancreatitis is the most common benign disease of the pancreas and may be acute or chronic, based on morphologic, clinical and histologic observations. Chronic pancreatitis (CP; Figure 1.9) is a persistent inflammation of the pancreas characterised by the loss of exocrine and endocrine parenchyma, irregular fibrosis, immune cell infiltration and ductal abnormalities (De Backer et al. 2002). Chronic pancreatitis typically manifests as abdominal pain and with increased symptoms of exocrine and endocrine insufficiency (such as mal-absorption and diabetes mellitus) as the disease progression occurs (De Backer et al. 2002). Several types of chronic pancreatitis exist and may mimic PDAC such as autoimmune, alcoholic, tropical and hereditary pancreatitis (Kloppel G, 2007) most common being the alcohol-induced. CP often exhibit duct like glands that are very similar to benign pancreatic ducts; produce an abundant fibrotic stroma of varying cellularity; and infiltrates pancreatic tissue without destroying it completely or replacing it. These features make it difficult to differentiate CP from PDAC (Klöppel and Adsay 2009).

1.3 b. PDAC and chronic pancreatitis

CP may be differentiated from PDAC by the following histopathology criteria:

1. Lobular pattern: When observed at low magnification, the remaining structures of CP; acinar, islets and small ducts retain their normal lobular arrangement. The formation of tubular complexes (ductal transformation) by the acinar may occasionally result in packed clusters that are evenly shaped, sized and spaced, and segregated from surrounding fibrous tissue. This is in contrast to PDAC, as well-differentiated PDAC form duct-like structures with

atypical shape that are distorted and haphazardly distributed (Klöppel and Adsay 2009).

2. Ductal contours and contents: Benign ducts have smooth, ripple-like contours with an open and round lumen. Benign ducts also retain their epithelium and their ducts rather than containing debris contain plugs and “concretions of secretions” which become calculi when calcified. Contrarily, ducts of PDAC are angular and “ruptured” (i.e. parts of the duct lacks epithelia and is lined by mesenchymal tissue). This leads to mucin leaking into the surrounding tissue attracting macrophages. PDAC ducts may also contain debris (Klöppel and Adsay 2009).
3. Stromal reaction and infiltration: A characteristic feature of PDAC is the concentration of a hyper-cellular stroma surrounding large neoplastic ducts. PDAC cells also erratically infiltrate the relatively acellular stroma either individually or in small cell clusters (Klöppel and Adsay 2009).
4. Extrapancreatic infiltration of tissue: A unique characteristic feature of PDAC is their ability to infiltrate nerve tissue, termed perineural invasion and is detected in almost all resected PDAC tissue. Perineural invasion occurs in the intra-pancreatic nerve fibres and nerve trunks in the retroperitoneal area behind the head of the pancreas, and around the common bile duct. PDAC cells invading the nerves show glandular differentiation. By contrast, benign ducts are rarely found around nerves and almost never show invasion to the perineurium. PDAC cells are also seen to infiltrate vascular tissues (usually involving veins); a feature used in diagnosis. Another feature is the location of solitary PDAC ducts as an island within fatty tissue with the ducts either

touching the fatty tissue or surrounded by inflammatory cells (Klöppel and Adsay 2009).

1.3 c. Cytological differentiation of chronic pancreatitis from PDAC

CP may be differentiated from PDAC by the following cytological criteria (Klöppel and Adsay 2009):

Chronic pancreatitis

a. Ducts of CP are composed of differentiated, equally sized epithelial cells.
b. Nuclei are round and located at the base of cell
c. Nuclei show no signs of nucleoli or at most small distinct nucleolus
d. There are no mitoses

Pancreatic ductal adenocarcinoma

a. Nuclear size variation among cells within an individual gland is 4:1
b. Larger nuclei, approximately 3 times lymphocyte
c. Nuclei with marked hyperchromatism and distinct and occasional multiple nucleoli
d. Presence of mitotic figures
e. Distinct loss of nuclear polarity

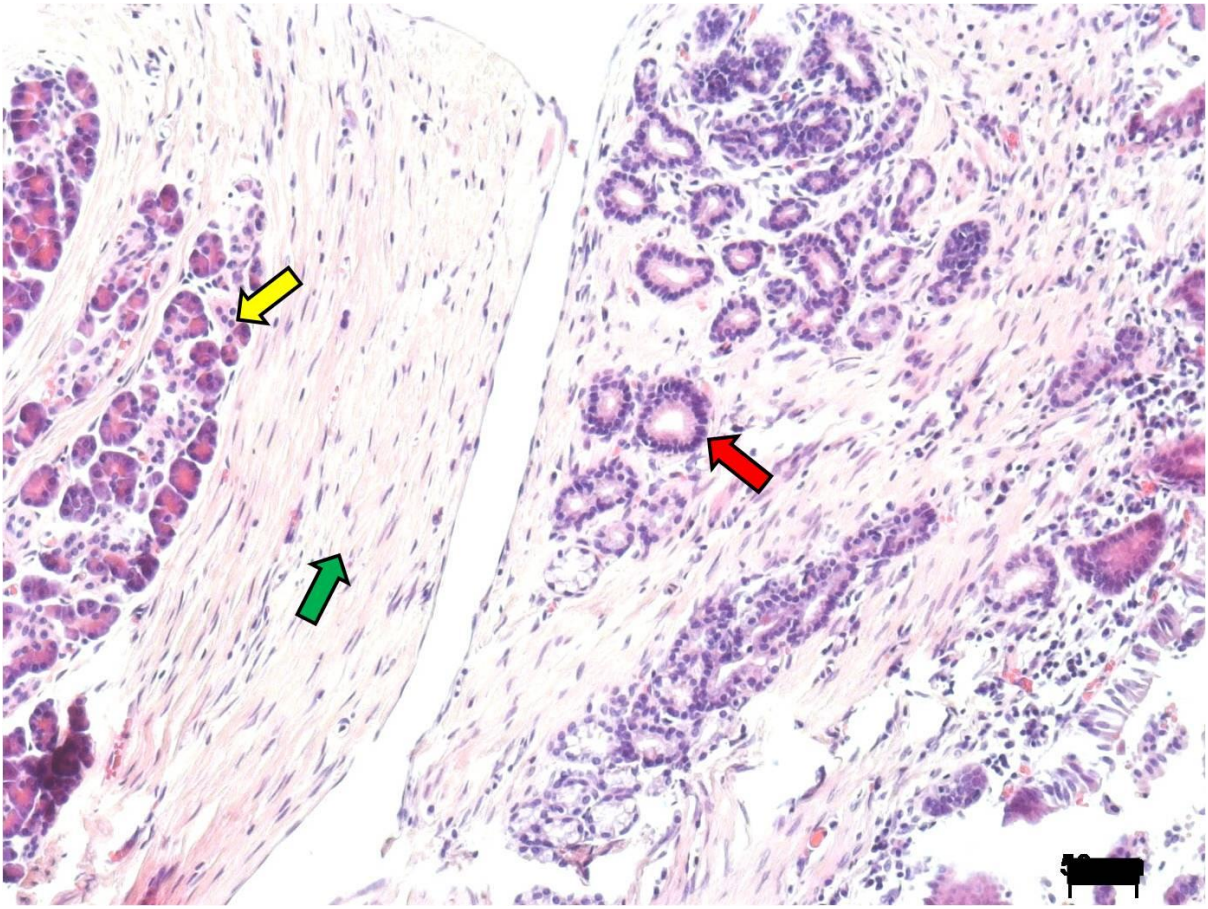

Figure 1.9 Chronic pancreatitis

A representative picture of chronic pancreatitis stained with haematoxylin and eosin; showing loss of exocrine and endocrine parenchyma, irregular fibrosis and ductal abnormalities. Ducts are smooth with ripple like contours and open and round contours, nuclei are also round and at the base of cell with no signs of nucleolus or mitosis (“red arrow”). Normal acinar cells (“yellow arrow”) retain their lobular pattern, stroma (“green arrow”) is not hypercellular and ducts do not infiltrate the stroma.

Scale bar 50µm.

1.3 d. Ampullary carcinoma

The pancreatic duct and bile duct merge at the ampulla of Vater forming a channel that drains these ducts into the duodenum. The ampulla of Vater is thus exposed to three different juices and is prone to tumours similar to those of the small intestine (Albores-Saavedra J, Menck 2000).(Fischer and Zhou 2004)

Ampullary carcinomas (Figure 1.10) are often symptomatic earlier due to biliary obstruction leading to persistent icterus. The jaundice may be waxing and waning type due to sloughing of ampullary tumour. This allows for 80% to 90% of tumours to be treated by surgery. The 5- year survival rate after tumour resection is 21% to 61% with a mean of 40% (Fischer and Zhou 2004).

1.3 e. PDAC and ampullary carcinoma

Like PDAC and other pancreatico-biliary diseases discussed earlier, ampullary carcinoma has an activating K-*ras* point mutation and genetic alterations for the tumour suppressor genes *CDKN2A*, *p53* and *SMAD4* have also been observed (Fischer and Zhou 2004). The frequency of K-*ras* mutations which is about 24% to 47% in ampullary carcinoma is considerably less than K-*ras* frequency of around 80% in PDAC (Howe, Klimstra et al. 1998).

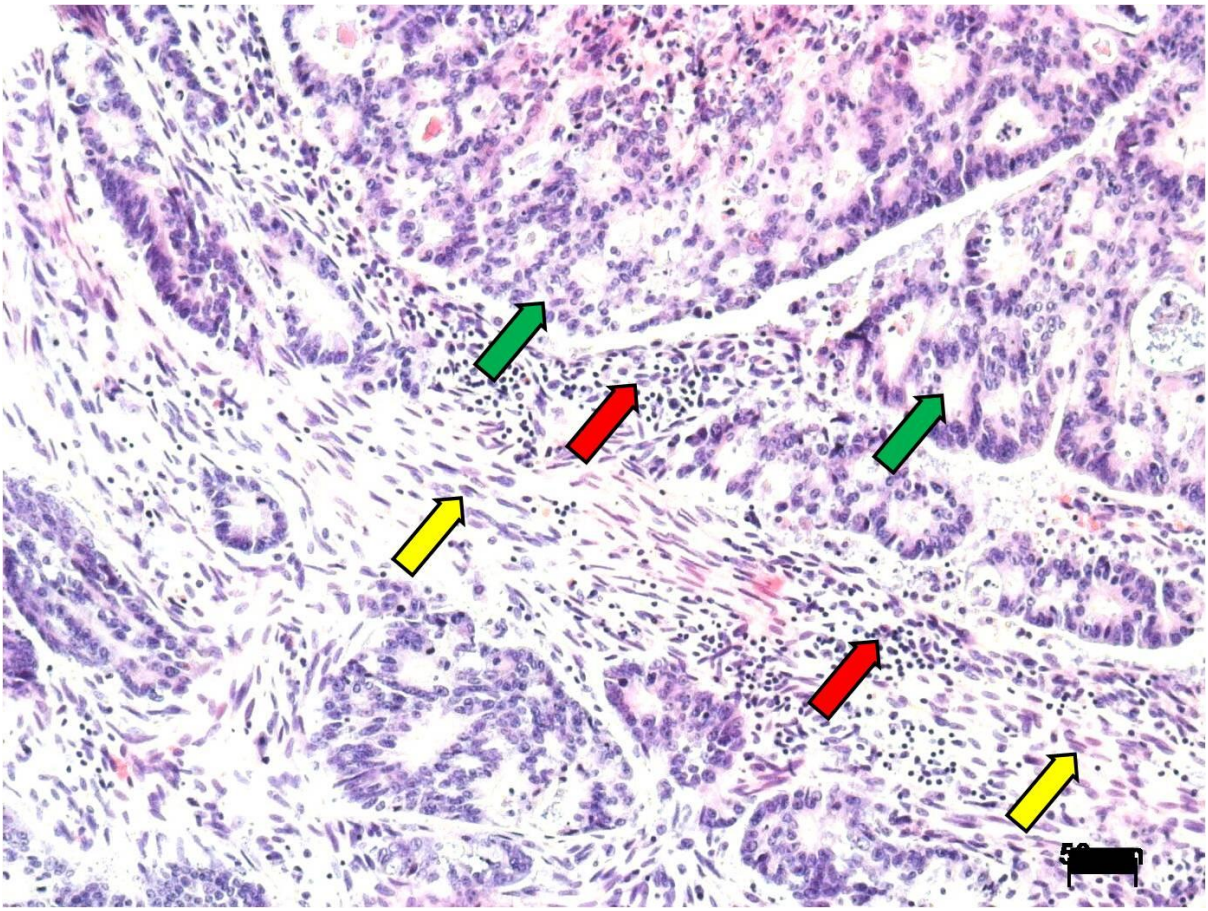

Figure 1.10 Ampullary carcinoma

A representative picture of Ampullary carcinoma stained with haematoxylin and eosin. “Red arrows” point at the immune/desmoplastic stroma, “green arrows” point at the tumour cells and “yellow arrows” point at the muscle layer of the bowel.

Scale bar 50µm.

1.3 f. Cholangiocarcinoma

Cholangiocarcinoma (Figure 1.11) arises from the epithelia of the biliary tract (Nakeeb A, Pitt HA 1996). The disease is found more in men (approximately 60%) usually in their 70's (West J, Wood H 1971- 2001), and most of whom were heavy smokers or diabetic (Endo I, Gonen M 2008). Cholangiocarcinoma has been associated to the following diseases: primary sclerosing cholangitis, hepatitis C, biliary infection (chronic or recurrent), hepatolithiasis, Caroli's disease and cirrhosis of the liver (Skipworth, Olde Damink et al. 2011).

Cholangiocarcinoma may be grouped as intrahepatic and extrahepatic (de Groen, Gores et al. 1999). Intrahepatic cholangiocarcinoma occur when the tumour is within the liver whereas extrahepatic cholangiocarcinoma may be distal (when the tumour occurs at the distal bile ducts) or hilar (when tumours occur at the bifurcation of hepatic ducts) (de Groen, Gores et al. 1999; Eckmann, Patel et al. 2011). Surgical resection remains the only "curative treatment" (Khan, Davidson et al. 2002) which is feasible in a minority of patients. As a result prognosis of biliary tumours is poor with 21.4% surviving up to 1 year, and 3.8% surviving up to 5 years after diagnosis (Coupland, Kocher et al.).

Patients with extrahepatic cholangiocarcinoma present with painless jaundice and approximately 10% present with signs of sepsis and cholangitis (Skipworth). Disease progression is gradual because of the gradual infiltration and spread of disease along the biliary tract that results in delayed cholestasis, hepatic failure and cholangitis (Skipworth). Majority of cholangiocarcinoma patients present late with biliary obstruction and sepsis, and death mostly results from recurrent biliary obstruction and sepsis rather than malignancy (Skipworth, Olde Damink et al. 2011).

1.3 g. PDAC and cholangiocarcinoma

The molecular characteristics of cholangiocarcinoma are similar to those of PDAC as both tumours carry mutations in K-*ras*, Tp53, SMAD-4 and p16 (Reeves and DeMatteo 2000; Khan, Davidson et al. 2002). The extensive desmoplastic reaction present in (extra-hepatic) cholangiocarcinoma (de Groen, Gores et al. 1999) is also similar to that seen in PDAC.

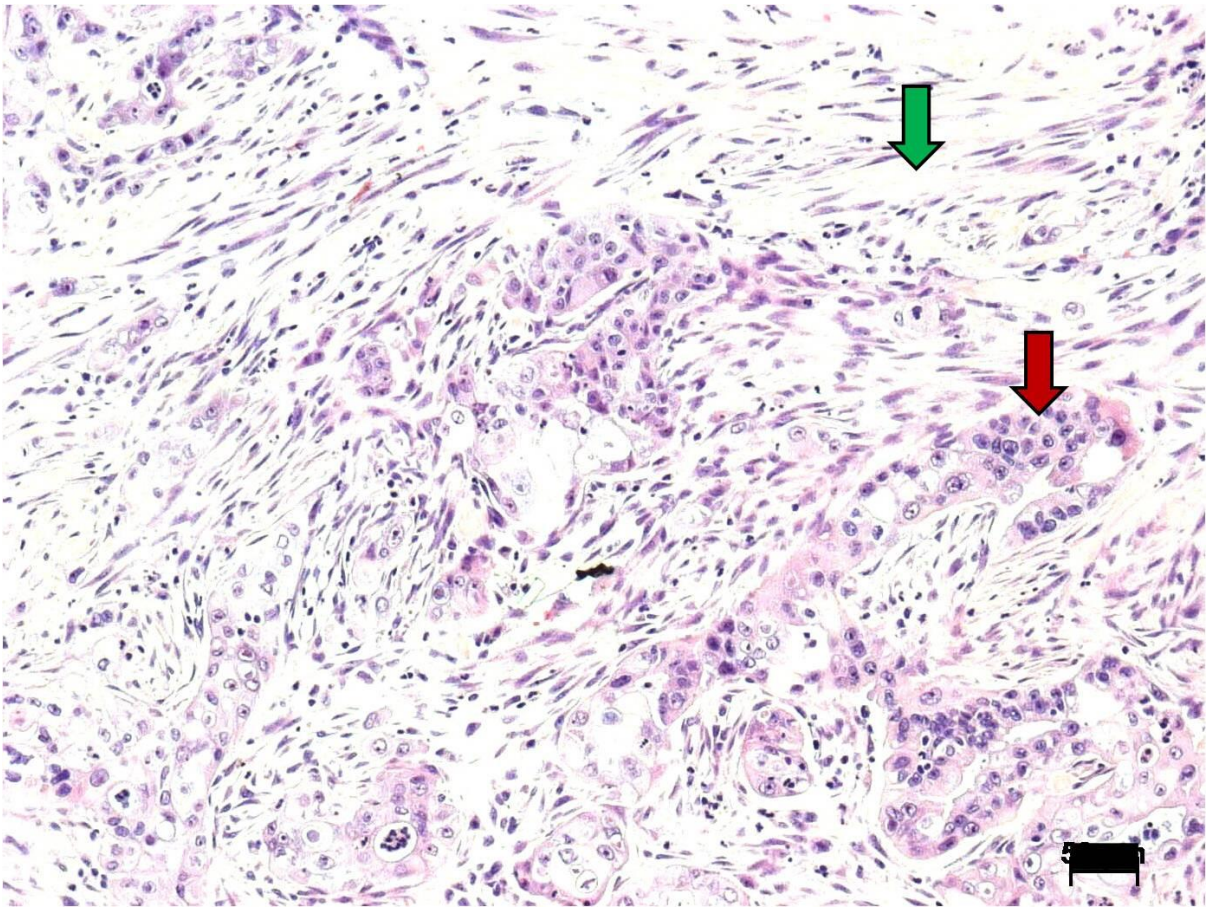

Figure 1.11 Cholangiocarcinoma

A representative picture of cholangiocarcinoma stained with haematoxylin and eosin.

“Red arrow” points at tumour and “green arrow” at stroma.

Scale bar 50µm.

Immune cells

1.4 a. Introduction

Risk of neoplasia is promoted by continued cell proliferation, the presence of growth factors, activated stroma, DNA damage causing agents and inflammatory cells amongst other micro-environmental factors (Coussens and Werb 2002).

Cancers have been known to express foreign antigens as a result of genomic instability and aberrant gene expression. These can be recognized by immune cells (Van den Eynde and van der Bruggen 1997; Clark, Hingorani et al. 2007). *In vitro* and *in vivo* studies have shown that immune cells are activated in response to cancers (Garside 1998). Tumour infiltrating lymphocytes have been associated with increased survival in patients with melanomas, colorectal carcinomas, ovarian cancers and breast cancers (Clemente, Mihm et al. 1996; Marrogi, Munshi et al. 1997; Naito, Saito et al. 1998; Zhang, Conejo-Garcia et al. 2003; Galon, Costes et al. 2006; Tosolini, Kirilovsky et al. 2011).

1.4 b. Inflammation

Inflammation is an integral early process in immune cell response to physiological processes such as wound healing and pathological processes such as infection. Inflammation often results from tissue injury where a network of chemical signals such as cytokines and chemokines initiate and sustain a host response designed to repair affected tissue (Coussens and Werb 2002). With the help of specific chemokines and cytokines (Balkwill & Mantovani, 2001), leukocytes are activated and they migrate from blood vessels to affected tissue.

The activation and migration of leukocytes occur in four steps (Coussens and Werb 2002):

1. Activation of the adhesion molecule family of selectins (L-, P- and E-selectins) that facilitate leukocyte rolling along the endothelium.
2. “Switching-on” of cytokine and chemokine signals that activate and upregulate integrins on leukocytes.
3. Tight adhesion of leukocytes, immobilizing them on the surface of the vascular endothelium via α_4 β_1 and α_4 β_7 integrins that bind to endothelial the vascular cell adhesion molecules (VCAM-1) and mucosal addressin cell adhesion molecule (MadCAM-1) respectively.
4. Transmigration of leukocytes through the endothelium to sites of inflammation by the help of proteases such as the Matrix Metalloproteinases (MMPs).

These steps will be described in more detail.

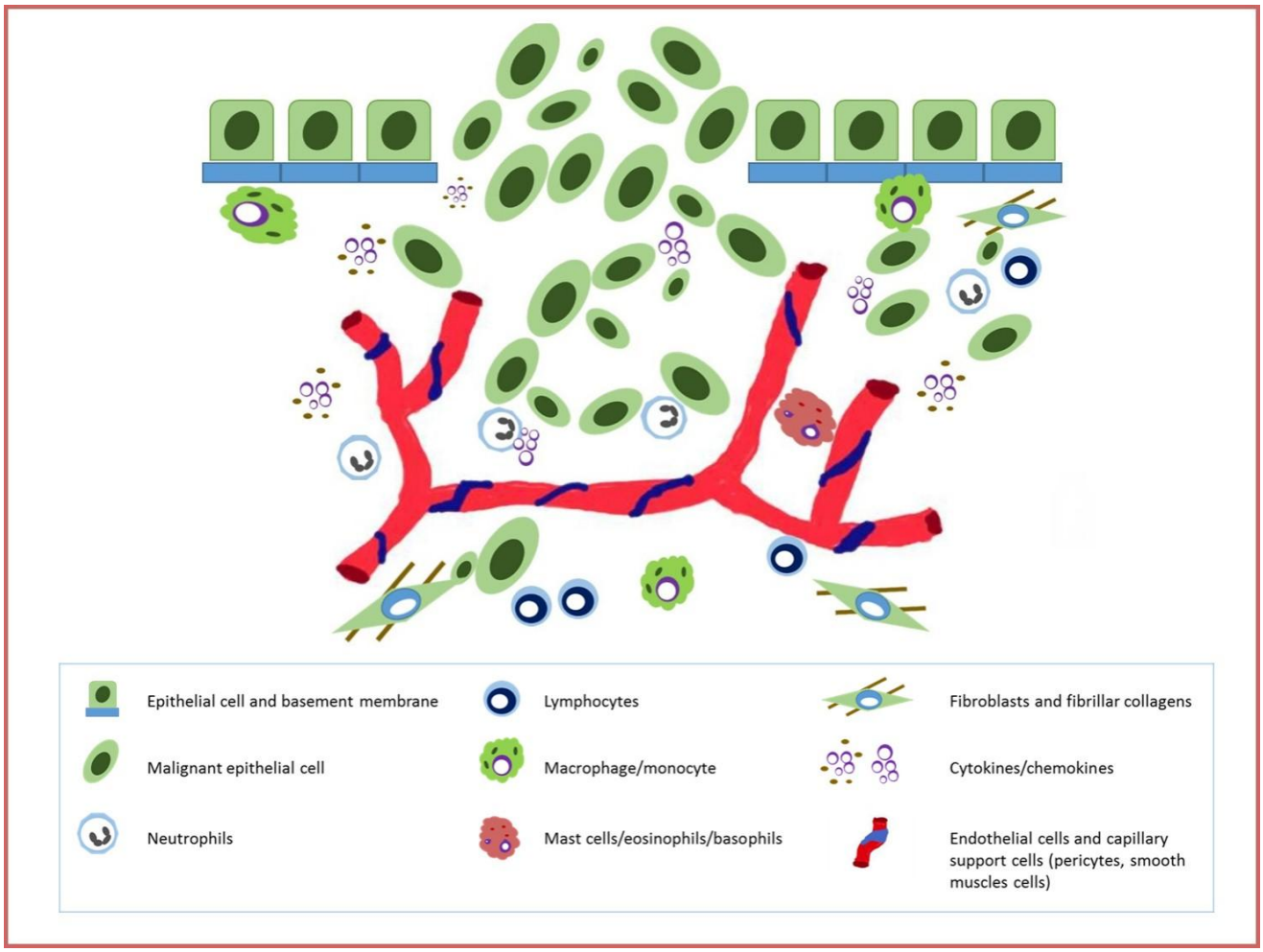

Figure 1.12 Microenvironment in pancreatic cancer

The microenvironment in pancreatic cancer is made up blood/lymphatic vessels where there may be transported and transplanted to other organs. There is an influx of immune cells that include neutrophils, macrophages and lymphocytes and a rich mixture of chemokines and cytokines that regulate these processes. A high proportion of the microenvironment is made up of myofibroblasts whose origin is believed to be stellate cells.

1.4 c. Immune cells: mechanism of action

Immune cells within the cancer tissue are morphologically organized in such a manner as to assist the complex cellular interactions needed for development, activation, migration, function and regulation of the various leukocytes (Campbell, Kim et al. 2003). This organisation is made possible by tissue and microenvironment specific lymphocyte homing due to the expression of surface adhesion molecules and chemo-attractant receptors such as CXCR5, VLA4 and P- and E- selectin ligands (Campbell and Koch 2011).

1.4 d. Lymphocyte homing

Inactivated lymphocytes continually re-circulate the body by crossing high endothelial venules into the lymph nodes where they remain from a few hours to a number of days (Smith 2003). In the absence of antigen specific recognition they exit into the circulation through lymph vessels and the thoracic duct (Smith 2003; von Andrian and Mempel 2003). Monocytes and neutrophils meanwhile circulate in the blood until when attracted by stimulant in target tissue (von Andrian and Mempel 2003). They then release cytokines and chemokines that attract lymphocytes to target tissues (Smith 2003).

Lymphocytes carry out precise effector functions that ensure host response to infection and inflammation as well as mediate homeostasis. T-cells, *in vivo,* show a migratory phenotype of an average speed of approximately 11µm/ minute with peak velocities exceeding 25 µm/ minute (Miller 2003) and they are approximately 100 times faster than fibroblasts and endothelial cells (Smith 2003).

The process of immune response wherein leukocytes migrate from the blood (in vessels) to target tissues is termed extravasation. The process involves a series of steps in sequence from tethering and rolling of leukocytes on the walls of blood vessels, to firm adhesion and protrusion through the endothelial barrier (diapedesis).

1.4 e. Migration

The migration of leukocytes is a complex process involving various integrins, motor proteins (such as myosins and kinesins), selectins, cytokines and chemokines. The adhesion of ligands of integrins (such as VCAM1 and ICAM1), chemokines and selectins with their respective receptors is a major driving force for migration. Activated endothelial cells express such proteins on their surface and these proteins control the different stages of leukocyte extravasation (Vicente-Manzanares and Sánchez-Madrid 2004).

Tethering, the initial attachment of leukocytes to the endothelial vessel wall, is mediated by the attachment of selectins to their ligands. Leukocytes express L-selectin which interacts with sialylated ligands expressed on the endothelium to mediate rolling (McEver 2002). P-selectin glycoprotein ligand 1 (PSGL1) expressed on the actin cytoskeleton of leukocytes also mediates rolling by interaction with P-selectin and E-selectin expressed by the endothelium (McEver and Cummings 1997).

Firm adhesion (leukocyte arrest) follows thereafter with the Intracellular adhesion molecule 1 (ICAM1) and Vascular cell adhesion molecule 1 (VCAM1) mediating this process. VCAM1 on endothelial vessel wall interacts with $\alpha_4\beta_1$ (very late antigen 4, VLA4) while ICAM1 interacts with β_2 integrins particularly leukocyte

function-associated antigen, LFA1 expressed on the membrane of the leukocyte (Barreiro 2002).

LFA-1 (CD11a/ CD18; $\alpha L\beta_2$), in addition to mediating adhesion, also promotes migration of leukocyte (Smith 2003). Andrew Smith and colleagues after exposing T-cells with active LFA-1 to immobilised ligand ICAM-1 observed that the T-cells polarised and begun to migrate approximately 2 minutes following contact with ICAM-1 suggesting induction of migration is a potent signalling function of LFA-1 (Smith 2003).

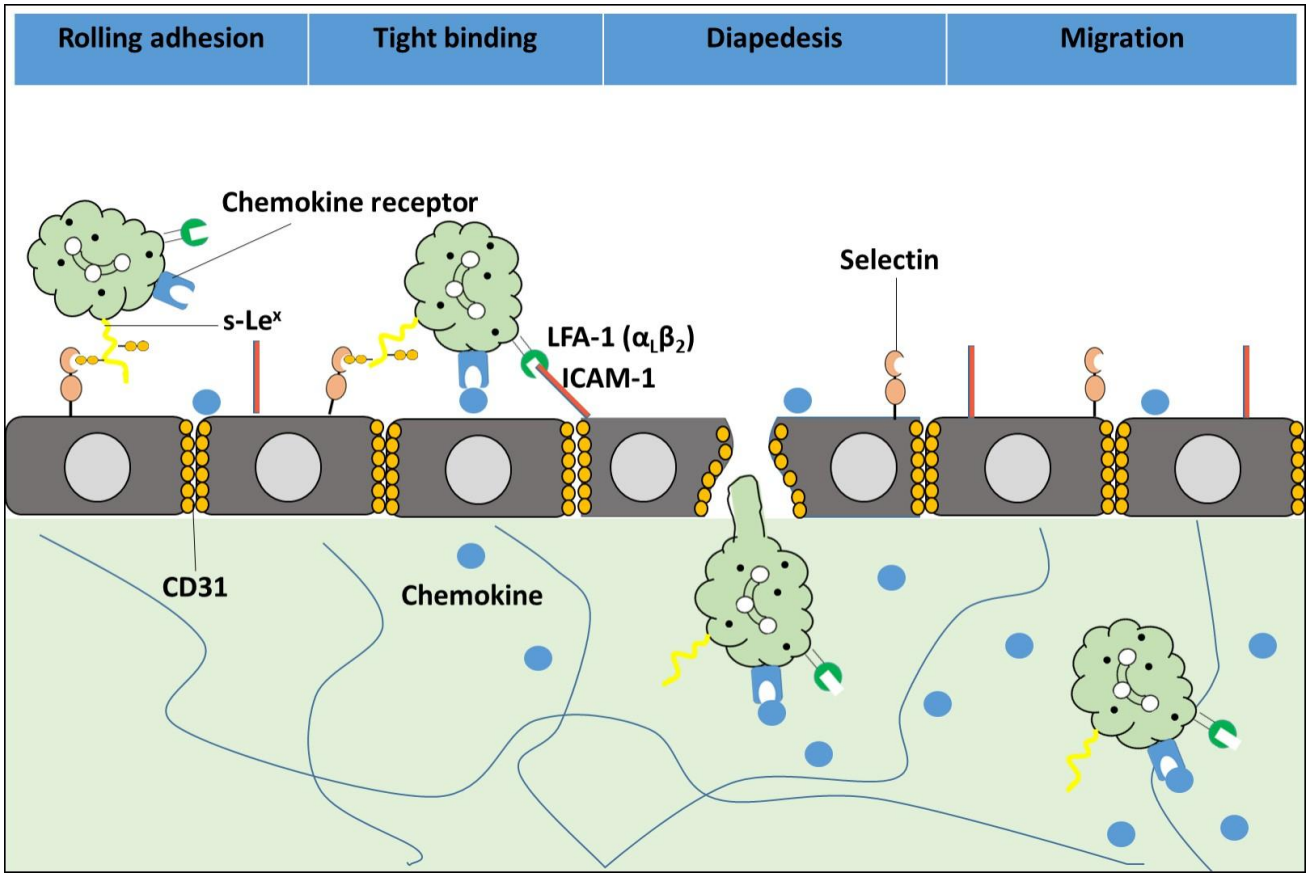

Figure 1.13 Representation of leukocyte chemotaxis

Leukocytes recirculate the body in blood vessels and in response to stimulants from tissue "tether" to selectins on endothelial vessel walls where they perform "rolling adhesion" from which "tight binding", usually involving ICAM-1/ VCAM-1 and their receptor on leukocytes, occur. Still in response to chemokine secretion from tissue, leukocytes protrude the endothelial barrier (diapedesis) on to target tissue where they migrate on tissue to target.

1.4 f. Chemokines

Chemokines were originally defined, based on their function, as soluble factors regulating specific migration of leukocytes during inflammation. This definition has now been modified to include all cell types including neoplastic cells (Rossi D & Zlotnik A 2000). In addition to recruiting leukocytes, chemokines also effects stromal and neoplastic cells (Coussens and Werb 2002). Tumour cells regulate their chemokine expression to help recruit inflammatory cells and help with their [tumour] growth and progression(Coussens and Werb 2002). For example, in Melanoma the chemokines GROα/ CXCL1, GROβ/ CXCL2, GROγ/ CXCL3 and IL-8/ CXCL8 have been demonstrated to control proliferation of neoplastic cells via an autocrine mechanism. Blocking GROα stops proliferation of melanoma *in vitro* while the overexpression of GROα, GROβ and GROγ in tumour derived cell lines enhances tumourigenicity and colony forming activity in nude mice (Richmond A & Thomas H, 1986; Norgauer J, Metzner B 1996; Balentien E, Mufson BE et al 1991; Owen JD et al 1997). Chemokines may also regulate angiogenesis where they have both pro-angiogenic and angiostatic effects and the balance of which may regulate the physiology of neoplastic cell. An example is the chemokine CXCL12/ SDF-1α that induces VEGF-A expression (Coussens and Werb 2002).

Ligand	Names	Receptors	Immune cell recruitment
CXCL1	Gro-a, growth related oncogene-a	CXCR1, CXCR2	MC, MO
CXCL2	Gro-ß, growth related oncogene-ß	CXCR2	MC, MO
CXCL3	Gro-g, growth related oncogene-g	CXCR2	MC, MO
CXCL4	PF-4, platelet derived factor 4	CXCR3	T
CXCL5	ENA-7A, epithelial cell derived neutrophil activating factor 78	CXCR2	MC, MO
CXCL6	GCP-2, granulocyte chemoattractant protein 2	CXCR1	MO, MC
CXCL7	NAP-2, neutrophil activating protein 2	CXCR2	MC, MO
CXCL8	IL-8, interleukin 8	CXCR1, CXCR2	MC, MO
CXCL9	MIG, monokine induced by interferon	CXCR3	T
CXCL10	IP-10, g interferon inducible protein 10	CXCR3	T
CXCL11	I-TAC, interferon inducible T-cell a-chemoattractant	CXCR3	T
CXCL12	SDF-1, stromal-derived factor-1	CXCR4	T, B, MO
CXCL13	BCA-1, B-cell activating chemokine 1	CXCR5	B
CXCL14	BRAK, breast and kidney chemokine	?	
CXCL16	Leukotactin-1	CXCR6	NK
CCL1	I-309	CCR8	T, NK
CCL2	MCP-1, monocyte chemoattractant protein 1	CCR2, CCR11	T, MC, MO
CCL3	MIP-1a, macrophage inflammatory protein 1a	CCR1, CCR3, CCR5	EO, MO, BO, T, NK
CCL4	MIP-1ß, macrophage inflammatory protein 1ß	CCR1, CCR5	MC
CCL5	RANTES, regulated on activation, normally T-cell expressed and secreted	CCR1, CCR3, CCR5	EO, MC, MO, BO
CCL7	MCP-3, monocyte chemoattractant protein 3	CCR1, CCR2, CCR3, CCR11	EO, MC, MO, BO MO
CCL8	MCP-2, monocyte chemoattractant protein 2	CCR1, CCR2, CCR3, CCR5, CCR11	MC, MO, BO

Table 1.2 Chemokines and their receptors (Iida and Grotendorst 1990; Ono, Nakamura et al. 2003; Bendall 2005; BENDALL 2005; Oo and Adams 2010)

Ligand	Names	Receptors	
CCL11	Eotaxin	CCR3	EO, MC, BO
CCL12	MCP-5, monocyte chemoattractant protein 5	CCR2, CCR11	MC, MO
CCL13	MCP-4, monocyte chemoattractant protein 4	CCR2, CCR3, CCR5, CCR11	EO, MC, MO, BO
CCL14	HCC-1, haemofiltrate CC chemokine or MIP-1d, macrophage inflammatory protein 1d	CCR1, CCR5	MC
CCL15	HCC-2, haemofiltrate CC chemokine-2 or Lkn-1, leukotactin 1	CCR1, CCR3	MC, BO
CCL16	HCC-4, haemofiltrate CC chemokine-4 or LEC, liver expressed chemokine	CCR1, CCR2, CCR8	MC, NK
CCL17	TARC, thymus and activation regulated chemokine	CCR4, CCR8	T, MC, MO, NK
CCL18	PARC, pulmonary and activation regulated chemokine	?	
CCL19	MIP-3ß, macrophage inflammatory protein 3b or ELC, Epstein–Barr virus induced receptor ligand chemokines	CCR7, CCR10, CCR11	T, DC, B
CCL20	MIP-3a, macrophage inflammatory protein 3a or LARC, liver and activation regulated chemokine	CCR6, CCR10	B, T
CCL21	SLC, secondary lymphoid tissue chemokine	CCR11	MO
CCL22	MDC, macrophage derived chemokine	CCR4	T, MC, MO, DC
CCL23	MPIF-1, myeloid progenitor inhibitory factor 1	CCR1	MC
CCL24	Eotaxin-2 or MPIF-2, myeloid progenitor inhibitory factor 2	CCR3	EO, MC, BO
CCL25	TECK, thymus expressed chemokine	CCR9, CCR11	DC, MO
CCL26	Eotaxin-3	CCR3	EO, MC, BO
CCL27	CTACK or ESkine	CCR10	T
CCL28	Mec	CCR3, CCR10	MC, BO, T
XCL1	Lymphotactin-a	XCR1	NK
XCL2	SCM1b or Lymphotactin-ß	XCR2	T
CX3CL1	Fractakine/neurotactin	CX3CR1	NK, MO

Table 1.2 (continued) Chemokines and their receptors (Iida and Grotendorst 1990; Ono, Nakamura et al. 2003; Bendall 2005; Oo and Adams 2010)

Macrophages

Macrophages have been found to promote solid tumour progression and metastasis. They are recruited by the tumour and "educated" by the tumour microenvironment to adopt a trophic role that encourages tumour cell migration, extracellular matrix breakdown and angiogenesis (Pollard 2004).

1.5 a. Role of Macrophages in Development

Macrophages are haematopoietic cells of the immune system that have repair functions. They are among the firsT-cells that migrate to crisis sites where they perform several functions. Some of the known functions of macrophages include: production of chemical messengers (cytokines and chemokines) that recruit other immune cells to sites of infection; production of growth factors, angiogenic factors and proteases that promote tissue repair; cytotoxic killing of pathogens by the production of reactive oxygen and nitrogen radicals; and the presentation of antigens to T-cells (Pollard 2004). Studies of mice with null mutations for colony stimulating factor 1 (csf-1), a growth factor for macrophages and other mononuclear phagocytic cells, show developmental defects including: osteopetrosis, impaired branching morphogenesis of the mammary gland and aberrant pancreatic morphogenesis (Cohen, Chisholm et al. 1996; Gouon-Evans, Rothenberg et al. 2000; Pollard 2004). These suggest that macrophages may play an important role in tissue morphogenesis during development and their natural developmental role may be employed by tumours to promote their own development (Gouon-Evans, Lin et al. 2002).

The complex tumour microenvironment of most solid tumours consists of Tumour Associated Macrophages (TAM), a class of macrophages that are thought to alter clinical outcome. Clinical data for breast, ovarian, prostate and cervical cancers have shown a strong correlation between the abundance of TAM and poor prognosis (Bingle, Brown et al. 2002)

1.5 b. TAMs and angiogenesis

Monocytes, the precursors of macrophages, migrate into crisis sites where they differentiate into macrophages with subsequent secretion of angiogenic molecules. Macrophages have been shown to be positively correlated with angiogenesis, with highly vascular tumours displaying abundant numbers of macrophages. The view that macrophages induce proliferation, migration and differentiation of endothelial cells was supported by the clustering of macrophages in high vascular regions, otherwise termed as “hotspots” by Leek *et al* (Leek, Lewis et al. 1996).

Macrophages produce Tumour Necrosis Factor-α (TNF-α) (Miles, Happerfield et al. 1994), CSF-1 receptor signalling in macrophages activates urokinase-type plasminogen activator (uPA), a protein that influences angiogenesis (Hildenbrand, Dilger et al. 1995). TAMs also release IL-2 which upregulates hypoxia inducible factor 1 alpha (HIF- 1α) through cyclooxygenase 2 (COX 2) resulting in an increase in the transcription of vascular endothelial growth factor (VEGF) (Jung, Isaacs et al. 2003), all of which are important for angiogenesis.

1.5 c. TAMs and tumour progression

Studies in mice with PyMT- induced tumours (Mammary tumours induced by the mammary-epithelial-restricted expression of the polyoma middle-T oncoprotein) (Lin, Nguyen et al. 2001) showed the presence of leukocytic infiltrates that coincided with areas of basement membrane breakdown and tumour cell egress at the time of malignant transition of which approximately 50% are TAMs, creating a portal through which tumour cells enter the surrounding stroma by the secretion of proteases by the TAMs on (Lin, Gouon-Evans et al. 2002).

TAMs also produce growth factors such as Fibroblast Growth Factor (FGF), Transforming Growth Factor –β (TGF-β), Hepatocyte Growth Factor (HGF), Platelet Derived Growth Factor (PDGF) and Epidermal Growth Factor Receptor (EGFR). These molecules influence the growth and migratory capability of tumour cells (Leek and Harris 2002).

1.5 d. Differentiation of Macrophage markers

Macrophages express a set of markers that mostly differ between humans and mice. Macrophage markers in humans include: CD68, CD163, CD16, CD312, and CD115. Macrophage markers in mice include: F4/80, CD11b, CSF-1R/ CD115 and an absence of Gr1(Qian and Pollard 2010).

1.5 e. Macrophage phenotypes

Macrophages have the capability to manifest distinct phenotypes in response to different microenvironment signals (Mantovani, Sica et al. 2004). Classical M1

macrophage phenotype is activated in response to microbial products and Interferon-γ and are characterised by high IL-12 and IL-23 production. M1 macrophages are mostly effector immune cells and produce large amounts of proinflammatory cytokines. Conversely M2 macrophage phenotype is activated by IL4, IL13, IL10 and glucocorticoids. TAMs are thought to have phenotypes and functions similar to M2 macrophages (Mantovani, Porta et al. 2006).

1.5 f. Characteristics of M1 macrophages (Mantovani, Sica et al. 2004; Mantovani, Porta et al. 2006)

1. High production of nitric oxide (NO)
2. High production of reactive oxygen intermediates (ROI)
3. High capacity to present antigen.

1.5 g. Characteristics of M2 macrophages (Mantovani, Sica et al. 2004; Mantovani, Porta et al. 2006)

1. Induction of adaptive Th2 immunity
2. Promotion of angiogenesis
3. Tissue repair and remodelling

Natural killer (NK) cells

1.6 a. Introduction

NK-cells are lymphocytes of the innate immune system with cytotoxic and cytokine effector functions that target pathogens and tumours (Trinchieri 1989; Vivier, Tomasello et al. 2008). They are widespread and can be found in lymphoid and non-lymphoid tissues and make up 2%- 18% of total lymphocyte fraction in human peripheral blood (Grégoire, Chasson et al. 2007). Human NK turnover is around 2 weeks (Zhang, Wallace et al. 2007). NK-cells have a detection system that involves activating and inhibitory cell surface receptors which when engaged with may lead to cytotoxic effector functions or the discrimination of self antigens produced by healthy 'self' cells (Vivier, Tomasello et al. 2008).

1.6 b. Functions of NK-cells

Receptors for the activation of NK-cells recognise the presence of ligands in distressed cells such as "stress- induced self ligands", the UL16 binding protein encoded by the gene ULBP and the major histocompatibility complex (MHC) class I chain related molecule (MIC) both recognised by NKG2D (Lanier 2005) and ligands from pathogens such as the Toll- like Receptor ligands (TLR) (Sivori, Falco et al. 2004). The exposure of NK-cells to ligands of TLRs *in vitro* leads to the production of interferon (IFN)- γ and enhances cytotoxicity (Vivier, Tomasello et al. 2008). NK-cells also express low affinity Fc receptor CD16 enabling them detect antibody coated targeT-cells and to exert antibody dependenT-cell cytotoxicity (ADCC) (Vivier, Tomasello et al. 2008).

NK-cells use inhibitory receptors to measure the absence of constitutively expressed self molecules on susceptible targeT-cells by binding MHC class I-specific ligands (Yokoyama and Plougastel 2003). They lose inhibition when they encounter MHC class I-deficienT-cells (Yokoyama and Plougastel 2003). MHC class I inhibitory receptors of include the killer cell immunoglobulin- like receptors (KIR) in humans and the lectin- like Ly49 dimers in mouse, as well as the lectin- like CD94- NKG2A heterodimers present in both humans and mice (Yokoyama and Plougastel 2003).

1.6 c. Regulation of NK cell

Natural killer cell function- cytotoxicity, regulation- is influenced by the cytokine profile of the tumour microenvironment and on the interaction of NK-cells with other immune cells, such as T-cells, macrophages and dendritic cells (Long E. O. 2007). IL-2 promotes proliferation, cytotoxicity and cytokine secretion of NK-cells (Trincheri 2004). Cytokines that activate NK cell effector functions include IL-12, IL-15, IL-18 and type 1 IFN (Walzer T, Dalod M 2005). NK-cells may be regulated by TGF-β and Tregs through a TGF-β dependent mechanism in both human and mice (Laouar YSutterwala F.S. 2005; Smyth M.J et al 2006). In mice, $CD8^+$ T-cells may work together with NK-cells as they infiltrate tumour; the mechanism is not yet understood (Shanker A 2007).

1.6 d. NK cell phenotypes

1.6 d. i. Mice

In mice NK-cells differentiate from $CD11b^{dull}CD27^{+}$ NK-cells to $CD11b^{+}CD27^{+}$ NK-cells (double positives) to $CD11b^{+}CD27^{dull}$ NK-cells. The latter two phenotypes show comparable characteristics in cytotoxicity and IFN- γ production *in vitro* with $CD11b^{+}CD27^{dull}$ NK-cells exhibiting senescence (Hayakawa and Smyth 2006).

1.6 d. ii. Humans

In humans NK-cells can be divided into $CD56^{dim}$ and $CD56^{bright}$ which differ in their homing properties. $CD56^{dim}$ $CD16^{+}$ constitutes around 90% of peripheral and spleen NK-cells and expresses perforin. They are cytotoxic and produce IFN-γ upon interaction with tumour cells *in vitro* (Anfossi, André et al. 2006). Most NK-cells in the lymph nodes and tonsils are $CD56^{bright}$ $CD16^{-}$ and lack perforin (Ferlazzo and Münz 2004). These cells produce cytokines such as IFN-y in response to stimulation with IL12, IL15 and IL18 (Cooper, Fehniger et al. 2001).

B-cells

1.7 a. Introduction

B-cells are components of the adaptive immune system and protect from a diverse range of infections. Activation of B-cell is mediated via recognition of antigen by B-cell receptor (BCR) resulting in the proliferation and differentiation of these cells (Harwood and Batista 2010). BCRs take up antigens into the processing pathway. Antigen processing and presentation in B-cells is mediated by membrane Ig and was

first demonstrated using normal B-cells to present rabbit anti-mouse Ig to rabbit Ig-primed T-cells (Chesnut and Grey 1981).

Activated B-cells differentiate into the following:

1.7 b. Antibody secreting plasma cells

Plasma cells are the sole secretors of antibodies (Shapiro-Shelef and Calame 2005). Marginal zone B-cells in response to antigen develop into plasma cells (Lopes-Carvalho and Kearney 2004). Plasma cells can be distinguished from mature B-cells as the plasma cells exhibit a small, dense and eccentric nucleus and voluminous cytoplasm containing significant amounts of rough endoplasmic reticulum and enlarged Golgi apparatus (Minges Wols 2006). Plasma cells are often resident in tissue of choosing and are not found in circulation. Antibody secreting cells in circulation en-route to tissue are plasmoblasts (Minges Wols 2006).

1.7 c. Memory B-cells

Memory B-cells are larger than naive B-cells and they express the co-stimulatory molecules CD80 and CD86, and CD11b (Alugupalli, Leong et al. 2004; Tarlinton 2006). In mice memory B-cells are characterised by their expression of CD38 and B220, their ability to bind small amounts of the lectin peanut agglutinin and the presence of somatically mutated variable (V) gene segments (Tarlinton 2006). While human memory B-cells are largely similar to those of mice, they also express CD27 (Tangye, Liu et al. 1998).

Memory B-cells are quiescent antigen experienced lymphocytes. They can be generated in response to T-cell dependent antigens (proteins) and T-cell independent antigens (carbohydrates) (Tarlinton 2006). Based on their expression profiles, memory B-cells have been divided into:

The conventional $B200^{+}$ memory B-cells which express memory B-cell markers- B220, CD19 and CD79b (McHeyzer-Williams, Cool et al. 2000).

Memory B-cells with down regulated expression of several B-cell lineage markers including B220, CD19 and CD79b) and upregulated expression of CD11b ($B220^{-}$ memory B-cells). These cells are enriched in the bone marrow and differentiate into plasma cells upon re-exposure to antigen (McHeyzer-Williams, Cool et al. 2000).

Another subset of $B220^{-}$ memory B-cells with the capability to differentiate into plasma cells with needing re-exposure to antigen has also been identified. These cells differentially express CD44 and CD138 (syndecan) and can be divided on the basis of expression into short-lived bone-marrow plasma cells and long-lived bone marrow plasma cells respectively (O'Connor, Cascalho et al. 2002).

T-cells

In order for T-cells to respond to pathogen, they require physical contact with antigens of such pathogens. T-cell receptors (TCR) recognises protein and lipid antigens bound to major histocompatibility complex (MHC) or CD1 respectively on cell surfaces (Germain RN, Stefanova I 1999; Porcelli SA, Modlin RL 1999).. Because there are an almost unlimited number of ways that an antigen octapeptide may form, the immune system has adapted T-cells to attack these, by varying TCRs

so that each T-cells is unique and specific to an antigen (Mackay 1999). Naive T-cells are T-cells that have not come in contact with antigen. In an adult, there are approximately between 25 to 100 million naive T-cells (Arstila TP, Casrouge A et al 1999). Naive T-cells encounter antigens carried by dendritic cells in secondary lymphoid organs (Banchereau J and Steinman RM 1998). These T-cells “home” to secondary lymphoid tissues and upon encountering and binding to the antigen presenting cell, are activated, and thus proliferate approximately a thousand times to form identical clones with similarly identical antigen specificity. Activated T-cells eventually acquire effector functions and “home” to inflamed sites where they interact with other cells of the immune system and antigen bearing parenchymal cells (Mackay 1999).

1.8 a. T-cell death

Several death pathways ensure there is balance in T-cell numbers:

Apoptosis: This is a programmed cell death that involves the participation of a cell in its own death. In cells, it is characterised by chromosomal condensation, fragmentation of the nucleus, fusion of cell membrane with the endoplasmic reticulum and cell fragmentation into “apoptotic bodies” which are consumed by surrounding cells (Kerr JF et al 1972). The activation of caspase is a vital biochemical process in apoptosis. Caspase cleaves essential cellular proteins such as Lamin, and activate dormant enzymes such as DNA fragmentation factor 40kDa ((DFF40), also called caspase activated DNase (CAD)) that degrade cellular contents (Shi Y, 2002). Programmed cell death in activated T-cells may be divided based on function into 2 major groups:

1. Activation induced cell death (AICD): thymocytes die after activation through their CD3 molecules (Lu and Finn 2007). *In vitro,* death of thymocytes and activated T-cells after stimulation of their T-cell receptors is mediated by tumour necrosis factor receptor (TNF-R) family members such as Fas, death receptors (DR3, DR4, DR5, DR6) and TNF-R1 (Lenardo M, Chan et al 1999). Stimulation of TCR on thymocytes or activated T-cells promotes expression of FAS/ APO-1 and its ligand. This results in "autocrine or paracrine activation of apoptosis" (Lu and Finn 2007).
2. Activated T-cell autonomous death (ACAD): also called cytokine withdrawal cell death or spontaneous involves the mitochondrial pathway which is regulated by BCL-2 family. T-cell death results after cytokine and growth factor secretion has ceased (Hilderman DA and Zhu 2002). Mice deficient in the BCL2 gene were seen to develop abnormalities such as atrophy of the spleen and thymus and a rapid apoptosis of lymphocytes (Veis DJ, Sorenson CM et al 1993).

Autophagy: this is an alternative to programmed cell death. Autophagy is a vital "catabolic metabolism that recycles building blocks for basal macromolecular synthesis when cells are under nutrient starvation conditions, degrades damaged organelles and eliminates pathogens that invade cells" (Lu and Finn 2007). It involves the isolation of cell organelles or a portion of cytosol in autophagosomes (double membrane vesicles). Autophagosomes coalesce with lysosomes to form autophagolysosomes leading to degradation (Levine B, Deretic V, 2007, Ohsumi Y, 2001).

Tumour mediated T-cell death: Fas (APO-1) has been found to be expressed in various types of cancers and may contribute to evasion of immune cells by tumour

(Lu and Finn 2007). Cancers with FasL expression include head and neck cancers, melanoma, colon and ovarian cancers (Whiteside TL, 2002). The FasL has been seen to be active in some of the above cancers. Expression of FasL was observed in areas of severe lymphocyte infiltration, with apoptotic lymphocytes also observed in such areas (Whiteside TL, 2002).

Fas (Apo-1) are a family member of the Tumour Necrosis Factor (TNF-1). Activation of Fas recruits Fas- Associated protein with Death Domain (FADD) to the cytoplasmic membrane. FADD then recruits pro- caspase 8 forming Death- Inducing Signalling Complex (DISC) as part of the process during apoptosis (Krammer PH, 2000).

The expression of FasL on tumours and their resistance to Fas-mediated apoptosis may provide proof for the hypothesis that tumours use FasL to pre-emptively attack lymphocytes (O'Connell J, Bennett MW, et al 1999).

1.8 b. CD8+ T-cells

CD8+ T-cells recognise pathogen derived peptides bound to major histo-compatibility complex I (MHC) class I molecules on infected cells (Wong and Pamer 2003). Peptides generated by protein degradation mediated by peptides are transported to the endoplasmic reticulum where they bind to newly synthesized MHC class I and are transported to the cell surface (Pamer and Cresswell 1998).

Naive $CD8^+$ T-cells are activated in secondary lymphoid organs such as the spleen in response to an infection. Dendritic cell population are preferred by $CD8^+$ T-cells to activate their differentiation. When antigen presentation occurs, naive $CD8^+$ T-cells may undergo approximately 19 cell divisions in the immediate week after priming and these divisions may represent approximately a 500,000 fold expansion

(Zhang and Bevan 2011). After antigen presentation, the activated T-cells upregulate CXCR3, an inflammatory cytokine receptor that allows their entry to peripheral tissues (Groom and Luster 2011).

When $CD8^+$ T-cells are activated they undergo striking metabolic changes such as an increase in iron, glucose and amino acid uptake. They also switch from oxidative phosphorylation to aerobic glycolysis in preparation for the requirements for building blocks of cells such as proteins, nucleic acid and lipids (Michalek and Rathmel, 2010).

In some cases, such as for non-inflammatory antigens and certain viral infections e.g. herpes simplex virus, $CD4^+$ T-cells aids in the activation of $CD8^+$ T-cells. In other cases as immune response to influenza, $CD8^+$ T-cells are activated independently of $CD4^+$ T-cells (Bevan 2004). In addition to their cytotoxic functions, $CD8^+$ T-cells may serve a regulatory role by "preventing excessive tissue injury" by the secretion of the immunosuppressive cytokine IL-10 once thought to be a T helper 2 (Th2) cytokine (Palmer et al 2010; Saraiva and O'Garra 2010).

After immune clearance, most effector cells disappear from the blood stream, however a heterogeneous population of memory cells remain which are capable of immune response to re-presentation of antigen (Jameson and Masopust 2009). These memory $CD8^+$ T-cells may be divided into 2 major groups based on their function and the expression of receptors that aid homing. These groups are:

1. Effector memory T-cells (T_{EM}) – these cells lack lymph node homing receptors but express receptors that aid migration to peripheral tissues.
2. Central memory T-cells (T_{CM}) – these cells express the lymph node homing molecules CD62L and CCR7.

Memory T-cells are different from naive T-cells by their continued presence at increasing frequencies, their distribution to a larger anatomy and the speed with which they can gain effector functions when they are reactivated (Kaech et al 2002). While $CD8^+$ memory T-cells have a profound role in immune protection from systemic infections, they are limited in their ability to tackle localized infections (Bachmann et al 1997, 2005; Jiang et al 2012; Mackay et al 2012). This is because they lose their ability to migrate to peripheral tissues as a result of their loss of expression of homing molecules for entry into peripheral sites, a reduction of the T_{EM} population and the conversion of T_{EM} towards a $CD62L^+$ T_{CM} phenotype (Gebhardt and Mackay 2012, Tripp et al 1995, Wherry et al 2003, Masopust et al 2010).

1.8 c. CD8+ effector molecules

CD8 + T-cells mediate their effector functions via the excretion of effector molecules listed below (Harty, Tvinnereim et al. 2000).

1. Direct cytolysis mediated by **perforin** release
2. Secretion of cytokines such as **tumour necrosis factor alpha (TNF-α)** and **interferon gamma (IFN-γ)**
3. Secretion of chemokines that attract other inflammatory cells to sites of infection

$CD4^+$ T-cells

$CD4^+$ T helper (T_H) cells are mediators of the immune system where they serve to coordinate the cellular components of the immune system and their response to pathogen (Dong 2008). They modulate immune protection by their ability to assist B-cells in making antibodies, recruit neutrophils, basophils and eosinophils to infected and inflamed sites and stimulate macrophages to develop microbicidal activity (Zhu and Paul 2008). Naive $CD4^+$ T helper cells differentiate into at least 4 subsets (T_H1, T_H2, T_H17 and iTregs (inducible Tregs)) in secondary lymphoid organs when stimulated by cytokines produced during early immune response (Mosmann and Coffman 1989; Zhu and Paul 2008).

The subsets of T helper cells are discussed below:

1.9 a. T_H 1 $CD4^+$ cells

T_H1 $CD4^+$ cells mediate immune response against intracellular pathogens (Mosmann and Coffman 1989) and are responsible for the induction of some autoimmune diseases (Zhu and Paul 2008). They can be characterised by their ability to secrete IFN-γ, lymphotoxin (LTα) and IL-2 (Mosmann and Coffman 1989). IFN-γ production enables these cells regulate antigen presentation and cellular immunity. Also the IFN- γ produced by T_H 1 cells inhibits the development of T_H 2 cells (Fitch, McKisic et al. 1993) and serves as a positive feedback amplifier. IL-2 is essential for CD4 T-cell memory as $CD8^+$ T-cell stimulated by IL-2 leads to the formation of CD8 memory T-cell (Williams MA, Tyznik AJ, 2006). T_H1 $CD4^+$ cells also express T-bet (T-box transcription factor). T-bet plays a crucial role in T_H1 cell development where it induces “both transcriptional competence of the locus

encoding IFN-γ and selective responsiveness to the growth factor IL-12" (Murphy and Reiner 2002).

1.9 b. T_H 2 $CD4^+$ cells

T_H 2 cells mediate immune response against extracellular parasites (Mosmann and Coffman 1989) and are involved in the induction of allergic diseases such as asthma (Zhu and Paul 2008). They produce cytokines such as IL-4, IL-5, IL-9, IL-10, IL-13 and IL-25. (Zhu and Paul 2008). IL-4 serves as a positive feedback amplifier. These cytokines may activate mast cells and eosinophils and a rise in IgE. Thus they have been implicated in allergic inflammation and atopy (Sergio 1994; Dong 2008). They also produce B-cell growth and differentiating factors (Mosmann and Coffman 1989) which may explain their role in humoural immunity and allergy. The production of IL-4 and IL-10 by T_H 2 cells inhibit the development and activation of T_H 1 cells (Sher and Coffman 1992; Moore, O'Garra et al. 1993; Anne 1998) hence T_H 2 cells are often described as anti-inflammatory.

1.9 c. T_H 17 $CD4^+$ cells

T_H17 $CD4^+$ cells mediate immune response against extracellular bacteria and fungi (Weaver CT, Harrington et al 2006) and they take part in the induction of organ-specific autoimmune diseases (Zhu and Paul 2008). They produce IL-17a, IL-17F, IL-21 and IL-22 (Dong 2006). IL-17a and IL-17f is associated with host defence against infections and autoimmune disease by recruiting macrophages and Neutrophils to sites of infection (Dong 2008; Zhu and Paul 2008). IL-21 serves as a positive feedback amplifier. T helper cells that express IL-17 do not express IFN-γ

and IL-4 (Infante-Duarte, Horton et al. 2000; Dong 2008). The differentiation of T_H 17 cells is mediated by transforming growth factor β (TGF β), IL-6, IL-21 and IL-23 (Dong 2008; Zhu and Paul 2008).

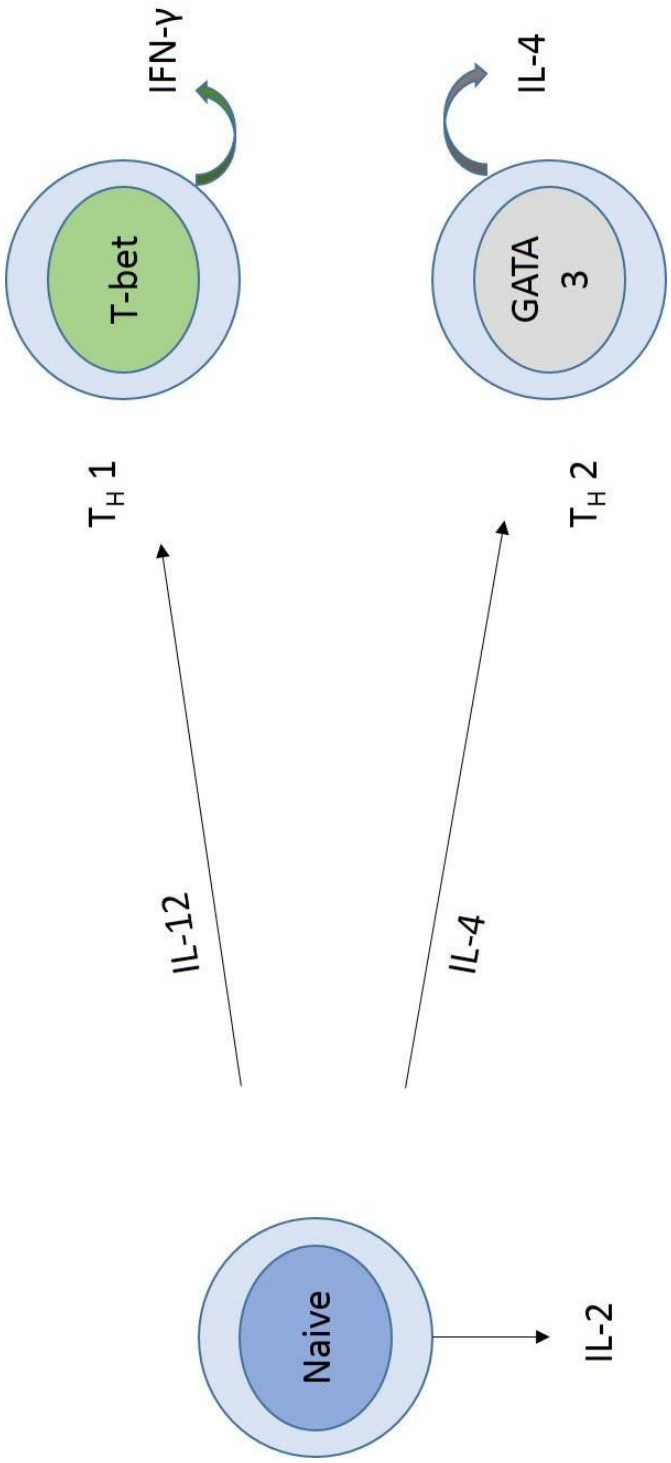

Figure 1.14 Original schematic of CD4$^+$ T-cell differentiation

Original schematic of naive CD4$^+$ T-cell (helper T-cell) differentiation into T helper 1 and T helper 2 cells in response to cytokine.

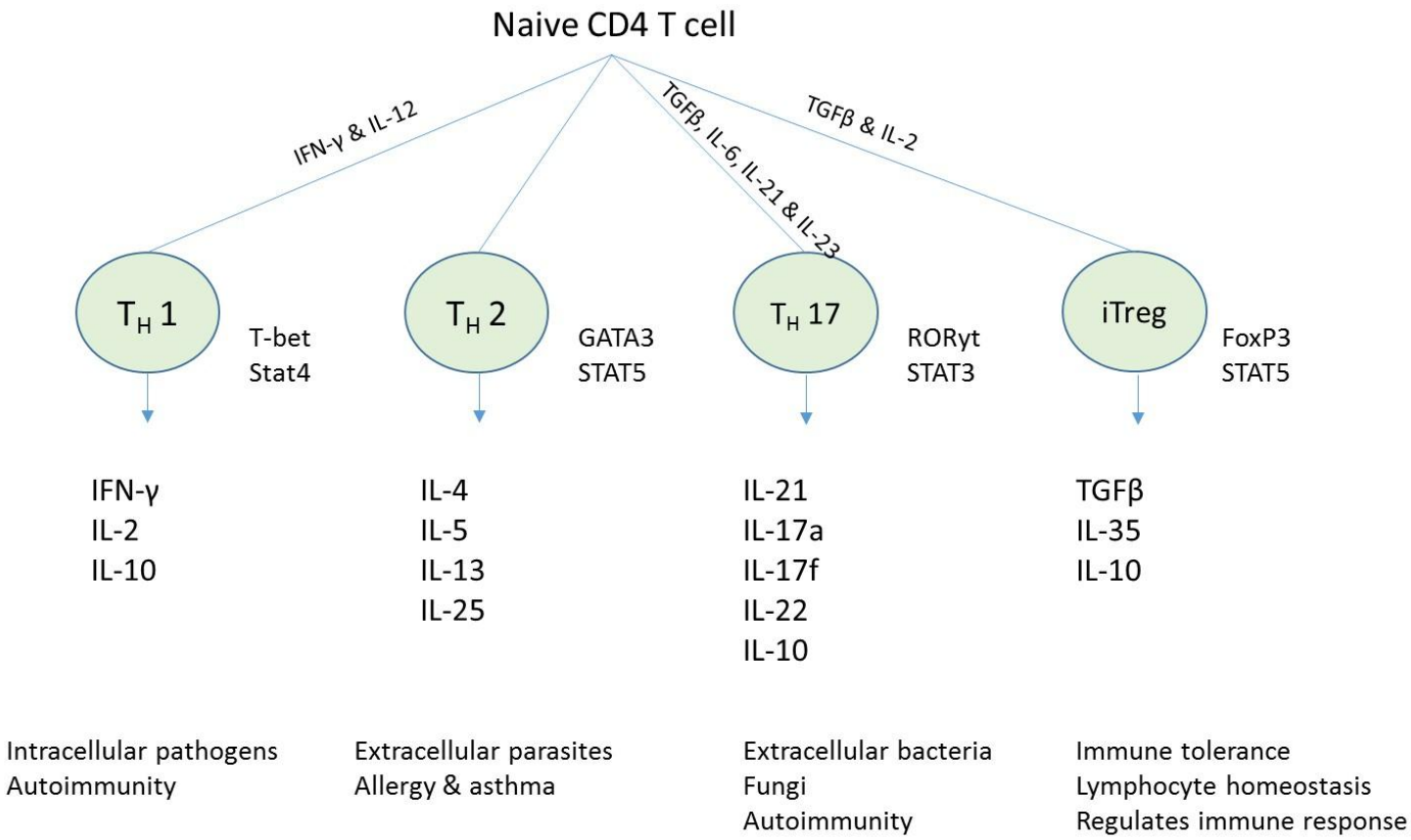

Figure 1.15 CD4$^+$ T-cell differentiation

CD4$^+$ T-cell differentiation into its subsets: T helper 1 (T_H1), T helper 2 (T_H2), T helper 17 (T_H17) and T regulatory cells (iT_{regs}), in response to cytokine stimuli, and their functions.

T regulatory Cells (T_{regs})

T_{regs} mediate immune homeostasis and prevent inflammatory diseases (Sakaguchi, Yamaguchi et al. 2008). They also regulate immunity to infections of viral and bacterial origin and protect from immunity directed towards tumour cells and transplanted tissue (Belkaid 2007). Deficiency in Tregs have been known to be a major causative factor in numerous autoimmune diseases (Campbell and Koch 2011) such as rheumatoid arthritis (Ehrenstein 2004), systemic lupus erythromatosis (Horwitz 2008) and multiple sclerosis (Viglietta 2004).

T_{regs} can be found in both lymphoid and non-lymphoid tissues even in the absence of inflammation (Sather, Treuting et al. 2007). They are also found in abundance within tumours where they seem to prevent tumour clearance (Nishikawa and Sakaguchi 2010).

1.10 a. Characterisation of T_{regs}

The characterisations of Tregs, all of which contribute to immunosuppression are seen below (Sakaguchi 2005):

1. Naturally occurring $CD4^{+}CD25^{high}$ Treg cells
2. Induced Treg cells e.g. Tr1 and TH3 cells
3. Treg cells developing in the periphery by the conversion of $CD4^{+}CD25^{-}$ to $CD4^{+}CD25^{high}$.

1.10 b. Markers of Tregs

CD25 (Interleukin 2 receptor α chain (IL-2Rα)) is a good marker of Tregs in experimental mice as the animals are bred in disease-free conditions. Humans differ in that they are constantly exposed to antigens which results in a significant fraction of recently activated $CD25^+$ effector T-cells (Beyer 2006). The transcription factor fork head box p3 (Foxp3) is a more specific marker and is uniquely expressed in Treg cells in mouse (Hori 2003). $CD4^+$ $CD25^+$ Tregs make up approximately 10% of the $CD4^+$ T-cells (Nishikawa and Sakaguchi 2010). Tregs are produced in the thymus as a functionally mature and distinct sub-population of T-cells but may be induced from naive T-cells ($CD4^+$ $CD25^-$) by antigen stimulation in the presence of high dosage of TGFβ (Nishikawa and Sakaguchi 2010).

1.10 c. Recruitment

For Treg cells to function properly in the modulating of both innate and adaptive immune responses to foreign antigens, the Tregs often have to come into physical proximity with their targets by migrating to their target tissues and microenvironment (Campbell and Koch 2011).

Tregs express a variety of such adhesion molecules and chemo-attractant receptors that modulate their migratory distribution to specific tissues and consequent functions (Suffia*, Reckling* et al. 2005). Genetic studies have highlighted the importance of several homing receptors for the appropriate distribution and function of Tregs to tissues. Many possible scenarios exist for the recruitment of Tregs to sites of inflammation. An example is the expression of the αE integrin chain (CD103) and Chemokine receptor CC-chemokine receptor 4 (CCR4),

and the ability to generate carbohydrate ligands for P-selectin and E-selectin by the action of α-(1, 3)-fucosyltransferase VII enzyme which are all important for the migration and retention of Tregs within the skin. Deletion of any of these molecules on Tregs results in the development of skin-specific autoimmunity and defective pathogen clearance during cutaneous infection (Suffia*, Reckling* et al. 2005; Sather, Treuting et al. 2007; Dudda, Perdue et al. 2008; Freyschmidt, Mathias et al. 2010; Campbell and Koch 2011). Treg recruitment is substantially increased during inflammation. The contribution of individual homing receptors to T-cell migration induced by inflammation vary considerably depending on tissue involved and type of inflammation (Campbell and Koch 2011).

1.10 d. Suppressive function of Tregs (immunoregulation)

T-cell Receptor (TCR) recognition is important in influencing phenotype, function and localisation of T-cells *in vivo*. Antigen specific activation of T-cells isolated from TCR null (TCR-) transgenic mice alters the expression of several homing receptors that determines their redistribution to non lymphatic tissues (Lee, Kang et al. 2007; Sather, Treuting et al. 2007; Campbell and Koch 2011). Because Tregs are broadly autoreactive (Picca, Larkin et al. 2006), a number of varying mechanisms are used by these cells to regulate immune responses. One is the expression of interleukin-10 (IL- 10) which is a cytokine deployed by Tregs that inhibits T helper cell responses during cancer, autoimmunity and infection (Asseman, Mauze et al. 1999). Deletion of IL 10 gene selectively in Treg cells in mice resulted in the development of spontaneous colitis and exaggerated immune responses in organs such as lungs and skin (Rubtsov, Rasmussen et al. 2008).

Another mechanism of immunoregulation by Tregs employs the expression of cytotoxic T lymphocyte antigen 4 (CTLA4). This is as a result of CTLA4 having the capacity to reduce immuno-stimulatory activity of Dendritic cells in the lymphoid tissues by downregulating their expression of co-stimulatory ligands CD80 and CD86 (Wing, Onishi et al. 2008; Campbell and Koch 2011). CTLA4 also ligates CD80 and CD86 to produce indoleamine 2,3- dioxygenase (IDO) (Onodera, Jang et al. 2009) which is an immunosuppressive enzyme.

Tregs also function in the down-regulation of immune responses in lymphoid tissues which allow for migration of T-cell from lymph node to tissue site of infection. This was exemplified by the depletion of Tregs in mice following mucosal herpes simplex virus infection (Lund, Hsing et al. 2008). A pronounced increase in T-cell activity was observed in the draining lymph nodes without a corresponding increase of T-cells, Natural Killers and Dendritic cells at the sites of infection (Lund, Hsing et al. 2008).

In addition to these varied responses employed by Tregs in the modulating of immune cells, Treg cells also produce immunosuppressive cytokines such as Transforming growth factor β (TGF- β), IL- 35 and adenosine or cyclic AMP that are metabolic inhibitors of effector T-cells (Campbell and Koch 2011).

1.11 Immune cell infiltration in PDAC

Recent significant findings of immune cell infiltration in PDAC are described below (Table 1.3). I will discuss these results again in context of my experiments.

Species	Methods	Results	Authors
Human/ Mice	FACS, histology, spheroid adhesion assays, transmigration assays assay, NOD/SCID mouse mode	An increase in $CD3^+$ cell infiltration was observed as measured by histology. T regulatory cells (T_{regs}) infiltrated pancreatic cancer more than adjacent non malignant pancreatic tissue and more than $CD4^+$ T-cells.	(Nummer, Suri-Payer et al. 2007)
Mice	FACS, histology, cellular proliferation assay, quantitative PCR, KPC mouse model	Infiltration of $CD3^+$, $CD4^+$, $C8^+$ cells were observed starting at pre-invasive disease. An increase of the immunosuppressive cells: MDSCs, Tregs, TAMs were also observed.	(Clark, Hingorani et al. 2007)
Mice	Immunohistochemistry, Immunofluorescence, FACS, Tg mouse model of LL2 Lewis lung carcinoma and subcutaneous mouse model of PDAC identifying stromal cells expressing Fibroblast activating protein -α (FAP) labelled with Diptheria toxin receptor (DTR)	Targeting DTR with Diptheria toxin ablated FAP expressing stromal cells. This caused a "rapid hypoxic necrosis" of both cancers and stromal cells which occurred in an interferon-γ and tumour necrosis factor- α dependent manner. However, this was not the case in Rag2- deficient mice.	(Kraman, Bambrough et al. 2010)
Human/ Mice	Human clinical trials, combining gemcitabine therapy with CD40 antibody (CD40 activates antigen presenting cells), KPC mouse models, ultrasound imaging, FACS, cytokine analysis, Immunohistochemistry	Regression of tumour was observed in some patients and similar results were observed in KPC mice. Macrophages were activated by CD40 antibody leading to tumour infiltration, stromal depletion, and tumour clearance mediated by activated macrophages.	(Beatty, Chiorean et al. 2011)

Table 1.3 Recent findings about immune cell infiltration in PDAC

Species	Methods	Results	Reference
Mice	KPC mouse model, FACS, T-cell suppression assay, arginase production, nitric oxide production, immunohistochemistry, immunofluorescence, cytokine analysis, shRNA	MDSCs derived from spleen or pancreas of diseased KPC mice suppressed the proliferation of CD8+ T-cells. Inhibition of inducible nitric oxide synthase and arginase abolished the ability of MDSCs to suppress T-cell proliferation. The development of MDSC is driven by granulocyte macrophage colony stimulating factor (GM-CSF) and abolishing GM-CSF inhibits the recruitment of MDSCs to tumours.	(Bayne, Beatty et al. 2012)
Human/ Mice	KPC mouse model, immunohistochemistry, immunofluorescence, flow cytometry, immunoblot analysis, quantitative RT-PCR, CD8+ depletion	An upregulation of GM-CSF in mouse ductal epithelia cells was observed and was found to be dependent on oncogenic Kras. GM-CSF was responsible for MDSC recruitment. In the absence of GM-CSF however, CD8+ cytotoxicity was responsible for tumour clearance.	(Pylayeva-Gupta, Lee et al. 2012)

Table 1.3 (continued), Recent findings about immune cell infiltration in PDAC

1.12 Summary

Immune cells have been implicated in cancers as having both immunosuppressive and tumour clearing roles. The interactions between infiltrating immune cells and the tumour microenvironment is not fully understood particularly in pancreatic cancers where there is a microenvironment rich with stromal elements that include stellate cells, fibroblasts and structural matrix components such as fibronectin and collagen. These stromal elements express chemo-attractive cytokines, adhesion molecules and receptors that interact with the infiltrating immune cells in a number of permutations. While many groups have focused on the capability of immuno-suppressive cells to inhibit cytotoxic immune cell mediated tumour clearance in PDAC, various groups however, have shown that the depletion of the pancreatic stroma have often culminated in tumour clearance again mediated by cytotoxic cells of the immune system, highlighting the potential immuno-suppressive role of stromal cells. Most of these studies have utilized genetically engineered mouse models with few investigating human tissue. I therefore sought to characterise immune cell infiltration *in situ* with a panel of immune cell markers that included $CD3^+$ (T-cells), $CD4^+$ (helper T-cells), $CD8^+$ (cytotoxic T-cells), $FoxP3^+$ (T regulatory cells) $CD20^+$ (B-cells), $CD56^+$ (Natural Killer cells) and $CD68^+$ (macrophages) using sophisticated and rigorous imaging system in a robust patient tissue microarray cohort consisting of PDAC and other pancreatico-biliary diseases. Because pancreatico-biliary diseases have varying overall patient survival outcomes, I hypothesised that the immune cell infiltration pattern of each disease could be associated to the overall patient survival outcome of that disease.

1.13 Aims and objectives

- To observe and quantify tissue immune cell infiltrate in PDAC and other pancreatico-biliary diseases
- To measure the immune cell densities in the distinct stromal sub-compartments of individual pancreatico-biliary diseases in an unbiased manner
- To identify immune cell markers of prognostic significance
- To observe the effects of altering PDAC-associated pancreatic stellate cells on immune cell infiltrate *in vivo*
- To investigate the mechanisms underlying immune cell infiltration in PDAC *in vitro*

2.0 Materials and Methods

2.1 Tissue microarray (TMA) construction

Tissue microarrays were constructed from the pancreatic tissues collected after establishing diagnosis following surgical resection of pancreas (either head or body or tail) in patients with the pancreatico-biliary diseases: ampullary carcinoma (AC), cholangiocarcinoma (CC), chronic pancreatitis (CP), mucinous cystic neoplasm (MCN) and duodenal carcinoma patients, and from biopsies for advanced stage (metastatic or locally advanced) pancreatic ductal adenocarcinoma (PDAC) patients. All samples were collected at Barts and The London NHS Trust (City and East London LREC 07/0705/87). 157 patients were sampled in total and 2 sets of tissue microarrays were constructed. The first set had been constructed beforehand and used for previous work (Froeling, Mirza et al. 2009; Froeling, Feig et al. 2011). The number of patients with each disease on the 2 sets of TMA's can be seen on table 2. 1.

TMA construction involved the following steps:

1. Review of cases: A representative slide of each patients donor block was cut and stained with hematoxylin and eosin (H&E). Multiple regions of tumour, stroma and normal pancreas were identified and circled with marker pens on H&E stained slides of the donor tissue blocks on the Axiophot microscope (Carl Zeiss MicroImaging LLC, New York, USA). The regions were colour coded; Red represented stromal regions, blue represented 'normal' pancreas and black represented tumour regions (Figure 2.1 A and B).

2. Design of TMA map: A map for each TMA slide was designed on Excel (Microsoft, Seattle, USA) to serve as a guide during TMA construction and as a reference during TMA analysis. The maps consisted of the donor block ID, the exact location of cases and their duplicates and the location of controls (Appendix 1).

3. TMA creation: Three cores each of tumour and stroma were sampled from most donor blocks. Also three cores of adjacent normal tissues were sampled from patients with neuroendocrine tumour, duodenal cancer and cholangiocarcinoma. Furthermore, one core of a normal human spleen was inserted in a recipient block using the TMA map as a guide. The size of individual cores was 1mm and the TMA construction was performed with the Tissue Arrayer Minicore® 3 (Alphelys, Plaisir, France) (Figure 2.2). Upon completion, recipient blocks were kept at 37°C overnight to ensure bonding of the cores with paraffin wax of the recipient block (Parsons and Grabsch 2009) and sent to pathology for sectioning to multiple (100) slides.

Examination with a light microscope of H&E stained tissue microarrays after construction showed the numbers of tumour, stroma and normal cores varied slightly from the original design. I observed in a few cases; a complete loss of cores, folding of the tissue core and very low numbers of tumours in a tumour case, or the presence of tumours in a stromal case. These variations can be attributed to technical reasons (such as during sectioning) and the three-dimensional nature of the donor tissue, as a TMA core is a section of the whole tissue. It has been reported that in gastric cancer TMAs, approximately 10% of cases cannot be analyzed due to these variations (Parsons and Grabsch 2009). However each patient had an

abundance of tumour cores for confident analysis. The average of a patients tumour cores made up the final score for the patient. All stages of TMA construction was supervised by Mr. Hemant Kocher.

Pancreatico-biliary disease	**Number of patients**		
	Batch A	**Batch B**	**Total**
Ampullary carcinoma	0	9	9
Cholangiocarcinoma	9	12	21
Chronic pancreatitis	0	4	4
Mucinous cystic neoplasm	0	6	6
Duodenal carcinoma	0	5	5
Normal	0	14	14
PDAC (resected)	63	0	63
PDAC (biopsy)	0	35	35
Total	72	80	157

Table 2.1 Pancreatico-biliary diseases: patient numbers on respective TMAs

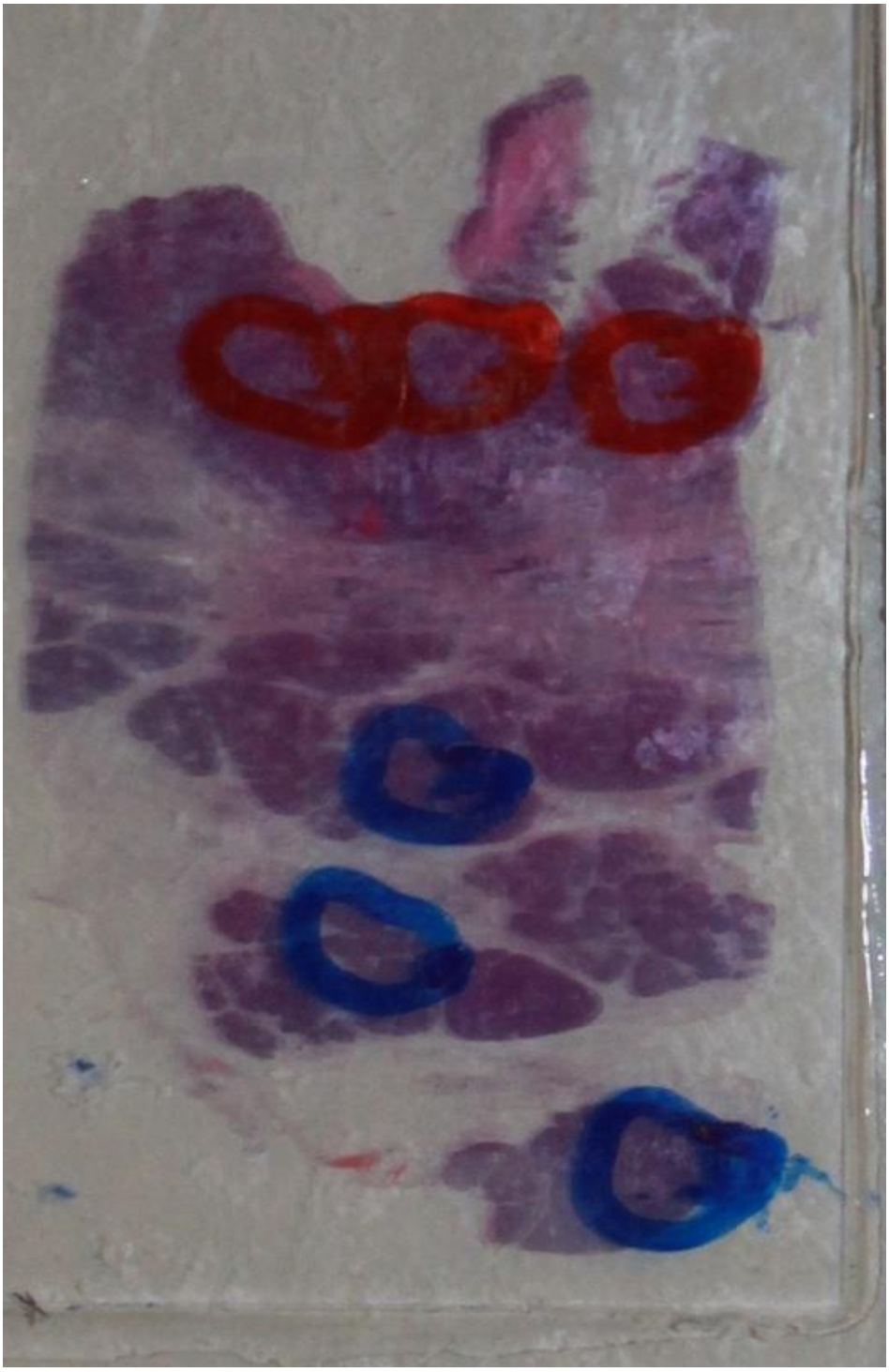

Figure 2.1 Marking slides for TMA construction

Regions of stroma (red) and normal pancreas (blue) were identified with the aid of bright field microscopy of H&E stained sections for resected pancreas for use in TMA construction.

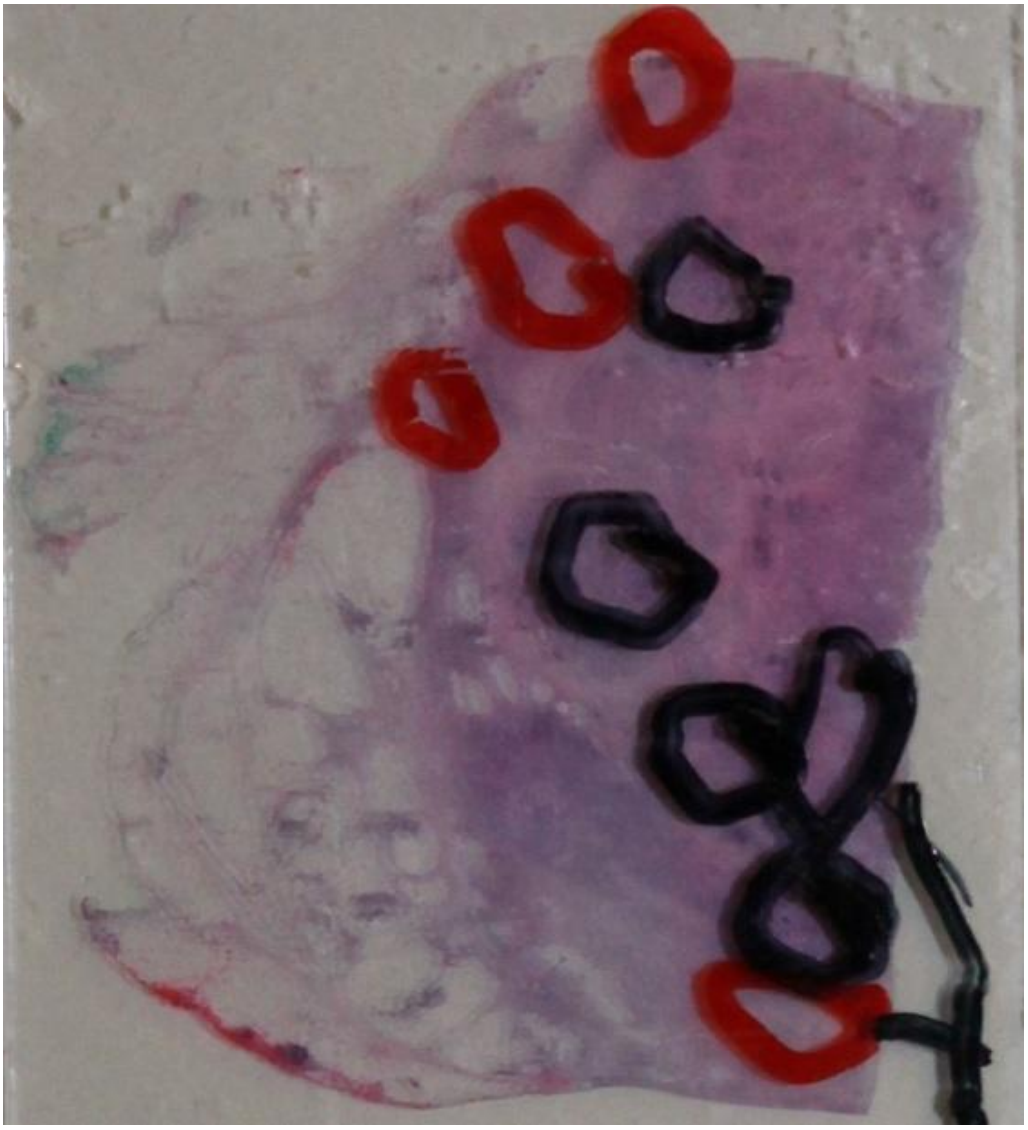

Figure 2.2 Marking slides for TMA construction

Regions of stroma (red) and tumour (black) were identified with the aid of bright field microscopy of H&E stained sections for resected pancreas for use in TMA construction.

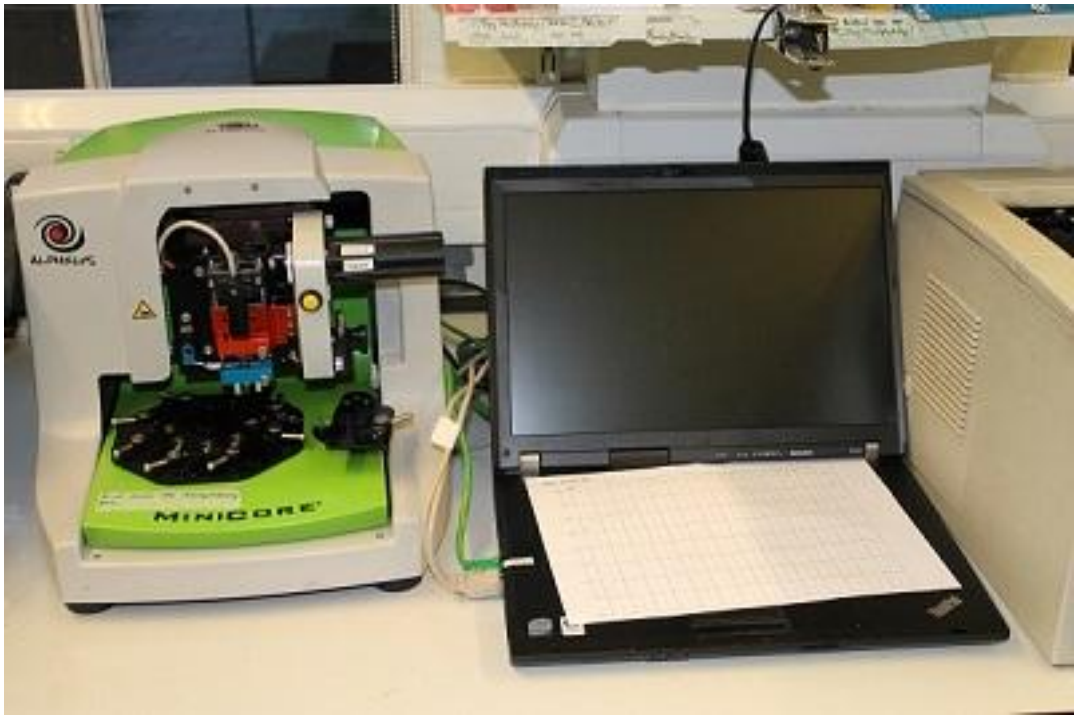

Figure 2.3 Minicore Arrayer

The Minicore arrayer (Alphelys, Plaisir, France) was used in the construction of specific tissue microarrays. The arrayer is connected to a computer which serves as an interface and a controller.

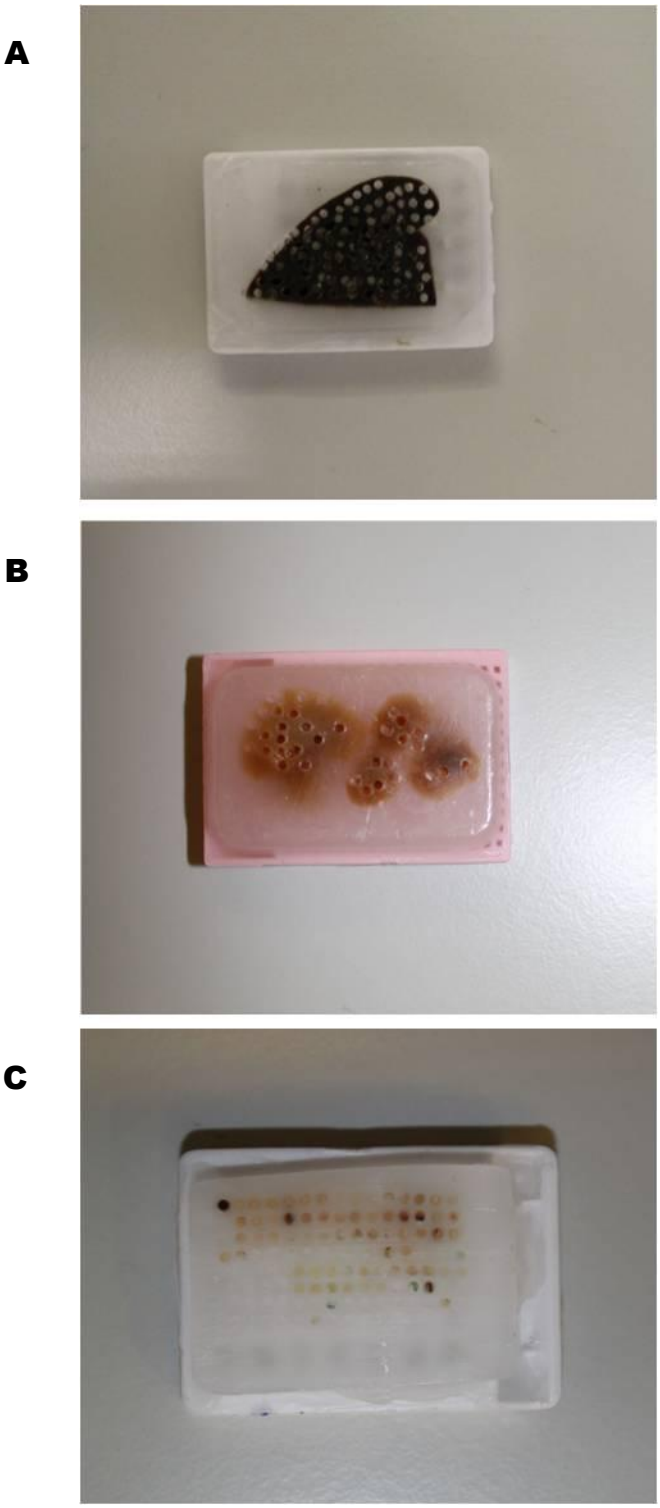

Figure 2.4 Donor and recipient blocks

A donor block of spleen tissue (A) that served as an internal control and a donor block of pancreas tissue (B). Tissue cores from A and B were inserted into recipient blocks which were then cut into 4µm thick sections. Sections were mounted on

positively charged Thermo Shandon slides (Fisher Scientific UK Ltd, Loughborough, UK) and stored in sealed slide boxes at room temperature.

Figure 2.5 TMA recipient block and slide

A representative recipient TMA block and H&E stained TMA slide of the block

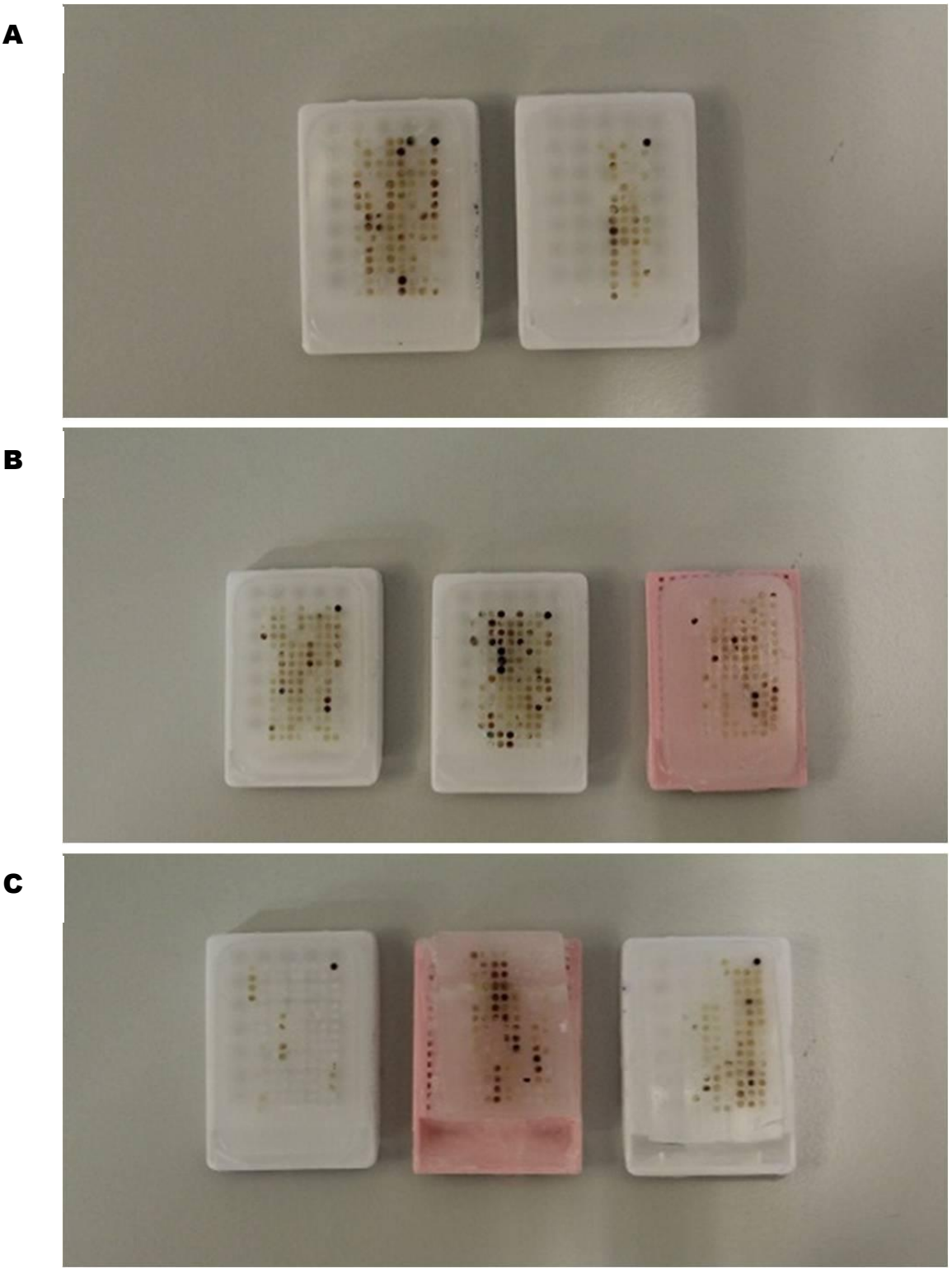

Figure 2.6 TMA blocks

Each set of recipient blocks represent a batch of TMAs.100 4µm sections were cut from each recipient block. (A) Mostly pancreatico-biliary diseases excluding PDAC. (B) Combination of PDAC and pancreatico-biliary diseases. (C) Mostly PDAC.

2.2 Immunohistochemistry

2.2 a. Human tissue microarrays

Immunohistochemistry is used to detect the location of antigenic epitopes (and therefore the respective proteins) in whole tissue sections, a feature which makes it a necessary tool in cancer research (Buchwalow and Böcker 2010). Since antibodies target specific antigens, specific proteins on tissue sections can be probed and visualized by chromogenic detection with the aid of a microscope. Chromogenic detection occurs where an enzyme that is conjugated to an antibody cleaves a substrate to produce a coloured precipitate (Buchwalow and Böcker 2010).

Substrates such as 3,3-diaminobenzidine (DAB; produces brown precipitate) and 3-amino-9-ethyl carbazole (AEC; produces red precipitate) produce their colours when they react with peroxidase enzyme in tissue, while the alkaline phosphate (AP; produces red, black, blue, etc., precipitates) produce their colours either by reduction of tetrazolium salts or by production of coloured diazo compounds (Buchwalow and Böcker 2010). AEC is soluble in alcohol and clearing agents but not DAB and AP; however, DAB and AP can be “dehydrated, cleared and mounted permanently”. These substrates can be used either in a single staining procedure or in multiple staining procedures of the same tissue section (Buchwalow and Böcker 2010).

Immunohistochemistry involves a series of steps:

1. Fixing and embedding of the tissue: The tissue was fixed in 10% neutral buffered formalin (Cellstor, CellPath Ltd. Newtown, UK) for 24 hours. Afterwards, they were embedded in paraffin and cut in a microtome to 5 microns, and affixed on to positively charged Thermo Shandon slides (Fisher Scientific UK Ltd, Loughborough, UK). The slides were left to dry

by leaving them at 60°C overnight and thereafter stored in a sealed slide box until further use.

2. Rehydration of tissue sections: Before staining, the slide was de-paraffinised and rehydrated as presence of formalin and paraffin and incomplete rehydration may lead to poor staining (Buchwalow and Böcker 2010). A number of incubation steps in xylene (Fisher Scientific UK Ltd, Loughborough, UK) and industrial methylated spirits (IMS) or ethanol (VWR International Ltd, Lutterworth, UK) were employed in the de-paraffinisation and rehydration of slides: slides were incubated in xylene in two steps for 5 minutes each, a single step of incubation of slides in 100% IMS for 5 minutes before a peroxidase blocking step of 10 minutes (discussed below). Afterwards, slides were incubated for 2 minutes each in 100% IMS, 80% IMS, 70% IMS and 50% IMS and a single incubation step of 1 minute in distilled water.

3. Peroxidase blocking: some tissue may contain endogenous peroxidase and using Horse Radish Peroxidase (HRP) conjugated antibodies may result in high non-specific background staining of tissue as a result of the reaction between the HRP conjugated antibodies and the endogenous peroxidase. To avoid this non-specific background staining I blocked endogenous peroxidase activity by incubating slides in 3% hydrogen peroxidase (H_2O_2) (Fisher Scientific UK Ltd, Loughborough, UK) in methanol (Fisher Scientific UK Ltd, Loughborough, UK) for 10 minutes.

4. Antigen retrieval: During fixation, methylene bridges are formed leading to cross-linking of proteins and masking of antigen sites (Metz, Kersten et al.

2004). Antigen retrieval is used to unmask antigens allowing for them to be detected by antibodies. I used heat induced epitope retrieval (HIER) with citrate buffer, pH 6.0 (Antigen unmasking solution, H3300, (Vector Laboratories, Burlingame, US)) method and enzymatic antigen retrieval with pepsin enzyme (Dako UK Ltd., Cambridgeshire, UK) (Shi, Shi et al. 2011).

Citrate buffer was added to a pressure cooker and let to boil on a hot plate with lid still open. Once boiling, slides were transferred into the pressure cooker and lid was closed and locked and left for 10 minutes.

Protease from *Streptomyces griseus*, type XIV (Sigma-Aldrich, Dorset, UK) at 0.5mg/ml of sterile PBS. Tissues on slides were outlined with a Dako pen (Dako UK Ltd., Cambridgeshire, UK) to retain liquid on tissue sections, and the slides were placed in a hybridiser (Dako UK Ltd., Cambridgeshire, UK) and pepsin solution added onto tissue sections. The temperature of the hybridizer was set to 37°C and slides were incubated for 10 minutes.

5. Staining: I stained tissues with the immune cell markers for the primary antibodies: $CD3^+$ (total T-cell population), $CD4^+$ (helper T-cells), $CD8^+$ (cytotoxic T-cells), $FoxP3^+$ (regulatory T-cells), $CD68^+$ (macrophages), $CD20^+$ (B lymphocytes), $CD56^+$ (natural killer cells) and $CD15^+$ and $myeloperoxidase^+$ (Neutrophils) (primary antibodies, antibody clones, manufacturers and dilutions I used are found on Table 2.2). I used spleen, tonsil and appendix as positive controls. All antibody incubations were carried out in a humidified chamber to avoid drying out of the tissue.

The Super Sensitive™ Polymer- HRP Detection System (Biogenex, Fremont, California) was used for the antibody labelling and detection. This system “uses a non-biotin polymeric technology wherein the secondary antibody conjugated to Poly-HRP reagent is bound to the primary antibody and is then visualized by the chromogen” (Biogenex 2013) The kit comes with a Super Enhancer™ reagent, a SS label, and 3,3’-diaminobenzidine (DAB) substrate (Biogenex, Fremont, California). I incubated the tissue sections with specific primary antibodies, after which the sections were incubated with the Super Enhancer™ reagent. The sections were then incubated with the SS label. The SS label is a “Poly-HRP reagent which is conjugated to anti-mouse and anti-rabbit secondary antibody” and subsequent incubation with DAB substrate makes the entire complex visible. The limitation of using this system is that it can primarily be used in human tissue and only to target antibodies raised in mouse and rabbit. However, because of the Super Enhancer™ component minuscule antibody signals from dilutions such as 1:1250 can be detected. This capability grossly reduces background non-specific staining. Antibodies were diluted in antibody diluents (Zytomed Systems, Berlin, Germany) or bovine serum albumin (BSA). The slides were incubated in the primary antibody for 40 minutes followed by incubation in the Super Enhancer™ solution for 20 minutes, then incubation is the secondary antibody (SS Label) and then 10 minutes in the DAB solution. Each incubation step was separated by washing slides three times in Tri Buffered Saline Tween-20 (TBST, Dako Wash Buffer, Dako UK Ltd., Cambridgeshire, UK). Slides were counterstained for two minutes with Mayer’s hematoxylin (Dako UK

Ltd., Cambridgeshire, UK) before dehydrating and mounting with DPX (a mixture of distryene, a plasticizer and xylene) mountant (Sigma-Aldrich, Dorset, UK).

Primary antibody	Species raised in	Supplier	Concentration of antibody (mcg/ml)	Dilution - IHC	Dilution mcg/ml
CD3 (clone SP7)	Rabbit	Labvision (CD-3-SP7)	1	1:500	0.002
CD4 (clone 4B12)	Mouse	Novacostra (NCL-CD4-368)	1	1:500	0.002
CD8 (clone C8/144B)	Mouse	Dako (M7103)	1	1:400	0.0025
CD20 (clone L26)	Mouse	Dako (M0755)	1	1:2000	0.0005
CD56 (clone ERIC-1)	Mouse	Serotec (MCA591)	1000	1:1200	0.833
CD68 (clone KP1)	Mouse	Dako (M0814)	1	1:8000	0.000125
FoxP3 (clone 263A/E7)	Mouse	Abcam (Ab20034)	1000	1:100	10
Myeloperoxidase	Rabbit	Dako (A0398)	1	1:8000	0.000125
FN	Rabbit	Abcam (ab299)	1	1:100	0.01
F4/80	Rat	eBioscience (14-4801)	500	1:200	2.5
CK7 (clone OV-TL 12/30)	Mouse	Dako (M701801-2)	1	1:200	0.005
CD8 (clone C8/144B)	Mouse	Dako (M710301-2)	1	1:50	0.02
CD8	Rat	Pierce antibodies (MA1-70041)	1	1:500	0.002
αSMA (clone 1A4)	Mouse	Dako (M085101-2)	1	1:100	0.01
CD11b (clone M1/70)	Rat	eBioscience (14-0112)	500	1:100	5

FN (clone FN-3E2)	Mouse	Sigma-Aldrich (F6140)	1	1:500	0.002
CD3	Rabbit	Abcam (ab5690)	200	1:20	10
CD8	Rabbit	Abcam (ab4055)	200	1:100	2
Alexa Fluor® 488	Goat	Invitrogen (A-11001)	2000	1:2000	1
Alexa Fluor® 555	Rabbit	Invitrogen (A-21431)	2000	1:100	20

Table 2.2 Details of antibodies used in immunohistochemistry (IHC) and immunofluorescence (IF)

2.2 b. Human whole tissue sections

Human whole tissue sections (4 patients) were stained using Bond-max™ Automated Immunostainer with Bond Polymer Refine Detection (all Leica Microsystems). The immune cell markers stained for were: T-cells (CD3), helper T-cells (CD4), cytotoxic T-cells (CD8), Neutrophils (CD15), B lymphocytes (CD20) and mast cells (MCT). Antibodies details for immunohistochemistry on human whole tissue sections and experimental conditions are seen below (Table 2.3). (Staining was performed by Dr. Moonim).

Antibody (clone)	**Supplier**	**Pre-treatment**	**Supplier Dilution**
CD3 (SP7)	Neomarkers	ER1 30 minutes	1:150
CD4 (4 B12)	Novocastra	ER2 30 minutes	1:80
CD8 (C8/144B)	Dako	ER1 30 minutes	1:80
CD15 (MMA)	Becton Dickinson	ER1 30 minutes	1:50

CD20cy (L26)	Dako	ER1 30 minutes	1:1000
MCT (AA1)	Dako	ENZ1 10 minutes	1:800

Table 2.3 Human whole tissue section IHC experimental conditions
ER1: Epitope Retrieval Solution 1 pH 6.0.

ER2: Epitope Retrieval Solution 2 pH 8.8.

ENZ1: Enzyme 1 Epitope Retrieval Solution.

2.2 c. Mouse Immunohistochemistry

Mouse whole tissue sections were probed for the immune cell markers F4/80 (macrophages), CD3 (T-cells) and $CD8^+$ (cytotoxic T-cells). Whilst the rest of the steps remained the same, to prevent non-specific binding of primary antibody, I performed a blocking step using normal serum from the same species that the biotinylated secondary antibody was raised in. I used the Vectastain® Elite ABC kit (Vector Laboratories, Burlingame, US). The ABC (Avidin Biotin Complex) system is used to amplify and detect the binding of primary antibody to its target antigen. This system utilizes the high affinity of avidin, a 68,000 molecular weight glycoprotein found in chicken egg white, for biotin (Hsu, Raine et al. 1981). The affinity of avidin to biotin is over one million times higher than the binding of an antibody to its antigen and is irreversible (Vectorlabs 2011). Avidin has 4 binding sites for biotin (Hsu, Raine et al. 1981) and because antibodies can be conjugated with biotin molecules, macromolecular complexes consisting of avidin, biotin and antibodies can be formed. This is exploited in the ABC system where a primary antibody is incubated with the

tissue section, afterwards, a biotinylated secondary antibody that is specific to the species in which primary antibody was raised is incubated with the tissue section. The ABC kit contains avidin DH and biotinylated horse-radish peroxidase which in a separate reaction is mixed together in a ratio that leaves some avidin unbound, forming a complex that the biotinylated secondary antibody binds to, resulting in more enzymes attached to the target protein than would be possible with an enzyme conjugated primary or secondary antibody. The peroxidase substrate 3,3'-diaminobenzidine produces a brown reaction on the site of the target proteins when incubated with the tissue sections.

2.3 Imaging and Image analysis with Ariol®

2.3 a. Introduction

Ariol ® (Leica Microsystems, Milton Keynes, UK) is a high throughput automated scanning microscope and image analysis system with applications in the clinical, genomic, research and pharmaceutical industries (Gokhale, Rosen et al. 2007; Minot, Kipp et al. 2009). The Ariol system is able to capture, store and analyse terabytes of imaging data and is approved by the FDA for *in vitro* diagnostic use of HER-2/ *neu*, nuclear Immunohistochemistry, specifically Oestrogen Receptor and Progesterone Receptor, pathVysion®- for counting probe signals in interphase nuclei in tissue sections, and detection of micro-metastasis in bone marrow (Microsystems 2011).

The Ariol system consists of a computer connected to a server to handle the large amounts of imaging data generated and is equipped with a barcode scanner, a microscope (the *Proscan 11*) with an automated mechanical stage embedded, and a

lighting system (*Olympus BX- UCB*) (Figures 2.7-2.10). The Ariol system can be programmed to capture whole tissue sections and tissue microarrays.

The use of the Ariol system is documented in primary colorectal adenocarcinoma (Ong, Kim et al. 2010), breast cancer (Turashvili, Leung et al. 2009; Bolton, Garcia-Closas et al. 2010; Zabaglo, Salter et al. 2010) and follicular lymphoma (Clear, Lee et al. 2010) research where it has been used to measure infiltrating T-cell subsets, oestrogen receptors α and β, progesterone receptors, aromatase, HER2 and sprouting blood vessels in immunohistochemical slides. Research assays that can be performed on the Ariol ® can be seen on Table 2.4.

Aesight; **Aesight_2**	cytoplasmic Immunohistochemistry
Angiosight	micro vessel density
Cellsight	detection of circulating tumour cells
Gensight	generic image capture such as Haematoxylin and Eosin (H&E)
ImmunoFluorescent	imaging of cells with a counterstain and fluorescent SpectraChromes
Kisight	nuclear IHC (Ki67, p53, p63)
Lymphsight	detection of tumour cells in lymph node tissue
Membrane	Her2/neu analysis in research only
Multistain	Gensight assay for slides with multiple stains (up to 4)
Ploidysight	measuring of DNA content of tumour cells using Blue Feulgen stain
TissueFISH	counting probe signals in interphase nuclei in tissue sections
SPOT	counting probe signals in interphase nuclei from cell suspensions
SPOT TissueFISH	detection of FISH spots in tissues
TMAsight	Tissue Microarrays and TMAsight sub assays

	(**TMAcytoplasm**, **TMAmembrane**, **and TMAnuclear**.

Table 2.4 Ariol embedded research assays (Ariol® "Help me" Manual)

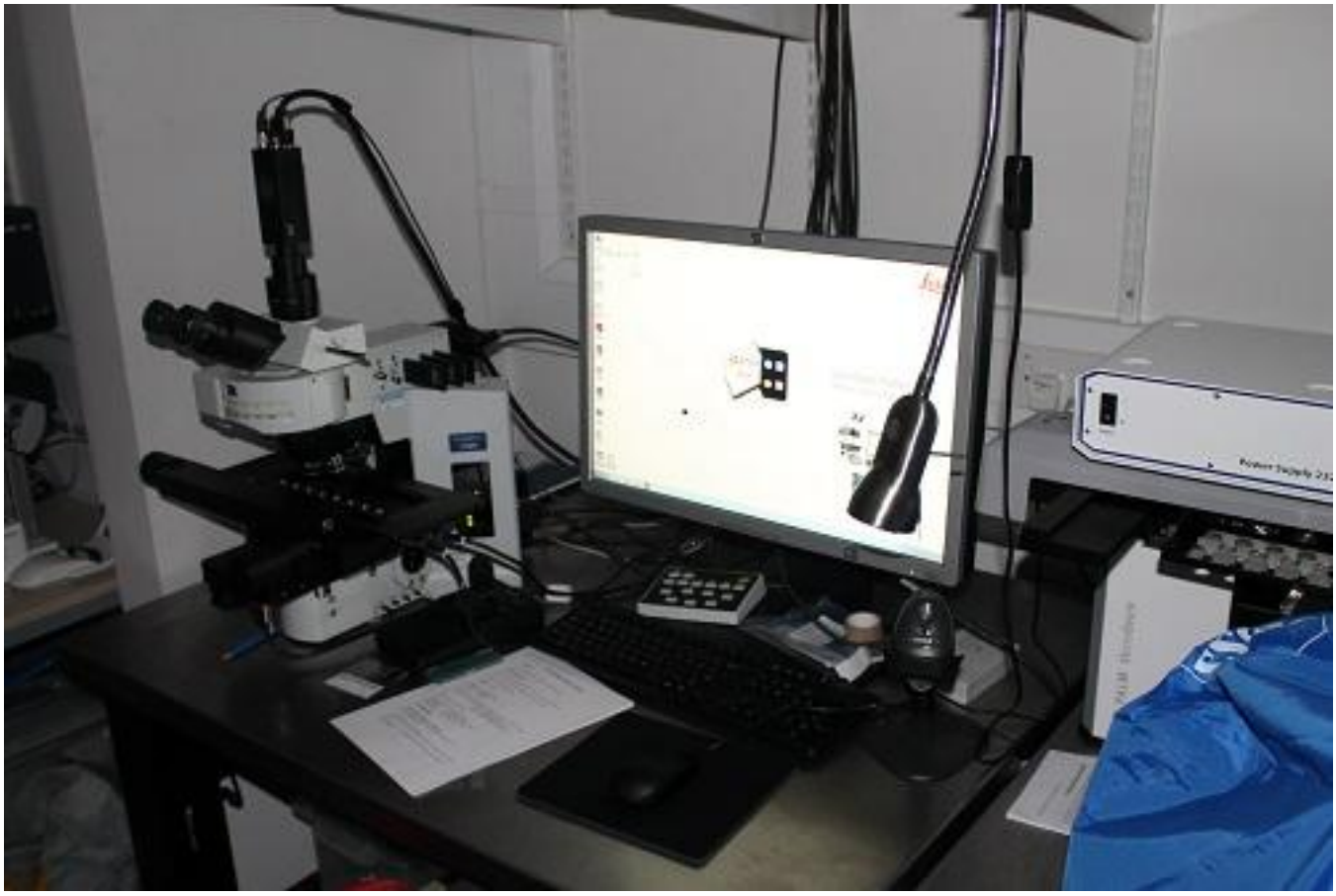

Figure 2.7 Ariol scanner

The Ariol scanner and analytical software (Leica Microsystems, Milton Keynes, UK) were used to scan immunohistochemically stained slides and to quantitatively score (count) positively and negatively stained cells.

Figure 2.8 Ariol barcode scanner

Each slide to be scanned is affixed with a unique barcode that registers information (such as slide template, assays etc.) pertaining to that slide. The Ariol barcode scanner is used to read these barcodes thus ensuring thoroughness and facilitating the high throughput capabilities of the Ariol scanner.

Figure 2.9 Ariol Slide Stage

The slide stage of the Ariol scanner is capable of holding and scanning 8 slides during a single session. The slide stage combined with the barcode scanner (Figure 2.7) enable for different arrays (Table 2.4) to be programmed for each slide.

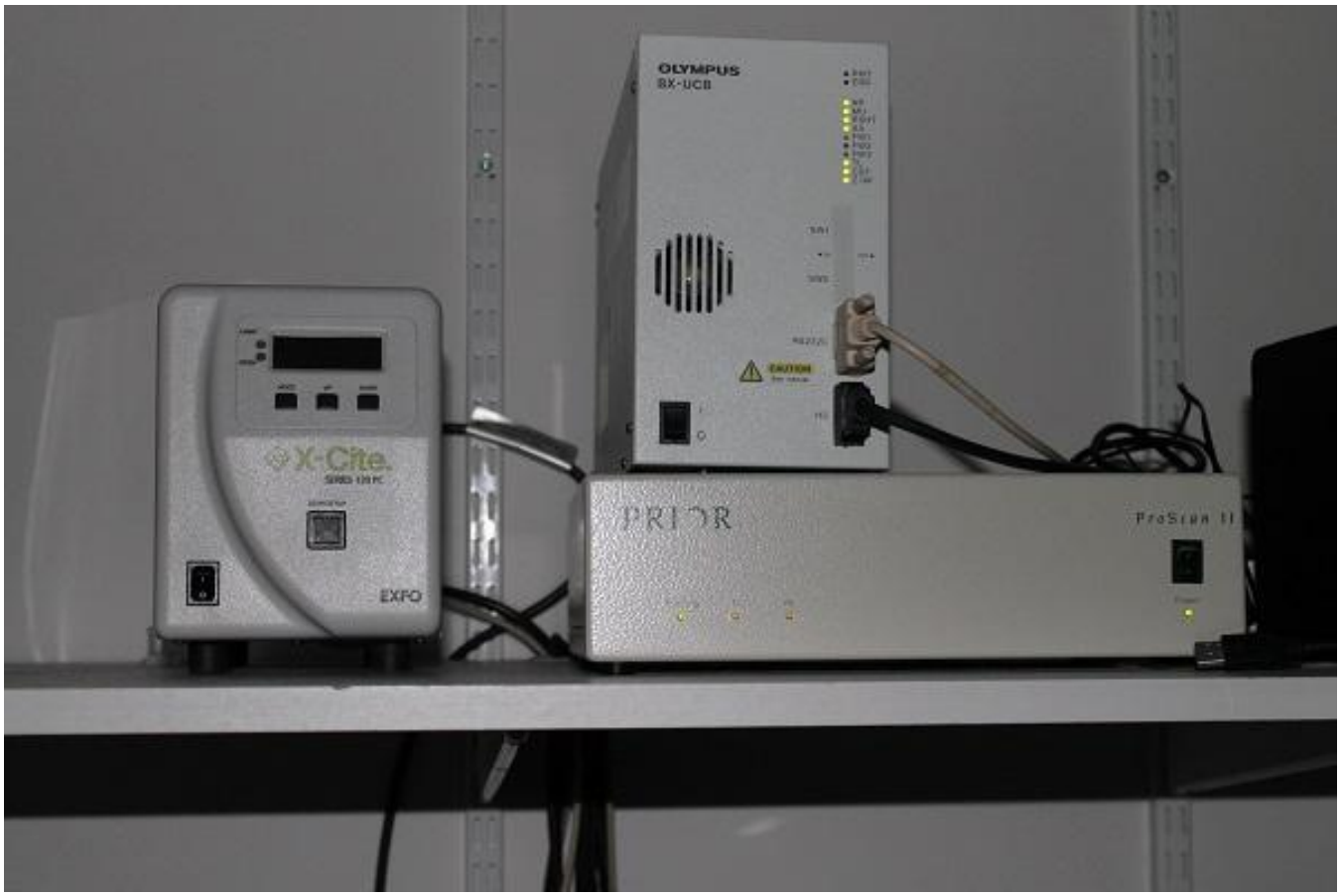

Figure 2.10 Light source for the Ariol

The Ariol scanner is able to perform immunohistochemistry, immunofluorescence and fluorescent *in situ* hybridization among others with the help of the light source.

2.3 b. Methods of immuno-scoring

Traditionally, biomarker quantification has relied exclusively on visual scoring performed by a pathologist or trained reviewer. This method is semi-quantitative and may be limited by inter-observer agreement (Kirkegaard, Edwards et al. 2006). In addition, the visual analysis of tissue samples is time consuming and prone to human errors. These create a need for a method of absolute quantification that is consistent, replicable, time saving, and have high throughput capabilities.

2.3 c. Automated methods of immunoscoring

Automated imaging analysis systems may offer solutions to the limitations listed above. The microscope component of the Ariol® is equipped with an automated mechanical stage capable of holding 8 slides and can be programmed to scan all 8 slides sequentially (the Ariol SL-50, another model formerly from Applied Imaging, Genetix Ltd (now Leica Microsystems), can scan 50 slides at a time). The barcode scanner hardware installed on the system ensures that every slide is unique allowing for the programming of different assays per slide. These make it possible to carryout high throughput analysis. The embedded software is equipped with applications that make it easy to parse scanned images into regions allowing for calculations within regions. This is useful for tumour microenvironment analysis. It is also equipped with user controlled thresholds for scoring based on size, colour, intensity, pattern and shape with which a trained user can teach the Ariol to discriminate a false positive from a truly positive stain. The high magnification of pixels also make it possible to differentiate shades of colours and cells juxtaposed to each other so that cells may be counted individually giving sufficient stringency to produce highly accurate, reproducible results. The output is quantitative with values

for useful parameters such as: counts (positive and negative), analysed area (μm^2), area of positive and negative straining (μm^2), mean intensity of colours, etc. Various imaging systems can be seen on Table 2.5.

Name	Manufacturer	References
Scanscope digital scanner, imagescope viewer, spectrum operating system	Aperio Technologies, Inc.	(Prasad and Prabhu 2011); (Fasanella, Leonardi et al. 2011); (Słodkowska, Markiewicz et al. 2011)
ACIS III®	Dako Ltd.	(Minot, Kipp et al. 2009); (Hanley, Siddiqui et al. 2009); (Bekkers, Bulten et al. 2003)
BLISS™ Virtual slide scanning system	Olympus Ltd.	(Rojo MG *et al* 2009)
Mirax HistoQuant	3DHistech Ltd.	(Varga, Ficsor et al. 2009); (Hadi, Mouchaers et al. 2011); (Nielsen, Lindebjerg et al. 2010)
Pathiam™	Bioimagene (Ventana Medical Systems, Inc.)	(Rojo MG *et al* 2009)

Table 2.5 Other types of Image analysis systems (Rojo, Bueno et al. 2010)

2.3 d. Advantages and validity of automated method

Automated imaging analysis systems need validation if they are to be preferred for routine immunocytochemistry analysis. The advantages above may proffer this, but would depend to a larger extent on the similarities between this method and a pathologists scoring. A number of assessments have been carried out to this effect. Ong and colleagues in seeking to measure the concordance, prognostic significance and time saving properties between visual scoring by pathologists and computer assisted pathological scoring stained for multiple markers (cytokeratin (CK) 7, CK20, cyclooxygenase-2, Ki67, p27 and p53) that exhibit either cytoplasmic or nuclear staining in 486 patients with primary colorectal carcinoma and scanned them with the Ariol SL-50. They observed that both human and computer assisted pathological scores correlated strongly, with all Kappa values greater than 0.8 (Cohen's Kappa is statistical measure of inter-rater agreement with a theoretical maximum of 1 and greater than 0.8 as very good), and that both methods showed the same biomarkers had significant association with survival. However the computer assisted method was found to be more time efficient for scoring larger number of slides. The limitation with this study however was the use of a single machine which led the authors to report that they could not comment on inter-machine variability (Ong, Kim et al. 2010).

In another study looking at three automated imaging analysis systems, the Ariol®, TMAx (*Beecher Instruments*) and TMALab II (*Aperio*), and their concordance among themselves as well as with visual pathological scoring in 440 breast cancer patients, the authors stained for oestrogen receptors α and β, progesterone receptors, aromatase, and human epidermal growth factor receptor 2 all chosen to reflect various staining patterns- nuclear, membranous and cytoplasmic. The

agreement between visual scoring and automated scoring of positive/ negative was excellent for ER- α and PR. Lower levels of agreement for ER- β, aromatase and HER2 were observed but more importantly, the scoring from all machines was similar. The authors concluded that automated image analysis systems can produce results in concordance with pathologists' scores, especially for markers with nuclear staining patterns and can provide standardised quantitative measurements of immunohistochemical staining (Bolton, Garcia-Closas et al. 2010). It is of note however that the authors measured the automated system's ability to call positive or negative staining and by doing so handed over discretionary powers to the automated systems.

2.3 e. Limitations of Ariol®

The Ariol software with all its capabilities is limited by its lack of user friendliness, archaic design and inflexibility. A likely comparison would be using a *Windows 98* operating system when you could use a *Windows 8* or a *Mac OS X Mountain Lion*. Such limitations consume time and effort. While it is possible to select a region and quantify the cells there, it is impossible to quantify the excluded region simultaneously and subsequently resulting in the user performing arithmetic calculations to get the cell counts of the excluded regions by performing separate time consuming analysis and deducting the selected region from the whole region.

The system is also expensive. It cost approximately $300,000 in 2005. Most users would have to spend hours on the system to gain expertise and to perform the many analyses that must be executed to overcome its inflexibilities, and because

researchers pay a service charge to use the system in most institutes, it is an expensive research tool.

For accurate results to be achieved, thresholds on what to quantify must be set. This is also consumes time, however, failure to set accurate thresholds on the software would result in inaccurate results.

2.3 f. Reasons for choosing Ariol®

In terms of the above assessments I would confer that the Ariol system is a robust imaging analyses system with limitations that can be overcome. It has been shown to very closely agree with pathological scoring (Bolton, Garcia-Closas et al. 2010). The training function overcomes many of the limitations this system may have towards more complex cytoplasmic and membranous staining patterns. After such training the quantitative output is accurate and precise. It is a very useful tool when the machines accuracy and high throughput capabilities work in concert with the discretionary powers of the trained reviewer.

2.3 g. Application

I used the Ariol® to perform quantitative analysis of immune cell markers for whole tissue sections and TMAs. I trained the software to distinguish and quantify positive and negative cells by their colour, shape, size and staining intensity (Figures 2.12 A-E). For immune infiltrate analysis, the tissue sections were classified into the juxta-tumoural compartment and the panstromal compartment. The juxta-tumoural compartment was defined as the region of stroma immediately juxtaposed to the

tumour (approximately 100μm) and the panstromal compartment was defined as the entire stromal region excluding the juxta-tumoural compartment. Immune cell infiltration close to the tumour was defined as having a significantly higher density of immune cells in the juxtatumoural compartment than the panstromal compartment, or having non-significant (equal) densities between the two compartments. To quantify immune cell densities within the juxta-tumoural compartment, I selected the region by drawing around it with the aid of a marker tool on the Ariol. Afterwards, the amount of positive cells in that region was quantified and divided by the amount of negative cells in the same region or by the analysed area. The resulting ratio is the density of the juxta-tumoural compartment. The same calculation was performed for whole TMA cores. The density of the juxta-tumoural compartment was then subtracted from the density of the whole core to give the panstromal density. The median of analysed tumour cores for each patient was calculated and the distribution of juxta-tumoural density relative to panstromal density for the patients was compared using Mann Whitney U test (Prism software (Graphpad)). The calculation is illustrated below (Figure 2.11).

An alternative method of quantification that required positive cells to be divided by the analysed area in μm^2 rather than number of negative cells was performed for one marker (CD68, a macrophage marker) as a control for choice of method of quantification.

2.3 h. Other imaging systems used

Axiophot microscope (Carl Zeiss MicroImaging LLC, New York, US) was used in routine immunohistochemistry image capture, for the semi quantitative image analysis of whole tissue sections and for marking H&E slides during TMA construction.

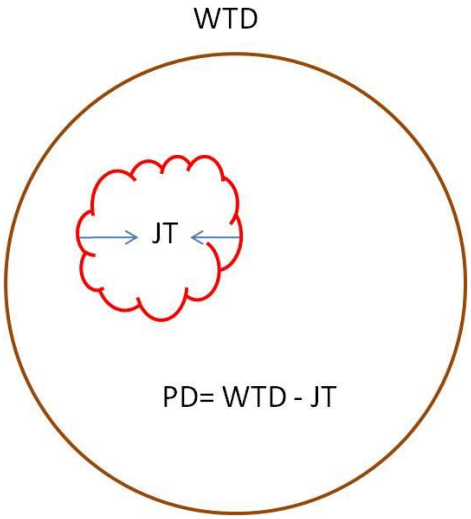

Whole TMA (core) density (WTD) = Number of positive cells in whole TMA (core)

Number of negative cells in whole TMA (core)

Juxta-tumoural density (JD) = Number of positive cells in juxta-tumoural compartment

Number of negative cells in juxta-tumoural compartment

Panstromal density (PD) = Whole TMA (core) density – Juxta-tumoural density

Figure 2.11 Illustration of Tissue microarray densities calculation

A

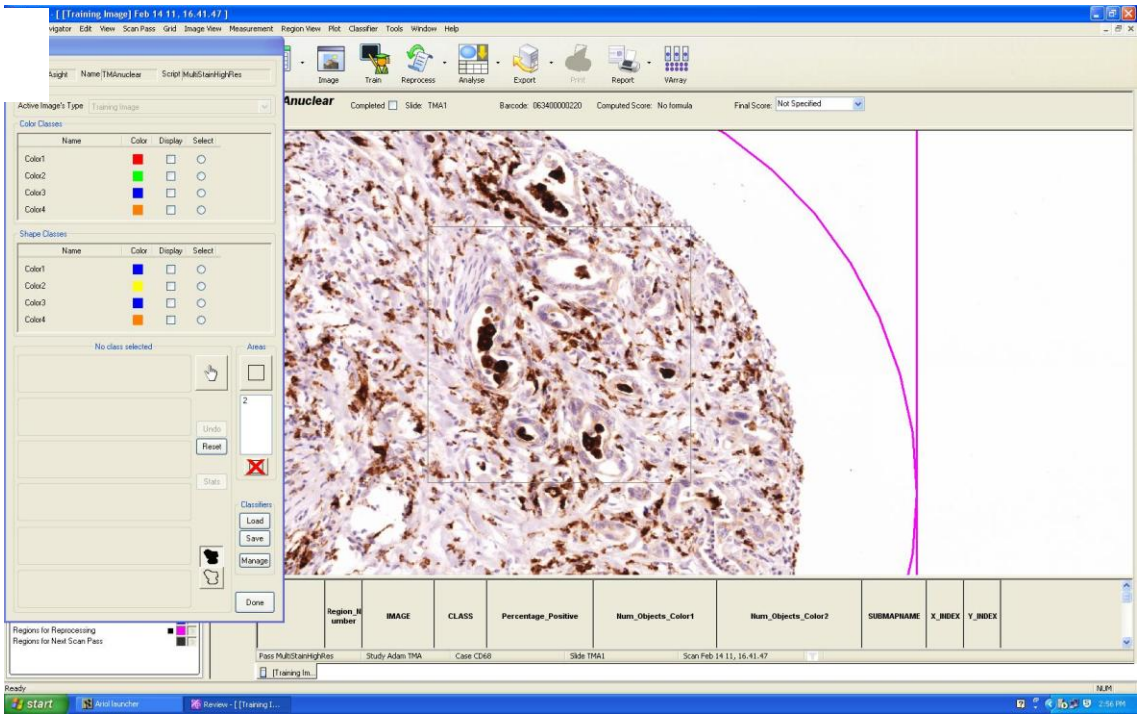
Anuclear
Completed
Slide: TMA1
Barcode: 063400000220
Computed Score: No formula
Final Score: Not Specified
Color Classes
Shape Classes
Color1
Color2
Color3
Color4
No class selected
Areas
Undo
Reset
Stats
Classifiers
Load
Save
Manage
Done
Regions for Reprocessing
Regions for Next Scan Pass
Region_Number
IMAGE
CLASS
Percentage_Positive
Num_Objects_Color1
Num_Objects_Color2
SUBMAPNAME
X_INDEX
Y_INDEX
Pass MultiStainHighRes
Study Adam TMA
Case CD68
Slide TMA1
Scan Feb 14 11, 16.41.47
Ready
start

B

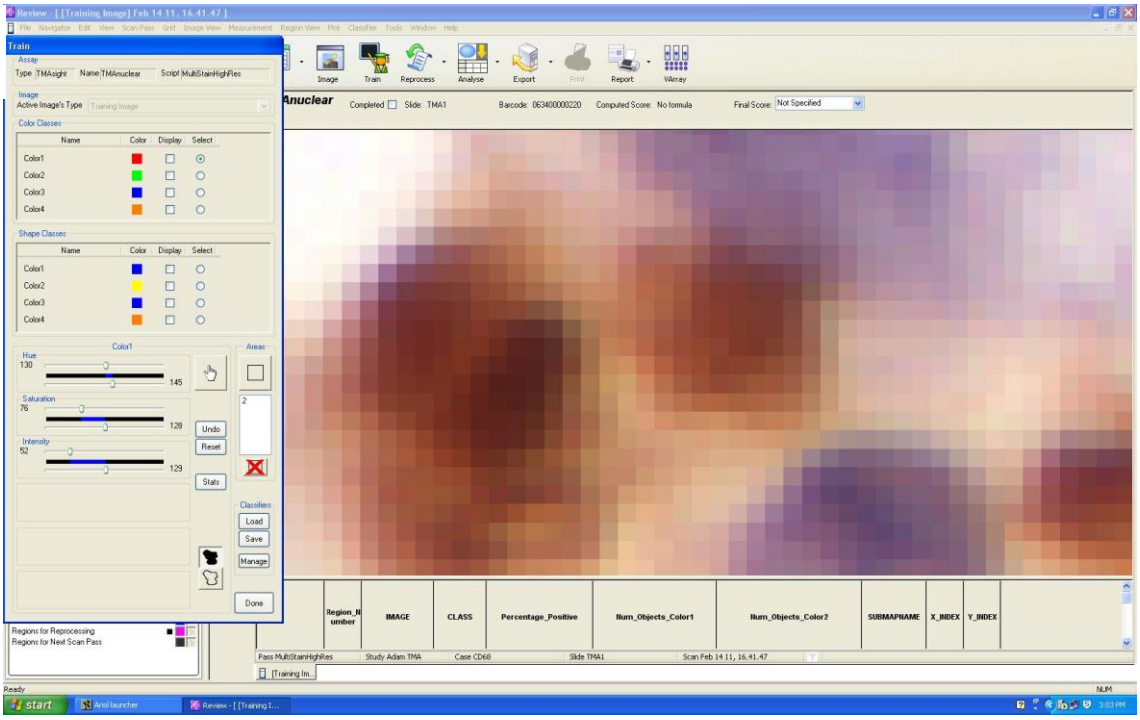
Train
Assay
Image
Anuclear
Completed
Slide: TMA1
Barcode: 063400000220
Computed Score: No formula
Final Score: Not Specified
Color Classes
Shape Classes
Color1
Color2
Color3
Color4
Hue
Saturation
Intensity
Areas
Undo
Reset
Stats
Classifiers
Load
Save
Manage
Done
Regions for Reprocessing
Regions for Next Scan Pass
Region_Number
IMAGE
CLASS
Percentage_Positive
Num_Objects_Color1
Num_Objects_Color2
SUBMAPNAME
X_INDEX
Y_INDEX
Pass MultiStainHighRes
Study Adam TMA
Case CD68
Slide TMA1
Scan Feb 14 11, 16.41.47
Ready
start

C

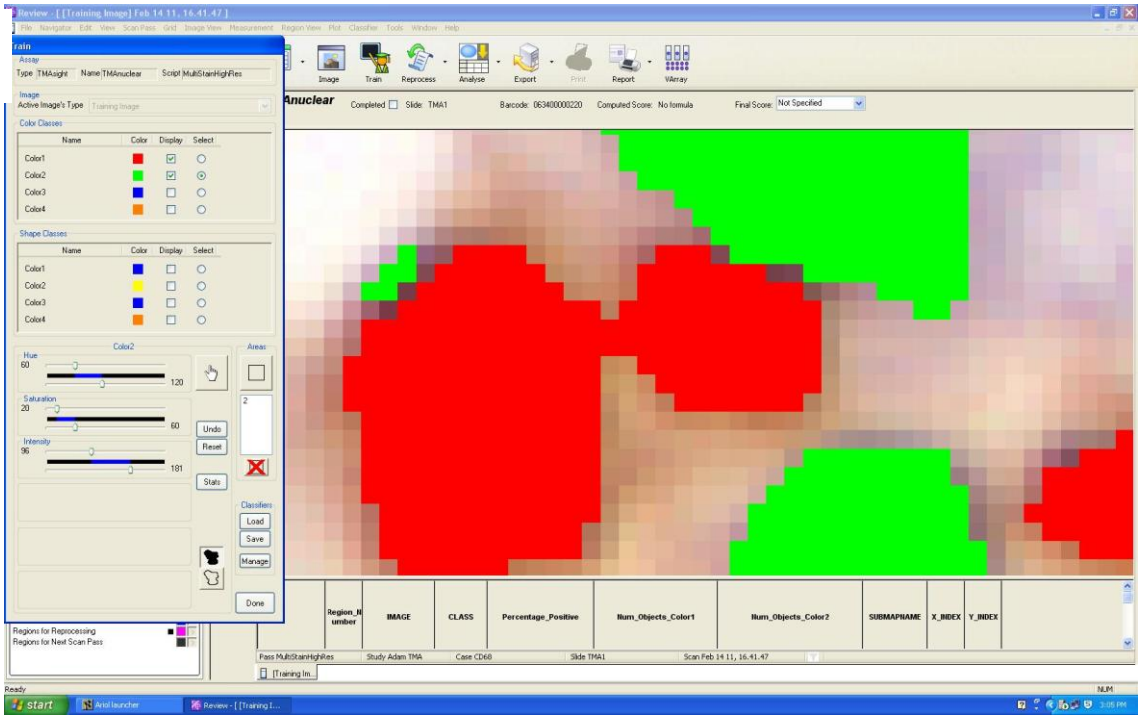

D

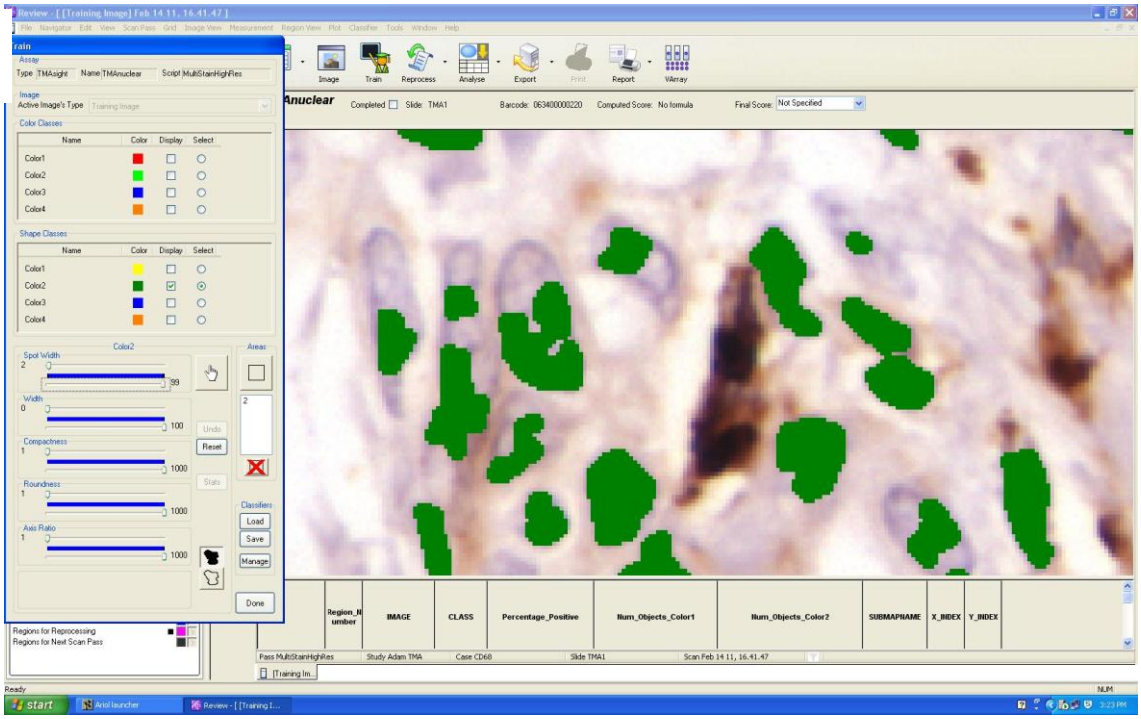

E

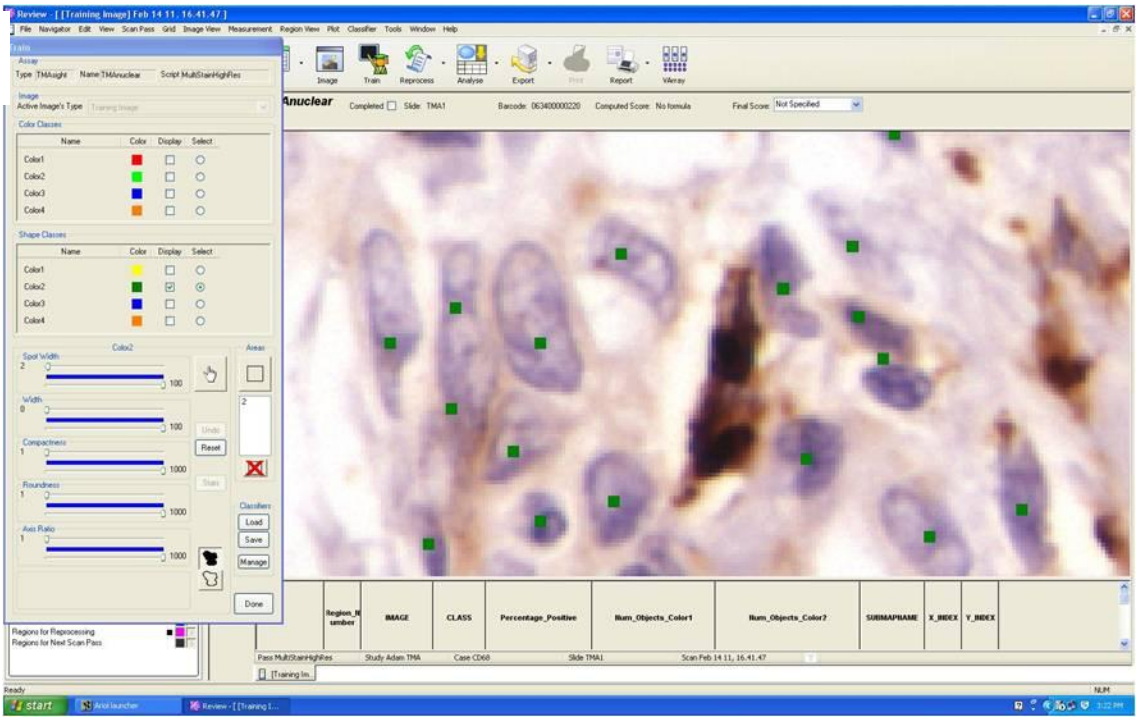

Figure 2.12 CD68 training using Ariol®

An example of training for quantification on the Ariol® using the marker for macrophages (CD68, brown) and hematoxylin (negative cells, blue) on a PDAC TMA core. The Ariol® can be taught to detect and quantify cells based on their colour, shape, staining intensity, and pattern of staining.

A. TMA core of PDAC stained for CD68: The Ariol® has the ability to quantify up to four markers on any given slide. The rectangular box to the left is the training interface and the square box on the core is the selected training region.

B. Magnification of image: Training on the Ariol® is performed at the pixel level thus image has to be magnified. Magnification enables the viewing of individual cells.

C. Training on colour: The TMA core has two stains, brown for CD68 (macrophages) and blue for hematoxylin (negative cells). The Ariol® was trained to detect brown staining (red) and blue (green). Care was taken to prevent overlapping of hue thresholds.

D. Training on shape: The Ariol® is able to detect the shape of individual cells (hematoxylin stained cells shown) using parameters such as width, spot width, roundness, compactness and axis ratio.

E. Quantification of cells: Using the algorithims created from training on colour and shape, the Ariol® is able to identify and quantify, quantitatively, individual cells (identification of hematoxylin stained cells shown).

2.4 X-Tile analysis

The X-tile software v.3.6.1 (Yale University) was used to analyse the role of the individual immune cell infiltrates on patient prognosis and survival.

The minimum p value method is traditionally used to assess the survival function of a population. This method is performed by dividing the cohort into high versus low expressers based on a single cut point and varying the cut point until a significant p value is reached, usually the lowest p value. A Kaplan-Meier graph of the survival function is then plotted for the minimum p value. This traditional method poses the risk of a high false positive rate of approximately 40 percent compared to the nominal 5 percent because of multiple testing, and has very small p values which are not often replicable (Altman, Lausen et al. 1994) .

Therefore correction is required for multiple testing. The x-tile software performs a number of statistical simulations such as the cross validation tests and Monte Carlo simulation of minimum p value to correct for multiple testing. The cross validation involves the random splitting of the dataset into two halves, finding the optimal cut point of one half of dataset and dividing the second half of dataset by the cut point of the first dataset. It then does the same for the second half of dataset and performs a survival analysis of the entire dataset based on these optimal cut points. Because the initial split is random, no two cross validations would give the same results. The software corrects for the random splits by performing the cross validation analysis 100 to 1000 times depending on the users settings and averages the results. It also plots a graphical heat map of the p values of the dataset which shows the quality of a marker for prognosis (Figure 2.13).

Monte Carlo simulation (or Monte Carlo method) is a mathematical technique that uses random numbers and probability statistics to perform risk analysis and has a range of applications, including in biology, atomic physics, economic and transportation. This technique makes it possible to examine very complex systems than would otherwise not be possible. The Monte Carlo simulation performs analysis "by building models of possible results by substituting a range of values- a probability distribution- for any factor that has inherent uncertainty" (Corporation 2013). It then calculates results multiple times, each time using a set of random values from the probability distribution that are different from the last time and the resulting outcome from that sample is recorded. Monte Carlo simulation performs this hundreds to thousands of times, the result of which is a probability distribution of possible outcomes.

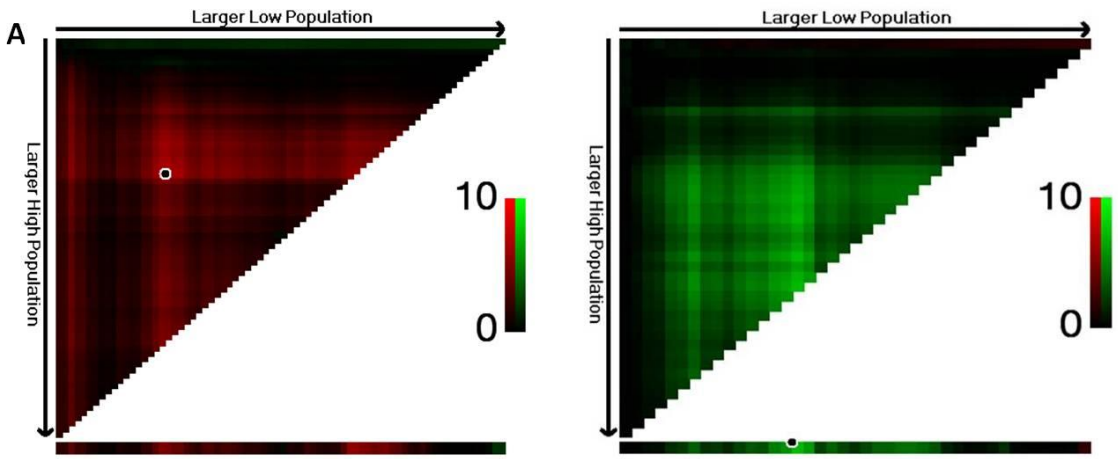

Figure 2.12 X-Tile heat maps

Heat maps produced by the X-Tile software. The triangle represents a population where 2 cuts are applied so that there is a middle population (3 populations) and the rectangle represents a population with a single cut applied (2 populations). Each pixel represents a data point where a cut has been applied. (A) Red denotes that the marker being investigated has a negative correlation with survival i.e. a high density of the marker results in poor prognosis. The spot with white border is the minimum p value in a 3 population cohort. (B) Green denotes that the marker being investigated has a positive correlation with survival i.e. a high density of the marker results in good prognosis. The black spot is the minimum p value in a 2 patient cohort.

2.5 Treatment of pancreatic stellate cells with all-trans retinoic acid (ATRA)

2.5 a. Pancreatic stellate cells

Pancreatic stellate cells (PSCs) are the main cells producing desmoplastic reactions in pancreatic ductal adenocarcinoma (Hwang, Moore et al. 2008; Vonlaufen, Joshi et al. 2008). PSCs are normally quiescent, a phenotype characterised by their ability to "store retinyl palmitate, retinol esterification, expression of the cytofilaments desmin and vimentin" (Bachem, Schünemann et al. 2005). However, PSCs may be activated by growth factors such as platelet-derived growth factor (PDGF), fibroblast growth factor (FGF) and transforming growth factor beta (TGFβ), cytokines and oxidant stress which results in a myofibroblast phenotype with subsequent transcriptional changes (Bachem, Schünemann et al. 2005; Froeling, Feig et al. 2011). Patients with PDAC have a relative deficiency of fat soluble vitamins such as vitamin A, due to the absence of biliary and pancreatic secretions (Froeling, Feig et al. 2011). Pancreatic stellate cell line (PS1) and primary pancreatic stellate cell line can be activated *in vitro* by growing on plastic and exposure to ethanol and can be rendered quiescent *in vivo* and *in vitro* by treatment with all-trans retinoic acid (ATRA) (Froeling, Feig et al. 2011).

2.5 b. All-trans retinoic acid (ATRA)

All-trans retinoic acid (ATRA) is a metabolic product of retinol and the active form of vitamin A. Retinoids have important roles in biological processes including development of embryonic structures, development of the central nervous system, maintenance of epithelial surfaces, immune competence and reproduction (Blomhoff and Blomhoff 2006; Clemens, Flower et al. 2013). Retinoic acids mediate their actions by nuclear retinoid receptor proteins, the retinoid acid receptors (RARs) and retinoid "X" receptors (RXRs). Retinoic acids role in biological processes involve the

binding to and activating of the RAR, which regulate the expression of several genes (Maden 2007).

2.5 c. *In vitro* treatment of pancreatic stellate cells

Because PSC are cultured on plastic *in vitro*, they retain an activated phenotype. To render the pancreatic stellate cells quiescent, ATRA (Sigma-Aldrich, Dorset, UK) was diluted from a stock solution of 10 mM in 100% ethanol to give 1mM ATRA. PS1s (pancreatic stellate cell line) were then treated in tissue culture every day for 7 days with 1mM ATRA in RPMI containing 10% foetal bovine serum (FBS) at a dilution of 1:1000 and under subdued light conditions. To control for quiescence, PS1 cells of the same lineage and passage were treated simultaneously with 100% ethanol (vehicle) only in RPMI containing 10% FBS at the same dilutions as ATRA treatment. These cells became our activated pancreatic stellate cell phenotype. After the 7 day treatment, media was aspirated off the cells and the cells were washed with fresh media 3 times. The conditioned media was collected after 24 hours. Conditioned media from cancer cells lines AsPc 1 and Capan 1 was also collected.

2.5 d. Storage conditions of ATRA

Upon purchase of ATRA (molecular weight 300.44), it was diluted in 100% ethanol to give a stock solution of 10 mM. The stock solution was covered in kitchen foil and stored at -80°C. A working solution of 1mM was normally made as described above and was stored in -20°C. All experiments were performed in subdued light.

2.6 *In vitro* migration assays

2.6 a. Hypothesis

I hypothesised that cytokine changes that occur when pancreatic stellate cells are turned quiescent may result in the differential (if any) migration of immune cells to the different pancreatic stellate cell phenotypes. To test this hypothesis, I modelled a simple migration assay of T-cells to the conditioned media of pancreatic stellate cell phenotypes using 6.5mm Transwell® with 5.0µm Pore Polycarbonate Membrane sterile Insert (Corning Life Science BV, Amsterdam, The Netherlands). Transwell® permeable supports are devices used to study anchorage-dependent and anchorage-independent cells and are available in a range of diameters, membrane types and pore sizes. They are used in *in vitro* studies that include transport and permeability, cell polarity, drug transport, chemotaxis, invasion, co-culture, endocytosis, tissue remodelling, *in vitro* fertilization and microbial pathogenesis (Incorporated 2010).

2.6 b. Parameters

In designing the migration experiments, certain factors such as membrane types, pore sizes, pore density, duration of incubation, starting number of cells and method of quantification had to be determined. These factors will be discussed below in relation to the Transwell® product (Corning Life Science BV, Amsterdam, The Netherlands).

2.6 b. i. Diameters

The Transwell® comes in diameters of 6.5mm, 12mm, 24mm and 75mm.

2.6 b. ii. Type of membrane

There are three membrane types; polycarbonate, polyester (PET) and collagen-coated polytetrafluoroethylene (PTFE).

The polycarbonate membrane is thin and translucent, and has 6 pore sizes: 0.1 µm, 0.4 µm, 3.0 µm, 5.0 µm, 8.0 µm and 12.0 µm. They are treated for optimal attachment of cells.

Polyester membranes are microscopically transparent and they provide better cell visibility under phase contrast microscopy which allows for the assessment of viability and monolayer formation. It has four pore sizes: 0.4 µm, 1.0 µm, 3.0 µm and 8.0 µm.

Collagen-coated PTFE membranes are transparent when wet. They promote cell attachment, spreading and visualization during culture. They are coated with types I and III collagen derived from bovine placenta and they have 2 pore sizes: 0.4 µm and 3.0 µm.

2.6 b. iii. Pore sizes

Pore sizes are a very important consideration as choosing the wrong pore size may inhibit migration of cells as a result of the pore being too small for a cell type, or they may induce the falling through of cells, making it impossible to quantify chemotaxis towards a gradient. Cell migration occurs in pore sizes of 3.0 µm or higher and because activated T-cells are approximately 10.0 µm in diameter (Nexcelom 2013), 3.0 µm and 5.0 µm pore sizes are recommended. I performed

optimization experiments with Transwells® of both pore sizes and chose 5.0 µm pore sized Transwells®.

2.6 b. iv. Pore density

Only the polycarbonate and polyester have defined pore densities. The polyester membranes have lesser pore densities than the polycarbonate membranes. The pore density of the 5.0 µm polycarbonate Transwell® is 4×10^5 pores/ cm^2 whereas the pore density of the 5.0 µm polyester Transwell® is not nominally defined.

2.6b. v. Starting number, Duration and Quantification

I started with 1×10^5 T-cells. I performed optimization experiments in which I let cells migrate for 5 and 8 hours and I chose final 8 hour duration. Cells were counted on the Casy® cell counter (Roche Diagnostics Ltd, Burgess Hill, UK).

2.6 c. Method

As T-cell migration to pancreatic stellate cell and cancer conditioned media had not been documented in literature, we optimised the experiment by performing pilot assays with 3 µm and 5 µm transwells; 5 and 8 hour incubation times; condition media collected with or without FBS in different growth media, RPMI and DMEM + E4 (50:50). We observed the best distinctions using sterile 6.5mm Transwells® with 5.0µm pore polycarbonate insert (Corning Life Science BV, Amsterdam, The Netherlands); 8 hour incubation time, condition media of cells grown in 10% FBS and RPMI 1640. RPMI with 10% FBS and 0% FBS were used as positive and negative controls respectively.

The experiments were performed by aliquoting 500 µl aliquot of conditioned media in the lower compartment. This served as chemo-attractant. 1×10^5 $CD3^+$,

$CD4^+$ and $CD8^+$ T-cells, separately, were resuspended in 200 µl of RPMI 1640 without FBS were placed in the upper compartment of the Transwell® insert and incubated for 8 hours. Immune cells used were from healthy donor patients (isolation of immune cells is discussed below). The media in the lower compartment was collected and cells were counted with the Casy® cell counter (Roche Diagnostics Ltd, Burgess Hill, UK).

2.7 Isolation of immune cells from blood

2.7 a. Introduction

Blood from PDAC patients were collected at Barts Health NHS Trust (City and East London LREC 07/0705/87). Healthy donor lymphocytes were obtained from Buffy coats prepared by the National Blood Service, NHS Blood and transplant (Brentwood, United Kingdom) as approved by the North London Research Ethics Committee.

Mononuclear cells (consisting of lymphocytes and monocytes) were isolated from blood using the density gradient media Lymphoprep™ (Axis-Shield Plc, Dundee, Scotland). Separation of mononuclear cells was possible because they have lower density than red blood cells and polymorphonuclear cells (granulocytes). Mononuclear cells have a density below 1.077g/ml and therefore can be isolated by centrifugation on an isosmotic medium with density of 1.077g/ml. The red blood cells and polymorphonuclear cells are deposited at the bottom, and the mononuclear cells are kept at the medium interface (i.e. the Lymphoprep™ media separates mononuclear cells from non mononuclear cells). Serum is deposited on top of mononuclear layer. The mononuclear layer is called Buffy coat.

Specific immune cells such as CD3, CD4 and CD8+ were isolated by positive selection. The principle involves labelling the immune cell of interest with magnetically labelled MicroBeads (Miltenyi Biotec, Surrey, UK) specific to that immune cell of interest. The cell suspension is then passed through a column in a magnetic field and positively labelled cells are retained in the column, and the non labelled cells are deposited in a collection tube. This non labelled fraction can still be labelled for other immune cells. I used the autoMACS® Pro separator (Miltenyi Biotec, Surrey, UK) (Figure 2.13) to isolate individual immune cells. The autoMACS® Pro may be used to separate cells either using positive or negative selection.

2.7 b. Method

Immune cell isolation was carried out in sterile condition in a laminar flow hood. Blood was diluted with PBS in a 1:1 ratio and afterwards added to Lymphoprep™ media in a 2:1 ratio (with Lymphoprep™ media being the lesser fraction). Utmost care was taken in the addition of blood to Lymphoprep™ media so as not to contaminate the layer: media was added to tube first and then tilting the tube at a 45 degrees angle, blood was slowly added. The mixture was then centrifuged at a speed of 1500rpm and at 22°C for 25 minutes.

After centrifugation, care was taken to ensure that layers were not mixed and with the use of a plastic pipette, serum layer was carefully aspirated off and stored at -80°C. Also with a plastic pipette, the mononuclear layer was carefully aspirated off, transferred to a new tube and filled up with MACS buffer (prepared by diluting MACS BSA Stock Solution 1:20 with autoMACS® Rinsing Solution (all Miltenyi Biotec, Surrey, UK)) and re-centrifuged at a speed of 1500rpm at 4°C for 5 minutes.

PBMCs were labelled with MicroBeads and left to incubate at 2-8°C for 15 minutes and separation was performed with the “POSSEL” program on the autoMACS® Pro. “POSSEL” is used in the isolation of cells with normal antigen expression and with frequencies higher than 5%, and is the program of choice when purity is the highest priority. The protocol in the MicroBead kit was followed.

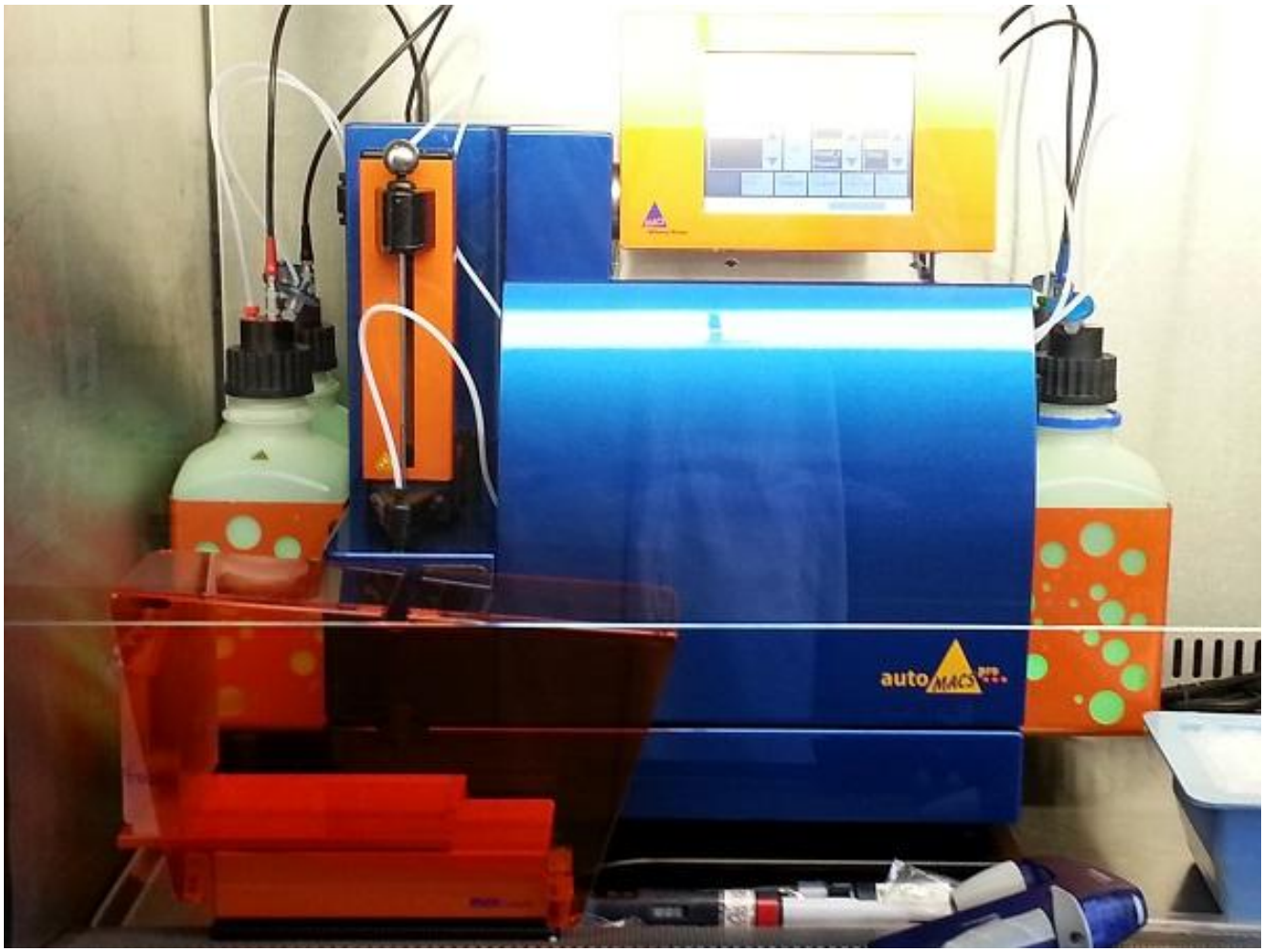

Figure 2.14 autoMACS® Pro separator (Miltenyi Biotec, Surrey, UK)

2.8 Adhesion assays

I modelled adhesion experiment to observe and measure if $CD3^+$ and $CD8^+$ T-cells have differential affinity, *in vitro,* for activated and quiescent pancreatic stellate cells. The rationale behind this experiment was that T-cells do not adhere to glass (Kirby, Wheeler et al. 2003) and thus if T-cells remained after incubation and a rigorous wash process, then they might have formed adhesion complexes with receptors or ligands on the PS1 cells. Quantifying the number of adhered T-cells to activated PS1 cells versus the adhesion of T-cells to quiescent PS1 cells might then show if there was differential adhesion.

I plated PS1 cells on 10mm glass cover slips that had been carefully inserted into 6 well plates The PS1 cells were treated with either ATRA or ethanol for 7 days as described previously. At the end of treatment, on the 8^{th} day, media was aspirated off and replaced with either 5×10^4 $CD3^+$ or $CD8^+$ in RPMI 1640 media with 10% FBS and incubated in 37°C for 1, 2 and 8 hours. Afterwards, media was removed from wells and cover slips were washed three times with PBS. The cover slips were harvested and fixed in Cellstor Neutral Buffered Formalin (Cellpath Ltd. Newton, UK) for 20 minutes. Cellstor buffer was removed and the cover slips were washed 3 times with PBS and stored at 4°C in PBS containing 0.1% sodium azide.

The glass cover slips were stained by immunofluorescence and the number of adhered T-cells relative to PS1 cells was counted on the Axioplan microscope (Carl Zeiss MicroImaging LLC, New York, US) based on cell morphologies and staining patterns. The counts were performed at x63 magnification because of the size of the T-cells, and were performed by dividing the number of adhered T-cells by number of

pancreatic stellate cells per high-power field to give ratios of T-cells adherent per stellate cell.

2.9 Immunofluorescence

Immunofluorescence was employed in the quantification of adhesion assays (above) and in the labelling of certain proteins on tissues. Immunofluorescence follows most of the same principles that govern immunohistochemistry (discussed previously) but differs primarily in its method of detection. In immunofluorescence antibodies are chemically conjugated to fluorescent dyes such the Alexa fluor dyes, fluorescein isothiocyanate (FITC) and tetramethyl rhodamine isothicyanate (TRITC). An automated imaging instrument capable of detecting fluorescent signals, such as the Zeiss Laser Scanning Microscope LSM 510 (Carl Zeiss Ltd. Cambridge, UK) can be used to quantify fluorescence.

Antibodies may bind directly or indirectly to the protein of interest. Direct immunofluorescence occurs when the fluorescent dye is conjugated to the primary antibody, whereas indirect immunofluorescence occurs when the fluorescent dye is conjugated to a secondary antibody. In most cases, mine included, indirect immunofluorescence is used. The advantages of indirect over direct immunofluorescence include: indirect method is not as expensive, signal is often amplified as more than a single secondary antibody may bind to the primary antibody whereas in the latter conjugation is on the single primary antibody and there is greater sensitivity in the indirect fluorescence method.

Immunofluorescence may be used to evaluate cell suspensions, cultured cells and tissues and they can be used on fresh and fixed samples, the former of which is not possible in immunohistochemistry.

Details of antibodies used are on Table 2.2.

2.10 Gene expression microarray analysis

Pancreatic stellate cells were plated on plastic and Matrigel and treated with 1µm and 10 µm of all trans retinoic acid (ATRA) for 7 days, after which triplicates were extracted using TRIzol (Invitrogen). 250ng of RNA was labelled using Illumina TotalPrep RNA amplification kit (Ambion, manufacturer's instructions were followed) and hybridized to Illumina Human-6 v2 Expression BeadChips (46,713 probes). Statistical analyses were performed using Bioconductor (Bioconductor 2013) packages with R statistical environment (R-Project 2013). The above was carried out by Froeling et al (Froeling, Feig et al. 2011).

I selected genes involved in migration and adhesion by comparing selecting upregulated and downregulated genes and comparing these to information on the genetics database, GeneCards (Genecards 2013). A summary table of selected genes and their functions can be seen below in table 2.6.

Genes	ILMN_ID	Description	Function	P1vsC.x	M1vsC.x	P10vsC.x	P1vsM1.x
IL8	ILMN_1666733	Interleukin 8	T-cell, Neutrophil, Basophil but not Monocyte chemotactic factor	1.2611	2.3026	-2.228	-1.042
MYL7	ILMN_16818 7	Myosin light chain 7, regulatory	Motor proteins, regulatory	1.2971	0	0	0
MYL4	ILMN_16842 5	Myosin light chain 4, protein coding	Motor proteins	0	0	-1.184	0
CXCL12 / SDF1	ILMN_1803825	Stromal cell derived factor	Migratory for lymphocytes and monocytes, negative regulator of adherence on monocytes through lyn kinase	0	0	-1.485	0
IL6	ILMN_1699651	Interleukin 6	B-cell stimulating factor	0	0	-1.393	0
CCL2	ILMN_1720048	Chemokine Ligand 2	Chemoattractant for monocytes	1.0182	1.1034	0	0
ITGA4	ILMN_1747052	Integrin alpha 4	Receptors of Fibronectin and VCAM1	1.125	1.0862	0	0
VCAM1	ILMN_1766955	Vascular cell adhesion molecule 1	Adhesion molecule, binds VLA4 on lymphocytes	0	0	-1.12	0
SOCS1	ILMN_1774733	Suppressor of cytokine signalling 1	Negative regulation of cytokines	0	0	-1.286	0
IL1B	ILMN_1775501	Interleukin 1 beta	stimulates thymocyte proliferation and B-cell maturation, involved in inflammatory immune response	1.788	2.3256	0	0
FN1	ILMN_1778237	Fibronectin 1	Binds cell surfaces, involved in adhesion, migration and wound healing	0	0	-1.362	] 0
CXCL6	ILMN_1779234	Chemokine (C x C motif) ligand 6	Neutrophil chemotactic protein	0	0	-1.072	0
TNFAIP6	ILMN_1785732	Tumour necrosis factor alpha- induced protein 6	Contains hyaluronan binding domain, involved in cell migration and extracellular matrix stability	0	0	-2.039	0

IL11	ILMN_1788107	Interleukin 11	Stimulates T-cell dependent development of immunoglobulin producing B-cells	0	0	-1.294	0
ICAM1	ILMN_1812226	Intercellular adhesion molecule 1	Ligands for Lfa1 proteins, involved in cell adhesion and migration	1.0787	1.0601	0	0

Table 2.6 Putative genes involved T-cell chemotaxis

Table showing mRNA gene expressions of pancreatic stellate cell line (PS1) when treated with ATRA versus controls (vehicle treated cells).

ILMN_ID: Illumina identifier

P1vsC.x: Fold change in gene expression when PS1 is treated with 1mM ATRA on plastic vs. control.

M1vsC.x: Fold change in gene expression when PS1 is treated with 1mM ATRA on Matrigel vs. control.

P10vsC.x: Fold change in gene expression when PS1 is treated with 10mM ATRA on plastic vs. control.

P1vsM1.x: Fold change in gene expression when PS1 is treated with 1mM ATRA on plastic vs. PS1 treated with 1mM ATRA on Matrigel.

Function of genes were obtained from the genetic database, GeneCards (Genecards 2013).

2.11 Enzyme linked immunosorbent assay (ELISA)

Quantikine® ELISA kits (R & D Systems, Abingdon, UK) were used to measure the concentrations of candidate chemokines and cytokines secreted by the activated and quiescent pancreatic stellate cell phenotypes. Stellate cell conditioned media was used and collected as previously described. The proteins measured included Interleukin 1 beta (IL-1β/ IL-1F2), Interleukin 8 (IL-8/ CXCL8), Stromal cell derived factor 1 alpha (SDF-1α/ CXCL12), Intracellular adhesion molecule 1 (sICAM-1/ CD54) and Monocyte chemotactic protein 1 (MCP-1/ CCL2). The protocols provided with the kit were strictly followed.

The Quantikine® ELISA (R & D Systems, Abingdon, UK) measures proteins in cell culture supernates, serum, urine and plasma. It can be used to determine "relative mass values of proteins of interest" and utilizes a quantitative sandwich ELISA approach. Monoclonal antibodies specific for the protein of interest are pre-coated onto a microplate. Antibodies in samples when added bind to immobilised antibodies on microplate. The final output is colourimetric.

Optical densities of colours were read with Dynex microplate reader and protein concentrations were calculated with Dynex Revelation 4.04 software (Dynex Technologies, Virginia). A primary test filter of 450 wavelengths and a secondary test filter of 560 wavelengths were used.

2.12 RNA interference (RNAi)

RNAi is a technique used to perform post-transcriptional gene silencing in cells. During RNA interference, the RNase II enzymes Dicer and Drosha process double stranded RNA (dsRNA) or micro RNA (miRNA) into 19~21 base pairs small interfering RNA (siRNA) (Hamasaki, Suzuki et al. 2012). siRNA is then loaded to the protein complex RNA-induced silencing complex (RISC). During assembly, RISC unwinds the two siRNA strands retaining one strand which is used to recognise and bind to the target mRNA. The RNase H enzyme, Argonaute (Slicer), degrades the target mRNA leading to gene silencing.

Because stromal cell derived factor 1 alpha (SDF-1 α / CXCL12) is chemotactic to T-cells (Kryczek et al 2007) and based on the expression results obtained from the ELISAs, I used siRNA to silence CXCL12 in PS1 cells.

I used CXCL12 GeneSolution siRNA (Qiagen, West Sussex, UK) to silence CXCL12 gene expression in PS1 cells and Allstars Negative Control siRNA (Qiagen, West Sussex, UK) as a control. Opti-MEM® reduced serum media (Life Technologies Ltd. Paisley, UK) was used to dilute the siRNA and transfection of the siRNA was performed with INTERFERin™ (Polyplus-transfection SA, France). The protocol provided with the INTERFERin™ was adhered to for transfection.

To optimize the siRNA experiments, concentrations of 1nm, 10nm and 50nm were employed. I incubated the cells with the transfection mix at 37°C for 96 hours after which I took the media off. RPMI with 10% FBS was put on the cells and incubated at 37°C for 24 hours and then collected. ELISA was used to measure the amount of protein in supernatant. All conditioned media were stored at 4°C for a maximum of 3 months.

2.13 Mouse experiments

Most genetically engineered mouse models use recombinases (e.g. bacteriophage-P1-derived Cre recombinases) to excise DNA sequences that are flanked by specific short repeats (called loxP sites) and are based on a Cre/loxP model (Mazur and Siveke 2011). In this model, mutant *Kras*$^{LSL\text{-}G12D}$ knock in allele and silenced by the insertion of a LoxP-flanked STOP element is activated by excision of the STOP element driven by the Cre-recombinase (Mazur and Siveke 2011). *Pdx1-Cre* transgenic knock in strains are used to target pancreatic progenitor cells and are activated during early pancreatic development. Because PDX1 is expressed in the stomach, duodenum and epidermis, extra-pancreatic tumours may arise in such mouse models and because *Pdx1-Cre* is activated in early embryogenesis, the mouse model does not reproduce the intermittent acquisition of mutations as is the case in humans. However, this mouse model most closely relates to the human PDAC condition as it exhibits the hallmark signs of PDAC such as PanINs that progress to invasive and metastatic disease (Mazur and Siveke 2011).

Genetically engineered mouse model KPC (***LSL-Kras$_{G12D}$/+; LSL-Trp53$_{R172H}$/+; Pdx-1-Cre*** **mice**) were treated with ATRA dissolved in sesame oil. Dosage of 10mg/kg was administered daily for 5 days. 6 mice were treated with ATRA only while 4 mice were treated with vehicle only. One ATRA treated mice was given 3 doses as it was enrolled at advanced stage PDAC. The whole pancreas, spleen and salivary gland were harvested and mounted on a single slide. The salivary gland and spleen serve as controls (Froeling, Feig et al. 2011).

KPC mice were then stained for the immune markers: $CD3^+$, $CD8^+$ and F4/80.

2.14 Flow cytometry

Flow cytometry is used to analyse the expression of cell surface markers and intracellular molecules and in characterising and defining cell types in heterogeneous cell population by measuring the fluorescent intensity produced by fluorescent labelled antibodies. The procedure consists of the following (Rahman 2006; Abcam 2013):

1. Fluidics: The fluidics system of a flow cytometer consists of a core through which the cell suspension is run through, and is enclosed by a sheath containing a faster flowing fluid called sheath fluid. This fluid creates an effect called hydrodynamic focusing which results in particles being passed through the laser light individually.

2. Forward and side scatter measurements: There are a number of detectors on a flow cytometer. One is found in the front of the light beam (forward) and several others are on the side of the beam (side scatter), and as cells pass through the beam they will scatter light which is detected by these forward and side scatter detectors. The forward scatter is dependent on cell size and the side scatter is dependent on the density of the cells (i.e. organelles, granules). Populations can be distinguished based on their forward scatter and side scatter characteristics.

3. Measurement of fluorescence: When excited by a laser, fluorochromes labelled to target proteins will emit light that corresponds to their excitation wavelengths. This fluorescence can be detected individually and analysed. The flow cytometer has a set of filters and mirrors that categorize forward and side scatter and fluorescence dependent on their wavelength. Each sensor,

called photomultiplying tubes (PMT), detects fluorescence only at a specified wavelength.

4. Staining: I used the direct staining method in which the primary antibody is directly conjugated to a fluorochrome. The advantages of this method are that there is only one incubation step and it eliminates the possibility of non-specific binding from secondary antibody.

Fluorescent activated cell sorting (FACS) buffer was always used freshly made and consisted of PBS with 2% foetal calf serum (FCS) and because it was always freshly made it was of no use adding azide. The procedure was performed on ice and antibodies were incubated for 30 minutes at 4°C in the dark. Analyses were also carried out the same day as it was not useful to fix the cells with paraformaldehyde. A list of the antibodies, their conjugates and other details are in table 2.7 below.

Primary antibody (clone)	Species raised in	Supplier (order number)	Conjugate	Gene
CD3 (UCHT1)	Mouse	Biolegend (300419)	PE/Cy7	CD3
CD4 (RPA-T4)	Mouse	eBiosciences (47-0049)	APC-eFlour® 780	CD4
CD8a (RPA-T8)	Mouse	eBiosciences (45-0088)	PerCP-Cy5.5	CD8
CD184 (12G5)	Mouse	BD Pharmingen™ (560936)	APC	CXCR4
CD45RA (H100)	Mouse	BD Pharmingen™ (561882)	FITC	PTPRC
CD197 (3D12)	Rat	eBioscience (12-1979)	PE	CCR7

Table 2.7 Flow cytometry antibodies and conjugates

3.0 Results

3.1 Introduction

PDAC have a pronounced desmoplastic reaction (Neesse, Michl et al. 2011). Activation of quiescent pancreatic stellate cells (PSC), the chief event in this process, is reversible as shown by Froeling et al (Froeling, Feig et al. 2011). Investigations with the aid of *in situ* hybridization by Iacobuzio-Donahue and colleagues have delineated invasive tumours into five distinct compartments based on differential gene expression as well as morphology: neoplastic epithelium, endothelium, inflammatory, panstromal and juxtatumoural stroma. (Iacobuzio-Donahue, Argani et al. 2002). The juxtatumoural stroma and panstromal regions of PDAC were delineated based on their differential expressions of the genes; Matrix metalloproteinase 11 (MMP11), Apolipoprotein C-1 (Apo C1) and Apolipoprotein D (Apo D), which are preferentially expressed in the juxtatumoural region, and Matrix metalloproteinase 2 (MMP2) which is preferentially expressed in the panstromal region (Iacobuzio-Donahue, Ryu et al. 2002; Ricci, Kern et al. 2005). This delineation was arrived at with the aid of serial analysis of gene expression (SAGE) libraries and *in situ* hybridization (Ryu, Jones et al. 2001; Iacobuzio-Donahue, Ryu et al. 2002; Ricci, Kern et al. 2005) and these differences in gene expression of the stroma may suggest differential interactions of stromal regions with immune cell infiltrate. The juxtatumoural stroma is defined as the region of stroma immediately adjacent to the tumour epithelial cells and the panstroma as the total stromal region excluding the juxtatumoural stroma (Ricci, Kern et al. 2005).

In this chapter I quantified the density of an array of immune cells in infiltrating cancers, particularly PDAC and other pancreatico-biliary diseases. In addition to quantifying the total tissue immune cell infiltrate of the various cancers, I also sought

to measure immune cell migration towards the tumour cells. In order to achieve this we defined the juxtatumoural stroma and panstromal compartments as described earlier in methods and measured density in the individual compartments.

There is a paucity of blood vessels within the immediate vicinity (juxtatumoural stromal compartment) of pancreatic tumours and an increase in blood vessel density further away (panstromal compartment) from the tumour and affixed within the stromal matrix in both human and KPC mice tissues (Olive, Jacobetz et al. 2009). In response to chemokine secretions resulting from inflammation, immune cells extavasate blood vessels where they are in circulation unto tissue and with the help of adhesion molecules such as VCAM-1 and ICAM-1 migrate to the site of inflammation as they require direct contact to perform their functions (von Andrian and Mackay 2000; Campbell, Kim et al. 2003; von Andrian and Mempel 2003). Because the majority of blood vessels in PDAC are found in the panstromal compartment, immune cells need to actively migrate across the stroma to the tumour, this, we called immune cell infiltration to the tumour.

I hypothesised that a defect in immune cell infiltration will occur when the immune cell density in the panstromal compartment is significantly more than the density in the juxtatumoural compartment. The corollary will then be that a no defect in immune cell infiltration will occur when the immune cell density in the juxtatumoural compartment is significantly higher than the density in the panstromal compartment or when there is no significant difference between these two stromal compartments. I also describe the effect of these immune cells on overall patient survival.

The juxtatumoural stroma and panstromal compartments have also been used in the delineation of breast cancer stromal reaction. The juxtatumoural stromal cells were found to express the gene Osteonectin differentially from the panstromal cells (Iacobuzio-Donahue, Argani et al. 2002) suggesting differences between tumour types or organs.

3.2 Immune cell staining of whole tissue sections

Whole sections of 4 PDAC patients were stained by immunohistochemistry for the T-cell markers (Figure 3.1); T-cells ($CD3^+$), helper T-cells ($CD4^+$), cytotoxic T-cells ($CD8^+$) and other immune cells (Figure 3.2); ($CD20^+$) and Neutrophils ($CD15^+$) and quantified quantitatively with Ariol as described previously. As the sample size was small we did not achieve significant results however we observed sequestration of $CD3^+$, $CD4^+$, $CD8^+$ and $CD20^+$ in the panstromal compartments and sequestration of $CD15^+$ in the juxtatumoural compartment. These observations formed our hypothesis of immune cell migration in PDAC, where some immune cells (such as the Neutrophils) are able to extravasate the blood vessels to the tissue and are able to perform chemotactic migration to the tumour, whereas other immune cells (such as the T-cells) are able to extravasate the tissue but seem sequestered by the stroma.

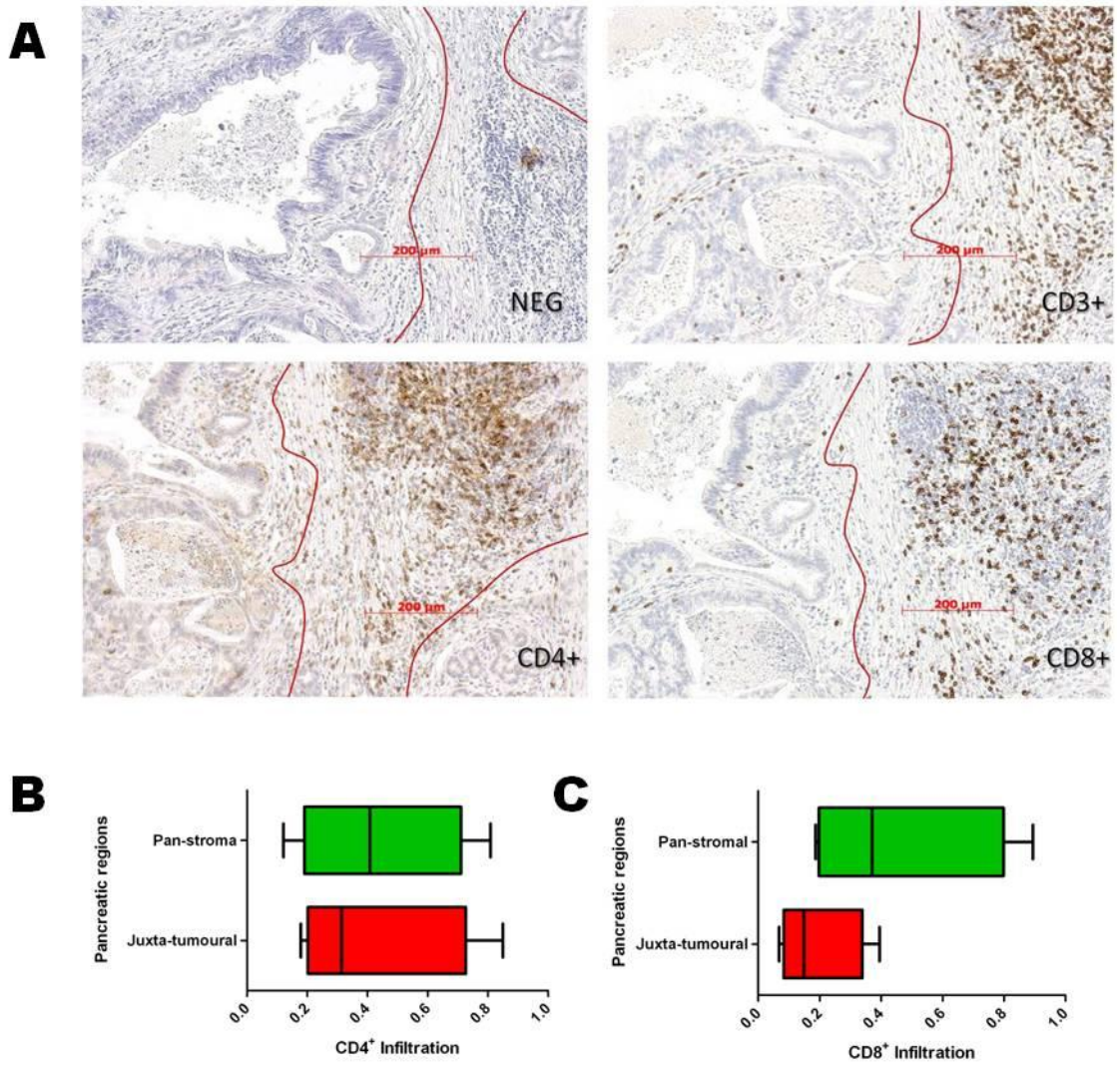

Figure 3.1 T-cell infiltration in whole tissue sections

(A) $CD3^+$, $CD4^+$ and $CD8^+$ staining compared with a negative control in tissue sections of the same PDAC patient. T-cells are sequestrated in the panstromal compartment indicating a lack of infiltration of these immune cells. Consecutive sections have been used for ease of comparison.

(B, C) Box and whiskers diagram showing the median and inter-quartile range of the subsets; helper T-cells ($CD4^+$) and cytotoxic T-cells ($CD8^+$) in the juxtatumoural stromal and panstromal compartments. There is no defect in infiltration of $CD4^+$ T-

cells; this is not the case for $CD8^+$ T-cells which are sequestered in the panstromal compartment.

Number of patients: 4; Scale bars: 200μm

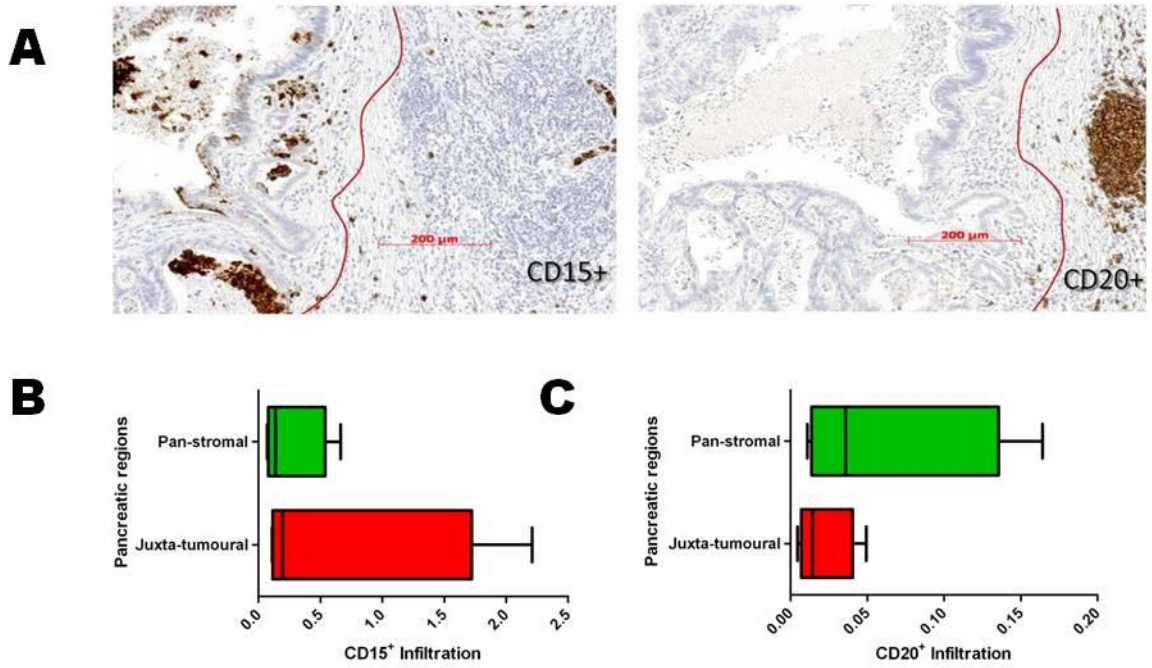

Figure 3.2: Other immune cell infiltration in whole tissue sections

(A) Neutrophil ($CD15^+$) and B-cell ($CD20^+$) staining compared with a negative control in tissue sections of the same PDAC patient. $CD15^+$ cells are sequestrated in the juxtatumoural compartment indicating an infiltration of neoplasia by this immune cell type. $CD20^+$ cells cluster in the panstromal compartment but are not seen infiltrating the neoplasia.

(B, C) Horizontal box and whiskers diagram showing the median and inter-quartile range of $CD15^+$ and $CD20^+$ cells in the juxtatumoural stromal and panstromal compartments.

Number of patients: 4; Scale bars: 200µm

3.3 a. Validation of method of quantification of whole tissue sections on tissue microarrays (TMA)

In order to increase the power of our quantification of immune cell infiltration on human tissues I chose to use TMAs. The benefits of TMAs include: high throughput capability, uniform staining of all TMA cores within a slide and less variation between slides as the quantity of slides are reduced when using TMAs compared to slides of whole sectioned tissue, and also using TMAs would introduce a separate method of quantifying immune cell infiltration.

To ascertain whether tissue microarrays (TMAs) could be used in the quantification of immune cell densities, I stained a TMA for $CD8^+$ T-cells and selected 4 random PDAC patients' samples from the TMA. I quantified the density of $CD8^+$ T-cells in the juxtatumoural and panstromal regions and compared this to the same four patients' tissues stained for individually in whole tissue sections (Whole tissue sections were stained by immunohistochemistry and performed by Dr. Moonim). I observed a similar distribution of densities using both methods (Figure 3.3). I chose TMA to analyse immune cell densities because of its high throughput capability.

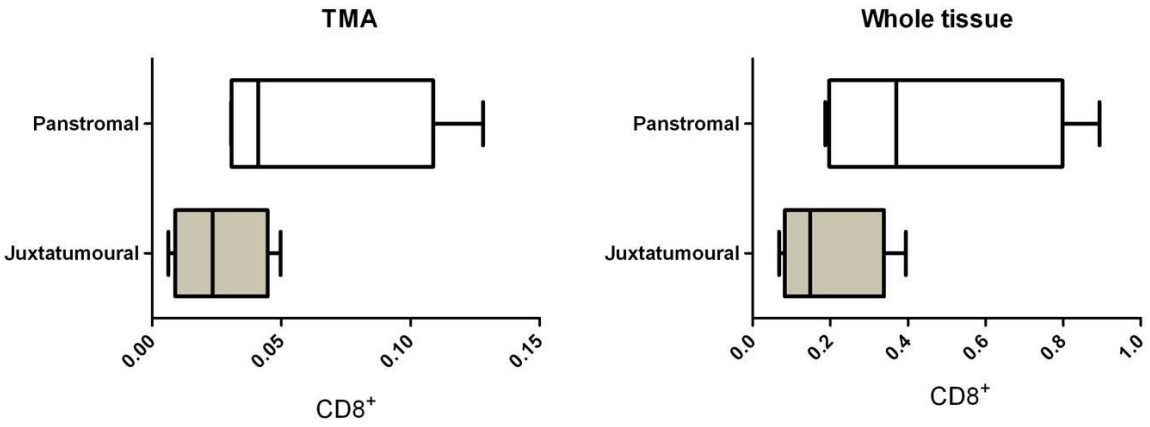

Figure 3.3: Comparison of immune cells density done in tissue microarray and whole tissue sections

Horizontal box and whiskers diagram representing immune cell densities on TMAs (A) and whole tissue sections (B) using the method described in chapter 2 (section…). Each graph is representative of four patients. In TMAs the median of all cancer cores for each patient was calculated and used to represent the patient. Both methods showed the same trend.

Boxes represent median with interquartile ranges (25^{th} and 75^{th}) with whiskers representing the range.

3.3 b. Comparison of two methods to calculate immune cell density: as a proportion of all cells and numbers per unit area

Furthermore, in order to satisfy the validity of approach, I quantified immune cell density by two methods. The first method involved quantifying both the number of positively and negatively stained cells and dividing the number of positively stained cells by the number of negatively stained cells. The second method involved counting only the number of positively stained cells and dividing these by the analysed area. For accuracy with the second method, I excluded ductal spaces (equation and result are shown in Figure 3.4). I chose the former method so as to take into account the variations in size of ductal spaces of neoplasms, especially as some immune cells such as neutrophils were found within the ductal lumens.

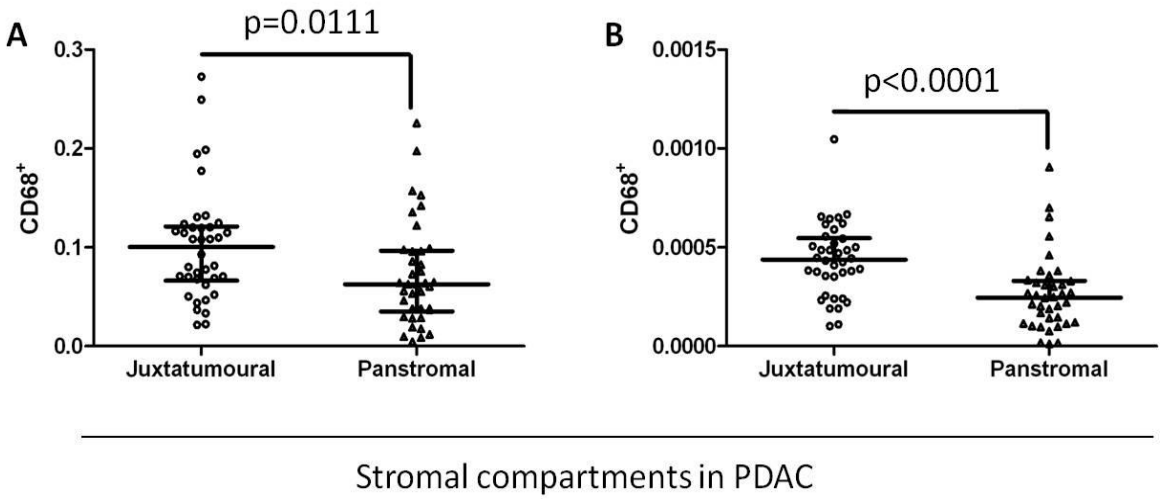

Density= Number of positive cells / Number of negative cells

Density= Number of positive cells / Analysed area

Figure 3.4: Comparison of immune cells density performed by two different methods

Immune cells were stained and analyzed as described earlier. The analysis of immune cell density was carried out by two distinct methods. In (A) the stromal compartments were analyzed by dividing the number of positively stained nuclei with the number of negatively stained nuclei to give a proportion of cellular population. In (B) the positively stained nuclei number was divided by the analysed area to give an estimate of immune cell density. Both methods demonstrated statistically significant result.

Each data point represents a single patient (median scores of all TMA cores (n=6)). Lines represent median with interquartile ranges (25^{th} and 75^{th}).

Mann Whitney U test; p-values are two-tailed.

3.4 Immune cell infiltration in pancreatico-biliary diseases

I performed an unbiased, automated survey of immune cell infiltrate (T-cells, $CD3^+$; helper T-cells, $CD4^+$; cytotoxic T-cells, $CD8^+$; regulatory T-cells, $FoxP3^+$; B-cells, $CD20^+$; and macrophages, $CD68^+$) on pancreatico-biliary cancers such as PDAC, ampullary carcinoma (AC) and cholangiocarcinoma (CC) and on the borderline malignant condition: mucinous cystic neoplasm (MCN); chronic inflammation: chronic pancreatitis (CP); and normal donors which served as controls (Figures 3.6 and 3.7). A normal spleen core was embedded in each TMA slide to serve as a positive control for immunohistochemical staining (Figure 3.5)

$CD3^+$, $CD4^+$ and $FoxP3^+$ cell densities were higher in all the malignant tumours (PDAC, CC, AC) with adverse prognosis (Coupland, Kocher et al. 2012) (Figure 3.7). Conversely, the density of $CD8^+$ T-cells infiltrate for PDAC was comparable to chronic pancreatitis and was lesser as compared to AC and CC. This defect in infiltration of cytotoxic T-cells has been observed in experimental animal studies for PDAC (Clark, Hingorani et al. 2007; Bayne, Beatty et al. 2012; Pylayeva-Gupta, Lee et al. 2012). In contrast, the infiltrate of other immune cells in PDAC was similar to the other malignant Pancreatico-biliary tumours. For the first time ever, we have looked at the defect in immune cell infiltration in a large cohort of PDAC patients compared with other pancreatico-biliary diseases.

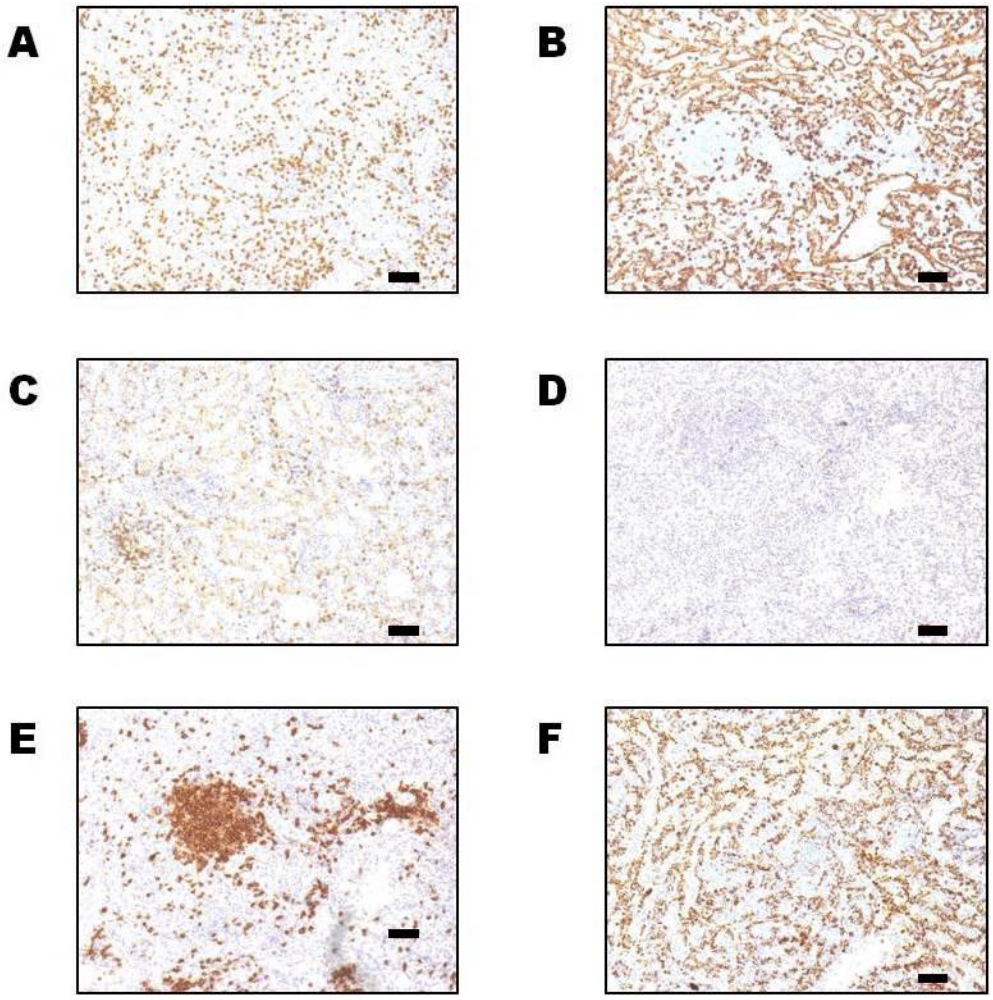

Figure 3.5 Immune cell positive controls with normal spleen

Each TMA core had a core consisting of normal spleen that served both as a positive and internal control during each immunohistochemistry staining. From the top: (A) T-cells, $CD3^+$; (B) helper T-cells, $CD4^+$; (C) cytotoxic T-cells, $CD8^+$; (D) regulatory T-cells, $FoxP3^+$; (E) B-cells, $CD20^+$; (F) macrophages, $CD68^+$.

Scale 50µm. Magnification 10x.

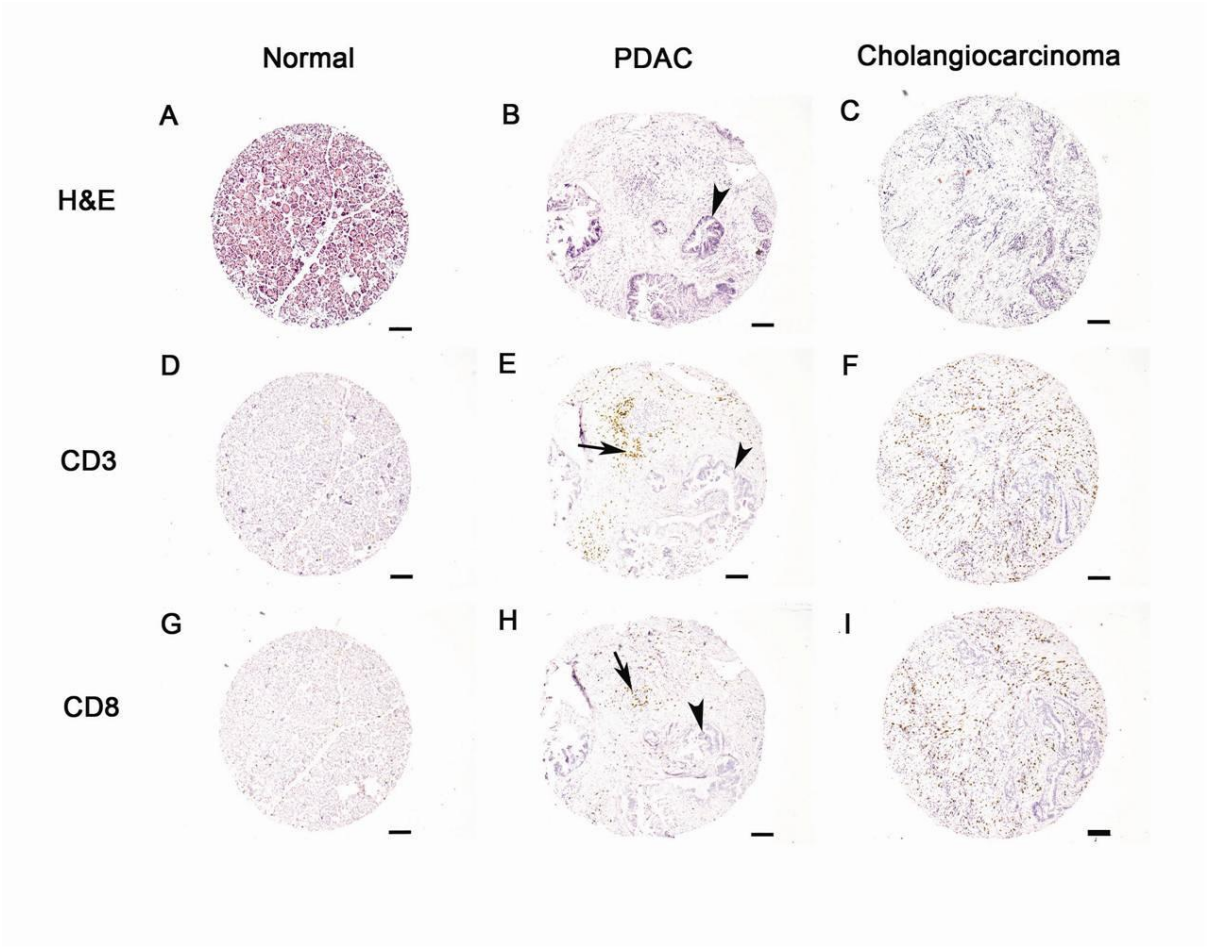

Figure 3.6: Immune cell distribution in patients with normal histology, PDAC and cholangiocarcinoma.

The panel shows representative H&E, $CD3^+$ and $CD8^+$ immunohistochemistry images of normal (A, D, G), PDAC (B, E, H) and cholangiocarcinoma (C, F, I) TMA cores. The arrow heads point at tumours and arrows at positively stained immune cells. Fewer $CD3^+$ and $CD8^+$ T-cells can be observed in normal cores. In PDAC, $CD3^+$ and $CD8^+$ T-cells are seen to aggregate in the panstroma, away from the juxtatumoural stroma. $CD3^+$ and $CD8^+$ are seen to be dispersed all over cholangiocarcinoma tissues. All T-cells are sequestered in the panstromal compartment where they appear to be in close association with stellate cells.

Scale bars: 100μm; Magnification 10x.

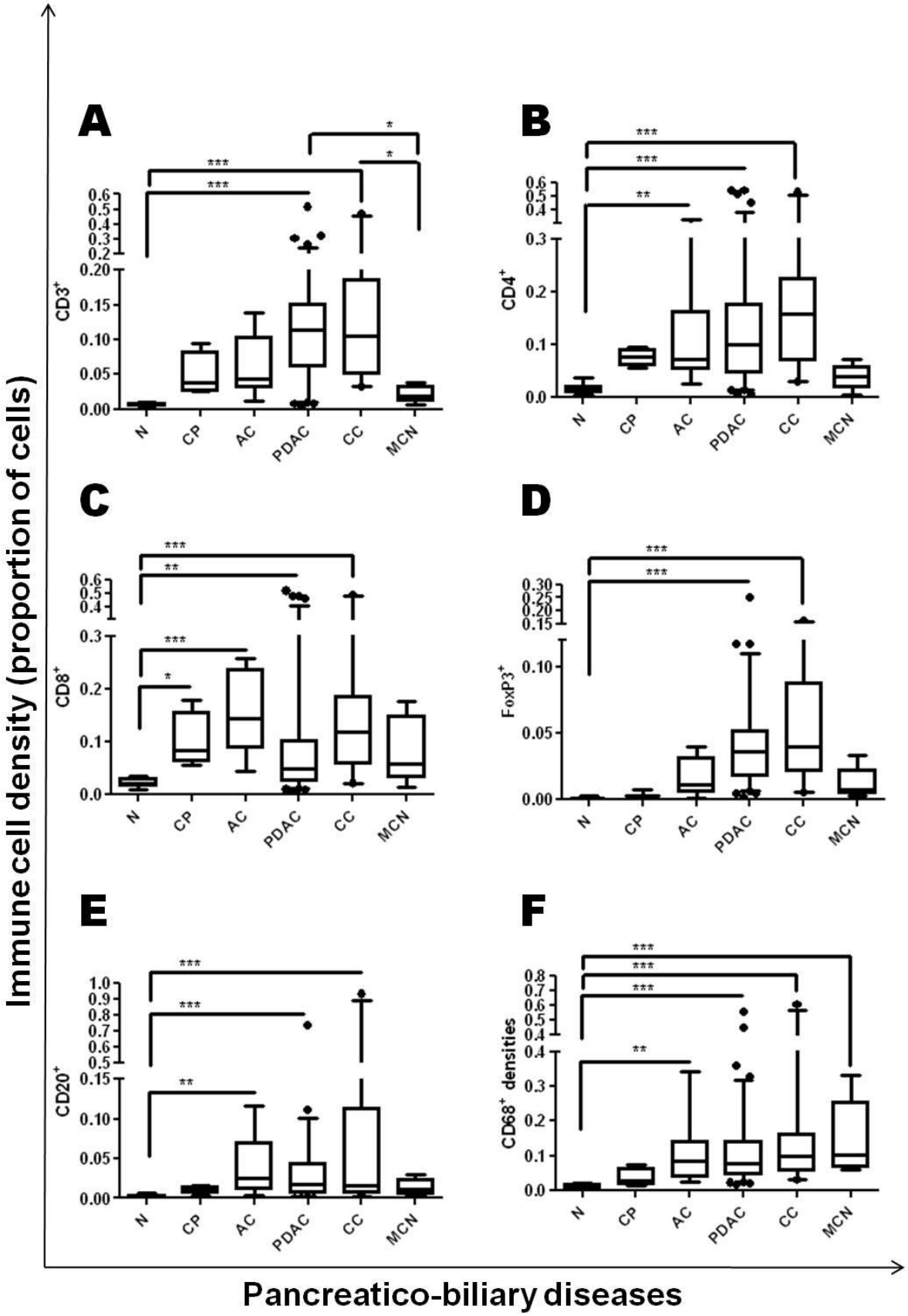
A
B
C
D
E
F
CD3+
CD4+
CD8+
FoxP3+
CD20+
CD68+ densities
N
CP
AC
PDAC
CC
MCN
Immune cell density (proportion of cells)
Pancreatico-biliary diseases

Figure 3.7 Immune cell infiltrate in human pancreatico-biliary diseases

Immune cells (T-cells, $CD3^+$(A), helper T-cells, $CD4^+$(B), cytotoxic T-cells, $CD8^+$(C), , $CD20^+$(D), regulatory T-cells, $FoxP3^+$(E), and macrophages, $CD68^+$(F)) infiltrates were measured in pancreatico-biliary diseases (chronic pancreatitis (CP), mucinous cystic neoplasms (MCN), ampullary carcinoma (AC), pancreatic ductal adenocarcinoma (PDAC), cholangiocarcinoma (CC)) and normal tissues (N) using Ariol software.

Box (median with interquartile ranges (25^{th} and 75^{th})) and whisker (5^{th} and 95^{th} percentiles) plots (outliers are represented by individual dots) demonstrate that all diseases demonstrate varied density and profile of immune infiltrate suggesting disease-specific responses of the immune system. Cholangiocarcinoma patients have the densest immune infiltrate and this may be related to biliary tract infection and/or intervention close to the tumour prior to resection. Inflammatory conditions (CP) and borderline neoplasms (MCN) have less immune infiltrate than all cancers.

Kruskal-Wallis p value< 0.0001 for all immune cells. Dunn's post test was used to compare columns. *** p< 0.001; ** p= 0.001 to 0.01; * p= 0.01 to 0.05;

Number (range) of patients for the whole chart: Normal (11-14), chronic pancreatitis (4), mucinous cystic neoplasms (6), ampullary carcinoma (9), pancreatic ductal adenocarcinoma (93-98), and cholangiocarcinoma (21).

3.5 Differential immune cell infiltrate in stromal sub-compartments of PDAC

Of the T-cell subsets, we observed sequestration in the panstromal compartment of regulatory T-cells ($Foxp3^+$, (Figure 3.11)) and cytotoxic T-cells ($CD8^+$, (Figure 3.10)), whereas helper T-cells ($CD4^+$, (Figure 3.9)) infiltrated the juxtatumoural compartment confirming our observations of $CD8^+$ and $CD4^+$ infiltration in whole tissue sections. Other immune cells that were equally sequestrated by the panstromal compartment included B-cells ($CD20^+$, (Figure 3.12)) and natural killer cells ($CD56^+$, (Figure 3.13)). By contrast macrophages ($CD68^+$, (Figure 3.14)) and neutrophils ($myeloperoxidase^+$ (Figure 3.15)) infiltrated the juxtatumoural compartment and were often seen in pancreatic ductal spaces. The observation of $CD68^+$ macrophages infiltrating the juxtatumoural compartment has previously been reported (Ricci, Kern et al. 2005) and neutrophil infiltration of the juxtatumoural compartment in TMAs also supported our observation of Neutrophil infiltration in whole tissue sections with $CD15^+$ staining.

The differential immune cell infiltration observed in PDAC could plausibly be attributed to a defect in the circulation of immune cells in the blood or a defect in their tissue migration. Hence to investigate the role that immune cell circulation might have in the differential immune cell infiltrate to the tumour of PDAC patients we calculated for associations between macrophages ($CD68^+$), T-cells ($CD3^+$), neutrophils ($myeloperoxidase^+$) and circulating monocytes, lymphocytes and neutrophils respectively. We found there were no correlations between circulating immune cells and the densities of same immune cells in the whole tissue, juxtatumoural stroma or panstromal compartments (Figures 3.18- 3.20); hence

eliminating a defect in immune cell circulation as a potential reason for the differential immune infiltrate.

In a separate TMA analysis of immune cell infiltration in advanced PDAC patients (Figure 3.16 and 3.17), T-cells ($CD3^+$), cytotoxic T-cells ($CD8^+$), helper T-cells ($CD4^+$) and B-cells ($CD20^+$) were sequestered in the panstromal compartment and did not infiltrate the juxtatumoural compartment, whereas, T regulatory cells ($FoxP3^+$), and Macrophages ($CD68^+$) had equal densities in both the juxtatumoural and panstromal compartments and as such infiltrated the juxtatumoural compartment. This indicates that immune infiltrate defects of cytotoxic T-cells and B-cells are a feature of PDAC regardless of disease progression as they are both present in early and advanced stage PDAC. While macrophage density between stromal compartments lost significance, the density was almost doubled.

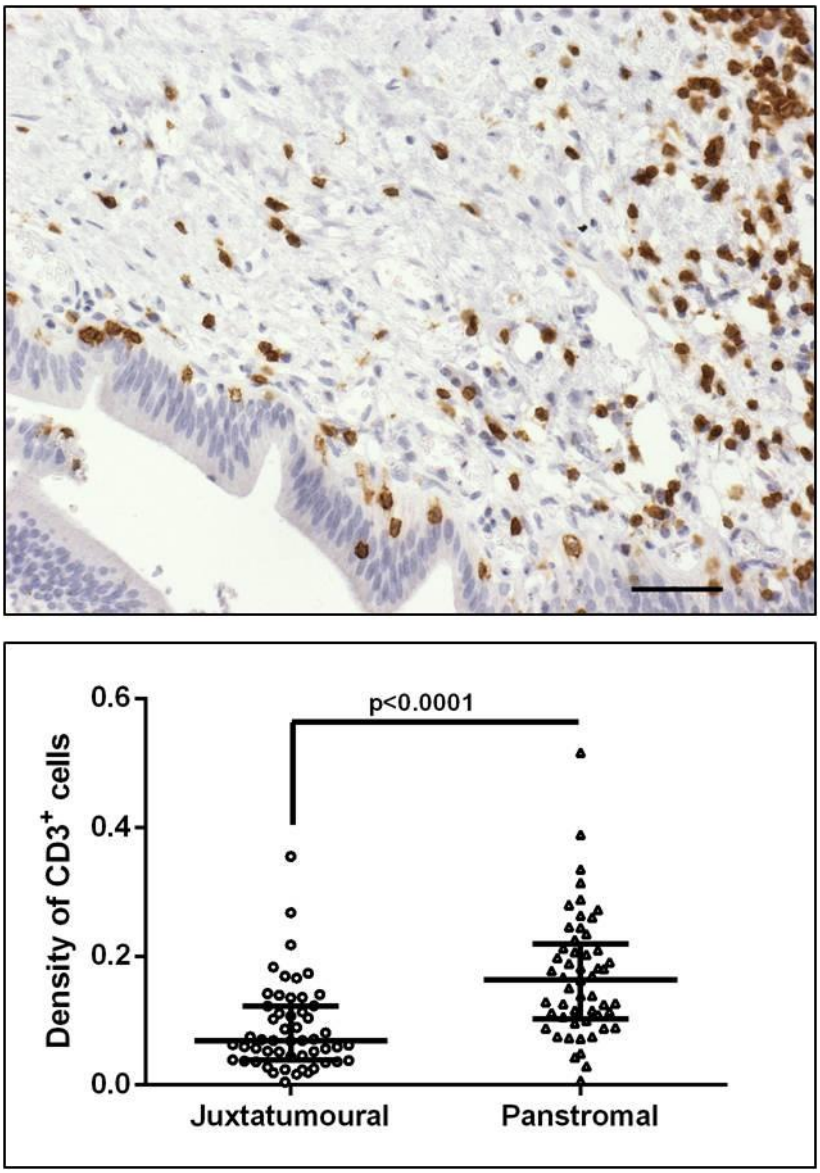

Figure 3.8: Stromal compartment specific $CD3^+$ cell infiltration in human PDAC

Direct comparison of stromal compartments ('juxtatumoural' defined as within 100μm of tumour and the rest of the tumour stroma as 'panstromal') demonstrate a defect in $CD3^+$ (T-cell) infiltration as evidenced by the significantly higher density in the panstromal compartment compared to juxtatumoural compartment.

Each data point represents a single patient (median scores of all TMA cores (n=6)). Lines represent median with inter-quartile ranges (25^{th} and 75^{th}).

Mann Whitney U test; p-values are two-tailed. Scale bars 100μm.

Number of patients: 53.

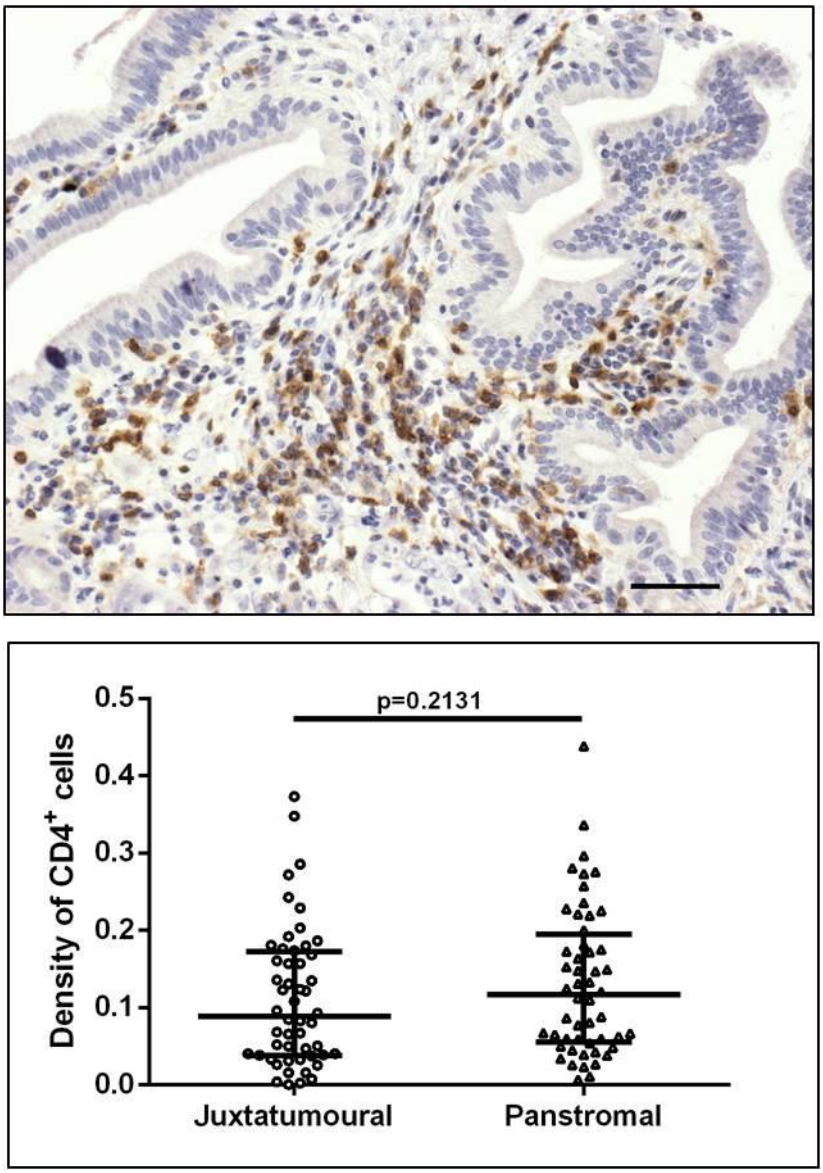

Figure 3.9: Stromal compartment specific $CD4^+$ T-cell infiltration in human PDAC

Direct comparison of stromal compartments ('juxtatumoural' defined as within 100μm of tumour and the rest of the tumour stroma as 'panstromal') demonstrate no defect in $CD4^+$ (helper T-cell) infiltration as evidenced by the equal densities in the panstromal and juxtatumoural compartments.

Each data point represents a single patient (median scores of all TMA cores (n=6)). Lines represent median with inter-quartile ranges (25^{th} and 75^{th}).

Mann Whitney U test; p-values are two-tailed. Scale bars 100μm.

Number of patients: 52

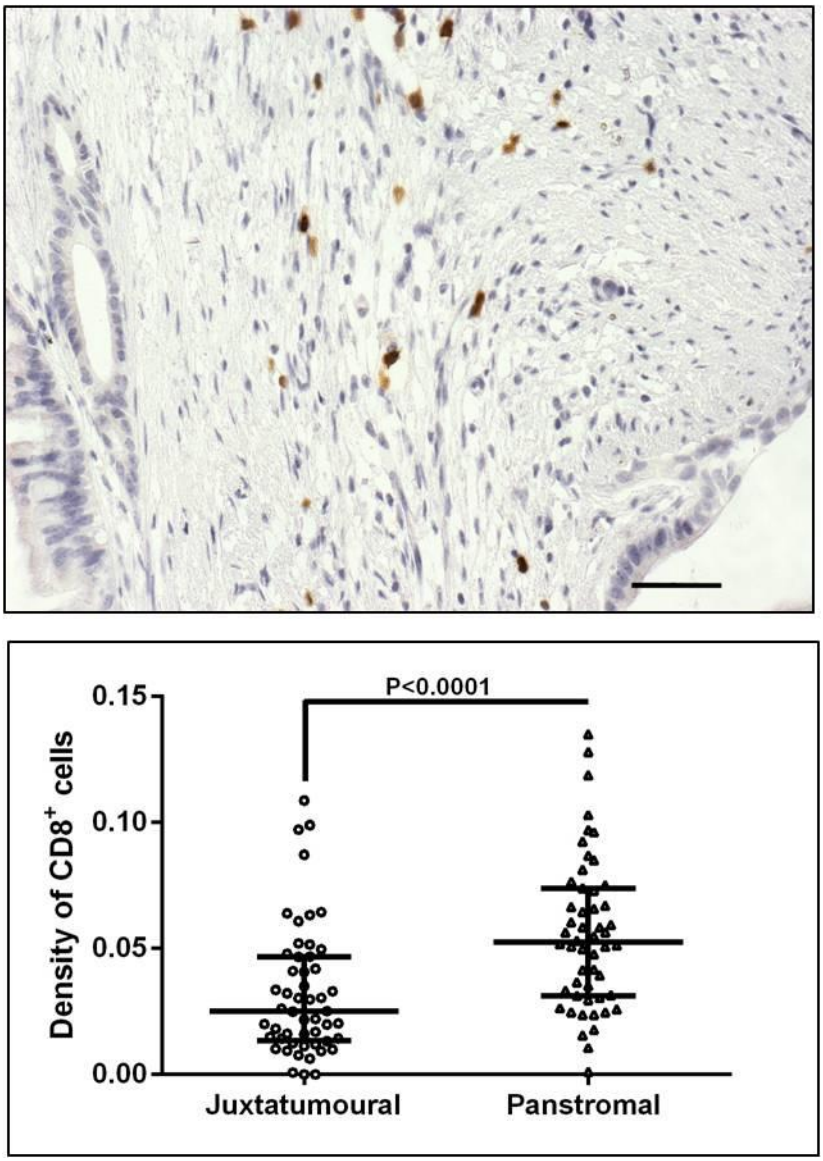

Figure 3.10: Stromal compartment specific $CD8^+$ T-cell infiltration in human PDAC

Direct comparison of stromal compartments ('juxtatumoural' defined as within 100μm of tumour and the rest of the tumour stroma as 'panstromal') demonstrate a defect in $CD8^+$ (cytotoxic T-cell) infiltration as evidenced by the significantly higher density in the panstromal compartment compared to juxtatumoural compartment.

Each data point represents a single patient (median scores of all TMA cores (n=6)). Lines represent median with inter-quartile ranges (25^{th} and 75^{th}).

Mann Whitney U test; p-values are two-tailed. Scale bars 100μm.

Number of patients: 52.

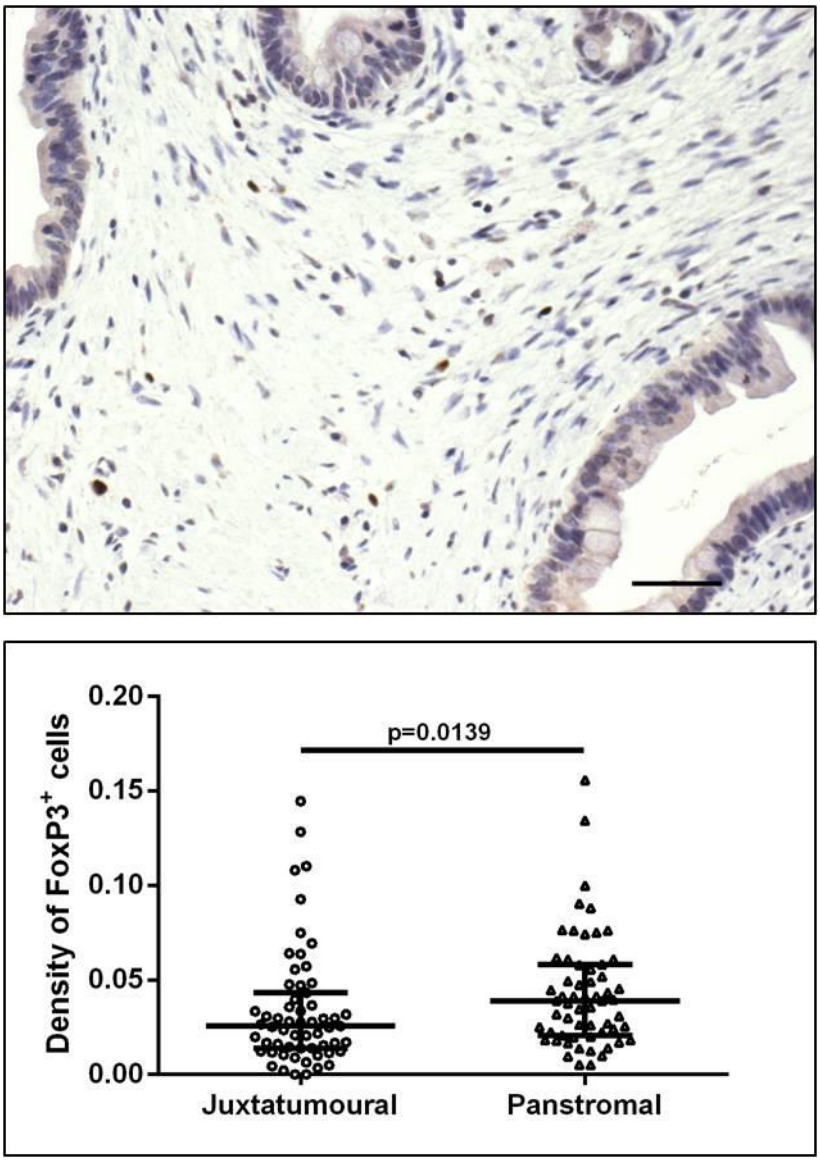

Figure 3.11: Stromal compartment specific FoxP3$^+$ cell infiltration in human PDAC

Direct comparison of stromal compartments ('juxtatumoural' defined as within 100µm of tumour and the rest of the tumour stroma as 'panstromal') demonstrate a defect in FoxP3$^+$ (T regulatory cell) infiltration as evidenced by the significantly higher density in the panstromal compartment compared to juxtatumoural compartment.

Each data point represents a single patient (median scores of all TMA cores (n=6)). Lines represent median with inter-quartile ranges (25th and 75th).

Mann Whitney U test; p-values are two-tailed. Scale bars 100µm.

Number of patients: 59.

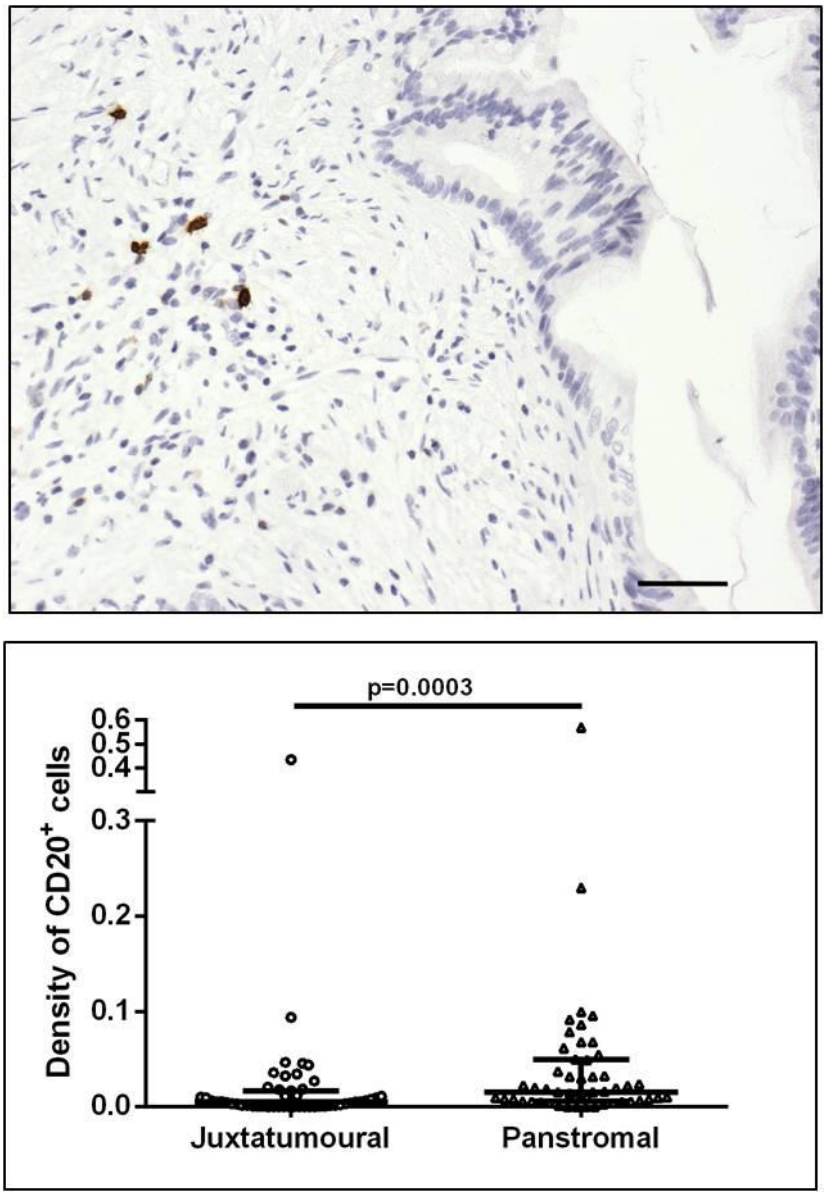

Figure 3.12 Stromal compartment specific CD20$^+$ cell infiltration in human PDAC

Direct comparison of stromal compartments ('juxtatumoural' defined as within 100µm of tumour and the rest of the tumour stroma as 'panstromal') demonstrate a defect in CD20$^+$ (B-cell) infiltration as evidenced by the significantly higher density in the panstromal compartment compared to juxtatumoural compartment.

Each data point represents a single patient (median scores of all TMA cores (n=6)). Lines represent median with inter-quartile ranges (25th and 75th).

Mann Whitney U test; p-values are two-tailed. Scale bars 100µm.

Number of patients: 51.

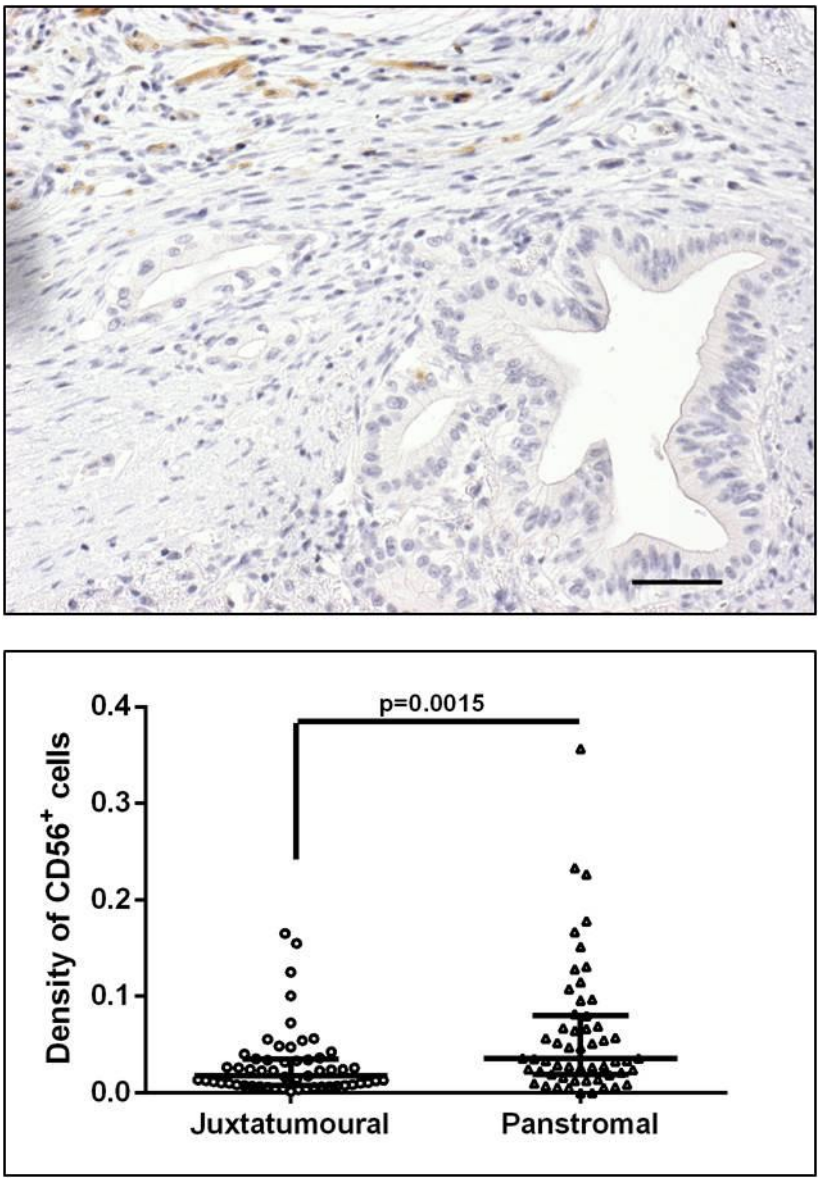

Figure 3.13 Stromal compartment specific CD56$^+$ cell infiltration in human PDAC

Direct comparison of stromal compartments ('juxtatumoural' defined as within 100μm of tumour and the rest of the tumour stroma as 'panstromal') demonstrate a defect in CD56$^+$ (Natural killer cell) infiltration as evidenced by the significantly higher density in the panstromal compartment compared to juxtatumoural compartment.

Each data point represents a single patient (median scores of all TMA cores (n=6)). Lines represent median with inter-quartile ranges (25th and 75th).

Mann Whitney U test; p-values are two-tailed. Scale bars 100μm.

Number of patients: 55.

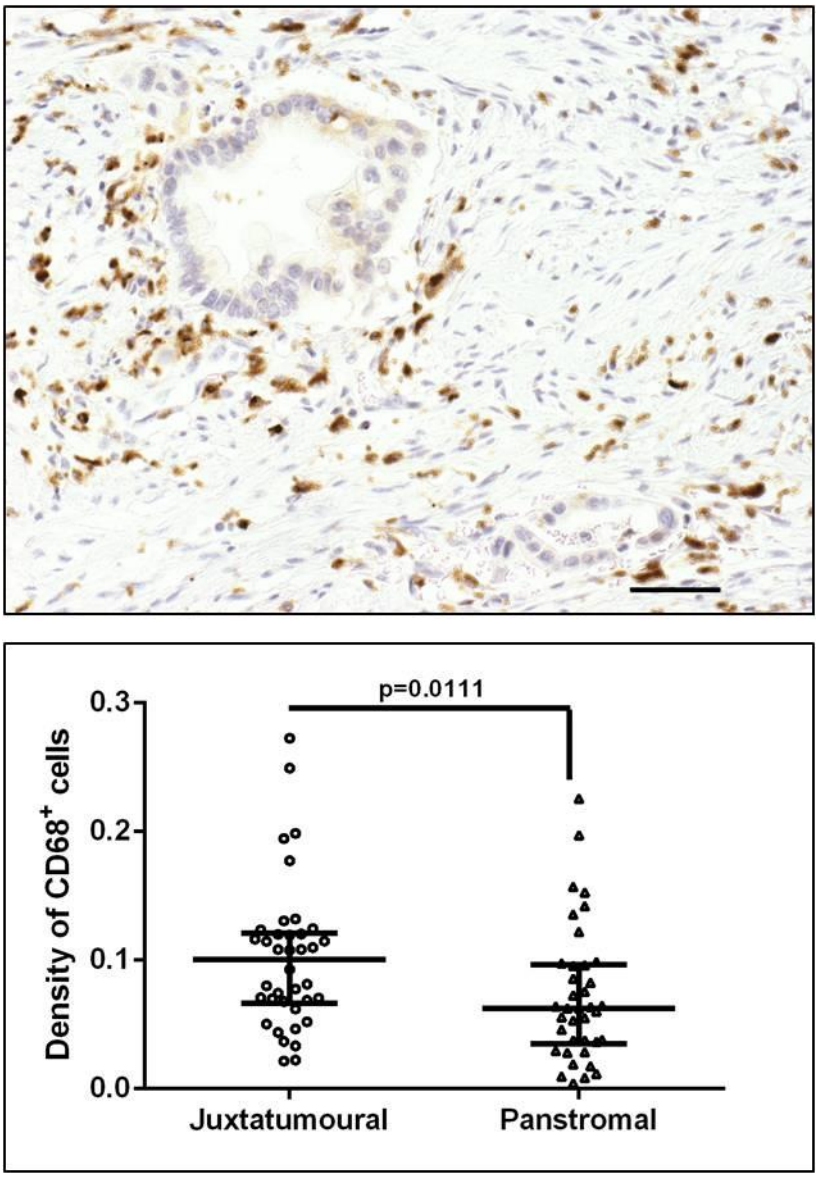

Figure 3.14 Stromal compartment specific CD68$^+$ cell infiltration in human PDAC

Direct comparison of stromal compartments ('juxtatumoural' defined as within 100µm of tumour and the rest of the tumour stroma as 'panstromal') demonstrate an infiltration of CD68$^+$ (Macrophages), evidenced by the significantly higher density in the juxtatumoural compartment compared to panstromal compartment.

Each data point represents a single patient (median scores of all TMA cores (n=6)). Lines represent median with inter-quartile ranges (25th and 75th).

Mann Whitney U test; p-values are two-tailed. Scale bars 100µm.

Number of patients: 52.

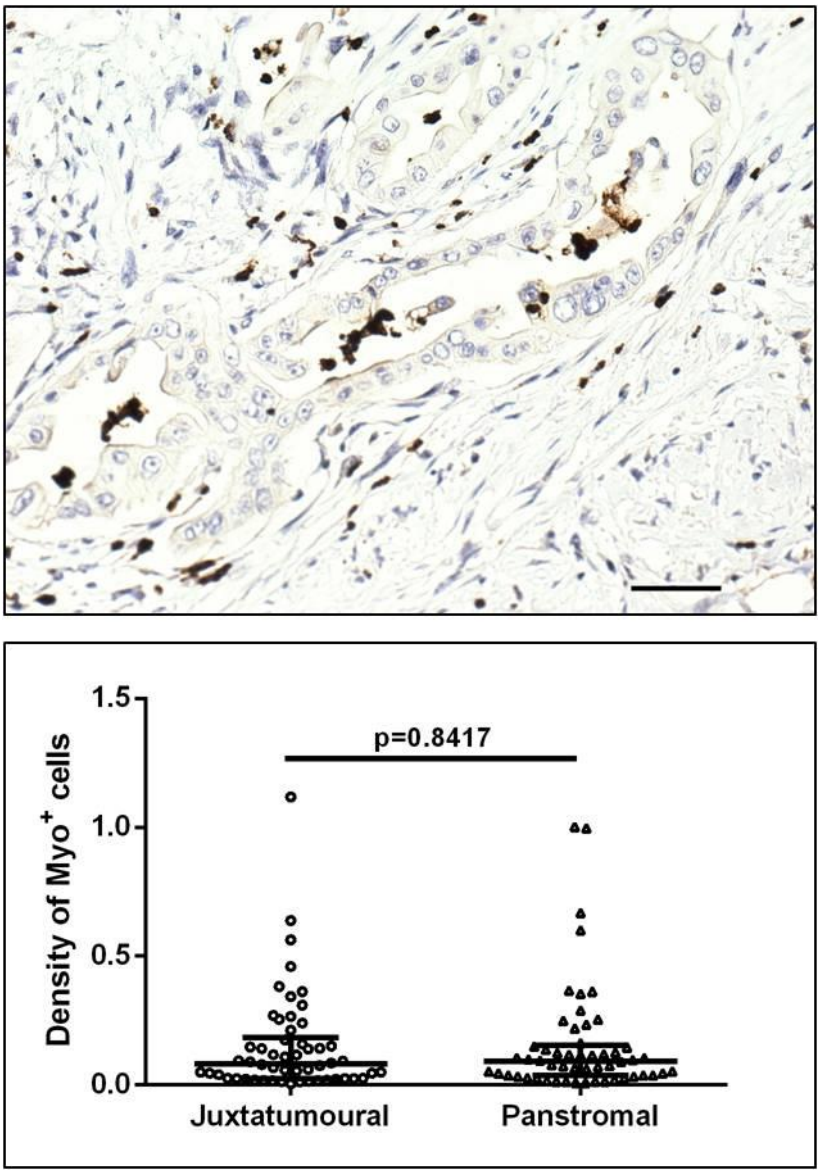

Figure 3.15 Stromal compartment specific Myeloperoxidase^{+} cell infiltration in human PDAC

Direct comparison of stromal compartments ('juxtatumoural' defined as within 100μm of tumour and the rest of the tumour stroma as 'panstromal') demonstrate no defect in myeloperoxidase^{+} (Neutrophils) infiltration as evidenced by the equal densities in the panstromal and juxtatumoural compartments.

Each data point represents a single patient (median scores of all TMA cores (n=6)). Lines represent median with inter-quartile ranges (25th and 75th).

Mann Whitney U test; p-values are two-tailed. Scale bars 100μm.

Number of patients: 54.

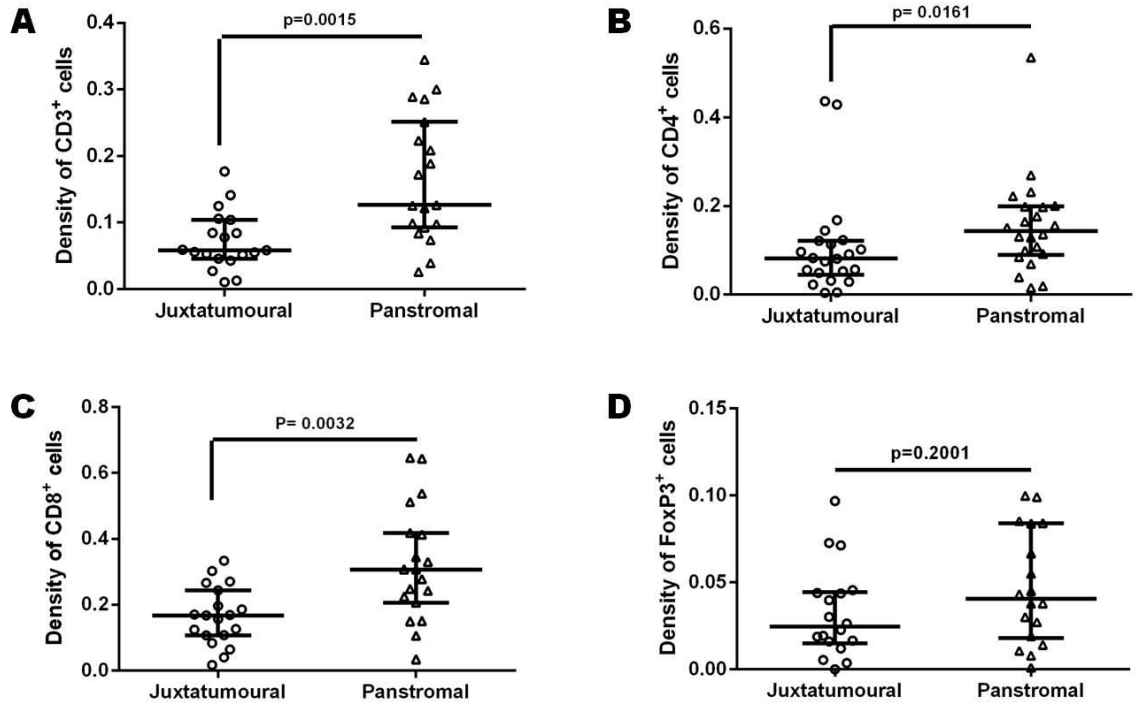

Figure 3.16: Stromal compartment specific T-cell infiltration in an independent cohort of advanced PDAC patients

Immune cells were stained and analyzed. This cohort was formed predominantly of patients with metastatic disease (TMA B); therefore, these tissues were obtained from biopsy specimens.

There was a defect in infiltration of T-cells ($CD3^+$ (A)), helper T-cells ($CD4^+$ (B)) and cytotoxic T-cells ($CD8^+$, (C)) but not in infiltration of T regulatory cells ($FoxP3^+$ (D)) suggesting that $FoxP3^+$ cells can access the tumour cells. $CD8^+$ findings are consistent with the primary cohort of patients suggesting that the exclusion of this immune cell from the immediate tumour microenvironment is consistent throughout the disease progression.

Mann Whitney U test; p-values are two-tailed.Number of patients analyzed for each marker: $CD3^+$ (n= 19), $CD4^{+,}$ (n= 22), $CD8^+$ (n=19) and $FoxP3^+$, (n= 18).

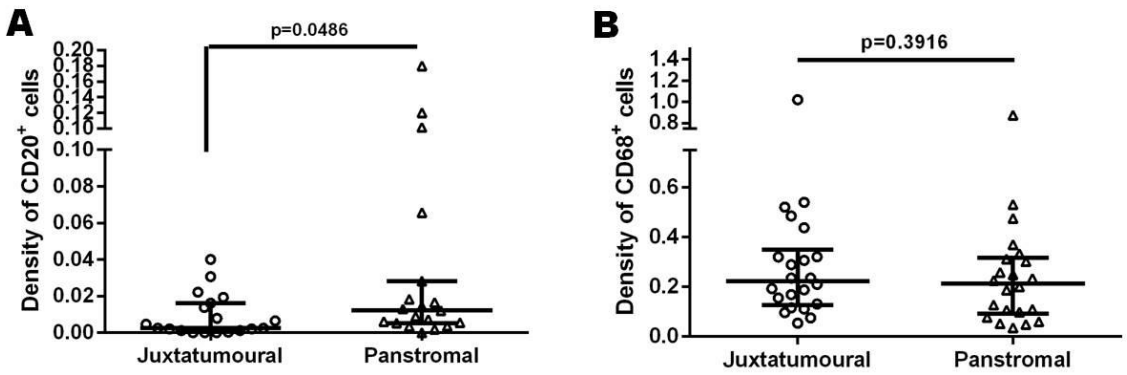

Figure 3.17: Stromal compartment specific immune cell infiltration in an independent cohort of advanced PDAC patients

Immune cells were stained and analyzed. This cohort was formed predominantly by patients with metastatic disease (TMA B); therefore, these tissues were obtained from biopsy specimens.

There is a defect in infiltration of B-cells ($CD20^+$, (A)) which is consistent with the primary cohort of patients suggesting that the exclusion of this immune cell from the immediate tumour microenvironment is consistent throughout the disease progression (similar to cytotoxic T-cells ($CD8^+$)). In contrast, macrophages ($CD68^+$ (B)) were not significant suggesting that they access tumour cells.

Mann Whitney U test; p-values are two-tailed.

Number of patients analyzed for each marker: $CD20^+$ (n= 19) and $CD68^+$ (n= 22)

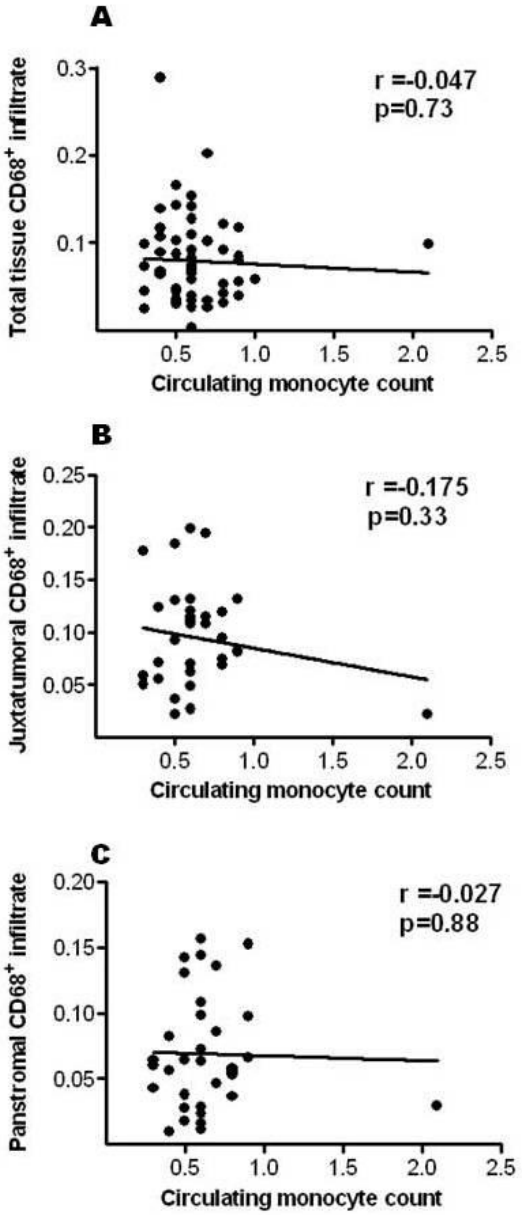

Figure 3.18: Correlation of circulating Monocytes with CD68$^+$ infiltrate in patients with PDAC (Figure provided by Dr. J Watt).

Correlation plots were constructed for circulating Monocytes and the CD68$^+$ immune cell infiltrate in whole tumour-stroma (A) and in distinct stromal compartments: juxtatumoural compartment (B) and panstromal compartment (C) in the PDAC patients. There was no correlation between these counts. Each data point represents one unique patient and the correlation line was plotted as shown with the values representing Pearson's Correlation Coefficient 'r' and the respective p-value.

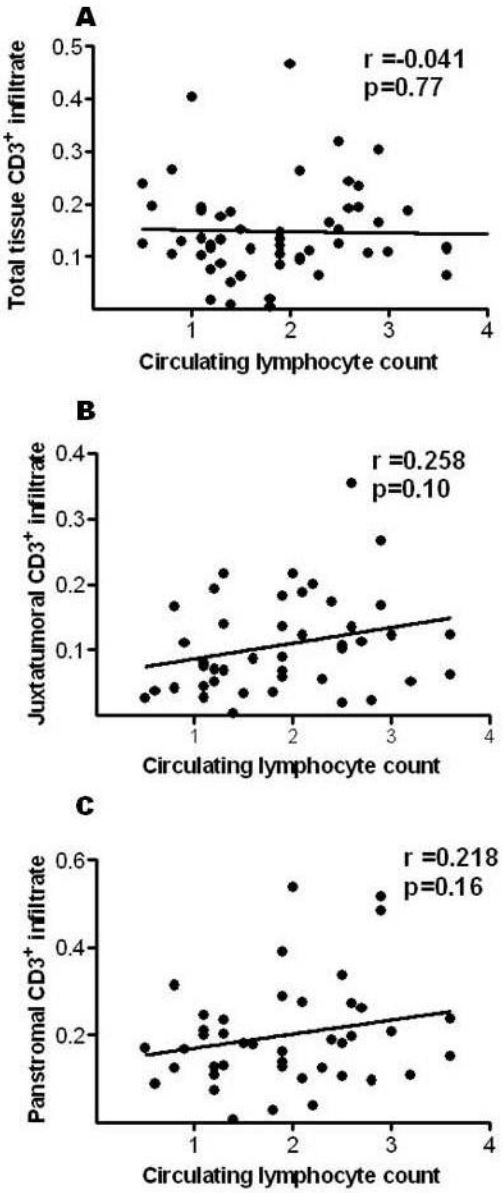

Figure 3.19: Correlation of circulating lymphocytes with CD3$^+$ infiltrate in patients with PDAC (Figure provided by Dr. J Watt).

Correlation plots were constructed for circulating lymphocytes and the CD3$^+$ immune cell infiltrate in whole tumour-stroma (A) and in distinct stromal compartments: juxtatumoural compartment (B) and panstromal compartment (C) in the PDAC patients. There was no correlation between these counts. Each data point represents

one unique patient and the correlation line was plotted as shown with the values representing Pearson's Correlation Coefficient 'r' and the respective p-value.

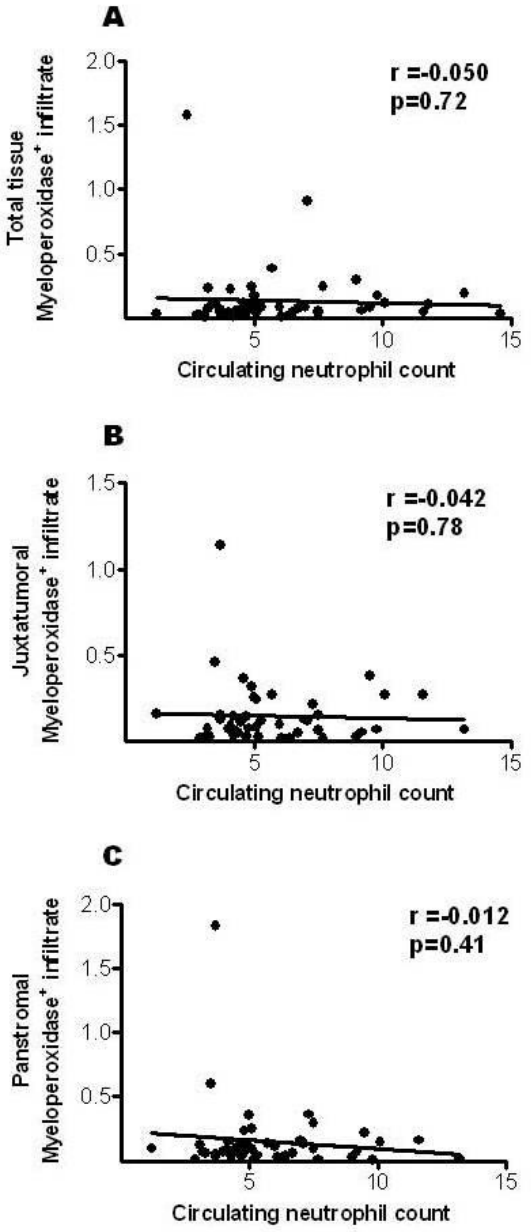

Figure 3.20: Correlation of circulating neutrophils with Myeloperoxidase$^+$ immune cell infiltrate in patients with PDAC (Figure provided by Dr. J Watt).

Correlation plots were constructed for circulating neutrophils and the Myeloperoxidase$^+$ immune cell infiltrate in whole tumour-stroma (A) and in distinct stromal compartments: juxtatumoural compartment (B) and panstromal compartment (C) in the PDAC patients. There was no correlation between these counts. Each data point represents one unique patient and the correlation line was plotted as shown

with the values representing Pearson's Correlation Coefficient 'r' and the respective p-value.

3.6 Differential immune cell infiltrate in stromal sub-compartments of other pancreatico-biliary cancers

Contrary to our observations of differential immune infiltrate in stromal sub-compartments in PDAC, we observed non-differential immune cell infiltrate (T-cells ($CD3^+$), helper T-cell ($CD4^+$), cytotoxic T-cell ($CD8^+$), T regulatory cell ($FoxP3^+$), B-cells ($CD20^+$) and macrophages ($CD68^+$)) in the stromal sub-compartments of ampullary carcinoma (Figures 3.21-3.26), cholangiocarcinoma (Figures 3.27-3.32), mucinous cystic neoplasm (Figures 3.33-3.38) and duodenal carcinoma (Figures 3.39-3.44).

This supports our earlier conclusion that differential immune cell infiltrate in stromal sub-compartments is specific to PDAC.

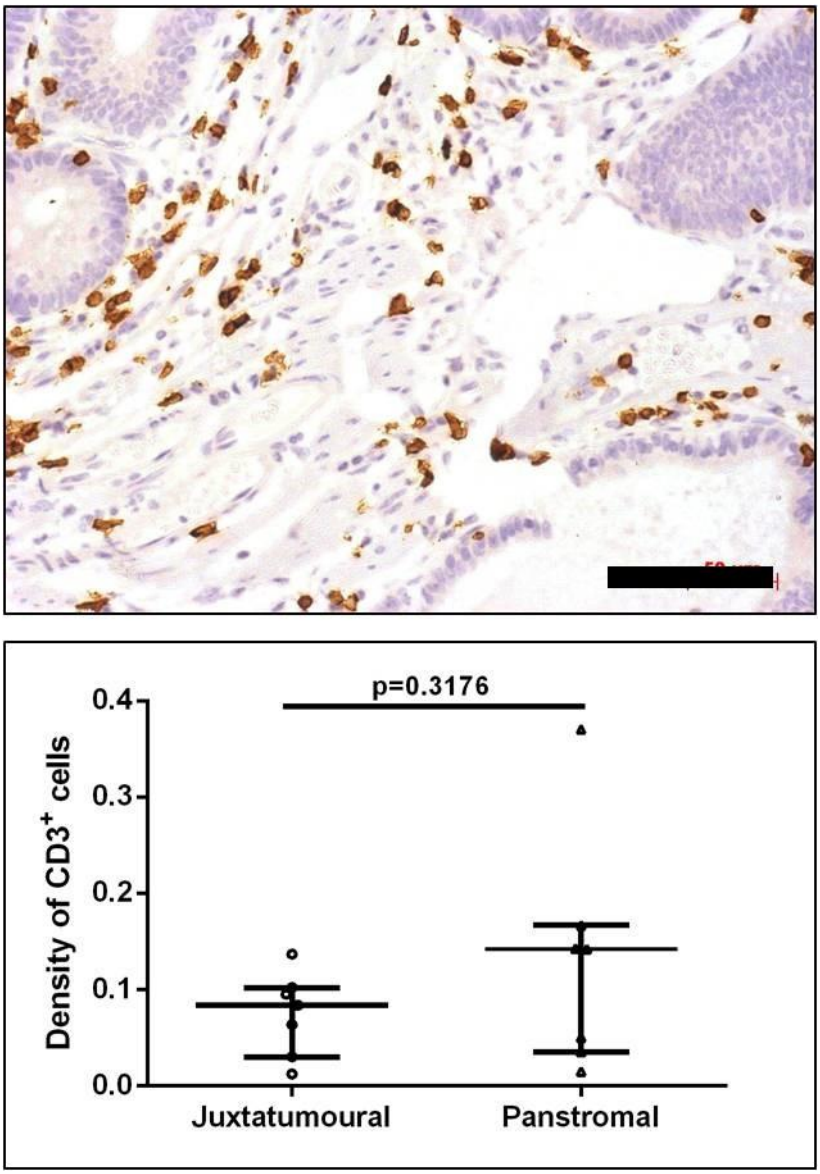

Figure 3.21 Stromal compartment specific $CD3^+$ cell infiltration in human ampullary carcinoma

Direct comparison of stromal compartments ('juxtatumoural' defined as within 100µm of tumour and the rest of the tumour stroma as 'panstromal') demonstrate no defect in $CD3^+$ (T-cell) infiltration as evidenced by the equal densities in the panstromal and juxtatumoural compartments.

Each data point represents a single patient (median scores of all TMA cores (n=6)). Lines represent median with inter-quartile ranges (25^{th} and 75^{th}).

Mann Whitney U test; p-values are two-tailed. Scale bars 100µm.

Number of patients: 7.

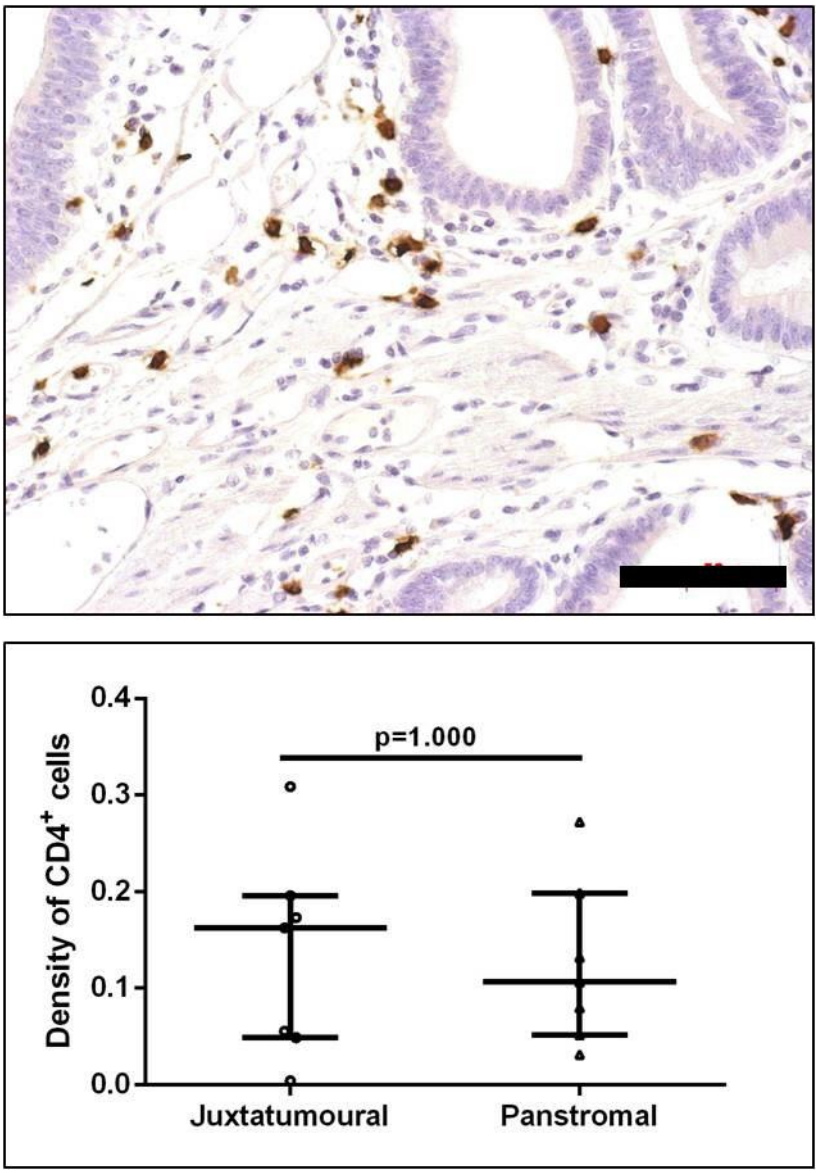

Figure 3.22 Stromal compartment specific $CD4^+$ cell infiltration in human ampullary carcinoma

Direct comparison of stromal compartments ('juxtatumoural' defined as within 100μm of tumour and the rest of the tumour stroma as 'panstromal') demonstrate no defect in $CD4^+$ (helper T-cell) infiltration as evidenced by the equal densities in the panstromal and juxtatumoural compartments.

Each data point represents a single patient (median scores of all TMA cores (n=6)). Lines represent median with inter-quartile ranges (25^{th} and 75^{th}).

Mann Whitney U test; p-values are two-tailed. Scale bars 100μm.

Number of patients: 7.

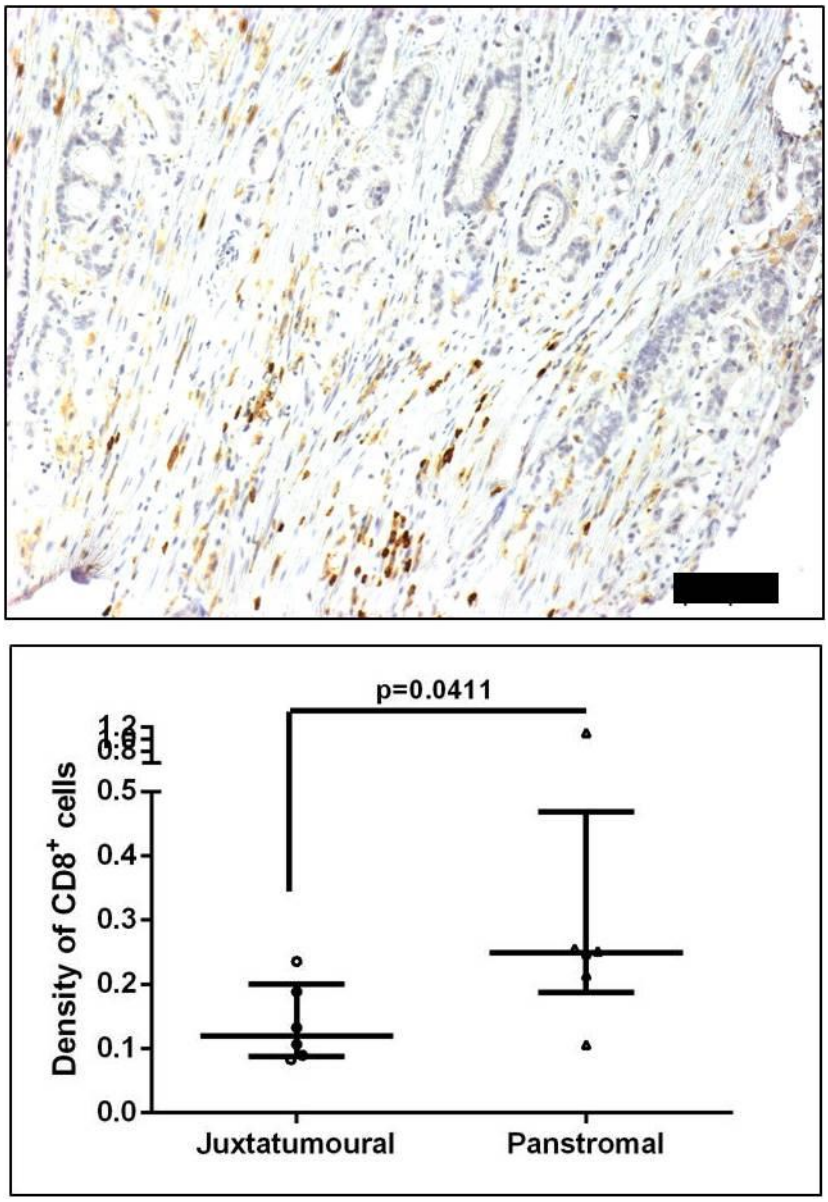

Figure 3.23 Stromal compartment specific $CD8^+$ cell infiltration in human ampullary carcinoma

Direct comparison of stromal compartments ('juxtatumoural' defined as within 100µm of tumour and the rest of the tumour stroma as 'panstromal') demonstrate a defect in $CD8^+$ (cytotoxic T-cell) infiltration as evidenced by the significant density in the panstromal compartment compared to the juxtatumoural compartments.

Each data point represents a single patient (median scores of all TMA cores (n=6)). Lines represent median with inter-quartile ranges (25^{th} and 75^{th}).

Mann Whitney U test; p-values are two-tailed. Scale bars 100µm.

Number of patients: 6.

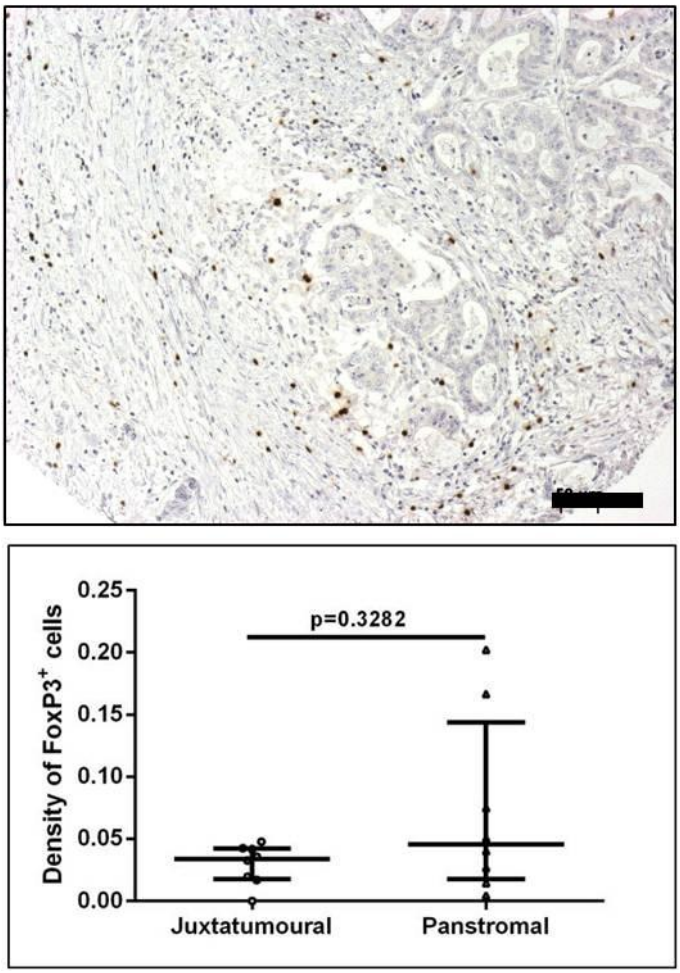

Figure 3.24 Stromal compartment specific FoxP3$^+$ cell infiltration in human ampullary carcinoma

Direct comparison of stromal compartments ('juxtatumoural' defined as within 100µm of tumour and the rest of the tumour stroma as 'panstromal') demonstrate no defect in FoxP3$^+$ (T regulatory cell) infiltration as evidenced by the equal densities in the panstromal and juxtatumoural compartments.

Each data point represents a single patient (median scores of all TMA cores (n=6)). Lines represent median with inter-quartile ranges (25th and 75th).

Mann Whitney U test; p-values are two-tailed. Scale bars 100µm.

Number of patients: 8.

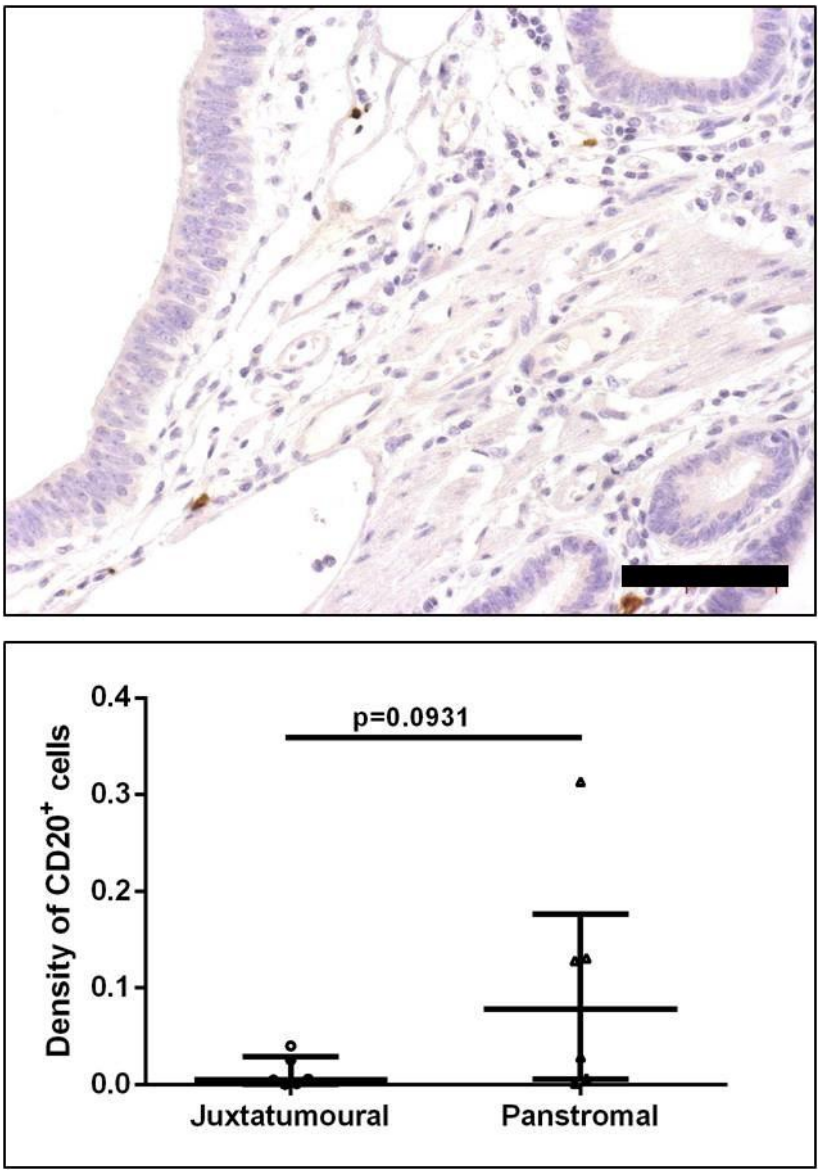

Figure 3.25 Stromal compartment specific $CD20^+$ cell infiltration in human ampullary carcinoma

Direct comparison of stromal compartments ('juxtatumoural' defined as within 100μm of tumour and the rest of the tumour stroma as 'panstromal') demonstrate no defect in $CD20^+$ (B-cell) infiltration as evidenced by the equal densities in the panstromal and juxtatumoural compartments.

Each data point represents a single patient (median scores of all TMA cores (n=6)). Lines represent median with inter-quartile ranges (25^{th} and 75^{th}).

Mann Whitney U test; p-values are two-tailed. Scale bars 100μm.

Number of patients: 6.

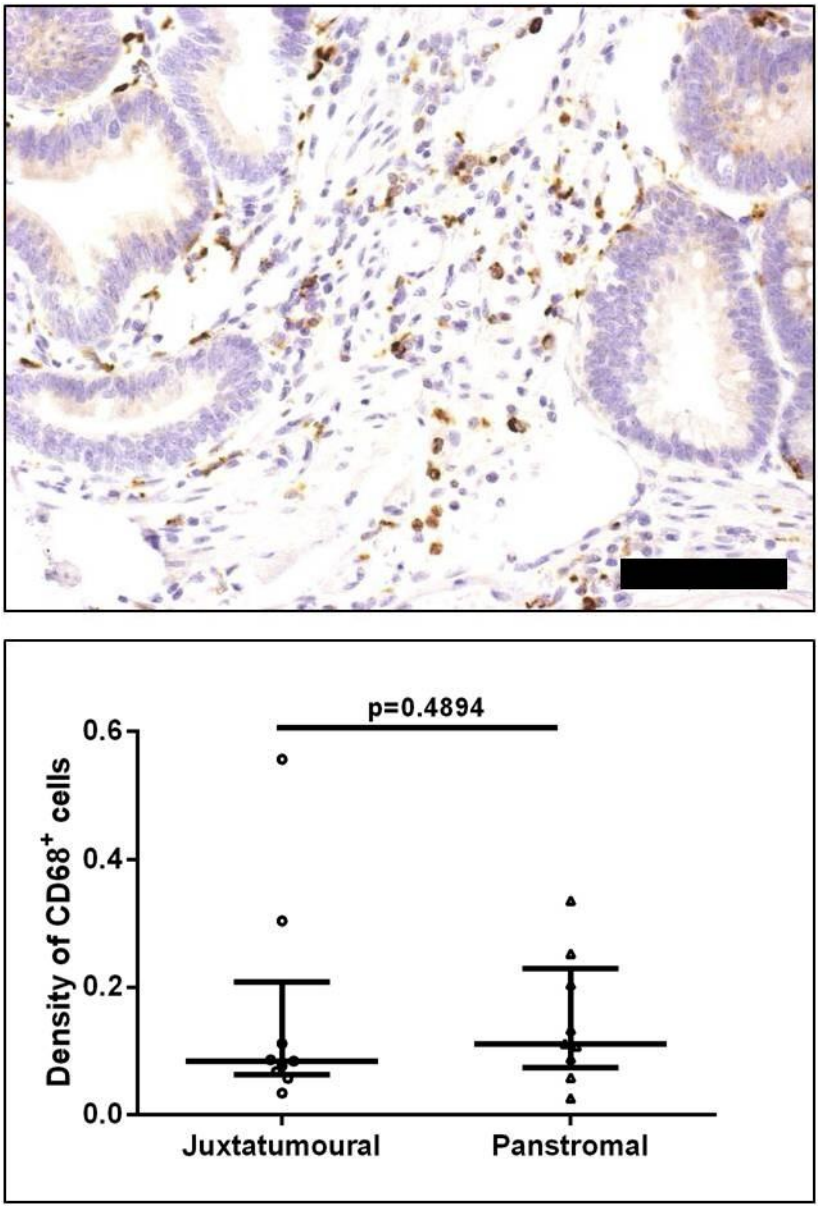

Figure 3.26 Stromal compartment specific CD68$^+$ cell infiltration in human ampullary carcinoma

Direct comparison of stromal compartments ('juxtatumoural' defined as within 100µm of tumour and the rest of the tumour stroma as 'panstromal') demonstrate no defect in CD68$^+$ (Macrophages) infiltration as evidenced by the equal densities in the panstromal and juxtatumoural compartments.

Each data point represents a single patient (median scores of all TMA cores (n=6)). Lines represent median with inter-quartile ranges (25th and 75th).

Mann Whitney U test; p-values are two-tailed. Scale bars 100µm.

Number of patients: 9.

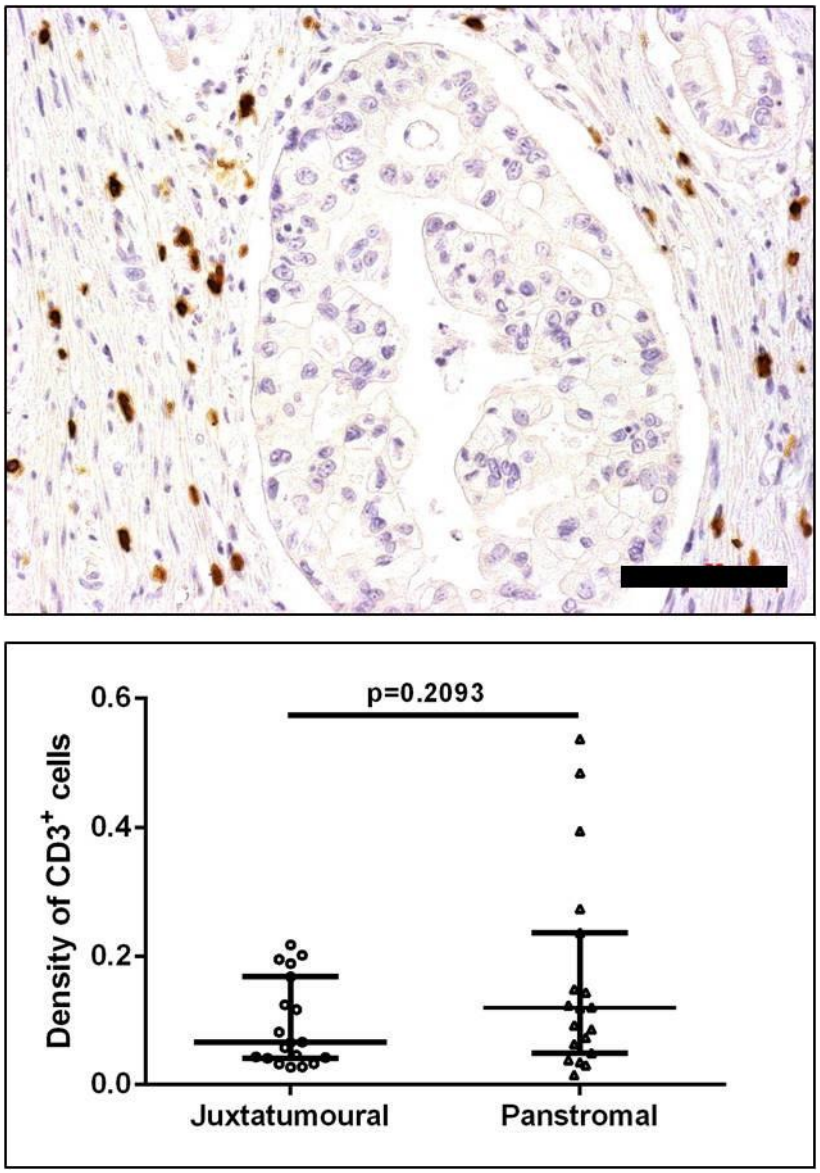

Figure 3.27 Stromal compartment specific $CD3^+$ cell infiltration in human cholangiocarcinoma

Direct comparison of stromal compartments ('juxtatumoural' defined as within 100μm of tumour and the rest of the tumour stroma as 'panstromal') demonstrate no defect in $CD3^+$ (T-cell) infiltration as evidenced by the equal densities in the panstromal and juxtatumoural compartments.

Each data point represents a single patient (median scores of all TMA cores (n=6)). Lines represent median with inter-quartile ranges (25^{th} and 75^{th}).

Mann Whitney U test; p-values are two-tailed. Scale bars 100μm.

Number of patients: 19.

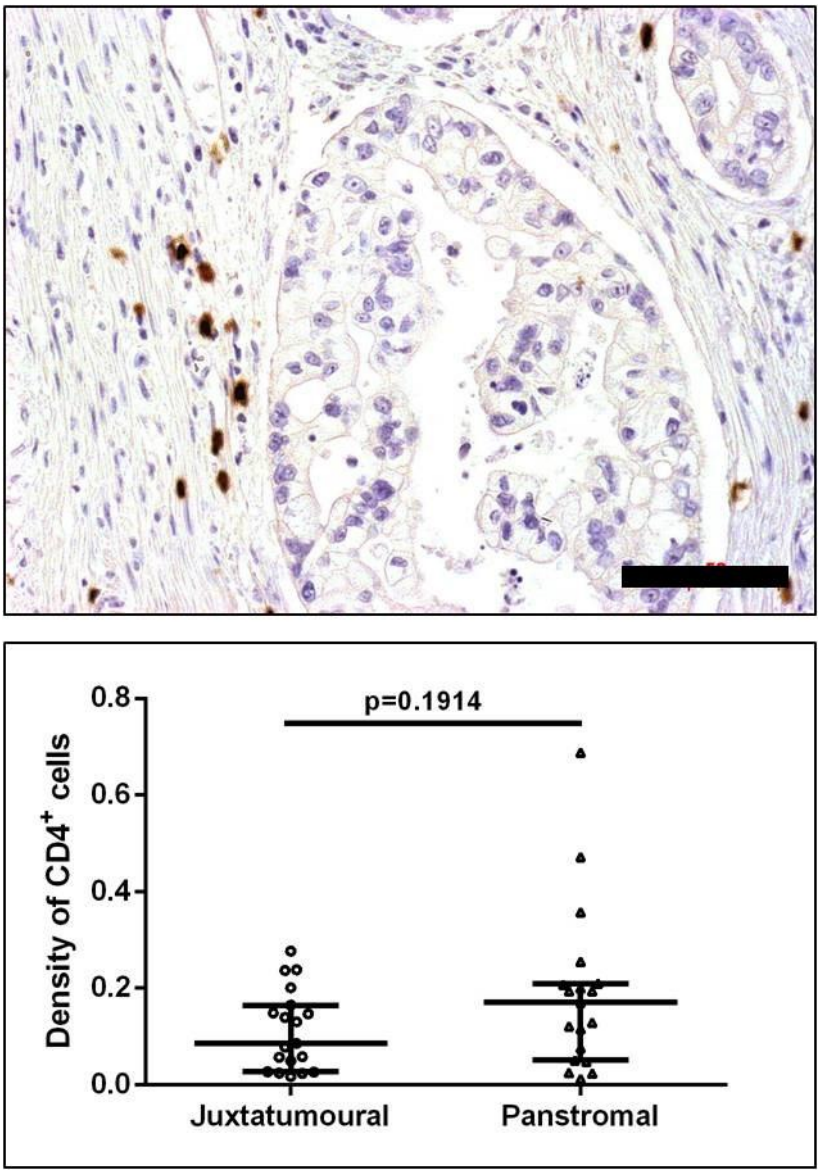

Figure 3.28 Stromal compartment specific $CD4^+$ cell infiltration in human cholangiocarcinoma

Direct comparison of stromal compartments ('juxtatumoural' defined as within 100μm of tumour and the rest of the tumour stroma as 'panstromal') demonstrate no defect in $CD4^+$ (helper T-cell) infiltration as evidenced by the equal densities in the panstromal and juxtatumoural compartments.

Each data point represents a single patient (median scores of all TMA cores (n=6)). Lines represent median with inter-quartile ranges (25^{th} and 75^{th}).

Mann Whitney U test; p-values are two-tailed. Scale bars 100μm.

Number of patients: 19.

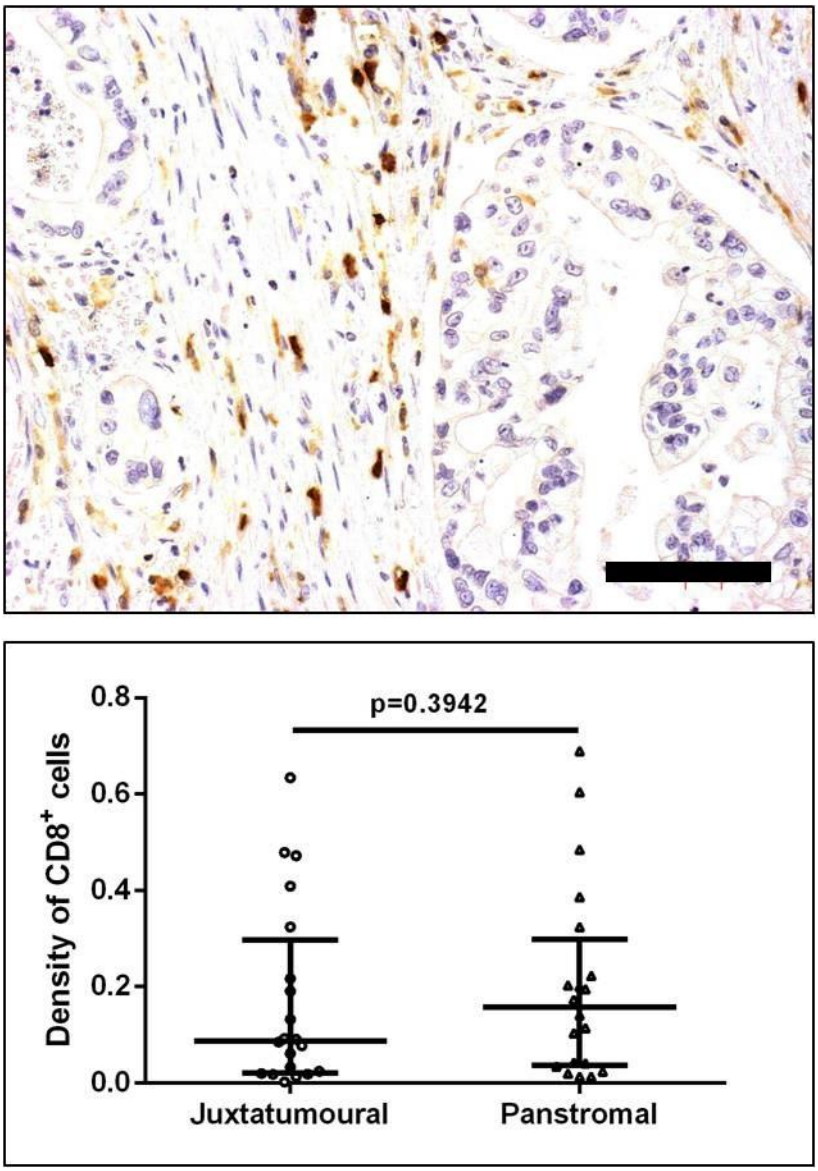

Figure 3.29 Stromal compartment specific $CD8^+$ cell infiltration in human cholangiocarcinoma

Direct comparison of stromal compartments ('juxtatumoural' defined as within 100μm of tumour and the rest of the tumour stroma as 'panstromal') demonstrate no defect in $CD8^+$ (cytotoxic T-cell) infiltration as evidenced by the equal densities in the panstromal and juxtatumoural compartments.

Each data point represents a single patient (median scores of all TMA cores (n=6)). Lines represent median with inter-quartile ranges (25^{th} and 75^{th}).

Mann Whitney U test; p-values are two-tailed. Scale bars 100μm.

Number of patients: 20.

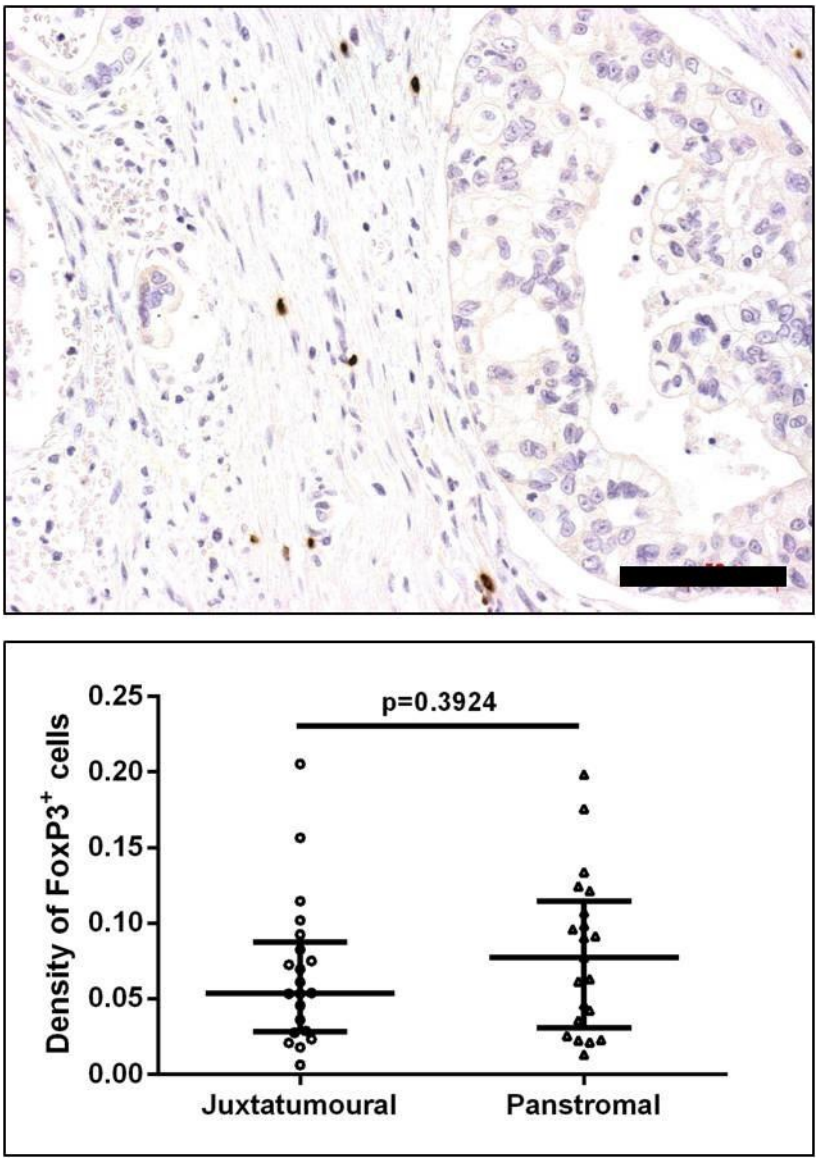

Figure 3.30 Stromal compartment specific FoxP3$^+$ cell infiltration in human cholangiocarcinoma

Direct comparison of stromal compartments ('juxtatumoural' defined as within 100μm of tumour and the rest of the tumour stroma as 'panstromal') demonstrate no defect in FoxP3$^+$ (Regulatory T-cell) infiltration as evidenced by the equal densities in the panstromal and juxtatumoural compartments.

Each data point represents a single patient (median scores of all TMA cores (n=6)). Lines represent median with inter-quartile ranges (25th and 75th).

Mann Whitney U test; p-values are two-tailed. Scale bars 100μm.

Number of patients: 21.

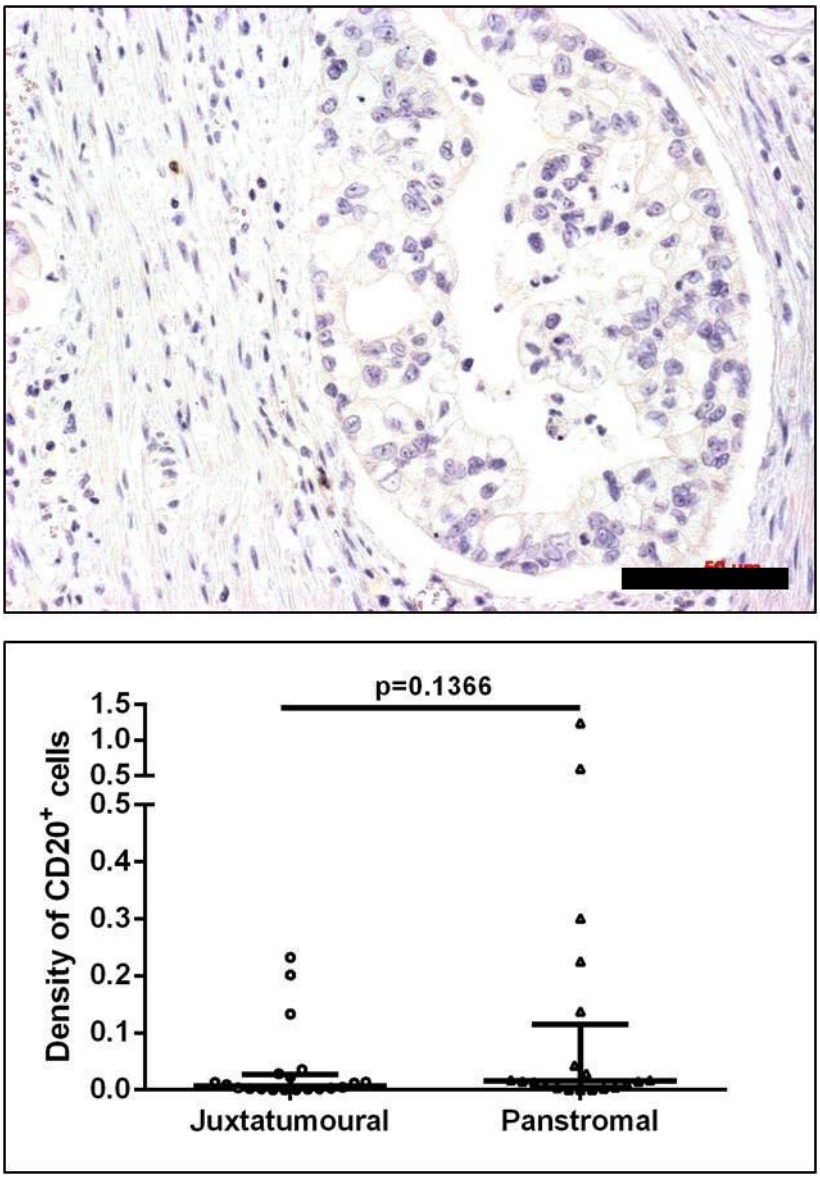

Figure 3.31 Stromal compartment specific $CD20^+$ cell infiltration in human cholangiocarcinoma

Direct comparison of stromal compartments ('juxtatumoural' defined as within 100µm of tumour and the rest of the tumour stroma as 'panstromal') demonstrate no defect in $CD20^+$ (B-cell) infiltration as evidenced by the equal densities in the panstromal and juxtatumoural compartments.

Each data point represents a single patient (median scores of all TMA cores (n=6)). Lines represent median with inter-quartile ranges (25^{th} and 75^{th}).

Mann Whitney U test; p-values are two-tailed. Scale bars 100µm.

Number of patients: 20.

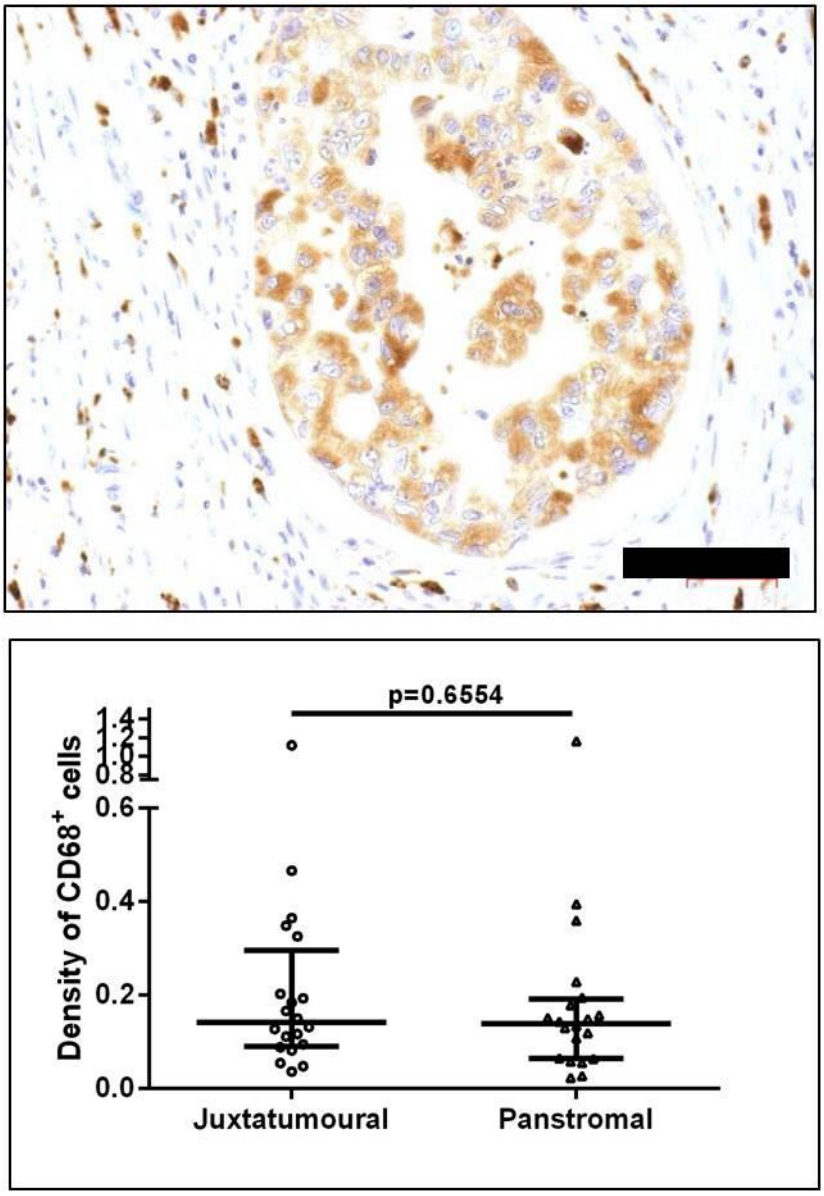

Figure 3.32 Stromal compartment specific CD68$^+$ cell infiltration in human cholangiocarcinoma

Direct comparison of stromal compartments ('juxtatumoural' defined as within 100μm of tumour and the rest of the tumour stroma as 'panstromal') demonstrate no defect in CD68$^+$ (Macrophages) infiltration as evidenced by the equal densities in the panstromal and juxtatumoural compartments.

Each data point represents a single patient (median scores of all TMA cores (n=6)). Lines represent median with inter-quartile ranges (25th and 75th).

Mann Whitney U test; p-values are two-tailed. Scale bars 100μm.

Number of patients: 21.

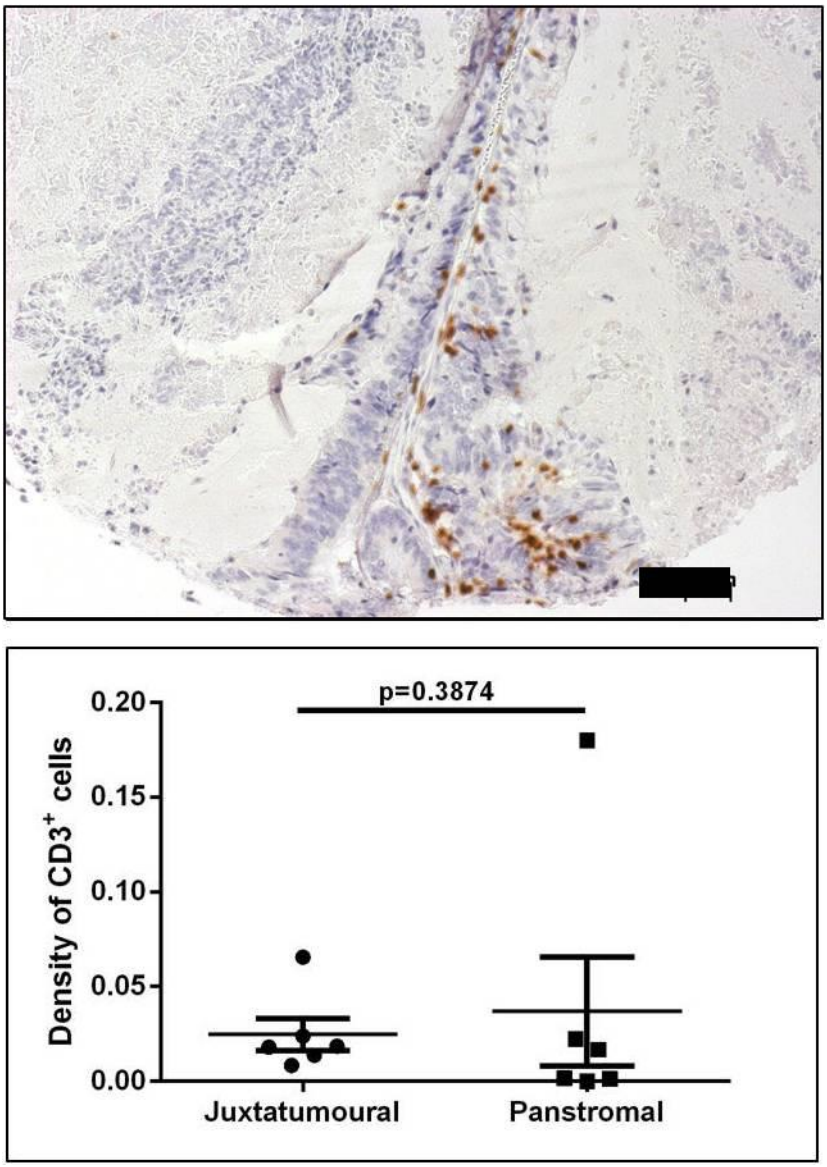

Figure 3.33 Stromal compartment specific $CD3^+$ cell infiltration in human mucinous cystic neoplasm

Direct comparison of stromal compartments ('juxtatumoural' defined as within 100μm of tumour and the rest of the tumour stroma as 'panstromal') demonstrate no defect in $CD3^+$ (T-cell) infiltration as evidenced by the equal densities in the panstromal and juxtatumoural compartments.

Each data point represents a single patient (median scores of all TMA cores (n=6)). Lines represent median with inter-quartile ranges (25^{th} and 75^{th}).

Mann Whitney U test; p-values are two-tailed. Scale bars 100μm.

Number of patients: 6.

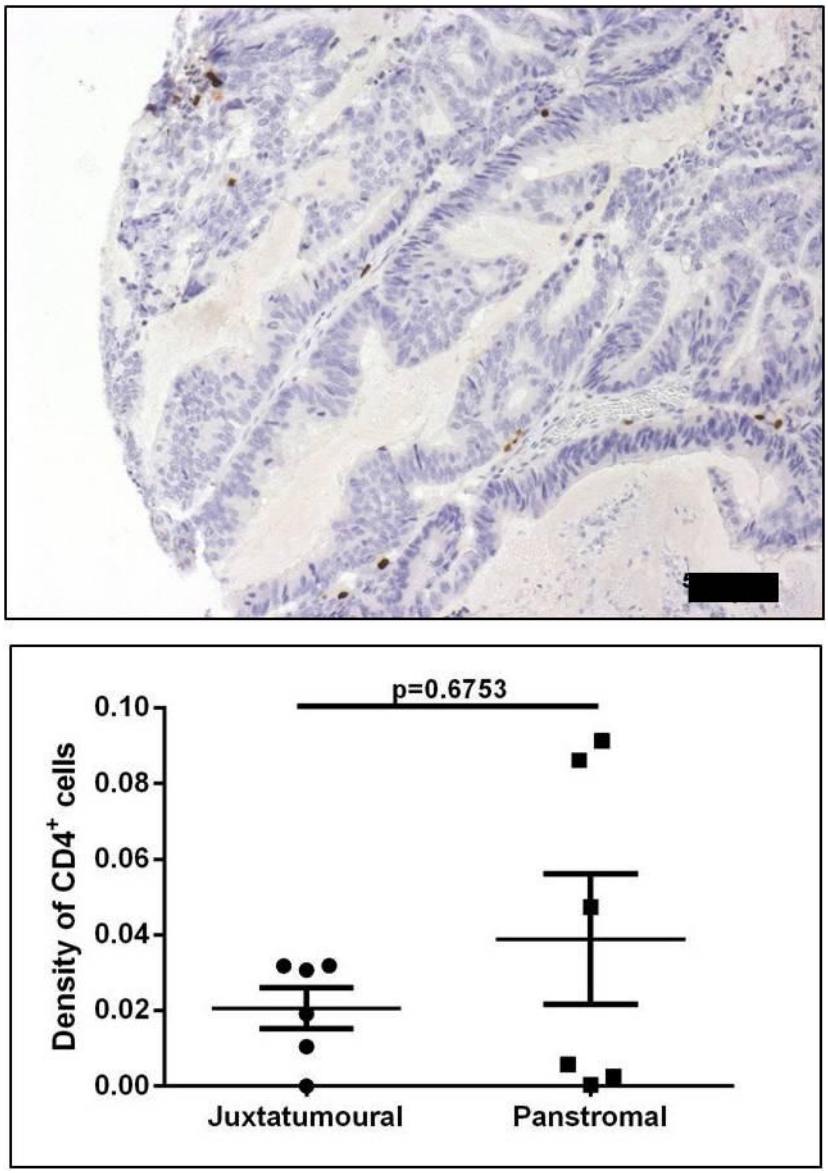

Figure 3.34 Stromal compartment specific $CD4^+$ cell infiltration in human mucinous cystic neoplasm

Direct comparison of stromal compartments ('juxtatumoural' defined as within 100µm of tumour and the rest of the tumour stroma as 'panstromal') demonstrate no defect in $CD4^+$ (T-cell) infiltration as evidenced by the equal densities in the panstromal and juxtatumoural compartments.

Each data point represents a single patient (median scores of all TMA cores (n=6)). Lines represent median with inter-quartile ranges (25^{th} and 75^{th}).

Mann Whitney U test; p-values are two-tailed. Scale bars 100µm.

Number of patients: 6.

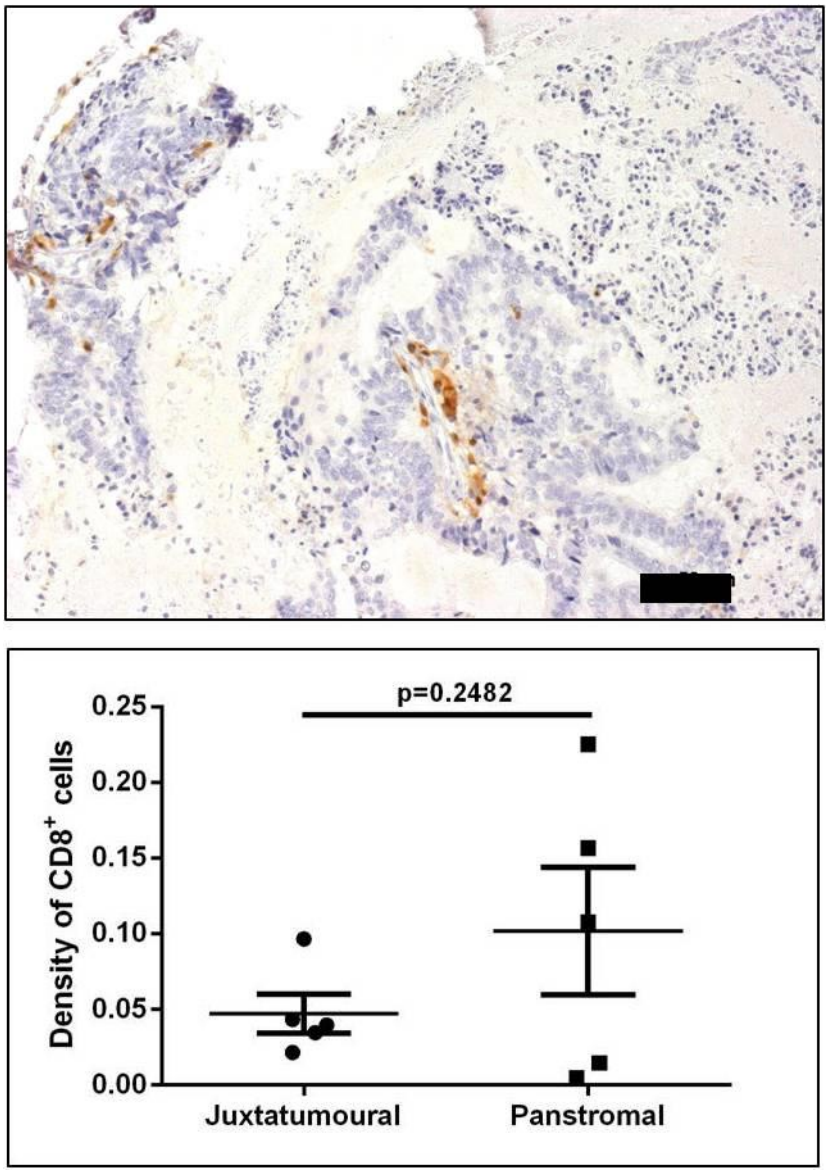

Figure 3.35 Stromal compartment specific $CD8^+$ cell infiltration in human mucinous cystic neoplasm

Direct comparison of stromal compartments ('juxtatumoural' defined as within 100μm of tumour and the rest of the tumour stroma as 'panstromal') demonstrate no defect in $CD8^+$ (cytotoxic T-cell) infiltration as evidenced by the equal densities in the panstromal and juxtatumoural compartments.

Each data point represents a single patient (median scores of all TMA cores (n=6)). Lines represent median with inter-quartile ranges (25^{th} and 75^{th}).

Mann Whitney U test; p-values are two-tailed. Scale bars 100μm. Magnification 20x.

Number of patients: 5.

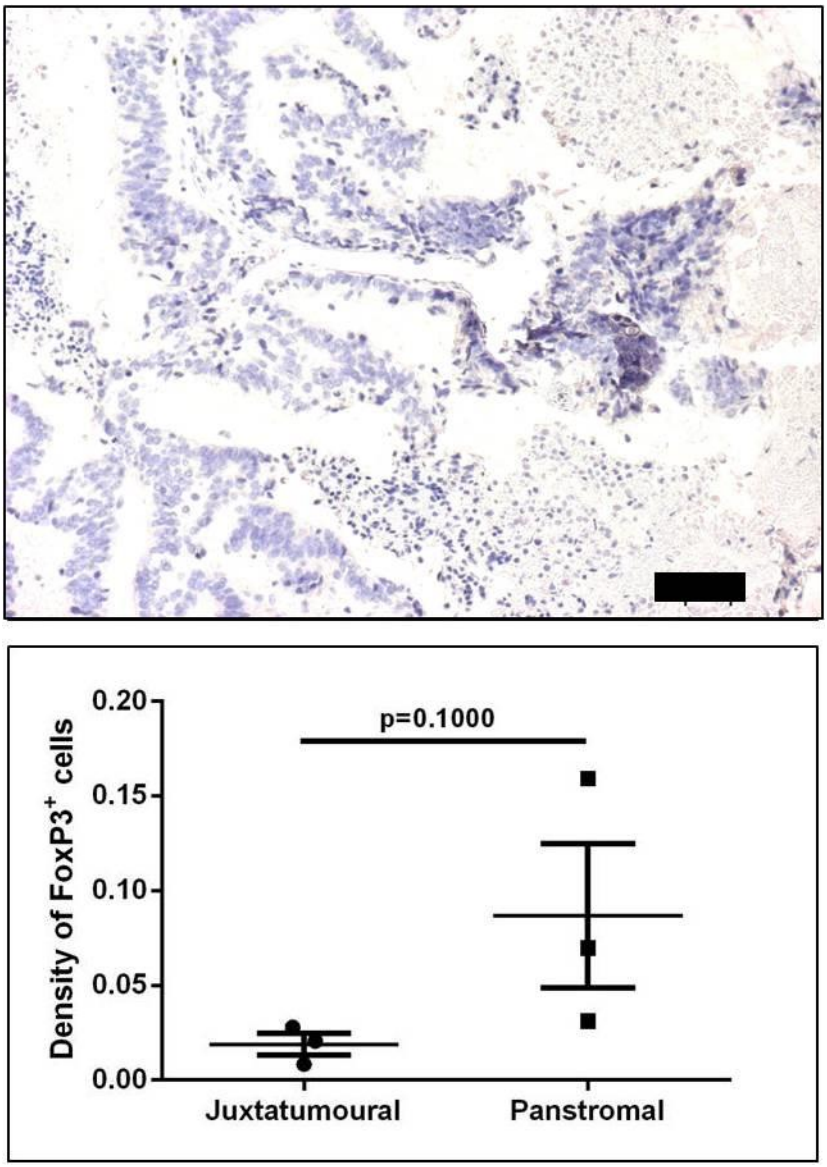

Figure 3.36 Stromal compartment specific FoxP3$^+$ cell infiltration in human mucinous cystic neoplasm

Direct comparison of stromal compartments ('juxtatumoural' defined as within 100μm of tumour and the rest of the tumour stroma as 'panstromal') demonstrate no defect in FoxP3$^+$ (T regulatory cell) infiltration as evidenced by the equal densities in the panstromal and juxtatumoural compartments.

Each data point represents a single patient (median scores of all TMA cores (n=6)). Lines represent median with inter-quartile ranges (25th and 75th).

Mann Whitney U test; p-values are two-tailed. Scale bars 100μm. Magnification 20x.

Number of patients: 3.

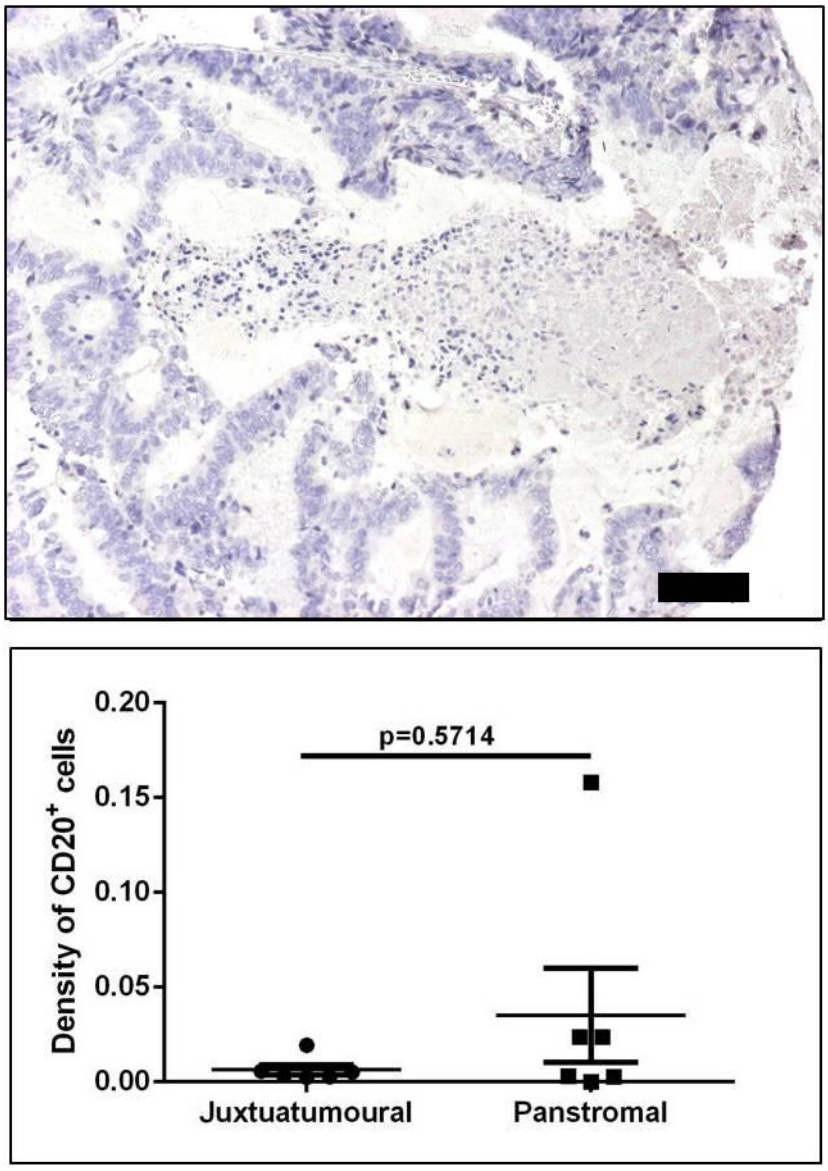

Figure 3.37 Stromal compartment specific $CD20^+$ cell infiltration in human mucinous cystic neoplasm

Direct comparison of stromal compartments ('juxtatumoural' defined as within 100μm of tumour and the rest of the tumour stroma as 'panstromal') demonstrate no defect in $CD20^+$ (B-cell) infiltration as evidenced by the equal densities in the panstromal and juxtatumoural compartments.

Each data point represents a single patient (median scores of all TMA cores (n=6)). Lines represent median with inter-quartile ranges (25^{th} and 75^{th}).

Mann Whitney U test; p-values are two-tailed. Scale bars 100μm.

Number of patients: 6.

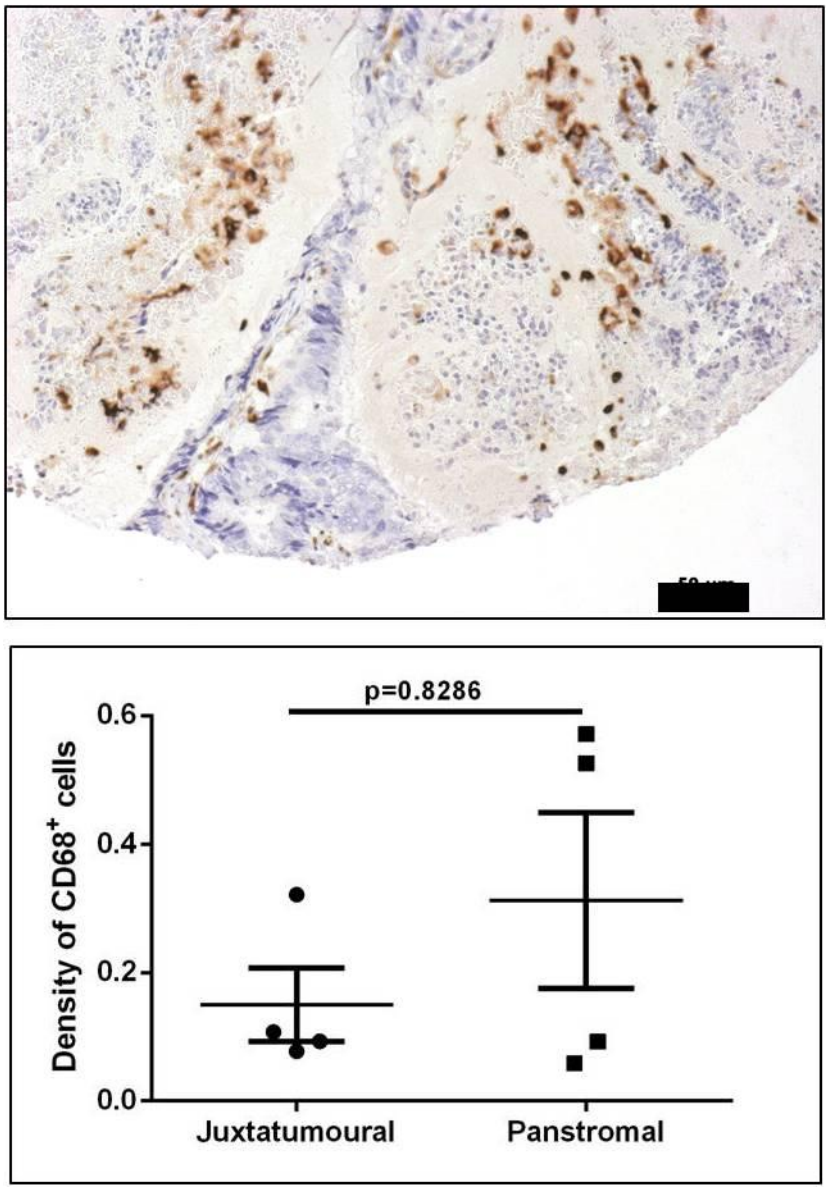

Figure 3.38 Stromal compartment specific $CD68^+$ cell infiltration in human mucinous cystic neoplasm

Direct comparison of stromal compartments ('juxtatumoural' defined as within 100µm of tumour and the rest of the tumour stroma as 'panstromal') demonstrate no defect in $CD68^+$ (Macrophages) infiltration as evidenced by the equal densities in the panstromal and juxtatumoural compartments.

Each data point represents a single patient (median scores of all TMA cores (n=6)). Lines represent median with inter-quartile ranges (25^{th} and 75^{th}).

Mann Whitney U test; p-values are two-tailed. Scale bars 100µm.

Number of patients: 4.

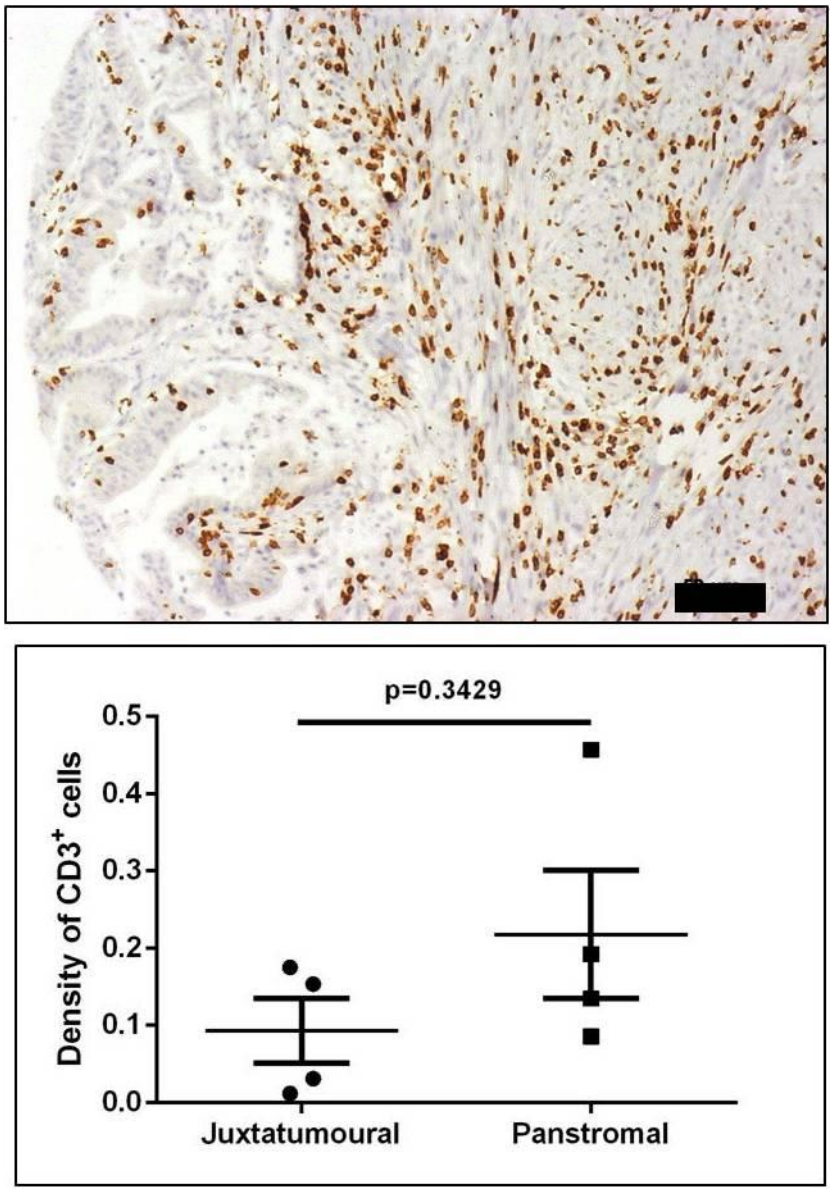

Figure 3.39 Stromal compartment specific CD3$^+$ cell infiltration in human duodenal carcinoma

Direct comparison of stromal compartments ('juxtatumoural' defined as within 100µm of tumour and the rest of the tumour stroma as 'panstromal') demonstrate no defect in CD3$^+$ (T-cell) infiltration as evidenced by the equal densities in the panstromal and juxtatumoural compartments.

Each data point represents a single patient (median scores of all TMA cores (n=6)). Lines represent median with inter-quartile ranges (25th and 75th).

Mann Whitney U test; p-values are two-tailed. Scale bars 100µm.

Number of patients: 4.

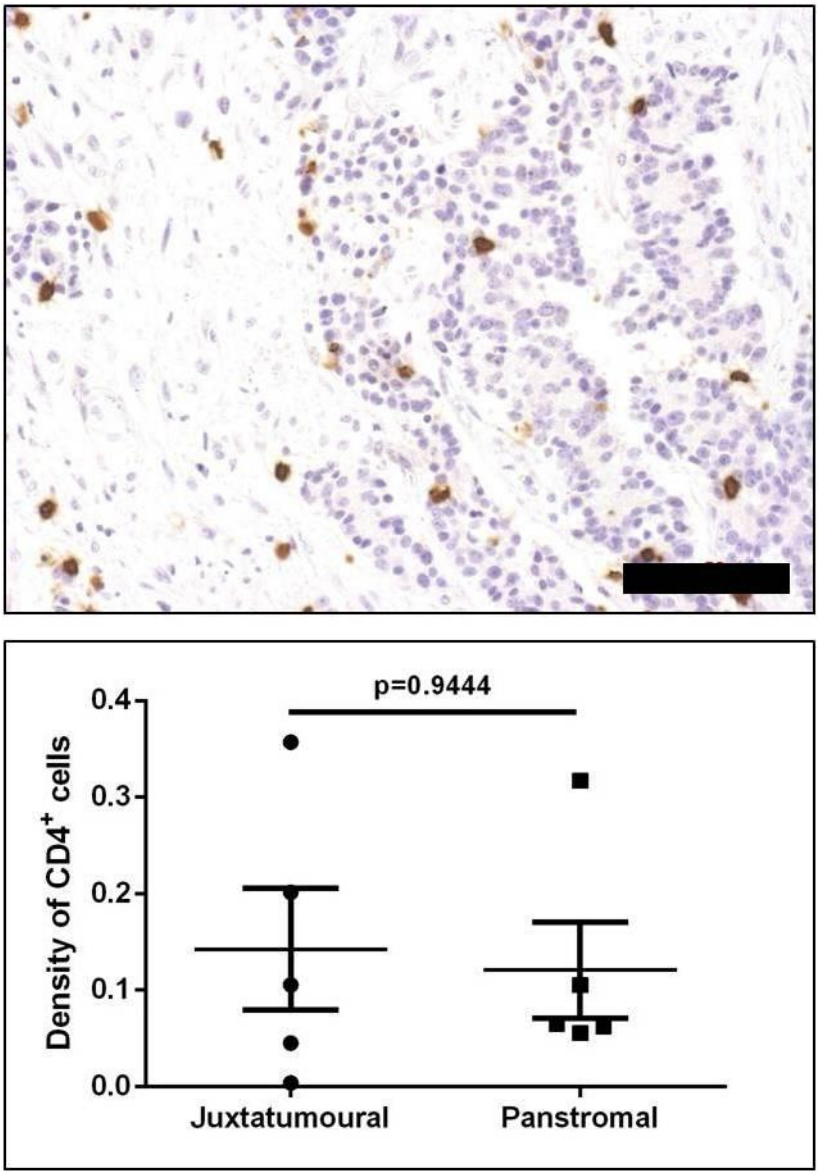

Figure 3.40 Stromal compartment specific $CD4^+$ cell infiltration in human duodenal carcinoma

Direct comparison of stromal compartments ('juxtatumoural' defined as within 100µm of tumour and the rest of the tumour stroma as 'panstromal') demonstrate no defect in $CD4^+$ (helper T-cell) infiltration as evidenced by the equal densities in the panstromal and juxtatumoural compartments.

Each data point represents a single patient (median scores of all TMA cores (n=6)). Lines represent median with inter-quartile ranges (25^{th} and 75^{th}).

Mann Whitney U test; p-values are two-tailed. Scale bars 100µm.

Number of patients: 5.

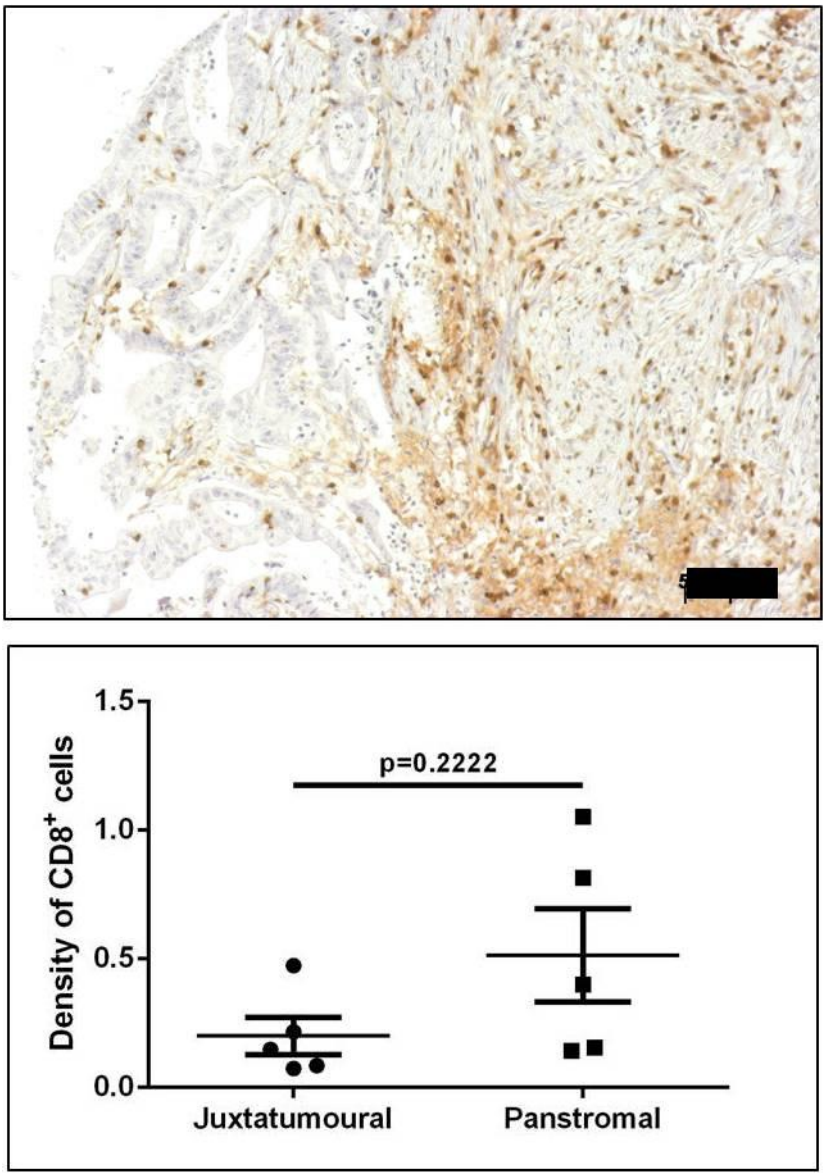

Figure 3.41 Stromal compartment specific $CD8^+$ cell infiltration in human duodenal carcinoma

Direct comparison of stromal compartments ('juxtatumoural' defined as within 100µm of tumour and the rest of the tumour stroma as 'panstromal') demonstrate no defect in $CD8^+$ (cytotoxic T-cell) infiltration as evidenced by the equal densities in the panstromal and juxtatumoural compartments.

Each data point represents a single patient (median scores of all TMA cores (n=6)). Lines represent median with inter-quartile ranges (25^{th} and 75^{th}).

Mann Whitney U test; p-values are two-tailed. Scale bars 100µm.

Number of patients: 5.

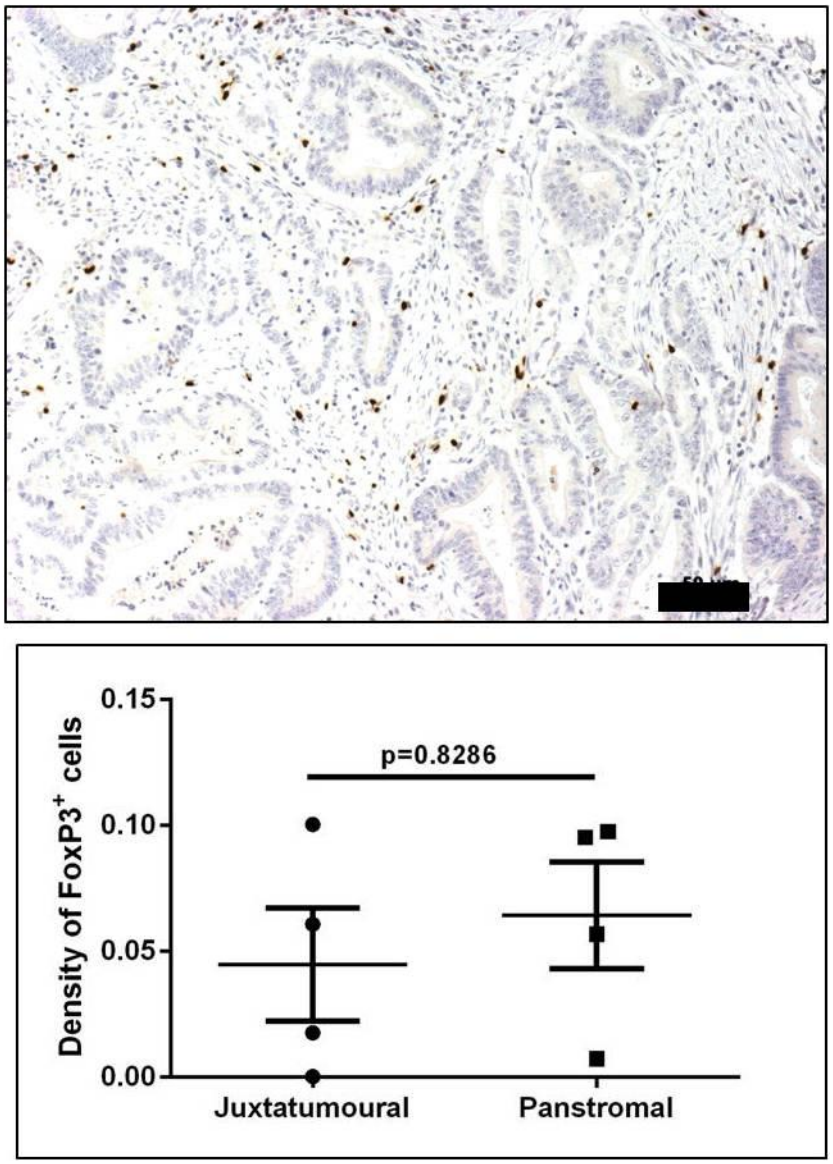

Figure 3.42 Stromal compartment specific FoxP3$^+$ cell infiltration in human duodenal carcinoma

Direct comparison of stromal compartments ('juxtatumoural' defined as within 100µm of tumour and the rest of the tumour stroma as 'panstromal') demonstrate no defect in FoxP3$^+$ (T regulatory cell) infiltration as evidenced by the equal densities in the panstromal and juxtatumoural compartments.

Each data point represents a single patient (median scores of all TMA cores (n=6)). Lines represent median with inter-quartile ranges (25th and 75th).

Mann Whitney U test; p-values are two-tailed. Scale bars 100µm.

Number of patients: 4.

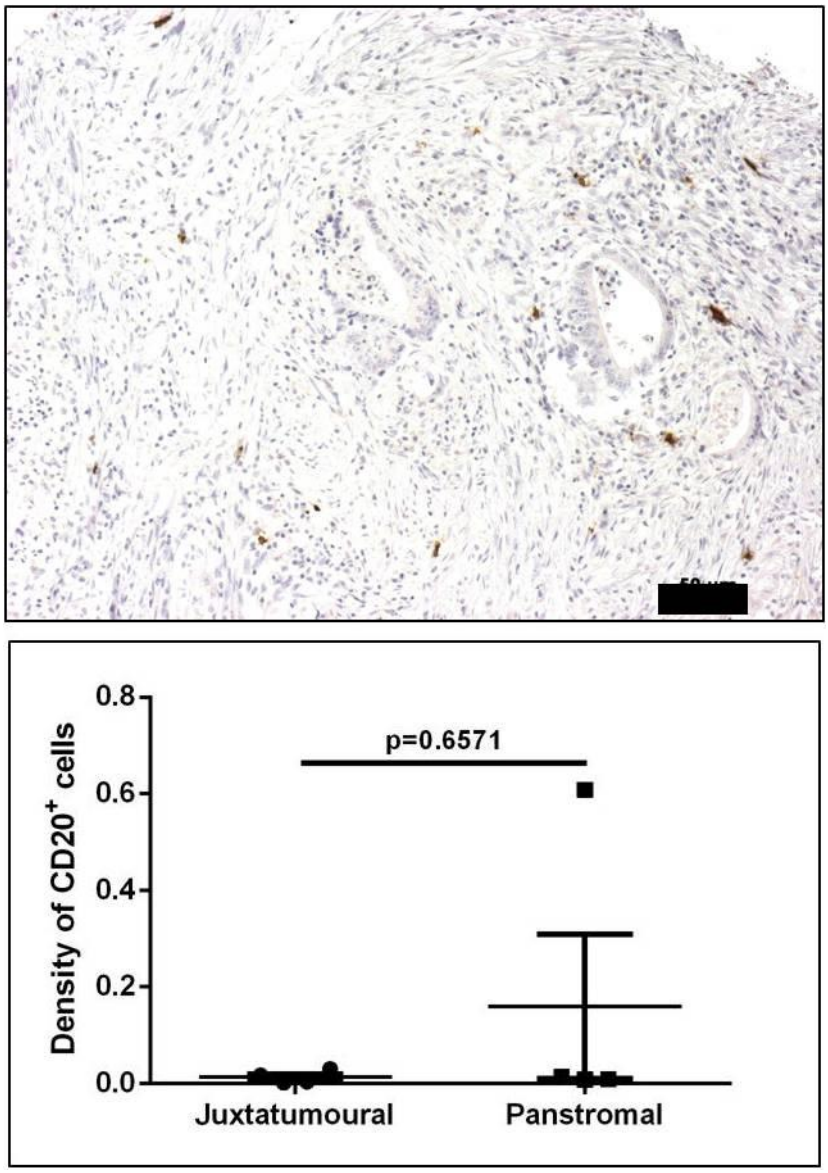

Figure 3.43 Stromal compartment specific $CD20^+$ cell infiltration in human duodenal carcinoma

Direct comparison of stromal compartments ('juxtatumoural' defined as within 100µm of tumour and the rest of the tumour stroma as 'panstromal') demonstrate no defect in $CD20^+$ (B-cell) infiltration as evidenced by the equal densities in the panstromal and juxtatumoural compartments.

Each data point represents a single patient (median scores of all TMA cores (n=6)). Lines represent median with inter-quartile ranges (25^{th} and 75^{th}).

Mann Whitney U test; p-values are two-tailed. Scale bars 100µm.

Number of patients: 4.

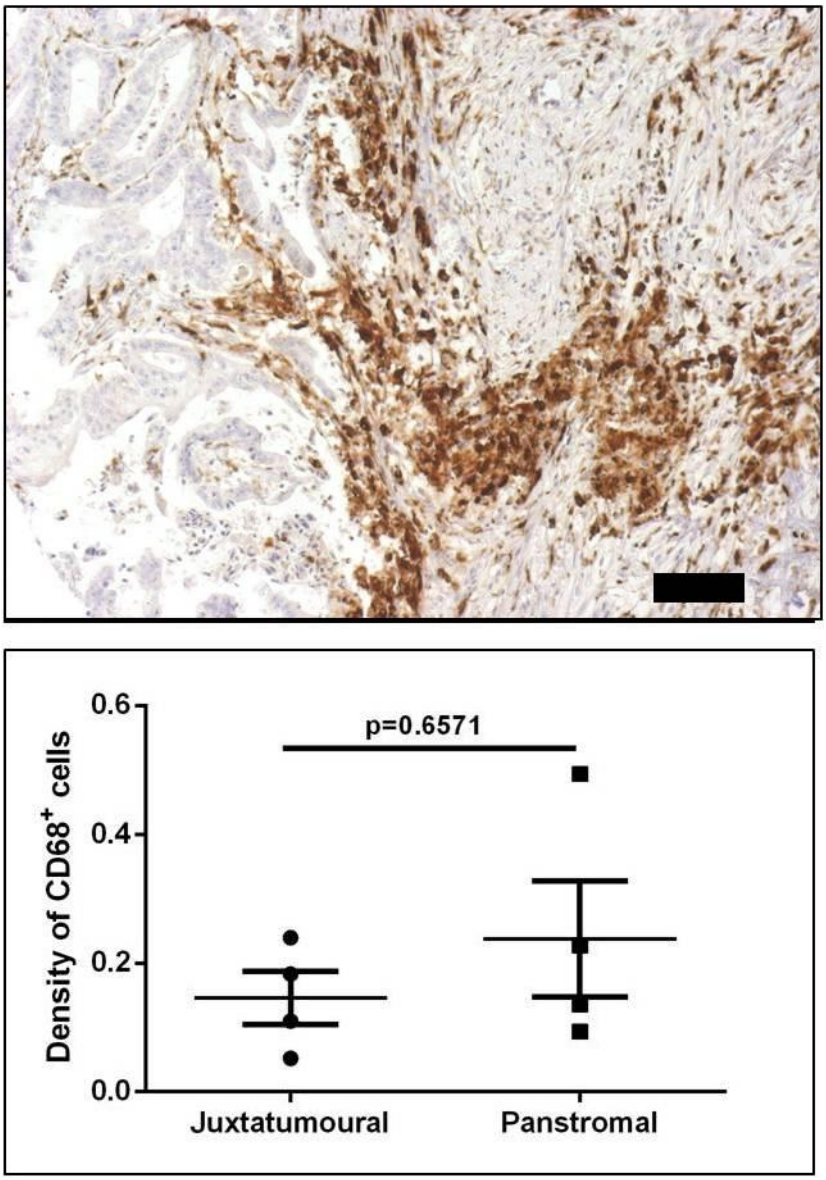

Figure 3.44 Stromal compartment specific CD68$^+$ cell infiltration in human duodenal carcinoma

Direct comparison of stromal compartments ('juxtatumoural' defined as within 100µm of tumour and the rest of the tumour stroma as 'panstromal') demonstrate no defect in CD68$^+$ (Macrophages) infiltration as evidenced by the equal densities in the panstromal and juxtatumoural compartments.

Each data point represents a single patient (median scores of all TMA cores (n=6)). Lines represent median with inter-quartile ranges (25th and 75th).

Mann Whitney U test; p-values are two-tailed. Scale bars 100µm. Magnification 20x.

Number of patients: 4.

3.7 Fibronectin is significantly upregulated in PDAC stroma

Fibronectin is an extracellular matrix (ECM) protein of approximately 440 kDa and mediates many important roles including cell adhesion, migration, wound healing, differentiation and growth (Pankov and Yamada 2002; Valenick, Hsia et al. 2005). A very large number of integrins bind to Fibronectin including α_4 β_1 (Very late antigen-4 (VLA-4)) and α_4 β_7 (Lymphocyte Peyer patch adhesion molecule (LPAM)) both of which are expressed on lymphocytes (Johansson, Svineng et al. 1997). α_4 β_1 integrins are expressed by leukocytes and mediate cell-cell and cell-matrix adhesion through their ligands vascular cell adhesion molecule (VCAM-1) and Fibronectin where they bind to the III_{14}-V region of Fibronectin. α_4 β_7 also bind to III_{14}-V region of Fibronectin, VCAM-1 and mucosal addressin cell adhesion molecule (MAdCAM-1) (Johansson, Svineng et al. 1997).

Using immunohistochemistry, I stained adjacent normal and cancer tissue from PDAC patients with Fibronectin. Quantification was performed by scoring individual slides on intensity and degree of staining and adding these two scores. This was performed six times for each slide and a median value of all six scores was calculated. The scoring range was 0 to 4; with zero being no staining and 4 being very positively stained. We observed an upregulation of Fibronectin in the stroma of cancer tissue, while Fibronectin in adjacent normal tissues of the same patients were mostly negative ($p<0.0001$; Figure 3.45, A, B and E). We also observed a denser staining of Fibronectin in the panstromal compartment of those patients (Figure 3.45, C) and the presence of immune cell infiltrates, a classical characteristic of most cancers (Clemente, Mihm et al. 1996; Naito, Saito et al. 1998; Zhang, Conejo-Garcia et al. 2003), within those densely stained areas of the panstromal compartment (Figure 3.45, D).

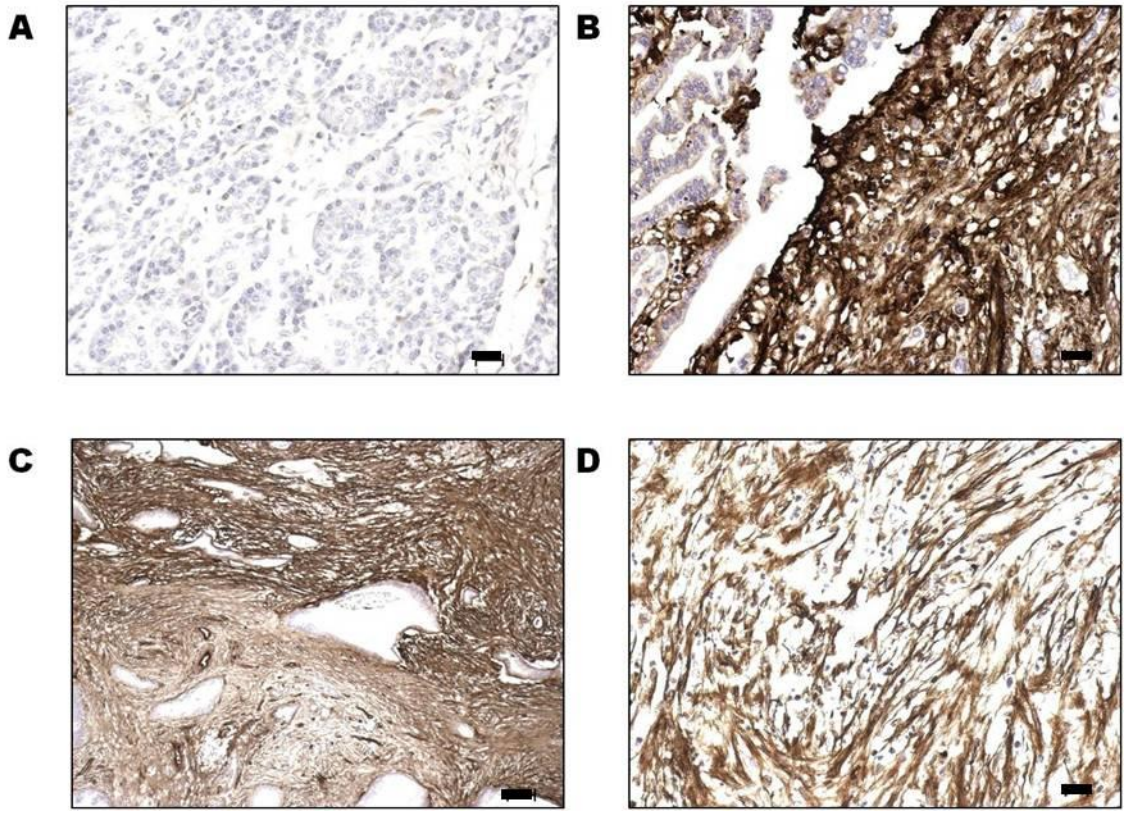
A
B
C
D

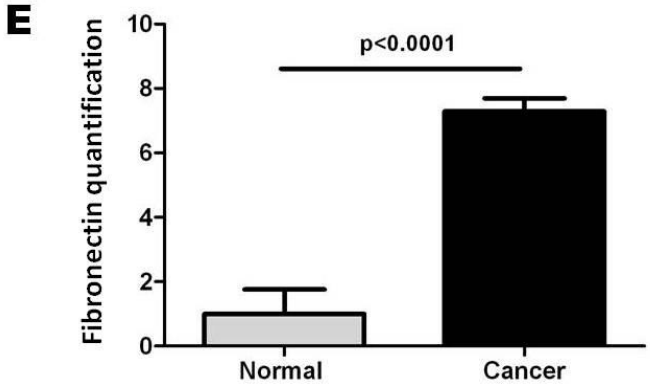
E
Fibronectin quantification
10
8
6
4
2
0
p<0.0001
Normal
Cancer

Figure 3.45 Fibronectin is upregulated in panstromal region of PDAC

Tissues from PDAC patients were stained for Fibronectin and analysed semi-quantitatively by colour intensity and area of positive staining under a light microscope.

(A) Adjacent normal tissues were mostly negative for Fibronectin with only a few regions staining lightly for Fibronectin (20x magnification). (B) Stromal regions of PDAC were positive for Fibronectin (20x magnification). This was not the case with the tumour epithelia. (C) Panstromal compartment of PDAC tissue had a denser staining of Fibronectin (5x magnification). (D) Immune cell infiltrates were observed within Fibronectin positive regions (20x magnification). (E) Quantification of Fibronectin in normal and cancer tissues, $p < 0.0001$, unpaired T test, p value is 2 tailed.

Number of patients: 7; Scale bars 50µm.

3.8 Correlation of differential immune cell infiltrate with patient survival

To test if the presence of immune cells in the pancreas, and their infiltration to close to the neoplasitic cells had an effect on the overall patient survival I performed Kaplan Meier survival analyses of the immune cells in whole tissues and the specific stromal compartments; Juxtatumoural stromal and panstroma. This was done with the X-TILE software (Camp, Dolled-Filhart et al. 2004). The X-Tile method is a versatile and perceptive tool for selecting cut-points based on traditional statistical tests and the plots provide a single comprehensive evaluation of all the possible ways a population can be divided either into low, medium and high marker expression (density in our case) or low versus high marker densities (Camp, Dolled-Filhart et al. 2004). The software represents the data in a right triangular heat map where each pixel represents a different cut-off point and a X^2 value is calculated for every possible division of the population shown on the heat map so that every pixel represents a X^2 value of an individual cut-point. This is done in a colour coded manner and the intensity of the colour of each cut-off point represents the strength of association of that cut-point with dark or black colours signifying low associations and bright colours signifying high associations. There two types of associations; direct associations (e.g., where having a high density of the marker may result in higher survival in patients or low marker density may result in poorer survival) are coloured green and inverse associations (e.g., where having a high marker density may result in poorer patient survival) are coloured red. The vertical axis of the right triangular heat map represents all possible patients with high immune marker density in the cohort with the size of the population increasing from top to bottom. The horizontal axis of the heat map represents all possible patients with low marker density in the cohort and size of the “low” population increases from left to right. Data

along the hypotenuse (which is the same data represented on the rectangle below the right triangular heat map) represents results from a single cut-point which divides patient data into two patient subsets: patients with high marker densities and patients with low marker densities. Data points away from the hypotenuse represent results from two cut-points that “define an additional ‘middle’ population” in addition to the earlier two subsets with the size of the middle population increasing with greater distance from the hypotenuse (Camp, Dolled-Filhart et al. 2004). A middle population may be considered in survival analysis with gene expression markers where a heterozygote population with a different phenotype from the homozygote dominant and homozygote recessive may exist. In our case only two subsets (high versus low) based on a single cut-point were relevant in assessing patient overall survival. The cursor can be moved manually over any cut-point to display survival curves however, an optimal division of the data can be selected by selecting the highest X^2 value. “Statistical significance is assessed by using the cut-point derived from a training set to parse a separate validation set using a standard log-rank test with p values obtained from a look up table” (Camp, Dolled-Filhart et al. 2004). The X-TILE creates individual training and validation cohorts (I set training and validation size ratio to 1:1) by making separate lists of censored and uncensored observations (censored: dead = 1; uncensored: alive = 0; lost to follow = 2) which are ordered by their follow up time. Patients are alternately assigned either to the training or validation cohorts by selecting every other patient as the software reads down the list. The base survival curve is normalized for both sets and this ensures that the same training and validation sets are created each time an analysis with the same marker is performed preventing the possibility of obtaining a different p value each time. The training and validation method provides a rigorous and statistical relevant manner of assessing p

value and overcomes the limitations of multiple cut-point analysis (Camp, Dolled-Filhart et al. 2004). Additional statistical significance using the X-TILE may be achieved by using Monte Carlo simulations (such as cross validation) and Miller-Siegmund p value correction (Altman, Lausen et al. 1994) .

Dichotomization into the juxtatumoural stromal and panstromal compartments indicated the effect on survival specific immune cells had relative to their position on the tissue (for instance, an proximity of a particular immune cell population to the tumour cells may have an effect on patient survival but not when the immune cells are sequestered in the panstromal compartment and vice versa, or the relative position of an immune cell infiltrate within the stroma may not influence patient survival).

We observed that high densities of $CD8^+$ (cytotoxic T-cells) in patients resulted in longer patient survival (p =0.0302; Miller-Siegmund p= 0.3555; cut off <0.07≥; Figure 3.45 A i). This is in line with work published by Tosolini and colleagues that found higher densities of $CD8^+$ Th1 cells in tumours correlated with increased disease free survival in colorectal cancer (Tosolini, Kirilovsky et al. 2011). Also high densities of $CD8^+$ T-cells in juxtatumoural stromal compartments resulted in patients having longer overall survival (p =0.0455; Miller-Siegmund p= 0.4639; cut off <0.05≥; Figure 3.45 A ii) but this was not the case in the panstromal survival analysis (p =0.0614; Miller-Siegmund p= 0.553; cut off <0.09≥; Figure 3.45 A iii). As more of the effect was observed when cytotoxic cells infiltrated the tumour, this could possibly indicate that $CD8^+$ T-cells are able to perform their cytotoxic function when

they infiltrate the tumour. Also X-Tile heat maps point to the potential multiple associations of $CD8^+$ cell densities with patient overall survival represented by the multiple bright green pixels (Figure 3.45 C ii). $CD8^+$ marker may be further investigated as a positive prognostic factor.

Patients with high densities of $FoxP3^+$ (T regulatory cells) have poorer survival (p =0.0016; Miller-Siegmund p= 0.0371; cut off <0.06≥; Figure 3.46 A i). This is also the case in the juxtatumoural stromal compartment (p =0.0019; Miller-Siegmund p= 0.0444; cut off <0.03≥; Figure 3.46 A ii). Also high densities of $FoxP3^+$ cells in the panstromal compartments show a reduced overall patient survival but loses significance as the Miller-Siegmund p value is not significant (p =0.0253; Miller-Siegmund p= 0.316; cut off <0.05≥; Figure 3.46 A iii). Of all the immune cell markers assessed, $Foxp3^+$ (T regulatory cells) was the only marker to have an additional level of significance as the Miller-Siegmund p value was significant in both tissue and juxtatumoural survival analysis. $Foxp3^+$ may be investigated further as a prognostic marker.

Survival analyses of other immune cells; (T-cells ($CD3^+$), helper T-cells ($CD4^+$), B-cells ($CD20^+$), Natural killer cells ($CD56^+$), Macrophages ($CD68^+$) and ratio of helper T-cells to cytotoxic T-cells ($CD4^+$/ $CD8^+$) were also carried out and discussed below. The summary of the results of the survival analyses for all immune cells are in table 3.1.

Overall patients with low densities of $CD3^+$ T-cells showed a trend towards surviving longer than patients with high densities (p =0.0151; Miller-Siegmund p= 0.2195; cut off <0.12≥; Table 3.1). Having higher or lower densities of $CD3^+$ T-cells in the juxtatumoural stroma did not have an effect on patient survival (p =0.10609; Miller-Siegmund p= 1; cut off <0.14≥; Table 3.1) however patients with a low density of $CD3^+$ T-cells in the panstromal compartments survived longer than patients with high $CD3^+$ T-cell ensities (p =0.018; Miller-Siegmund p= 0.2482; cut off <0.20≥; Table 3.1). $CD3^+$ T-cells densities are not a prognostic marker for PDAC.

Further introspection into $CD3^+$ subsets; $CD4^+$, $CD8^+$ and $FoxP3^+$ showed that patients with low densities of $CD4^+$ cells also demonstrated a trend towards surviving longer than patients having higher densities (p =0.0069; Miller-Siegmund p= 0.1217; cut off <0.19≥; Table 3.1). Survival analysis of $CD4^+$ in the juxtatumoural stromal compartment alone was not significant (p =0.0652; Miller-Siegmund p= 0.575; cut off <0.19≥; Table 3.1) whereas survival analysis of $CD4^+$ in panstromal compartment was significant (p =0.019; Miller-Siegmund p= 0.2586; cut off <0.16≥; Table 3.1) with low infiltrates surviving longer than high infiltrates. This indicates that $CD4^+$ T-cells (or a subset of them) may have an immunosuppressive function and may perform this function in the panstromal compartment (i.e. $CD4^+$ cells do not need to infiltrate the tumour to perform an immunosuppressive function). Observations for $CD8^+$ T-cells have been described earlier and contradicted survival outcomes of $CD3^+$ and $CD4^+$ T-cells. Observations for $FoxP3^+$ cells, also previously discussed above, were similar to survival outcomes of $CD3^+$ cells and $CD4^+$ T-cells and in contrast to $CD8^+$ T-cells.

$CD20^+$ B-cells survival analysis in patients was not significant (p =0.652; Miller-Siegmund p= 0.575; cut off <0.00≥; Table 3.1). However, survival analyses of

B-cells in the juxtatumoural stromal compartment showed a trend towards significance (p =0.0544; Miller-Siegmund p= 0.5174; cut off <0.01≥; Table 3.1) and was significant in the panstromal compartments (p =0.0128; Miller-Siegmund p= 0.1939; cut off <0.05≥; Table 3.1) with patients having low densities of $CD20^+$ surviving longer indicating a negative effect of $CD20^+$ B-cells in the panstroma but that does not necessarily increase as cells migrate. As with $CD8^+$ T-cells, patients with high densities of $CD56^+$ cells (p =0.0114; Miller-Siegmund p= 0.1782; cut off <0.02≥; Table 3.1) and high densities in the juxtatumoural stromal compartment (p =0.0359; Miller-Siegmund p= 0.3992; cut off <0.03≥; Table 3.1) demonstrated longer survival but this was not the case in the panstromal compartment p =0.2059; Miller-Siegmund p= 1; cut off <0.03≥; Table 3.1). This too may indicate the need for natural killer cells to infiltrate the tumour in other to perform anti-tumour function. Patients with low densities of $CD68^+$ demonstrated a tendency to longer survival than those with high densities (p =0.0269; Miller-Siegmund p= 0.3288; cut off <0.03≥; Table 3.1). Survival analyses of $CD68^+$ was not significant in the juxtatumoural stromal (p =0.138; Miller-Siegmund p= 1; cut off <0.12≥; Table 3.1) and panstromal compartments (p =0.1138; Miller-Siegmund p= 1; cut off <0.02≥; Table 3.1).

To see if the ratio of helper / cytotoxic T-cells has an impact on patient overall survival, I performed survival analysis of the $CD4^+/CD8^+$ ratio in PDAC patients. Patients with a low $CD4^+/CD8^+$ T-cells ratio had longer overall survival (p =0.0455; Miller-Siegmund p= 0.4639; cut off <2.00≥; Table 3.1). Survival analyses of $CD4^+/CD8^+$ T-cells ratio in the juxtatumoural stroma and panstroma compartments were not significant (Table 3.1).

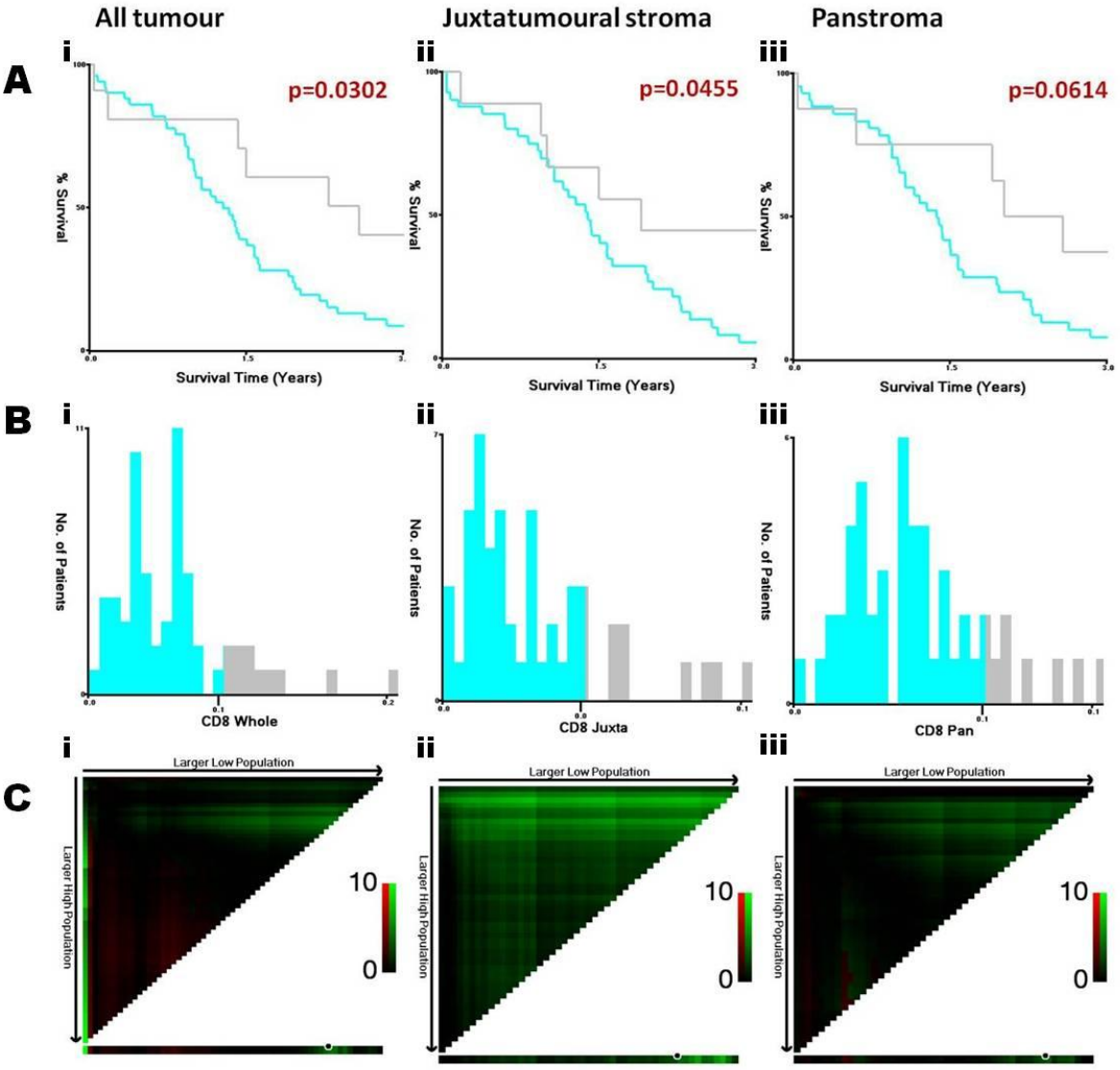

Patients with high immune cell

Patients with low immune cell

Figure 3.46 $CD8^+$ survival analyses

Density of $CD8^+$ T-cells in the whole tissue, the juxtatumoural stroma and the panstroma compartments of PDAC patients was correlated with their survival data using X-tile software (Yale). X-tile plots of the data are displayed in C i-iii. The right triangular plot shows the $_X^2$ log-rank values created when the cohort is divided into 3 populations based on two cut-points. The X axis represents all potential cut-points of a low subset from low to high (left to right) and the Y axis represents all potential cut-points of a high subset from high to low (top to bottom). The arrow represents the direction by which the subsets increase in size. The rectangular plot (below the right triangular plot (and the hypotenuse)) shows the $_X^2$ log-rank values created when the cohort is divided into 2 populations by the application of a single cut-point. The bright green colour indicates a direct association; in this case, having high densities of $CD8^+$ promotes longer patient survival. The cut-point, highlighted by the black/ white circle on the rectangular plot, is shown on a histogram (B i-iii) and Kaplan-Meier plots (A i-iii). P values were defined by using cut-points derived from a training set and applying them to a validation set. Miller-Siegmund p values were calculated to provide an additional level of significance to account for multiple comparisons.

(A) High densities of the $CD8^+$ marker demonstrated a tendency to longer survival in patients (i). The presence of high densities of the $CD8^+$ marker in the juxtatumoural stromal compartments also demonstrated a tendency to longer survival in patients (ii); this was not the case in the panstromal compartment (iii). (B) Histogram shows distribution of patients in whole tissue, juxtatumoural and panstromal survival analyses at the optimal cut-point. Blue

represents patients with low densities and grey represents patients with high densities. (C) Heat map shows the multiple potential associations of the $CD8^+$ marker in patient survival where each pixel is the $_X^2$ log-rank value with the bright green colour signifying a high association.

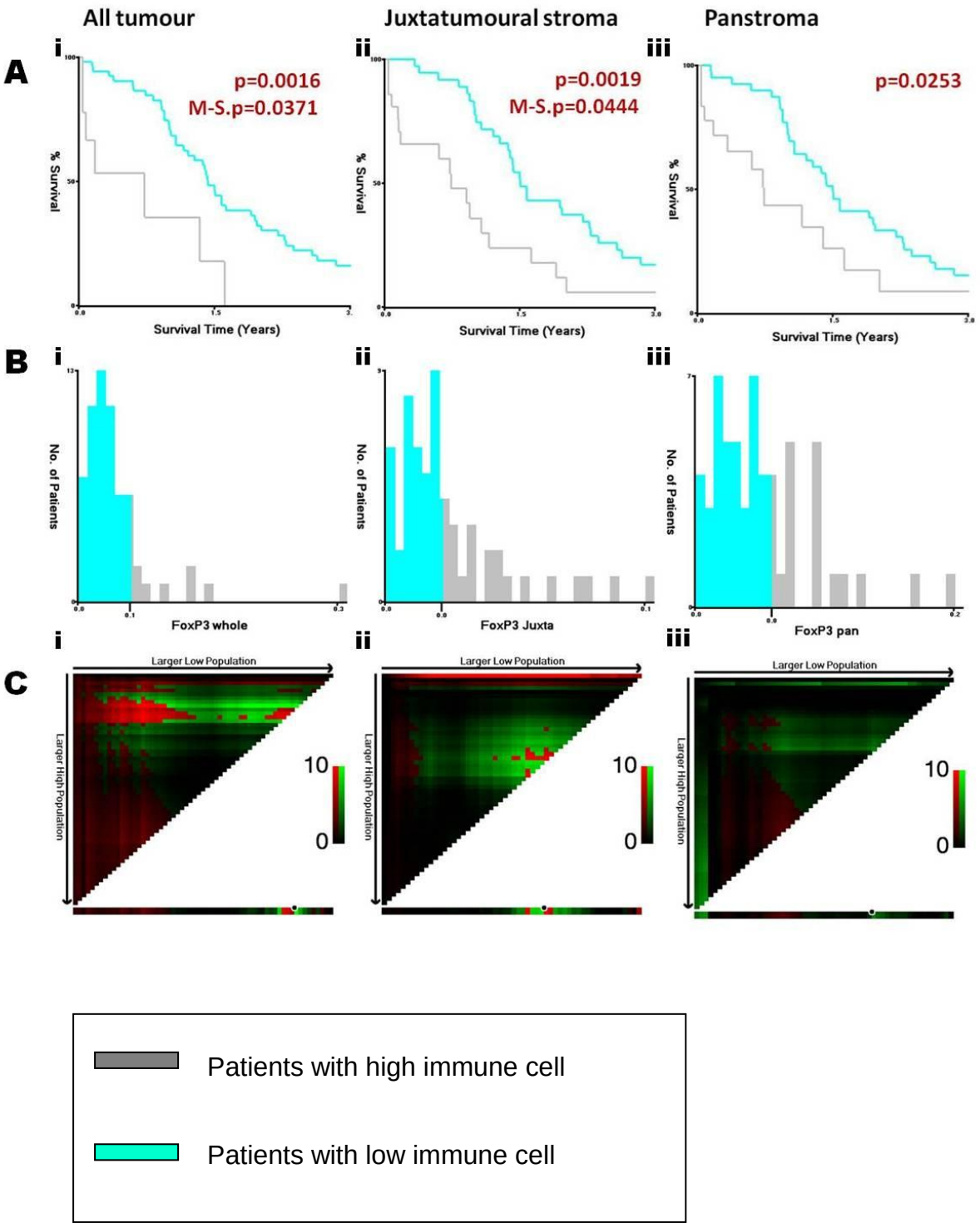
All tumour
Juxtatumoural stroma
Panstroma
A
i
ii
iii
p=0.0016
M-S.p=0.0371
p=0.0019
M-S.p=0.0444
p=0.0253
% Survival
Survival Time (Years)
B
No. of Patients
FoxP3 whole
FoxP3 Juxta
FoxP3 pan
C
Larger Low Population
Larger High Population
10
0
Patients with high immune cell
Patients with low immune cell

Figure 3.47 FoxP3$^+$ survival analyses

Density of FoxP3$^+$ T-cells in the whole tissue, the juxtatumoural stroma and the panstroma compartments of PDAC patients was correlated with their survival data using X-tile software (Yale). X-tile plots of the data are displayed in C i-iii. The right triangular plot shows the $_{X}^{2}$ log-rank values created when the cohort is divided into 3 populations based on two cut-points. The X axis represents all potential cut-points of a low subset from low to high (left to right) and the Y axis represents all potential cut-points of a high subset from high to low (top to bottom). The arrow represents the direction by which the subsets increase in size. The rectangular plot (below the right triangular plot (and the hypotenuse)) shows the $_{X}^{2}$ log-rank values created when the cohort is divided into 2 populations by the application of a single cut-point. The bright green colour indicates a direct association and the bright red colour indicates an inverse association; in this case, having low densities of FoxP3$^+$ promotes longer patient survival. The cut-point, highlighted by the black/ white circle on the rectangular plot, is shown on a histogram (B i-iii) and Kaplan-Meier plots (A i-iii). P values were defined by using cut-points derived from a training set and applying them to a validation set. Miller-Siegmund p values were calculated to provide an additional level of significance to account for multiple comparisons.

(A) Low densities of the FoxP3$^+$ marker demonstrated a tendency to longer survival in patients. Miller-Siegmund p value correction was also significant (i). The presence of low densities of the FoxP3$^+$ marker in the juxtatumoural stromal compartments also demonstrated a tendency to longer survival in patients with Miller-Siegmund p value also being significant (ii). Low densities of the FoxP3$^+$ marker in the panstromal compartment also resulted in longer patient survival however the additional level of significance was lost (iii). (B)

Histogram shows distribution of patients in whole tissue, juxtatumoural and panstromal survival analyses at the optimal cut-point. Blue represents patients with low densities and grey represents patients with high densities. (C) Heat map shows the potential associations of the FoxP3^{+} marker in patient survival where each pixel is the x^2 log-rank value. The cut-point falls on a red pixel which signifies an inverse association with patient survival.

MARKER	WHOLE TISSUE INFILTRATE			JUXTATUMOURAL TISSUE INFILTRATE			PANSTROMAL TISSUE INFILTRATE			Inference
	CUT OFF	P-VALUE	Miller-Siegmund p-value	CUT OFF	P-VALUE	Miller-Siegmund p-value	CUT OFF	P-VALUE	Miller-Siegmund p-value	
CD3	<0.12≥	0.0151	0.2195	<0.14≥	0.1069	1	<0.20≥	0.018	0.2482	↓
CD4	<0.19≥	0.0069	0.1217	<0.19≥	0.0652	0.575	<0.16≥	0.019	0.2586	↓
CD8	<0.07≥	0.0302	0.3555	<0.05≥	0.0455	0.4639	<0.09≥	0.0614	0.5553	↑
FoxP3	<0.06≥	0.0016	0.0371	<0.03≥	0.0019	0.0444	<0.05≥	0.0253	0.316	↓
CD20	<0.00≥	0.0652	0.575	<0.01≥	0.0544	0.5174	<0.05≥	0.0128	0.1939	↓
CD56	<0.02≥	0.0114	0.1782	<0.03≥	0.0359	0.3992	<0.03≥	0.2059	1	↑
CD68	<0.03≥	0.0269	0.3288	<0.12≥	0.138	1	<0.02≥	0.1138	1	↓
CD4/CD8	<2.00≥	0.0455	0.4639	<3.30≥	0.0783	0.6362	<4.60≥	0.1797	1	↓

Having a high density of immune cell marker promotes longer patient overall survival

Having a high density of immune cell marker promotes poorer patient overall survival

Table 3.1: Survival analyses of immune cell markers in PDAC

Results II

4.1 Introduction

In the previous chapter I demonstrated differential immune cell infiltrate specific for human PDAC tissue by probing for the immune cell markers ($CD3^+$, $CD4^+$, $CD8^+$, $FoxP3^+$, $CD20^+$, $CD56^+$, $CD68^+$ and $Myeloperoxidase^+$). We observed that while some immune cells such as Macrophages and Neutrophils had no defect in tumour infiltration (i.e., they could migrate on tissue into the juxtatumoural compartment and to the tumour cells), others such as cytotoxic T-cells and B-cells had a defect in reaching the tumour. Cytotoxic T-cell infiltration also suggested prognostic ability. We observed that these immune cells with infiltration defects were sequestered in the panstromal compartment which consists of activated stellate cells (a chief event in PDAC) (Figure 4. 1). Fortunately pancreatic stellate cell activation can be reversed *in vitro* and *in vivo* by treatment with all-trans retinoic acid (ATRA) (Froeling, Feig et al. 2011).

In this chapter I investigate with *in vivo* and *in vitro* experiments to understand the mechanisms hindering immune cell infiltration, particularly for cytotoxic T-cell infiltration.

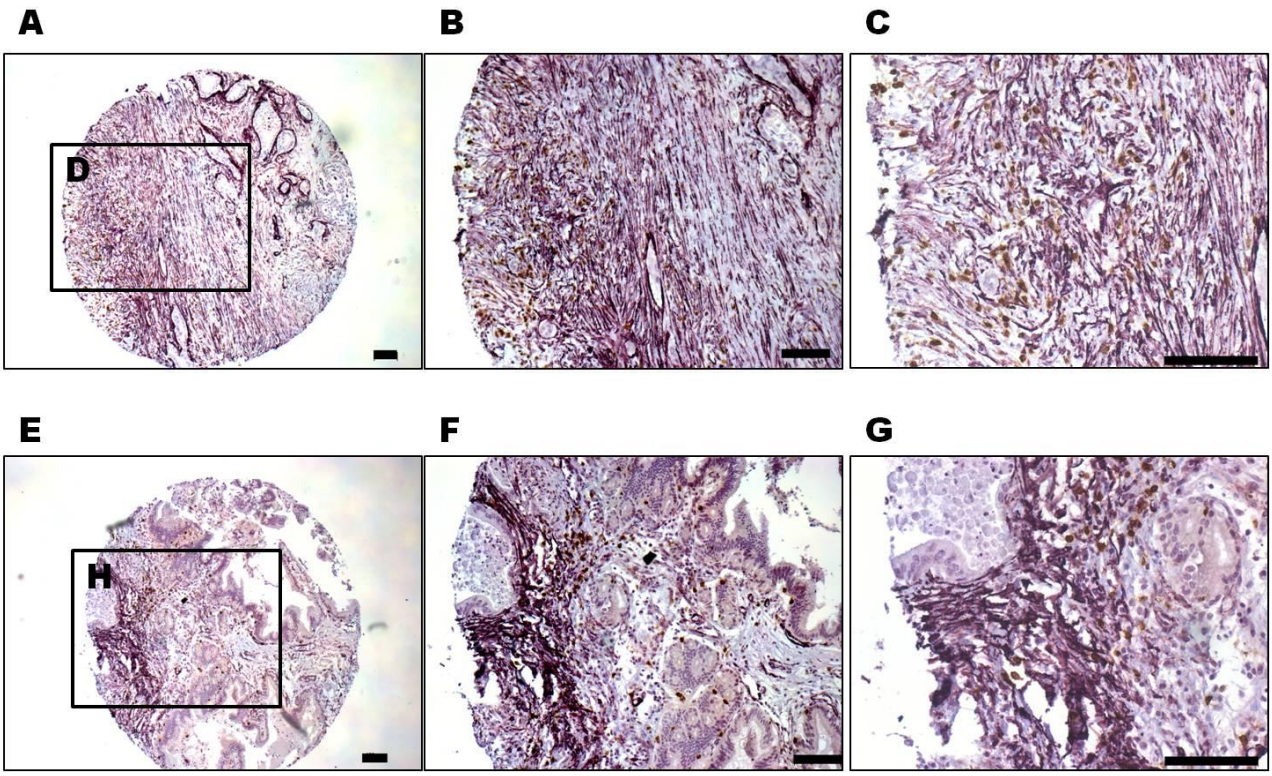

Figure 4.1: CD8+ T-cells are located in regions of tissue highly positive for the activated stellate cell marker, α-SMA

The figure above is a representation of pancreatic stellate cell tissues (TMAs) stained by immunohistochemistry for CD8 (brown) and α-SMA (purple). Regions of stroma positive for α-SMA were also densely populated with $CD8^+$ T-cells and in most cases $CD8^+$ T-cells can be seen juxtaposed to α-SMA positive cells.

Figures A-C represent the same TMA core at various magnifications (5x- 20x, respectively) where figures B and C are magnifications of the rectangle D. In the same manner, figures E-G represent the same TMA core at various magnifications (5x- 20x, respectively). Figures F and G are magnifications of the rectangle H.

All scale bars: 100μm

4.2 Stromal collapse reverses the juxtatumoural exclusion of cytotoxic T-cells in KPC mice but not $CD4^+$ T-cells, $F4/80^+$ macrophages, $CD11b^+$ MDSCs and $CD45R^+$ B-cells

KPC mice, a mouse model of PDAC (Clark, Hingorani et al. 2007) were treated with ATRA to transform activated stellate cells in the pancreas to a quiescent phenotype (treatment of KPC mice were performed at the Tuveson Laboratory and were performed by Drs. Feig and Froeling (Froeling, Feig et al. 2011)). I stained formalin fixed, paraffin embedded pancreas tissue slides for the cytotoxic T-cell marker, $CD8^+$ by immunohistochemistry.

I also observed similar sequestration of $CD8^+$ T-cells (Figure 4.2 A, B) and $CD45R^+$ B-cells (Figure 4.3 A, B) in the panstromal compartment of the most well characterized genetically engineered mouse model of human PDAC: KPC mice. Also similar to my observations in human PDAC, $F4/80^+$ macrophages (Figure 4.4 A, B) and $CD4^+$ T-cells (Figure 4.5 A, B) infiltrated in juxtatumoural compartment of KPC mice. $CD11b^+$ MDSCs were not sequestered in any of the stromal compartments (Figure 4.6 A, B). Froeling et al, had previously demonstrated that treating such mice with ATRA de-differentiates activated pancreatic stellate cells to a quiescent phenotype, thus mediating stromal collapse (Froeling, Feig et al. 2011). When we treated these mice with ATRA, $CD8^+$ T-cell infiltrate was enhanced allowing for $CD8^+$ T-cells to infiltrate the juxtatumoural compartment (Figure 4.2 A, C). Because the blood vessel density in KPC mice and human PDAC is significantly decreased in the immediate tumoural vicinity (Olive, Jacobetz et al. 2009), immune cells have to traverse the stromal compartments to access the tumour. These observations

suggest the possibility that the activated stellate cells compete with cancer cells for the T-cells infiltrating the PDAC tissues. It is therefore feasible that by adhering to $CD8^+$ T-cells, pancreatic stellate cells prevent the T-cells from accessing the tumour, in both human and mouse PDAC. Conversely, $CD45R^+$ B-cells (Figure 4.3 A, C), $F4/80^+$ macrophages (Figure 4.4 A, C), $CD4^+$ T-cells (Figure 4.5 A, C) and $CD11b^+$ MDSCs (Figure 4.6 A, C) infiltration patterns were not changed in KPC mice after treatment with ATRA.

In addition to the immune cells which I measured in ATRA and vehicle treated KPC mice, I measured the effect ATRA treatment had on Fibronectin expression in the stroma of KPC mice (Figure 4.7). The PDAC stroma of vehicle mice was strongly positive for Fibronectin (Figure 4.7 A, B), however, when these mice were treated with ATRA Fibronectin expression decreased significantly (Figure 4.7 A, C).

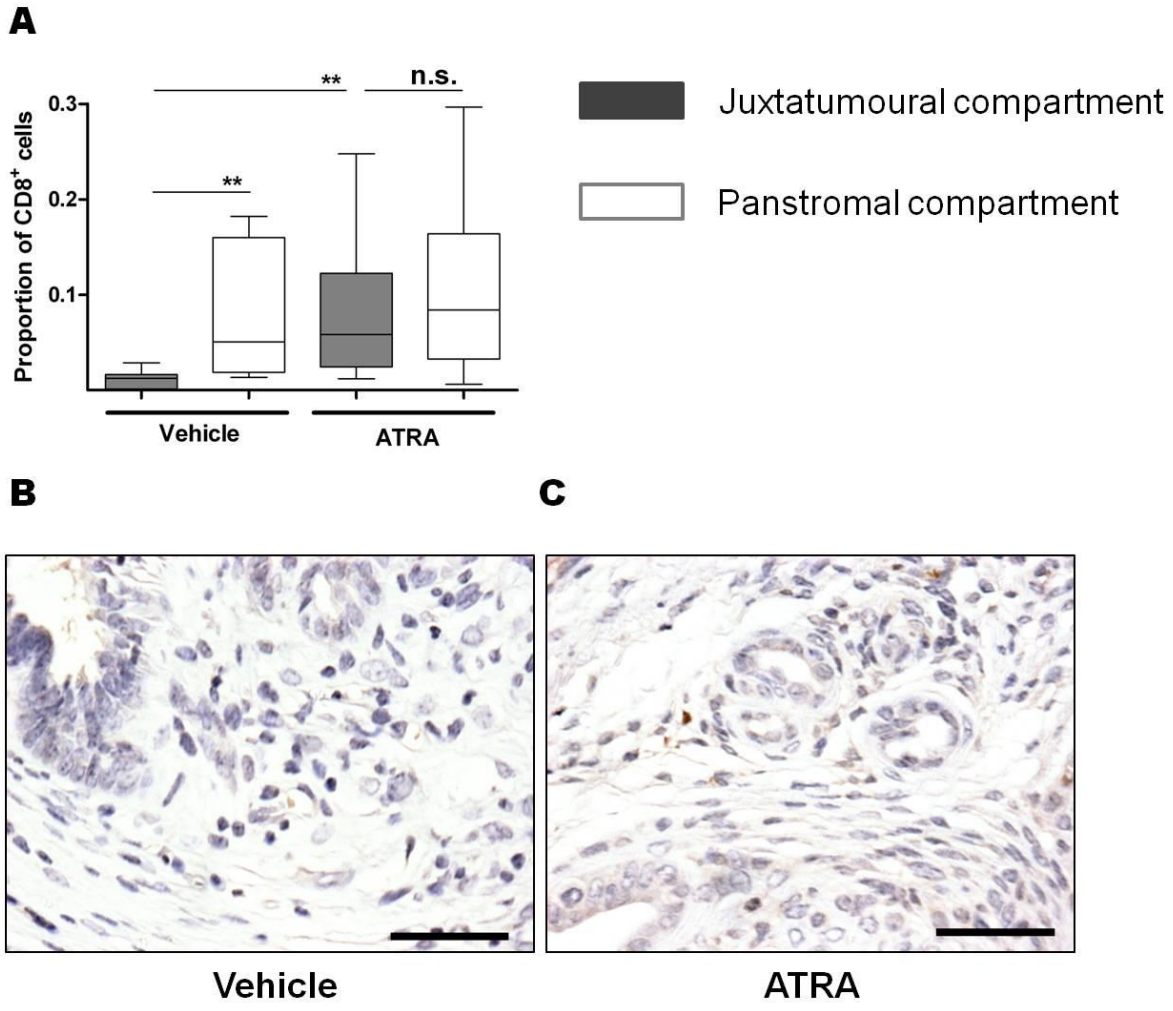

Figure 4.2: Stromal collapse reverses the juxtatumoural exclusion of CD8+ T-cells in KPC mice

Density of CD8+ T-cells in the juxtatumoural compartment of tumour bearing KPC mice (n=4) was less than the density in the panstromal compartment. However, there was no difference between stromal compartments when stellate cells of mice (n=6) were restored to quiescence by treatment with ATRA (A). Immunohistochemistry pictures representing mice that were treated with vehicle (control mice) (B) or treated with ATRA (C).

Data is represented by box (median with interquartile ranges (25^{th} and 75^{th})) and whisker (5^{th} and 95^{th} percentiles) plots. Outliers are represented by individual dots.

Scale bar: 100µm

Mann-Whitney U-test, all p-values are two-tailed.

** p= 0.001 to 0.01; n.s.= not significant

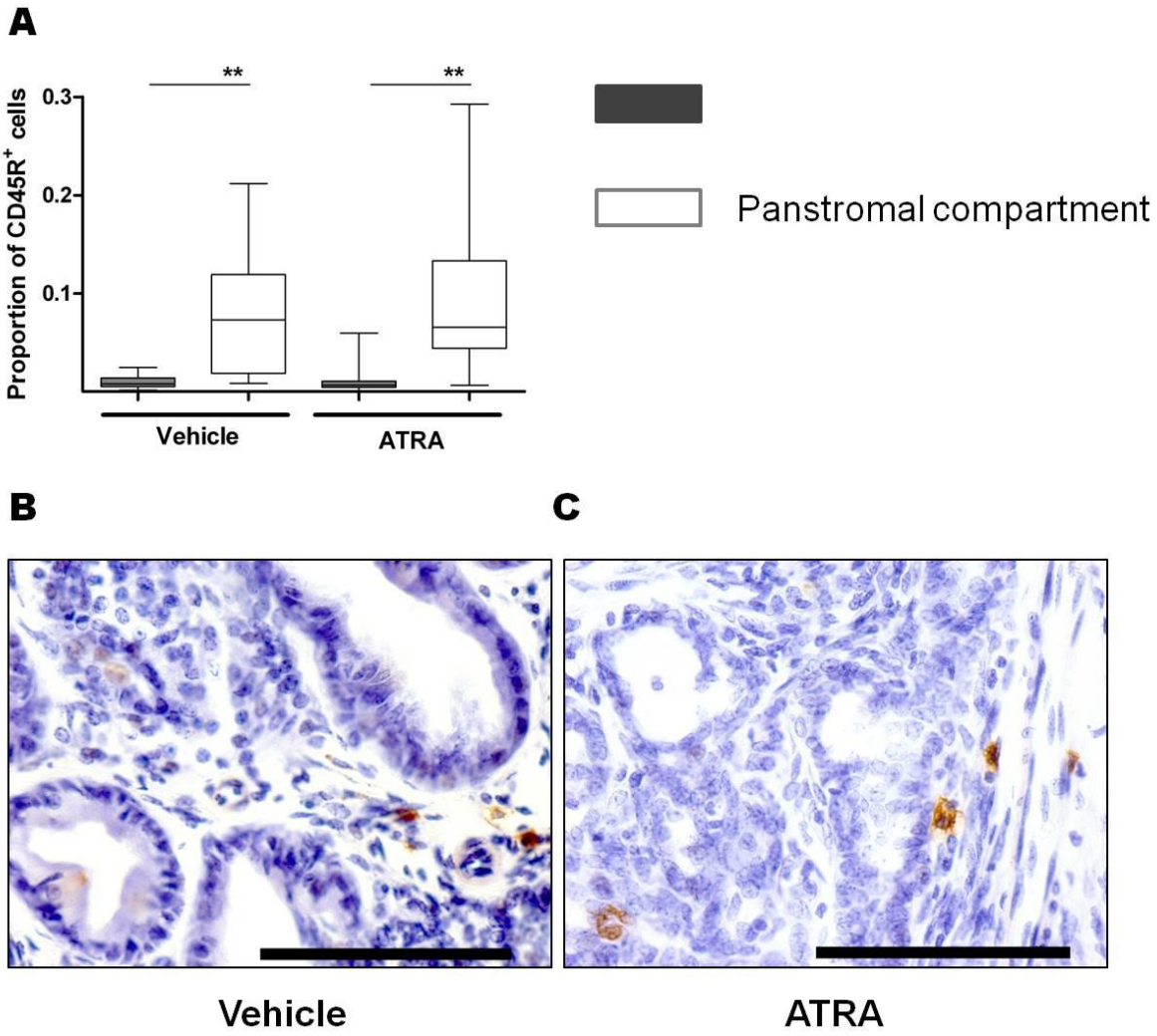

Figure 4.3: CD45R$^+$ B-cell infiltration in KPC mice remains unchanged after treatment with ATRA

CD45R$^+$ B-cell density in the panstromal compartment was significantly more than the density in the juxtatumoural compartment in vehicle treated mice (n= 4). After treating mice with ATRA, as previously described, there was no change in CD45R$^+$ B-cell infiltration (A). Immunohistochemistry pictures representing mice that were treated with vehicle (control mice) (B) or treated with ATRA (C).

Data is represented by box (median with interquartile ranges (25^{th} and 75^{th})) and whisker (5^{th} and 95^{th} percentiles) plots.

Scale bar: 100µm

Mann-Whitney U-test, all p-values are two-tailed.

** p= 0.001 to 0.01; n.s.= not significant

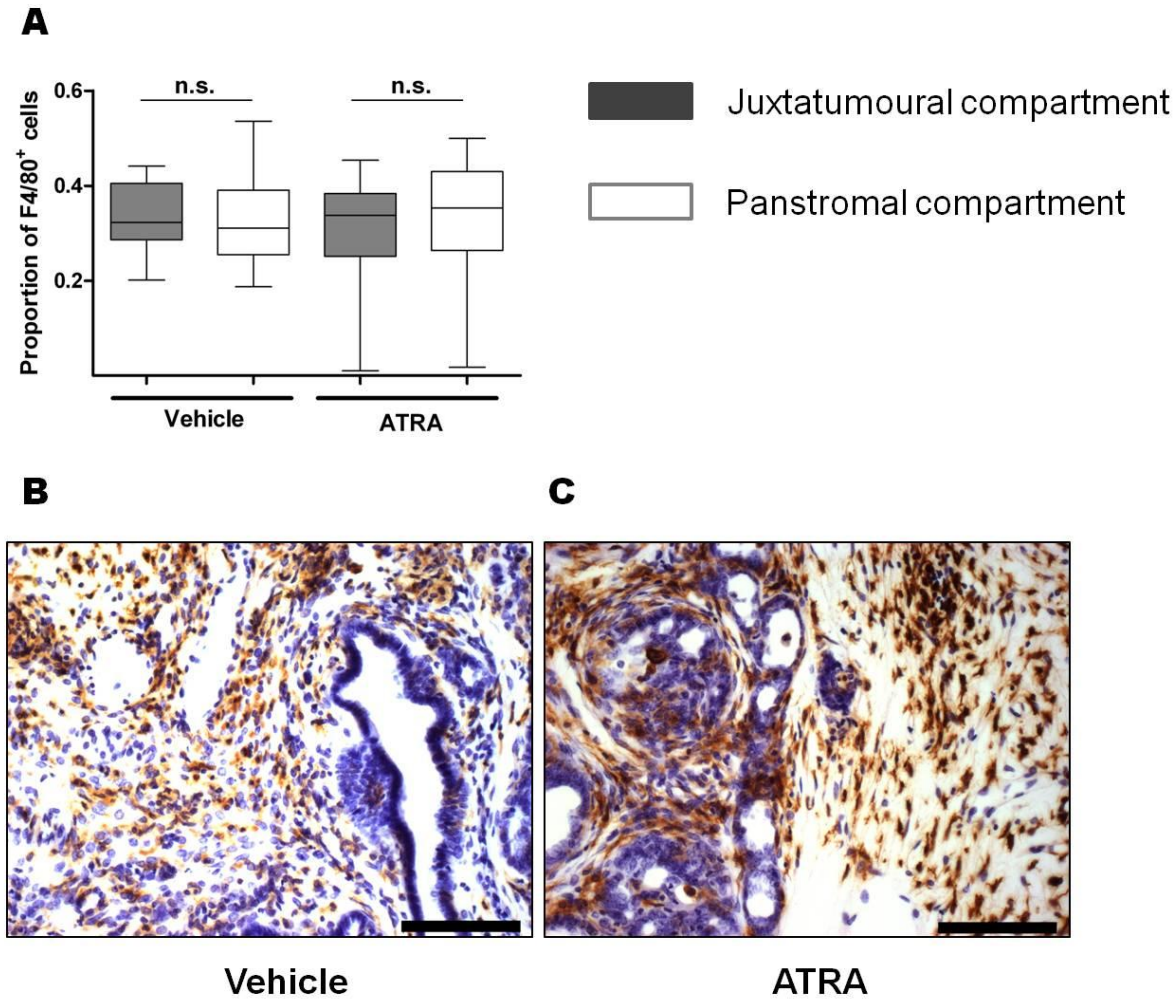

Figure 4.4: F4/80$^+$ macrophage infiltration in KPC mice remains unchanged after treatment with ATRA

Density of F4/80$^+$ macrophage in the panstromal compartment was similar to the density in the juxtatumoural compartment in vehicle treated mice (n= 4). This remained unchanged after KPC mice were treated with ATRA (A). Immunohistochemistry pictures representing mice that were treated with vehicle (control mice) (B) or treated with ATRA (C).

Data is represented by box (median with interquartile ranges (25th and 75th)) and whisker (5th and 95th percentiles) plots.

Scale bar: 100µm

Mann-Whitney U-test, all p-values are two-tailed.

n.s.= not significant

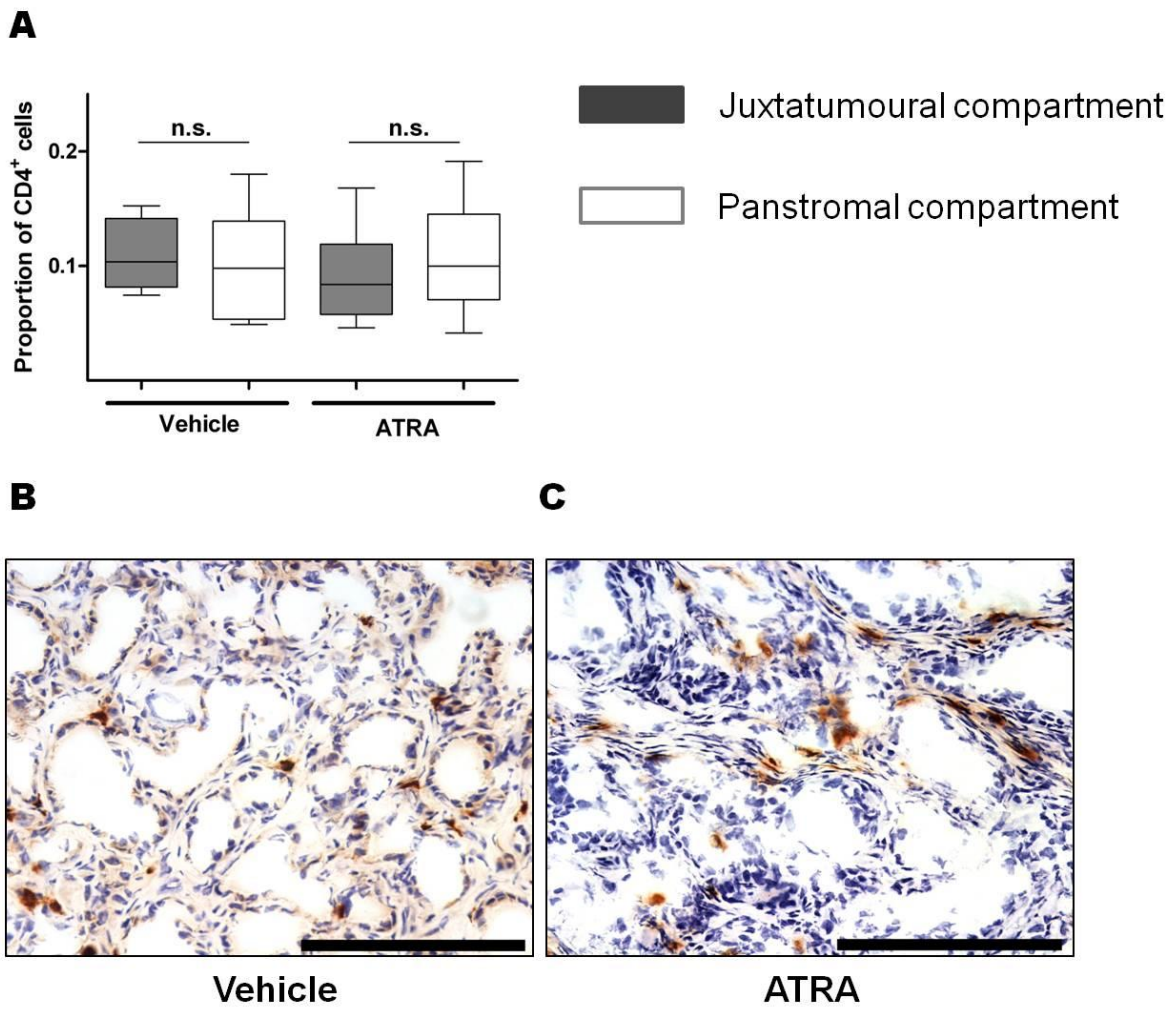

Figure 4.5: CD4$^+$ T-cell infiltration in KPC mice remains unchanged after treatment with ATRA

Density of CD4$^+$ T-cells in the panstromal compartment was similar to the density in the juxtatumoural compartment in vehicle treated mice (n= 4). This remained unchanged after KPC mice were treated with ATRA (A). Immunohistochemistry pictures representing mice that were treated with vehicle (control mice) (B) or treated with ATRA (C).

Data is represented by box (median with interquartile ranges (25th and 75th)) and whisker (5th and 95th percentiles) plots.

Scale bar: 100µm

Mann-Whitney U-test, all p-values are two-tailed.

n.s.= not significant

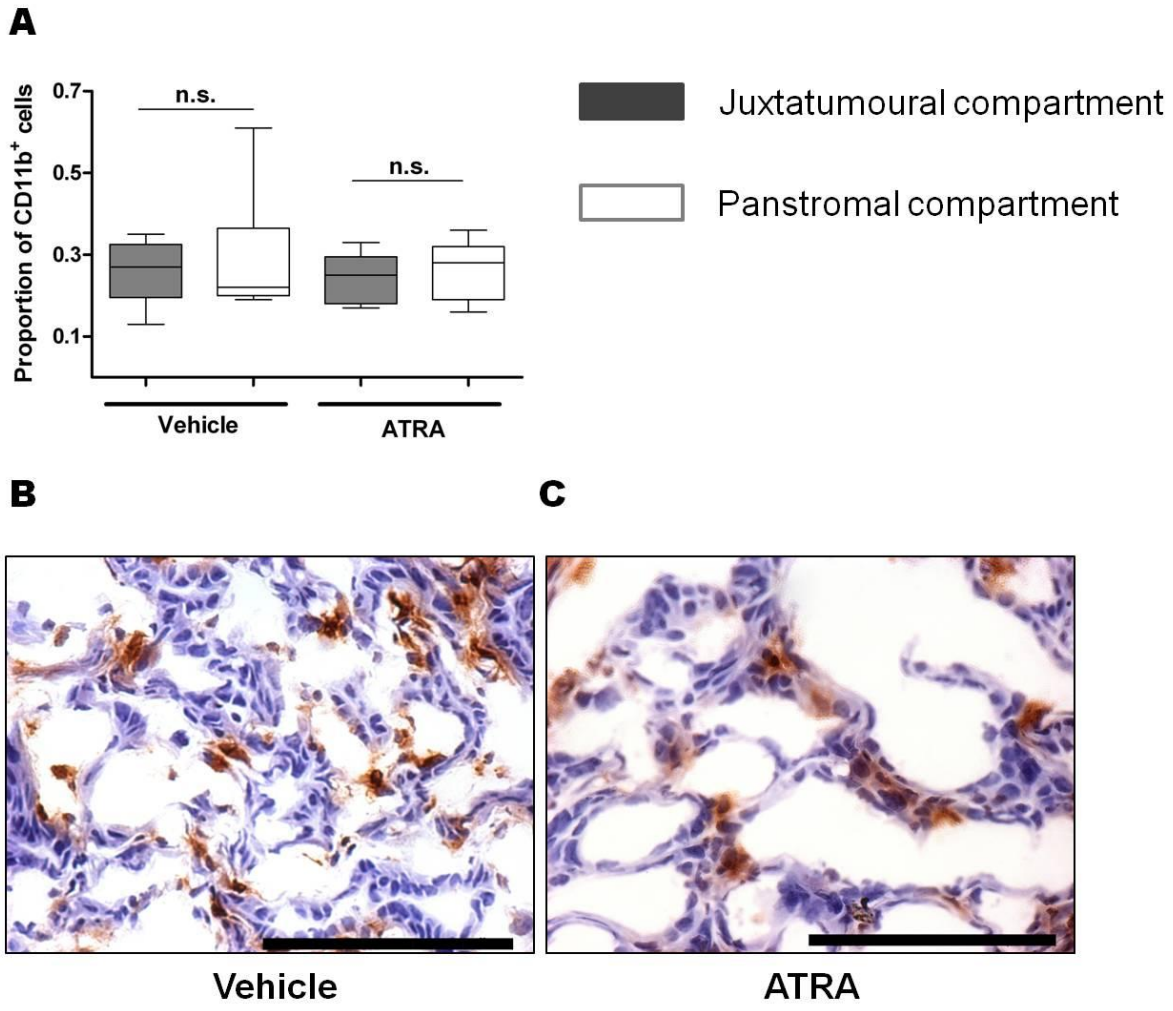

Figure 4.6: CD11b^{+} MDSC infiltration in KPC mice remains unchanged after treatment with ATRA

Density of CD4^{+} T-cells in the panstromal compartment was similar to the density in the juxtatumoural compartment in vehicle treated mice (n= 4). This remained unchanged after KPC mice were treated with ATRA (A). Immunohistochemistry pictures representing mice that were treated with vehicle (control mice) (B) or treated with ATRA (C).

Data is represented by box (median with interquartile ranges (25th and 75th)) and whisker (5th and 95th percentiles) plots.

Scale bar: 100µm

Mann-Whitney U-test, all p-values are two-tailed.

n.s.= not significant

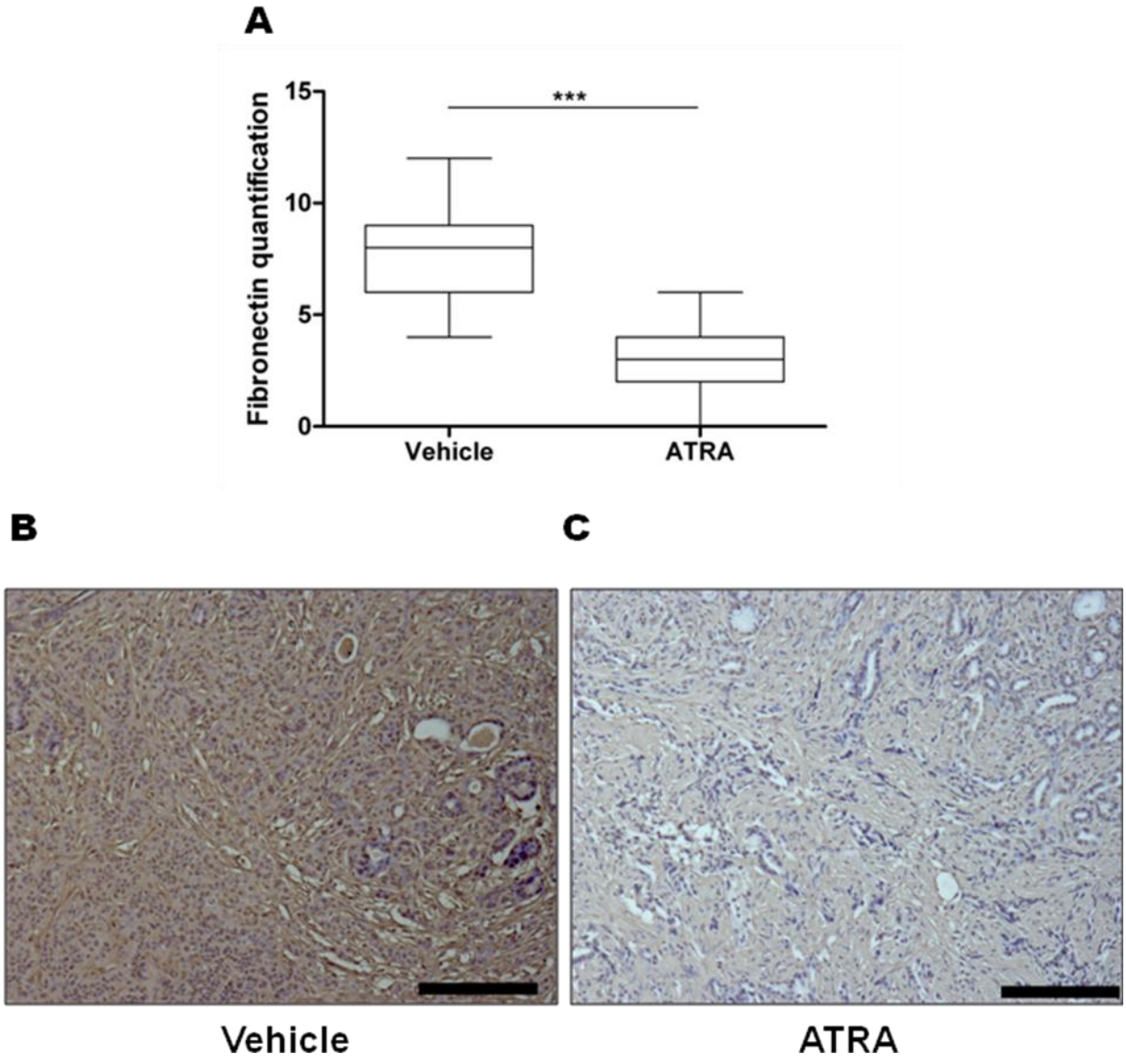

Figure 4.7: Expression of Fibronectin in the PDAC stroma of KPC mice is reduced after treatment with ATRA

PDAC stroma of KPC mice treated with vehicle (control mice) strongly expressed Fibronectin (A, B). However, when KPC mice were treated with ATRA Fibronectin expression decreased significantly (A, C).

Data is represented by box (median with interquartile ranges (25^{th} and 75^{th})) and whisker (5^{th} and 95^{th} percentiles) plots.

Scale bar: 100µm

Mann-Whitney U-test, all p-values are two-tailed.

*** p< 0.001

4.3 Optimization of Transwell® migration assay

To test our hypothesis that activated pancreatic stellate cells in PDAC may secrete chemokines which preferentially attract T-cells to them and thus prevent T-cell recruitment by the tumours, I modelled a migration assay using Transwells™ (Bleul, Fuhlbrigge et al. 1996; Ticchioni, Charvet et al. 2002; Meiron, Zohar et al. 2008; Borge, Nannini et al. 2010) as described in methods. As there were many variables to consider I performed optimization experiments.

4.3 a. Effects of serum on T-cell migration

$CD3^+$ T-cells were co-cultured in Transwell™ inserts with conditioned media of the cancer cell lines Capan 1 and AsPc 1 that had either been cultured in media containing 10% fetal bovine serum (FBS) or in media without FBS for 8 hours. RPMI with 10% FBS served as a positive control. This was because the cancer cell lines had been cultured in RPMI media with 10% FBS. $CD3^+$ T-cells migrated preferentially to the conditioned media of the cancer cell lines cultured with serum over control (Figure 4.8 B) but this was not the case for conditioned media of the cancer cell lines cultured in serum free media (Figure 4.8 A).

4.3 b. Effects of growth media on T-cell migration

T-cells are routinely cultured in RPMI media with serum, and pancreatic stellate cell line, PS1, is often cultured in DMEM/F12 media with serum but may also be cultured in RPMI media. To measure the effect of growth media on T-cell migration, I suspended $CD3^+$ cells in RPMI media without serum and co-cultured them in a Transwell™ insert with RPMI media, with and without serum, and with

DMEM media, with and without serum, for 8 hours. $CD3^+$ cells migrated preferentially to RPMI media with serum compared to RPMI media without serum (Figure 4.9). This differential migration was not as obvious in DMEM media with or without serum (Figure 4.9) indicating perhaps that $CD3^+$ cells are attracted to the DMEM media.

In addition, I suspended $CD3^+$ cells in DMEM without serum and co-cultured these in a transwell insert with DMEM with or without serum. Migration of $CD3^+$ cells was preferential to media containing serum over media without serum (Figure 4.9)

Also PS1 cell lines were cultured in RPMI or DMEM (both with serum) and their conditioned media was co-cultured with $CD3^+$ suspended in RPMI without serum. $CD3^+$ cells migrated preferentially to PS1 cells cultured in RPMI media (Figure 4.9).

Because of our doubts over the viability of T-cells suspended in DMEM media and the cross media migration when T-cells are suspended in one media and co-cultured with a different media, we opted to culture pancreatic stellate cells in RPMI media with serum.

4.3 c. Effects of pore size on T-cell migration

To check the effect that pore size of the transwell insert had on T-cell migration, I performed migration experiments with $CD3^+$ T-cell inserted into 5µm and 3µm pore sized transwells inserts. These were co-cultured with conditioned media from the cancer cell lines Capan 1 and AsPc 1, and the conditioned media from activated and quiescent pancreatic stellate cell line that resulted from treating PS1 cells with ATRA and ethanol respectively (previously discussed).

After 5 hours co-culture of $CD3^+$ T-cells in 5µm pore size transwell inserts with conditioned media, $CD3^+$ T-cells significantly migrated to activated pancreatic stellate cells over quiescent pancreatic stellate cells only (Figure 4.10 A).

After 8 hours co-culture of $CD3^+$ T-cells in 5µm pore size transwell inserts with conditioned media, $CD3^+$ T-cells significantly migrated to activated pancreatic stellate cells over quiescent pancreatic stellate cells and control (Figure 4.10 B).

After 8 hours co-culture of $CD3^+$ T-cells in 3µm pore size transwell inserts with conditioned media, $CD3^+$ T-cells significantly migrated to activated pancreatic stellate over control only (Figure 4.10 C).

I chose 5µm as the pore size of inserts as this gave the most significant results.

4.3 d. Effects of duration on T-cell migration

To study the effect duration of co-culture had on T-cell migration to activated and quiescent pancreatic stellate cells, I performed migration experiments with $CD3^+$ T-cells as described above and co-cultured for 1, 4 and 8 hours.

After 1 hour, migration to activated and quiescent PSC were similar to each other and to RPMI with 0% FBS (Figure 4.11 A, D). After 4 hours, migration of $CD3^+$ T-cells to activated PSC was significant over RPMI with 0% FBS and quiescent PSC (Figure 4.11 B, E). Migration of $CD3^+$ T-cell to activated PSC was also significant over RPMI with 0% FBS but not over quiescent PSC (Figure 4.11 C, F).

I adjusted $CD3^+$ T-cell migration data (shown; Figure 4.12) and all subsequent data for background by subtracting migration of T-cells to RPMI 0% (without FBS) from each value and normalised to RPMI with 10% FBS.

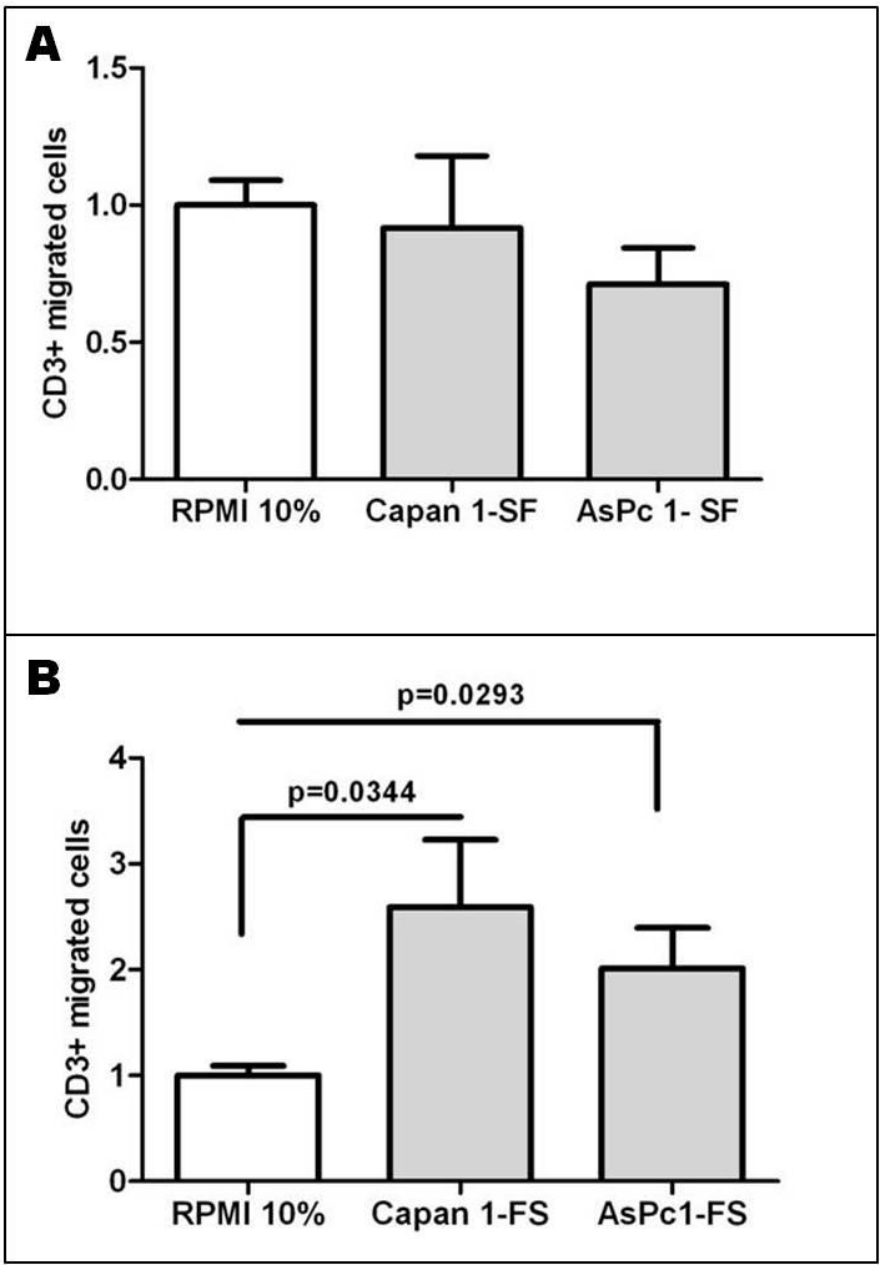

Figure 4.8: Effects of serum on migration

To assess the effect of serum in T-cell migration, migration assays to conditioned media collected with and without serum were performed. No significance was observed when T-cells migrated to conditioned media without serum (A), however, migration to cancer cell conditioned media were significantly more than control when serum was included (B).

SF: serum free; FS: full serum. Unpaired T test; p values are two tailed.

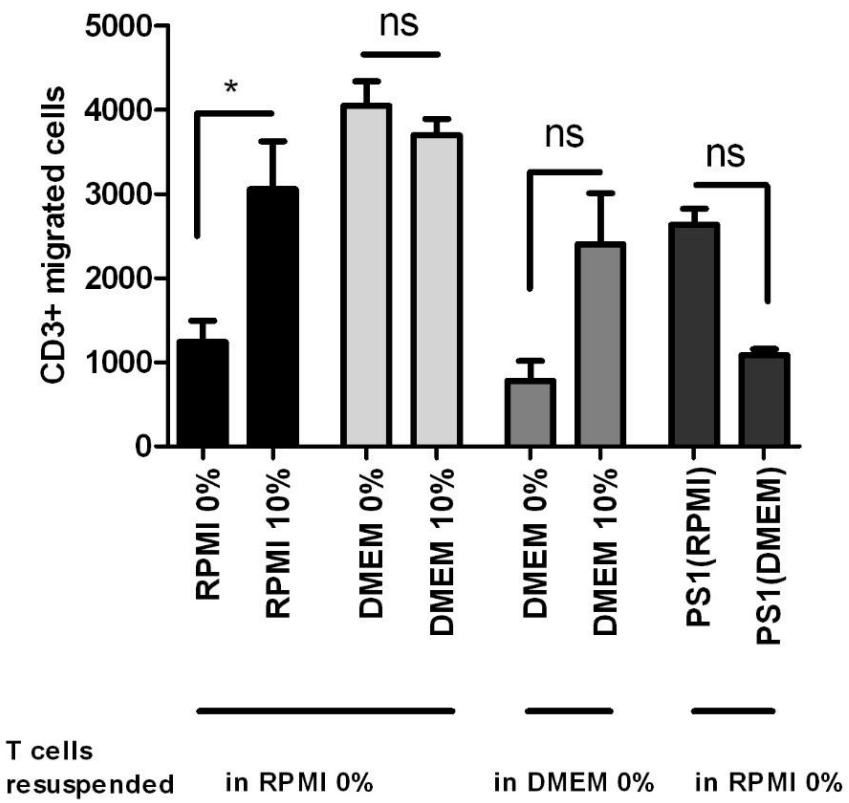

Figure 4.9: T-cell migration to growth media

$CD3^+$ cells migration to growth media (with 10% FBS or without FBS) was counted using the Casy counter. $CD3^+$ cells were suspended either in 0% RPMI or 0% DMEM and put in inserts. $CD3^+$ migration was significant between full serum media and without serum media when $CD3^+$ cells were suspended in the same growth media as the investigated condition (media in bottom well) but not when $CD3^+$ cells were suspended in a different media from media in the bottom well (highlighted in red). The difference in migration to RPMI with and without FBS when $CD3^+$ cells were suspended in 0% RPMI was significant. T-cells grow in RPMI media replete with FBS, hence we cultured PS1 cells in RPMI with 10% FBS.

Unpaired T test, p values are two tailed. * p= 0.01 to 0.05; ns= not significant

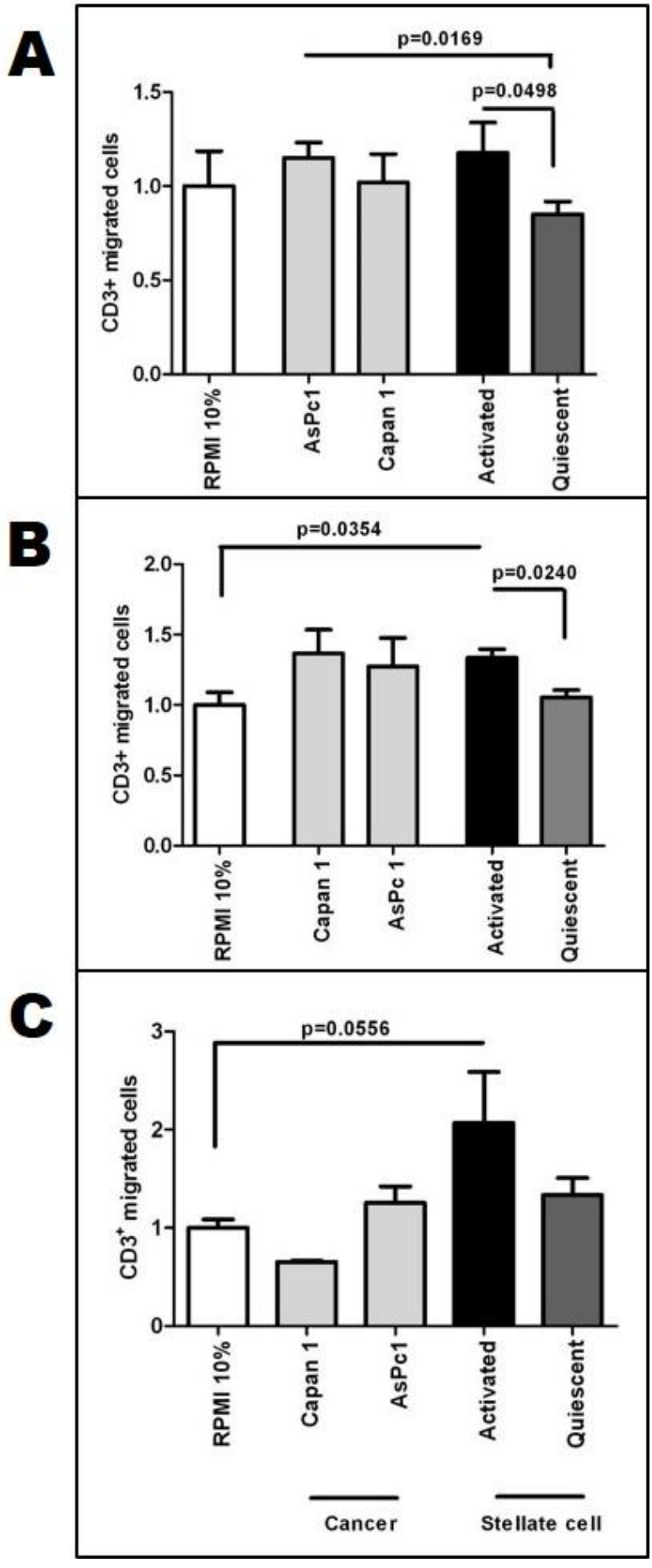
A
p=0.0169
p=0.0498
CD3+ migrated cells
1.5
1.0
0.5
0.0
RPMI 10%
AsPc1
Capan 1
Activated
Quiescent
B
p=0.0354
p=0.0240
CD3+ migrated cells
2.0
1.5
1.0
0.5
0.0
RPMI 10%
Capan 1
AsPc 1
Activated
Quiescent
C
p=0.0556
CD3+ migrated cells
3
2
1
0
RPMI 10%
Capan 1
AsPc1
Activated
Quiescent
Cancer
Stellate cell

Figure 4.10: Effects of pore size and duration on T-cell migration

$CD3^+$ migration experiments to determine transwell pore size and incubation time. $CD3^+$ was suspended in RPMI without serum and migrated to supernatant from pancreatic cancer cells (AsPc1 and Capan1), activated pancreatic stellate cells and quiescent pancreatic stellate cells. (A) 5 hour migration assays with 5µm pore sized transwells were performed. Migration of $CD3^+$ cells to activated pancreatic stellate cells was not significant over control, but significant over quiescent pancreatic stellate cells. Migration to AsPc1 was also significantly more than quiescent pancreatic stellate cell. (B) Migration assays were performed with 5µm pore size transwells and incubated for 8 hours. $CD3^+$ migrated to activated pancreatic stellate cells significantly more than quiescent pancreatic stellate cells and control. (C) Migration assays were carried out in 3µm pore size transwells and incubated for 8 hours. $CD3^+$ migration to activated pancreatic stellate cells compared to control was significant.

Unpaired T test; p values are two tailed.

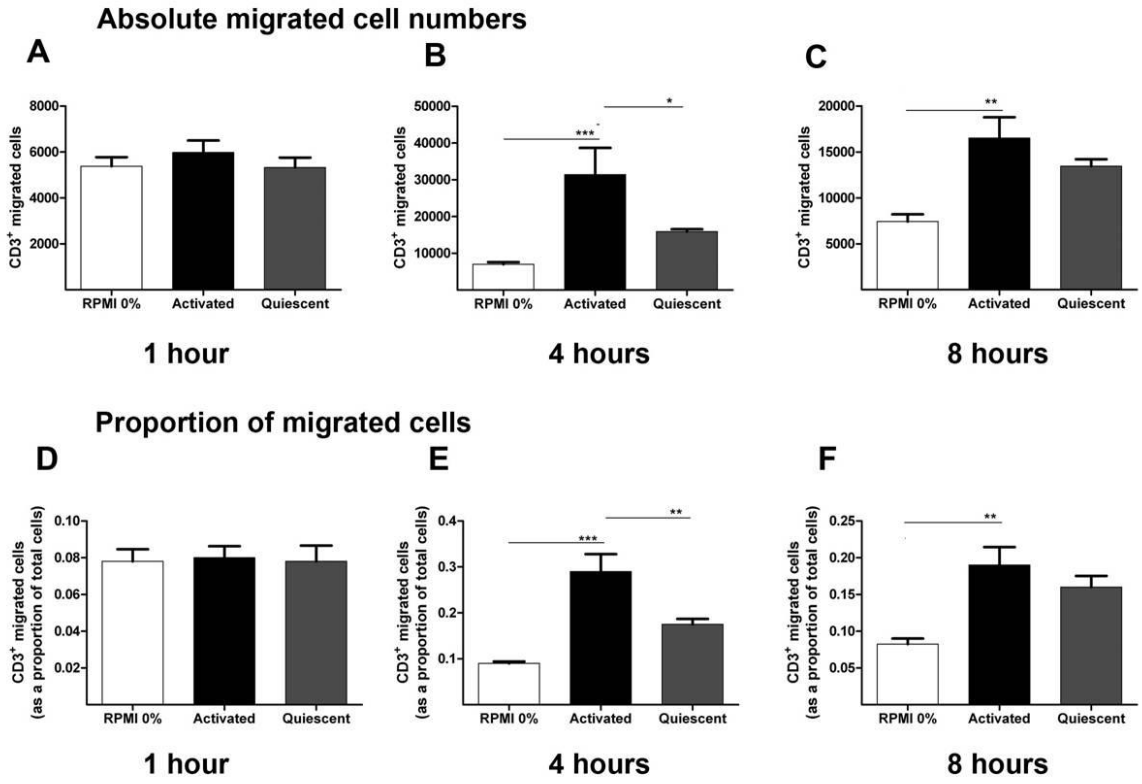

Figure 4.11: CD3$^+$ time point migration assays

Migration assay of CD3$^+$ T-cells from healthy donors towards the conditioned media of activated and quiescent pancreatic stellate cells, and RPMI without FBS. Migration of CD3$^+$ T-cells to RPMI without FBS was considered as background migration.

There were no differences between conditions when migration was terminated after one hour, however, observable, significant differences were observed at four and eight hour durations with differences between conditions at 4 hours being the most observable.

Mean and SEM are plotted. $CD3^+$ T-cell migration was calculated as “absolute migrated cells numbers” (A, B and C) and as “proportion of migrated cells” to the total amount of cells at the beginning of the assay (D, E and F).

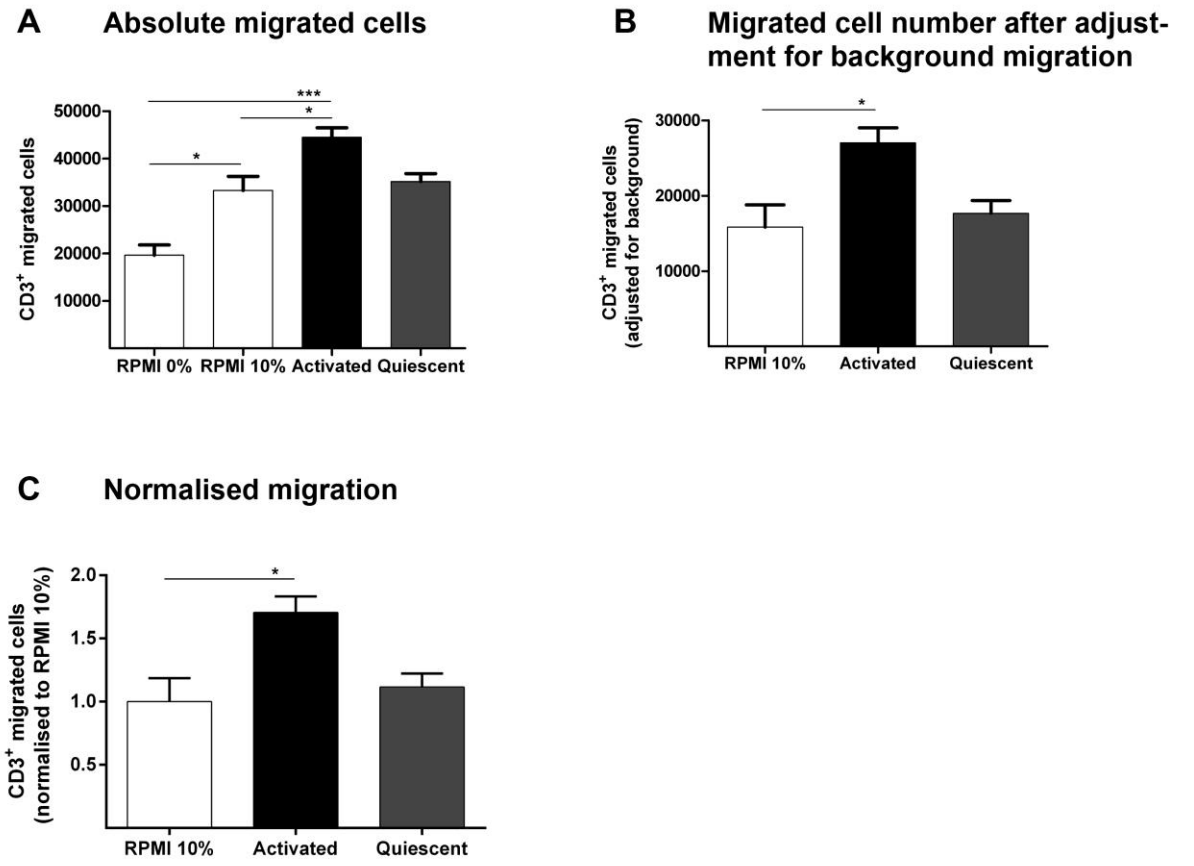

Figure 4.12: Normalisation of migration data

Migration assay of $CD3^+$ T-cells to RPMI without FBS (RPMI 0%), RPMI 10% (10% FBS) activated PSC and quiescent PSC was performed and data was plotted "Absolute migrated cells" (A). Migration values of RPMI 0% (which served as background migration) were subtracted from each value and plotted (B). Values were then normalised to RPMI 10% (serum directed migration) which then served as control.

4.4 Cytotoxic T-cells migrate preferentially towards activated pancreatic stellate cells

Pancreatic stellate cells may have an activated or quiescent phenotype that are accompanied by physiological and genetic changes (Froeling, Feig et al. 2011). We thus hypothesised that T-cells may migrate to the conditioned media of these phenotypes differentially. We found that $CD3^+$ (T-cells) migrated preferentially to the activated phenotype over quiescent while migration to quiescent was of a similar level as basal media (RPMI with 10% FBS) (Figure 4.13). T-cells also migrated to cancer cell (AsPc 1 and Capan 1) conditioned media more than RPMI with 10% FBS and conditioned media of quiescent pancreatic stellate cells (Figure 4.13).

The differential migration of helper T-cells ($CD4^+$) was not as dependent on conditioned media from cancer cells or stellate cells (no difference between 0% and 10% FBS media, Figure 4.14). Migration of $CD8^+$ T-cells to basal conditions (RPMI with FBS) was significantly less than cancer cells (Capan1) as well as activated pancreatic stellate cells (Figure 4.15). Also, migration of $CD8^+$ T-cells towards activated pancreatic stellate cell conditioned media was significantly more than quiescent pancreatic stellate cell or cancer cell conditioned media.

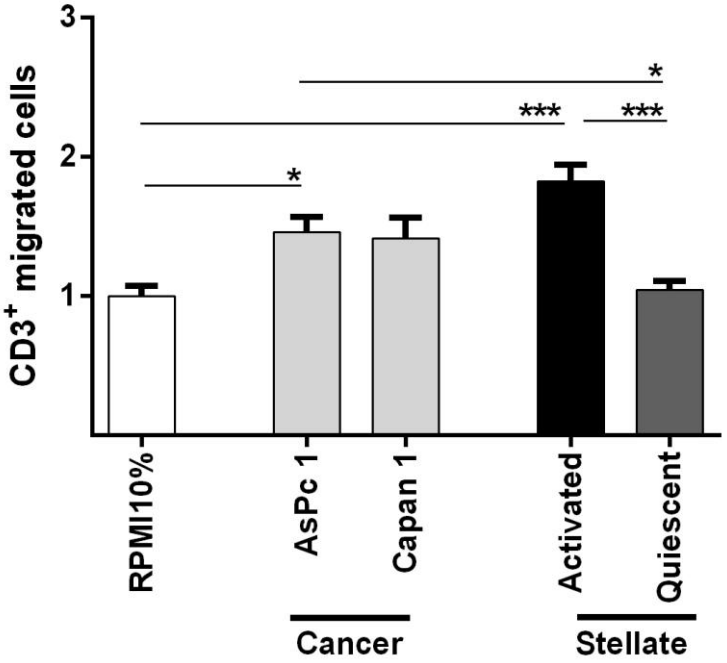

Figure 4.13 *In vitro* T-cell ($CD3^+$) migration assays

Transwell migration assay of immune cells from healthy donors (n=4) towards conditioned media (CM) from activated and quiescent pancreatic stellate cells and cancer cells (Capan1 and AsPc1). 0% RPMI (no serum) was considered as 'background' migration of T-cells, whilst 10% RPMI (10% FBS) was considered as basal serum-directed migration of T-cells. These two conditions served as internal controls. Values were normalised to RMPI 10% (Y axis).

We demonstrated a significant reduction of migration of $CD3^+$ T-cells to quiescent pancreatic stellate cell CM in comparison to activated pancreatic stellate cell CM. While $CD3^+$ cell migration to cancer CM was significant over basal medium, it was less than migration to activated pancreatic stellate cell CM.

Bar chart represents mean ± SEM. *** $p< 0.001$; ** $p= 0.001$ to 0.01; * $p= 0.01$ to 0.05, Comparisons were conducted with ANOVA with comparisons between columns using Bonferroni's Multiple Comparison Test.

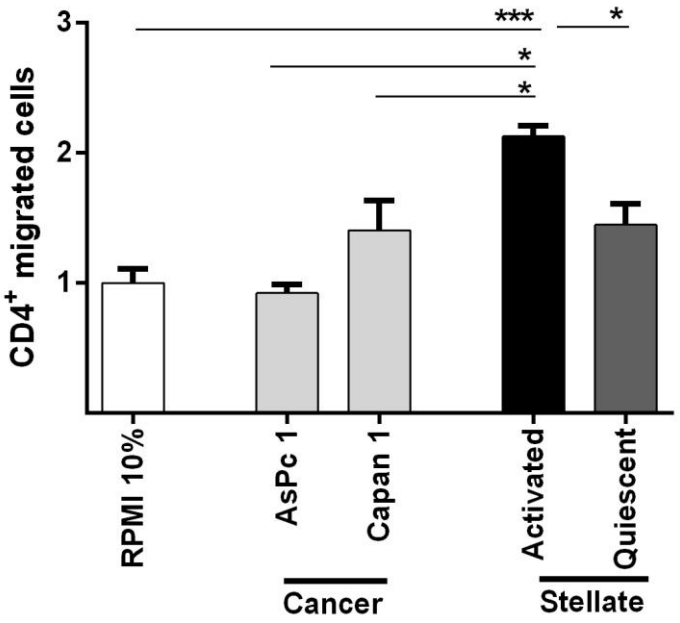

Figure 4.14 *In vitro* helper T-cell ($CD4^+$) migration assays

Transwell migration assay of immune cells from healthy donors (n=4) towards conditioned media (CM) from activated and quiescent pancreatic stellate cells and cancer cells (Capan1 and AsPc1). 0% RPMI (no serum) was considered as 'background' migration of T-cells, whilst 10% RPMI (10% FBS) was considered as basal serum-directed migration of T-cells. These two conditions served as internal controls. Values were normalised to RMPI 10% (Y axis).

We demonstrated a significant reduction of migration of $CD4^+$ T-cells to quiescent pancreatic stellate cell CM in comparison to activated pancreatic stellate cell CM. The relative migration of $CD4^+$ cells was minimal with little difference over the background level (RPMI 0%). Migration of helper T-cells towards activated pancreatic stellate cell CM was more than migration towards cancer cell CM.

Bar chart represents mean ± SEM. *** $p< 0.001$; ** $p= 0.001$ to 0.01; * $p= 0.01$ to 0.05, Comparisons were conducted with ANOVA with comparisons between columns using Bonferroni's Multiple Comparison Test.

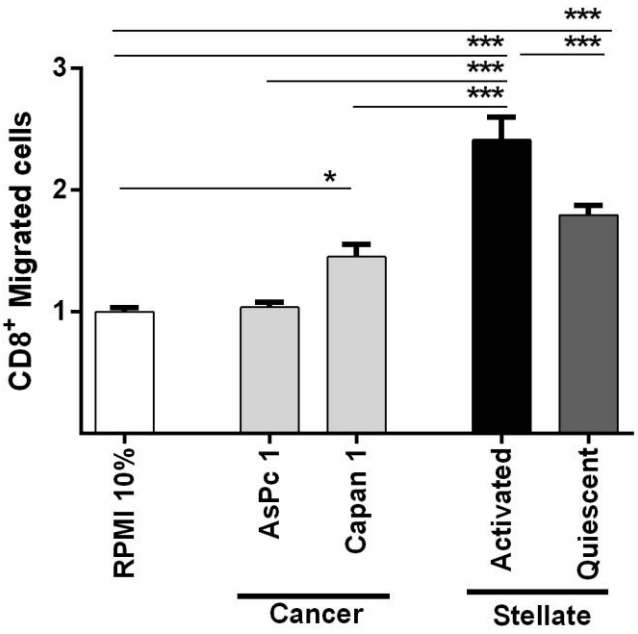

Figure 4.15 *In vitro* cytotoxic T-cell ($CD8^+$) migration assays

Transwell migration assay of immune cells from healthy donors (n=4) towards conditioned media (CM) from activated and quiescent pancreatic stellate cells and cancer cells (Capan1 and AsPc1). 0% RPMI (no serum) was considered as 'background' migration of T-cells, whilst 10% RPMI (10% FBS) was considered as basal serum-directed migration of T-cells. These two conditions served as internal controls. Values were normalised to RMPI 10% (Y axis).

The most dramatic, and perhaps clinically relevant, fold change in migration of T-cells with different conditioned media was seen with $CD8^+$ T-cells. We demonstrated a significant reduction of migration of $CD8^+$ T-cells to quiescent pancreatic stellate cell CM in comparison to activated pancreatic stellate cell CM. Migration of cytotoxic T-cells towards activated pancreatic stellate cell CM was more than migration towards cancer cell CM.

Bar chart represents mean ± SEM. *** p< 0.001; ** p= 0.001 to 0.01; * p= 0.01 to 0.05, Comparisons were conducted with ANOVA with comparisons between columns using Bonferroni's Multiple Comparison Test.

4.5 CD3+ T-cells adhere to pancreatic stellate cells

Our observations of sequestration in the panstromal compartment and differential migration between activated and quiescent pancreatic stellate cells informed our hypothesis that activated and quiescent stellate cells may have different adhesion properties that may variably interact with T-cells during infiltration. Thus we performed adhesion assays. The premise for this adhesion assay is that T-cells are routinely cultured in suspension and do not adhere to glass and after a rigorous wash step (performed three times), only T-cells adhered to pancreatic stellate cells will remain. The cover slip can then be fixed and adherent T-cells can be counted.

To determine the optimal time for co-culturing $CD3^+$ cells with pancreatic stellate cells, $CD3^+$ cells were counted after co-culturing for 1, 2 and 8 hours. 6 power fields per slide were sampled at random at a magnification of x63 and the ratio was obtained by dividing the number of adhered $CD3^+$ cells by the number of pancreatic stellate cells in each power field. The median of ratios per power field was calculated resulting in one data point per cover slip. There was no significant difference in adhesion among the time points (Figure 4.16 B). We therefore chose duration of 1 hour (Figure 4.16 A) and performed and quantified the assay on 6 cover slips at a sample rate of 6 high power fields per cover slip (Figure 4.17).

These *in vitro* observations, along with the previous *in vivo* observations suggest that activated pancreatic stellate cells, present abundantly in panstromal compartment, might attract and adhere to T-cells before they can access tumour.

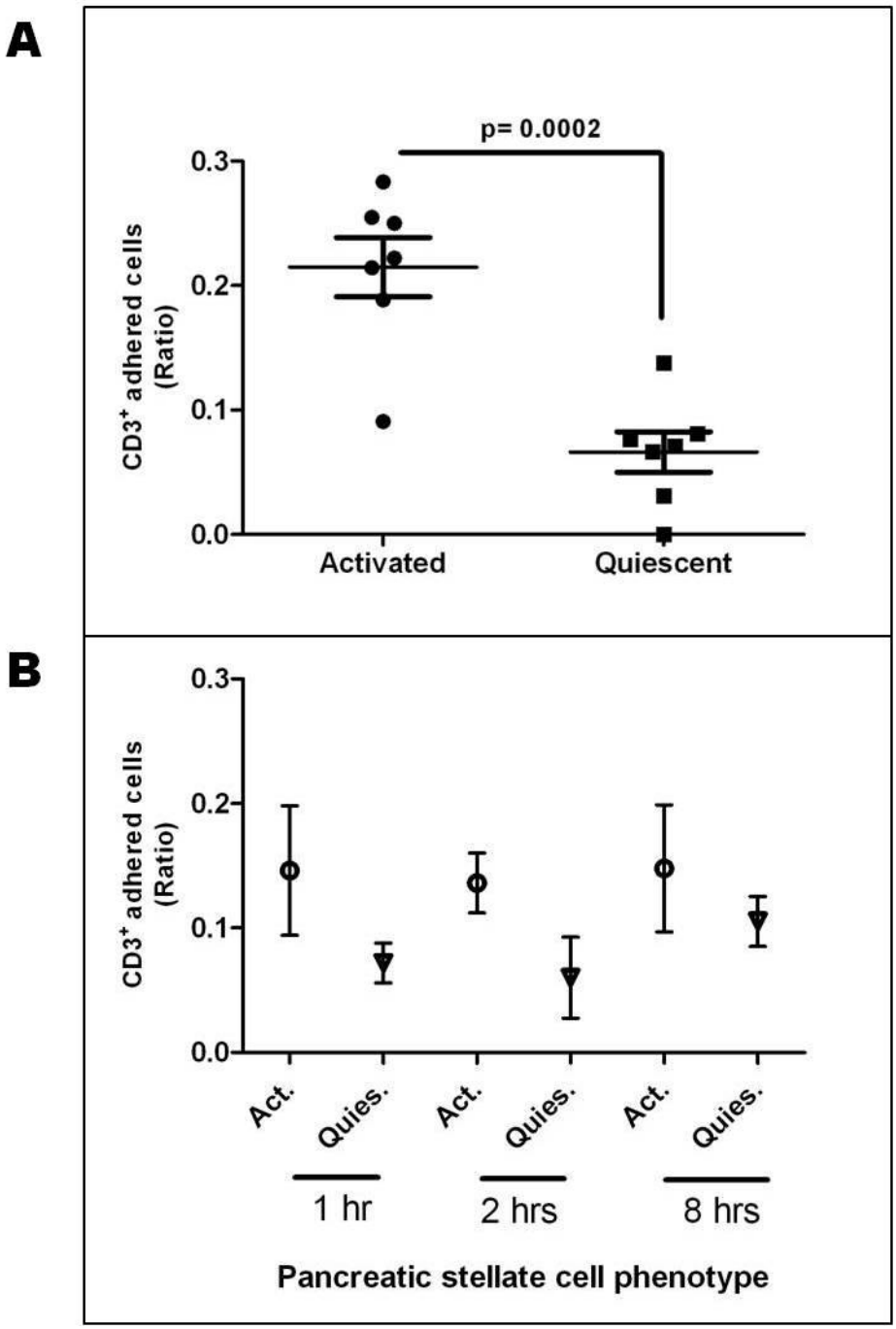

Figure 4.16 Optimisation of T-cell adhesion assay

The above graphs represent optimisation experiments of T-cell adhesion to quiescent and activated pancreatic stellate cells. The method has been described previously. Ratios were obtained by dividing the number of adhered $CD3^+$ T-cells by the number of pancreatic stellate cell per power field. (A) The graph is a

representation of adhesion of $CD3^+$ T-cells to quiescent and activated pancreatic stellate cells after 1 hour on one cover slip only. Each data point represents a power field. 7 power fields were sampled at random at a magnification of x63. Adhesion to activated pancreatic stellate cells was significantly more than quiescent phenotype ($p = 0.0002$; Unpaired T test, 2 tailed). (B) Time point experiments of $CD3^+$ T-cell adhesion to pancreatic stellate cell. $CD3^+$ T-cells and pancreatic stellate cell phenotypes were co-cultured for 1, 2 and 8 hours. 6 power fields per cover slip were sampled at random, at a magnification of x63 and median calculated to give one data point. 3 independent cover slips for each pancreatic stellate cell phenotype and time point were counted.

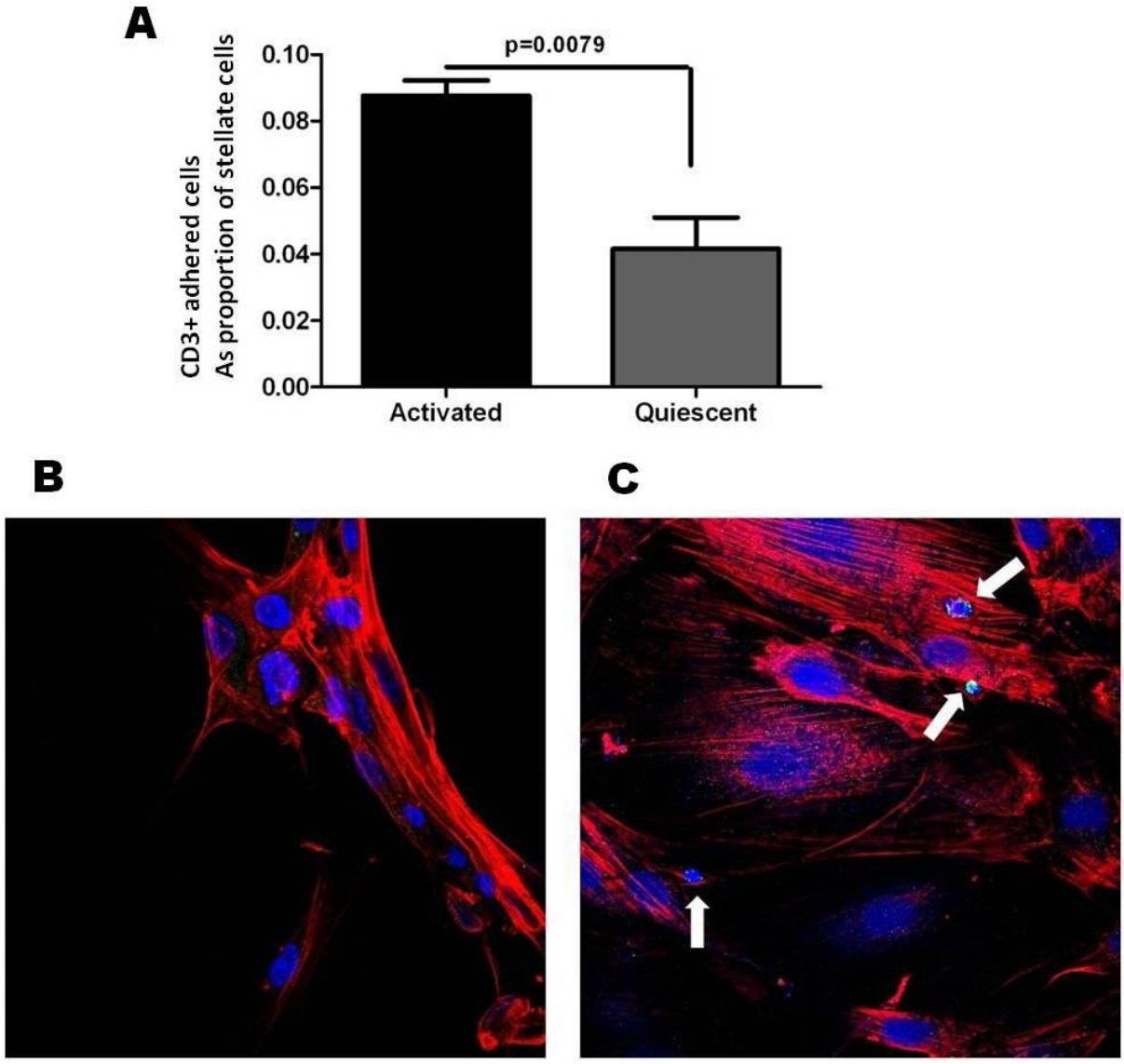

Figure 4.17 T-cell adhesion assay

The above figure represents T-cell adhesion to quiescent and activated pancreatic stellate cells. Ratios were obtained by dividing the number of adhered $CD3^+$ T-cells by the number of pancreatic stellate cell per power field (Y axis) to normalise for pancreatic stellate cell numbers. Cover slips were stained by immunofluorescence. Blue represents DAPI; Red represents F-actin; Green represents $CD3^+$ cells (T-cells). $CD3^+$ cells were identified based on their staining pattern and their cell

morphology (white arrows). 6 power fields per cover slip were sampled and median was calculated for all 6 power fields. A total of 6 cover slips were sampled.

(A) Adhesion of T-cells to activated pancreatic stellate cells were significantly more than the quiescent pancreatic stellate cells (Paired t-test; p-value is two-tailed).

(B) T-cells do not adhere to quiescent pancreatic stellate cells (C) T-cells adhere to activated pancreatic stellate cells (white arrows).

4.6 Pancreatic stellate cells secrete more CXCL12 upon activation

I re-analysed previously performed gene expression arrays (by Fieke Froeling). This has been discussed in materials and methods. We demonstrated that as a result of activation, secretion of a number of cytokines, chemokines and adhesion molecules is altered in pancreatic stellate cells (Froeling, Feig et al. 2011) (Figure 4.18).

I investigated putative migration inducing genes in conditioned media of activated and quiescent pancreatic stellate cells by enzyme linked immuno-assay. Quiescent pancreatic stellate cell secreted more Interleukin 8 (IL8) and soluble intracellular cell adhesion molecule 1 (sICAM 1/ CD54) compared to activated pancreatic stellate cells. Secretion of Monocyte chemotactic protein 1 (MCP1/ CCL2) was not altered when phenotypes of pancreatic stellate cells were changed. In contrast, activated pancreatic stellate cells secreted significantly higher stromal cell derived factor 1 alpha (SDF1α/ CXCL12) than quiescent pancreatic stellate cells (Figure 4.19).

A

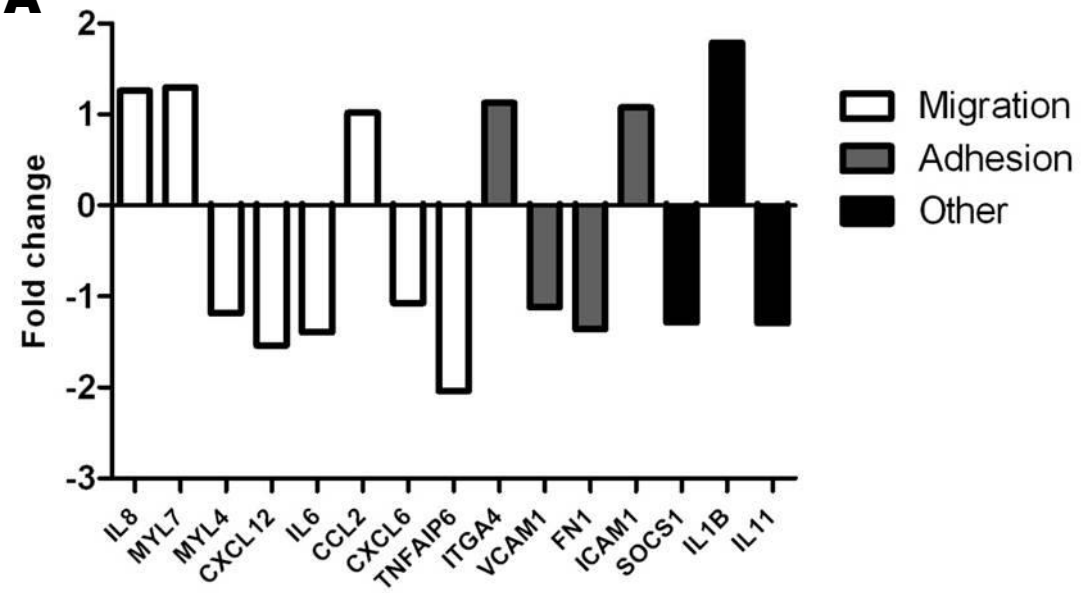

B

Cell adhesion pathway (Gene ontology: 0007155

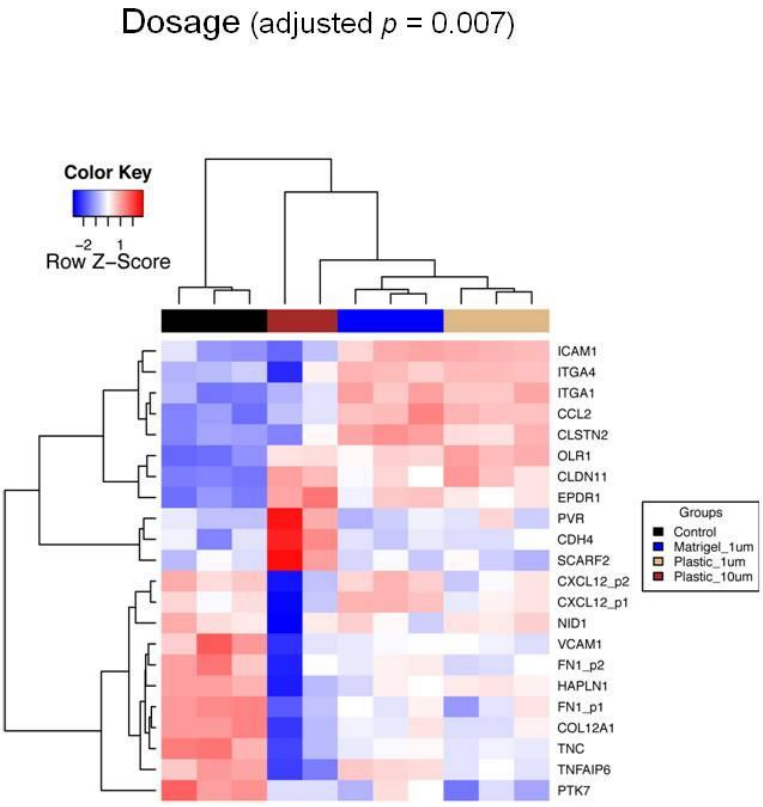

c Cell adhesion pathway (Gene ontology: 0007155

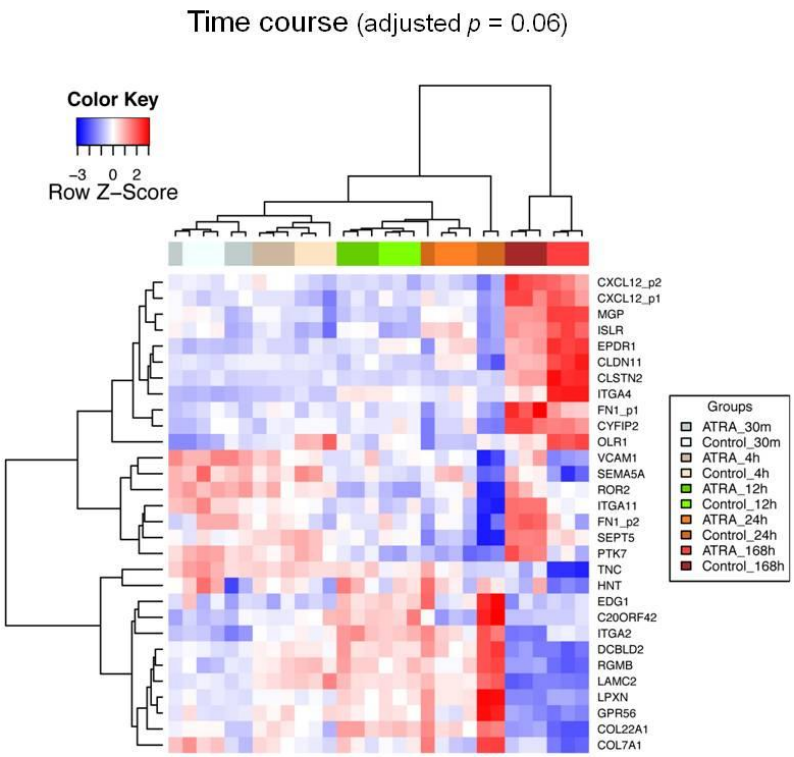

D Cytokine-cytokine receptor interaction (KEGG pathway)

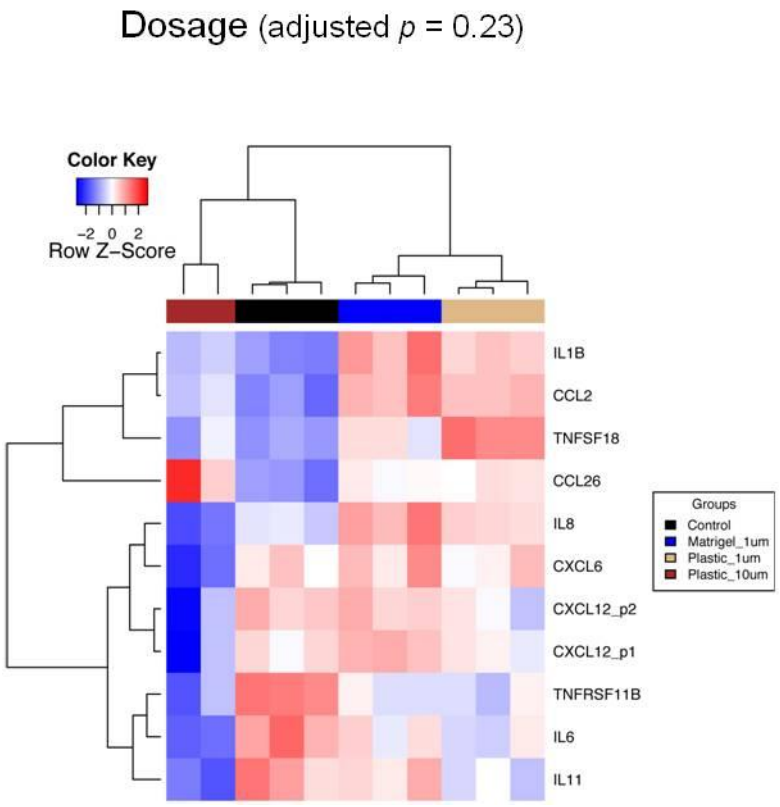

E Cytokine-cytokine receptor interaction (KEGG pathway)

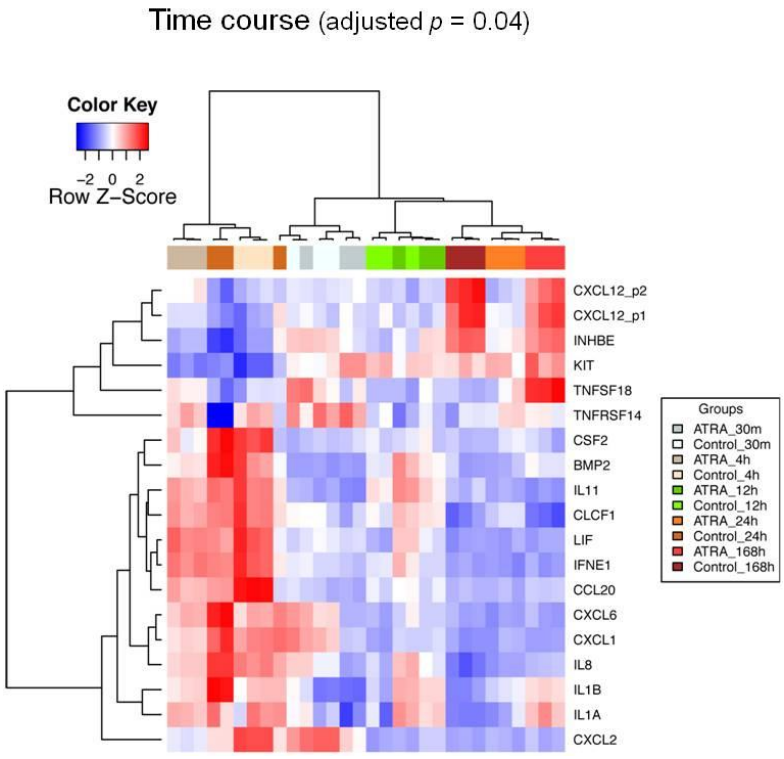

Figure 4.18 Gene expression changes upon activation of pancreatic stellate cells

Gene expression microarrays of quiescent pancreatic stellate cells compared to controls (activated pancreatic stellate cells). (A) Positive Y axis is “up-regulated in quiescent pancreatic stellate cells compared to activated pancreatic stellate cells”; negative Y axis is “down-regulated in quiescent pancreatic stellate cells compared to activated pancreatic stellate cells”. Gene functions were established from the genetic database, www.genecards.com and grouped as shown.

(B-E) Gene expression microarrays (as in A) were re-analysed for differentially expressed genes involved in cell adhesion (Gene Ontology GO:0007155) gene set enrichment test (p= 0.007). This was performed performed using DAVID (Benjamini-Hochberg test). Hierarchy clustering of all samples from activated pancreatic stellate cells (which served as control (black)) and quiescent pancreatic stellate cells when plated on Matrigel and treated with 1 μM ATRA (blue), when plated on Plastic and treated with 1μM ATRA (burlywood) and when plated on plastic and treated with 10 μM ATRA (dark brown), was performed based on the expression profiles of these differentially expressed probes using the Euclidean metric. Changes in gene expression from time-course experiments and changes in cytokine-cytokine receptor interaction pathway were also analysed.

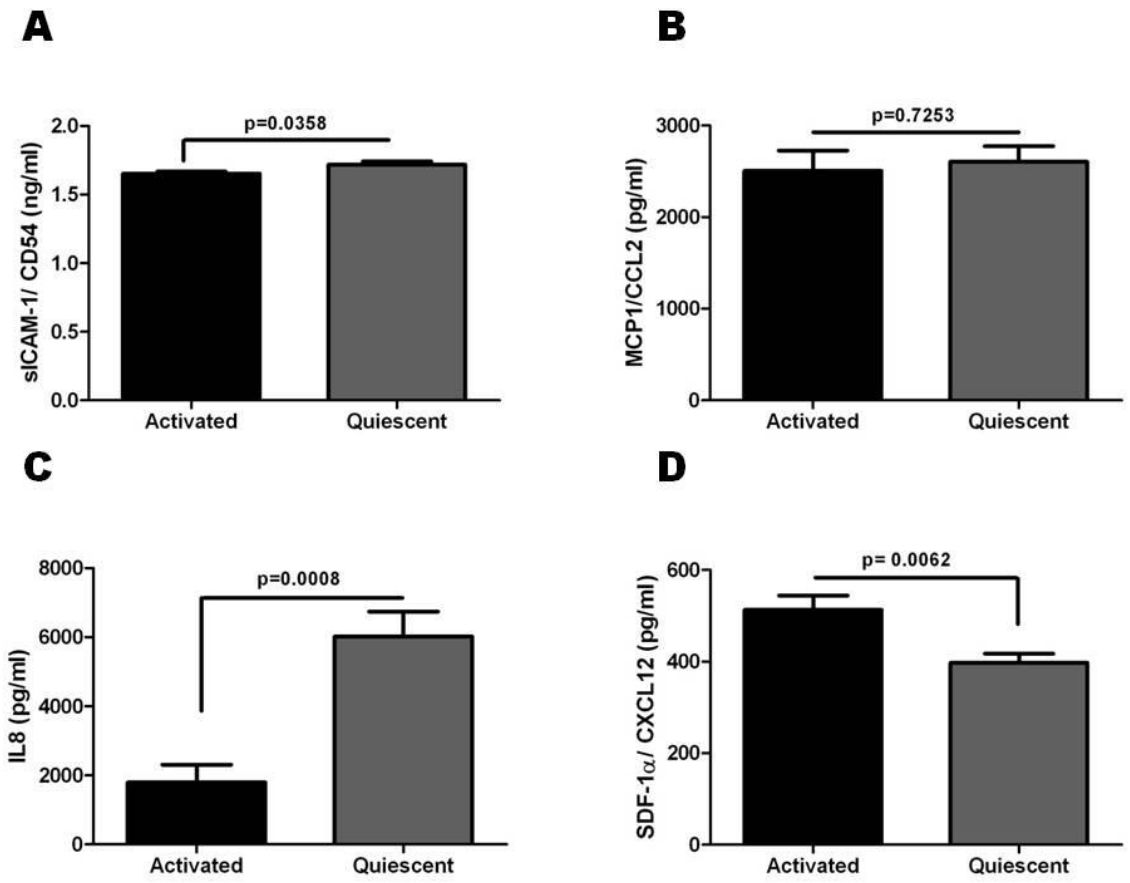

Figure 4.19 Changes in secreted protein concentration upon activation of pancreatic stellate cells

Concentrations of the above proteins in conditioned media collected from quiescent pancreatic stellate cells and activated pancreatic stellate cells using ELISA.

Surprisingly at protein level, there was no difference in the secretion between quiescent pancreatic stellate cell and activated pancreatic stellate cell for sICAM1/ CD54 (A) and MCP1/ CCL2 (B). However, confirming the gene expression data, activated pancreatic stellate cells secreted less IL8 than quiescent pancreatic stellate cell (C). The reverse was true for SDF-1α/ CXCL12 (D).

Bar chart represents mean ± SEM. Paired t-test; p values are two-tailed.

4.7 T-cell migration to activated pancreatic stellate cells is mediated by CXCL12

Following our observation that secretion of CXCL12 is reduced in quiescent pancreatic stellate cells compared to activated pancreatic stellate cells, and from the knowledge that CXCL12 is chemo-attractive to T-cells (Bleul, Fuhlbrigge et al. 1996; Ticchioni, Charvet et al. 2002; Meiron, Zohar et al. 2008; Borge, Nannini et al. 2010), I sought to knock down the gene CXCL12 in activated pancreatic stellate cells with siRNA constructs (method previously described).

To determine a suitable concentration of siRNA constructs, I used 2 siRNA constructs at 5nm, 10nm and 20nm concentrations each. After siRNA transfection, I measured the concentration of CXCL12 in the conditioned media of these cells with ELISA using CXCL12 in the conditioned media of untreated PS1 cells, scrambled RNAi transfected PS1 and activated and quiescent pancreatic stellate cells as controls. CXCL12 secretion was significantly reduced after RNAi at all concentrations. We chose to perform further experiments with siRNA constructs at 5nm to minimise off-target effects. Because two independent RNAi constructs achieved gene silencing, we believe that CXCL12 siRNA was specific (Figure 4.20).

To investigate the role of CXCL12 in pancreatic stellate cell migration, I knocked down CXCL12 by siRNA in activated pancreatic stellate cell line (PS1) (Figure 4.21 A) and primary stellate cells (PSC) (Figure 4.21 B), and measured CXCL12 secretion in conditioned media to confirm that RNAi transfection worked. Gene silencing was achieved in both cell types. Furthermore, I performed migration experiments with $CD8^+$ T-cells in both PS1 cell lines and PSCs (Figure 4.22 A and B,

respectively). There was a reduction in migration of $CD8^+$ T-cells to the conditioned media of activated pancreatic stellate cells down to a level similar to quiescent pancreatic stellate cells.

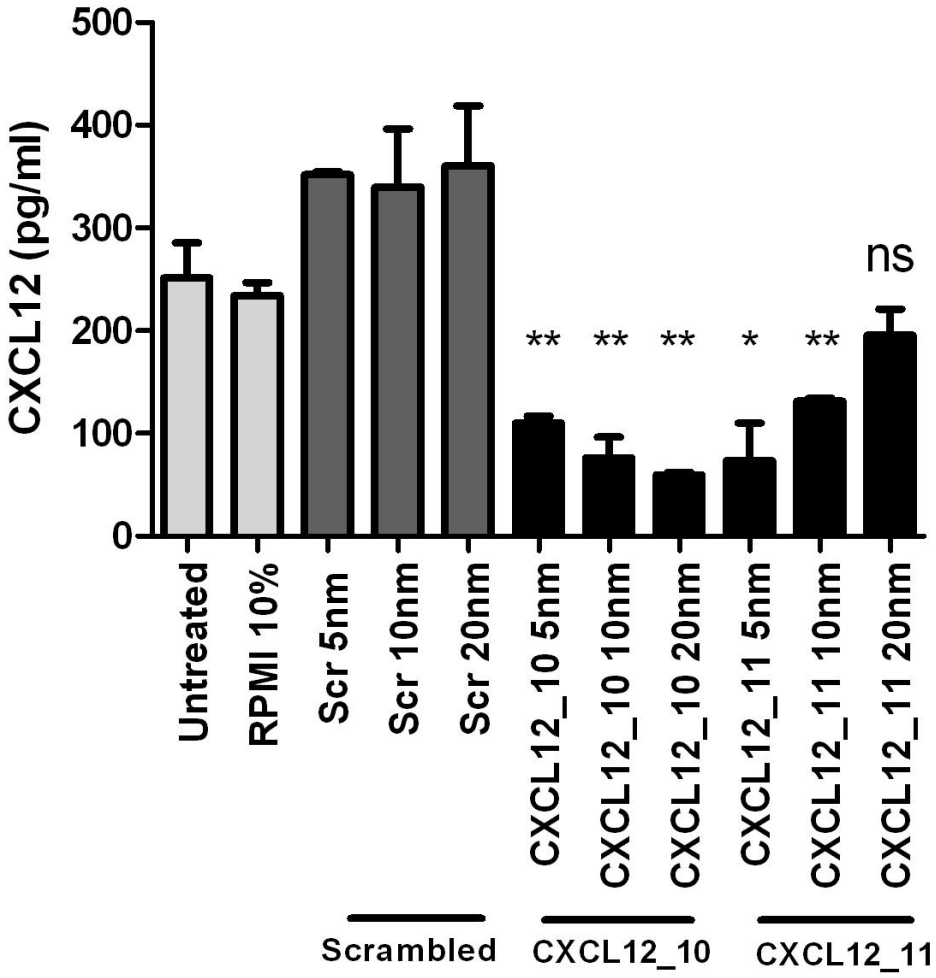

Figure 4.20 Optimization of RNAi transfection

CXCL12 was knocked down in pancreatic stellate cells with two siRNA constructs at 5nm, 10nm and 20nm. Protein concentration in the conditioned media after gene silencing was measured by ELISA and compared to pancreatic stellate cells without CXCL12 knock down (No CXCL12) and scrambled. Gene silencing was observed in all concentrations.

Bar chart represents mean ± SEM. *** p< 0.001; ** p= 0.001 to 0.01; * p= 0.01 to 0.05, Comparisons were conducted with ANOVA with comparisons between columns using Bonferroni's Multiple Comparison Test.

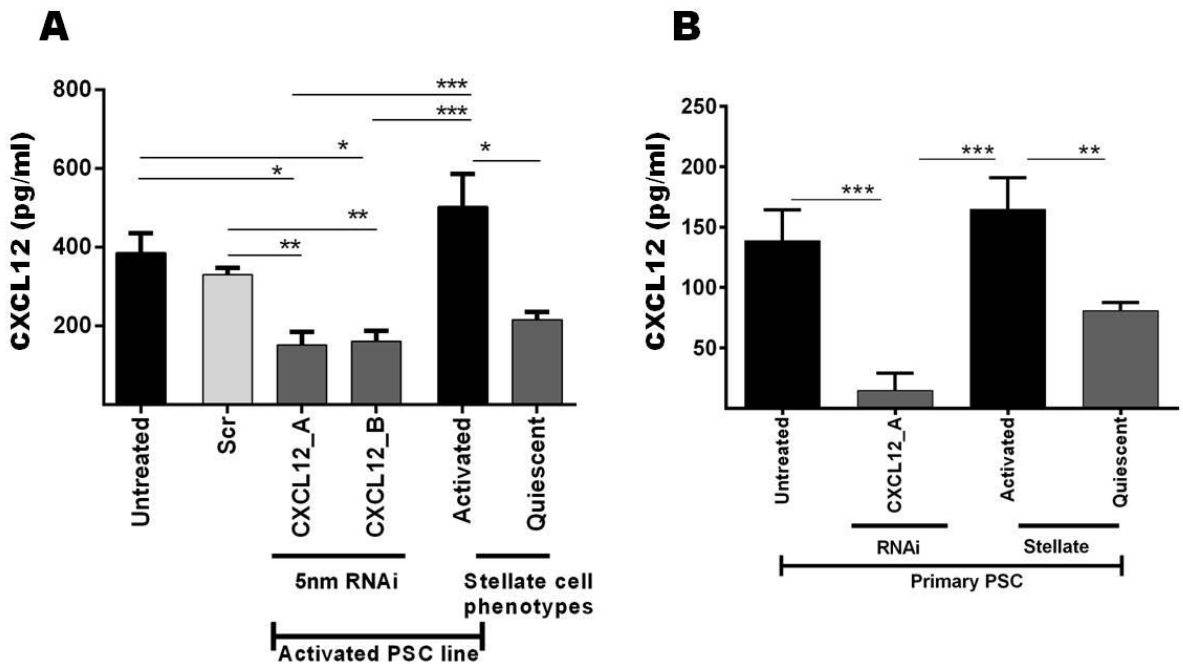

Figure 4.21 Gene silencing of CXCL12 in pancreatic stellate cell line and primary pancreatic stellate cells.

CXCL12 was knocked down in pancreatic stellate cell line (PS1: A) and primary pancreatic stellate cells (B) with two distinct targeting siRNAs and appropriate controls. CXCL12 secretion was measured in conditioned media by ELISA. Pancreatic stellate cells treated with siRNA for CXCL12 demonstrated significant reduction of CXCL12 secretion (A, B) which was equivalent to quiescent PSC levels.

*** p< 0.001; ** p= 0.001 to 0.01; * p= 0.01 to 0.05. Comparisons were conducted with ANOVA with comparisons between columns using Bonferroni's Multiple Comparison Test.

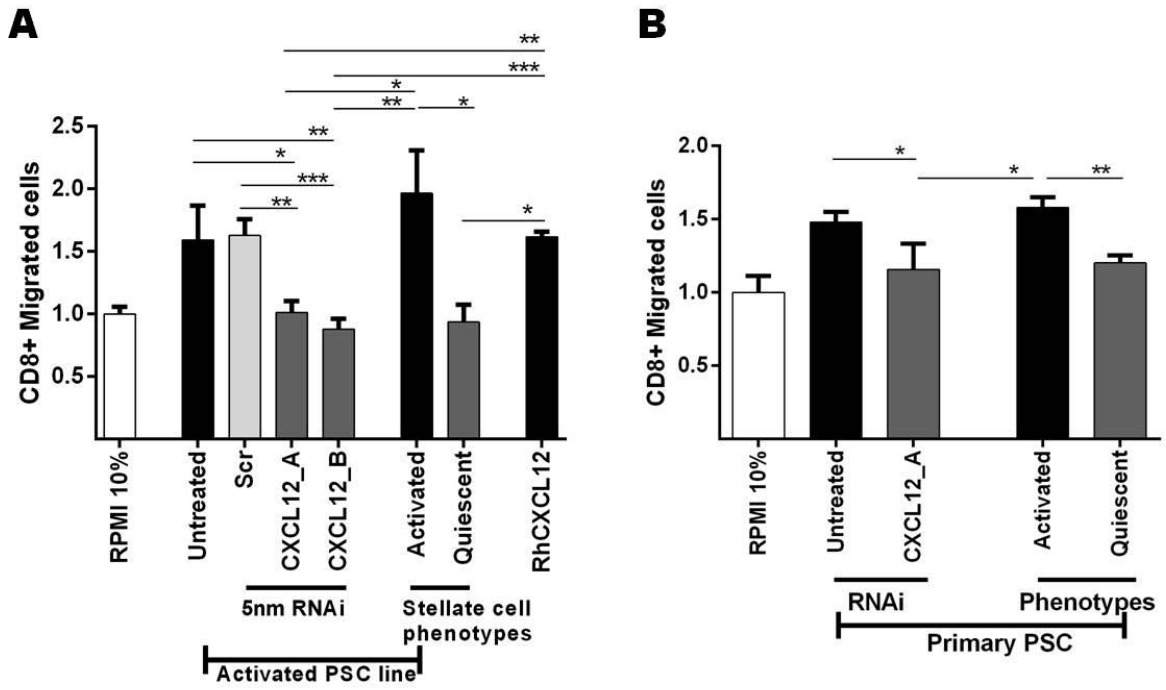

Figure 4.22 Migration of T-cell is dependent on CXCL12

Migration of $CD8^+$ T-cells to the conditioned media from CXCL12 knockdown pancreatic stellate cell line (PS1; A) and primary pancreatic stellate cell (PSC; B) demonstrated significant reduction, which was equivalent to quiescent pancreatic stellate cell levels. $CD8^+$ T-cells also migrated to recombinant CXCL12 (RhCXCL12) significantly over quiescent pancreatic stellate cell conditioned media.

*** p< 0.001; ** p= 0.001 to 0.01; * p= 0.01 to 0.05. Comparisons were conducted with ANOVA with comparisons between columns using Bonferroni's Multiple Comparison Test.

4.8 Natural killer cells, but not B-cells, also migrate preferentially to activated pancreatic stellate cells

In addition to investigating the migration of T-cells to both pancreatic stellate cell media, I investigated the migration of $CD19^+$ (B-cells) and $CD56^+$ (Natural killer cells) isolated from donor samples to the different stellate cell conditioned media. This was undertaken following our earlier observations that B-cells and Natural killer cells, along with cytotoxic T-cells did not infiltrate the juxtatumoural compartment of PDAC.

Natural killer cells significantly migrated to activated pancreatic stellate cells over quiescent pancreatic stellate cells and RPMI with serum (Figure 4.23).

In contrast to T-cells and Natural killer cells, migration of B-cells to conditioned media from activated and quiescent pancreatic stellate cells was not significantly different from migration to basal media (RPMI with serum) (Figure 4.24). We also observed that there was no difference in migration between activated and quiescent pancreatic stellate cell conditioned media. These observations may suggest that another mechanism exists to prevent B-cell migration to the tumour.

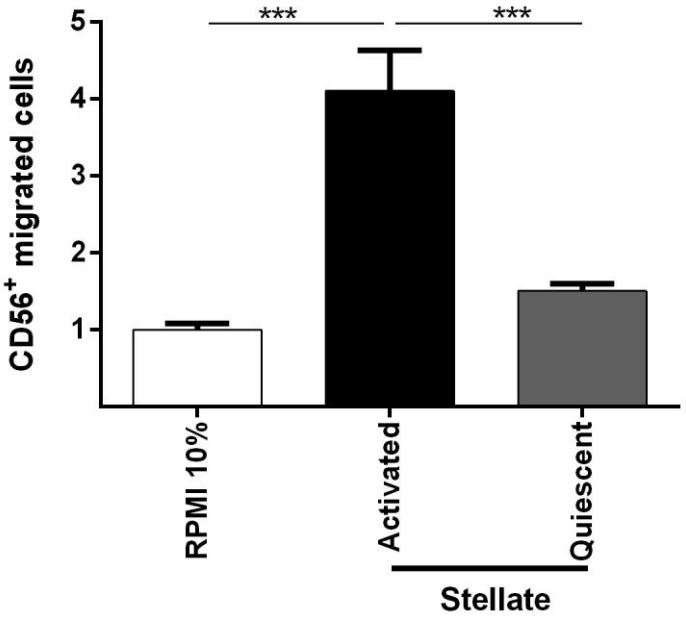

Figure 4.23 *In vitro* Natural killer cell ($CD56^+$) migration assays

Transwell migration assay of Natural killer cells from healthy donors towards conditioned media (CM) from activated and quiescent pancreatic stellate cells. Migration to 10% RPMI (RPMI with 10% FBS) was considered as basal serum-directed migration of Natural killer cells. Values were counted with Casy counter (Roche Diagnostics) and were normalised to the basal serum directed migration (Y axis).

$CD56^+$ cells migrated significantly to conditioned media from activated pancreatic stellate cells more than quiescent and basal media.

*** p< 0.001; ** p= 0.001 to 0.01; * p= 0.01 to 0.05. Comparisons were conducted with ANOVA with comparisons between columns using Bonferroni's Multiple Comparison Test.

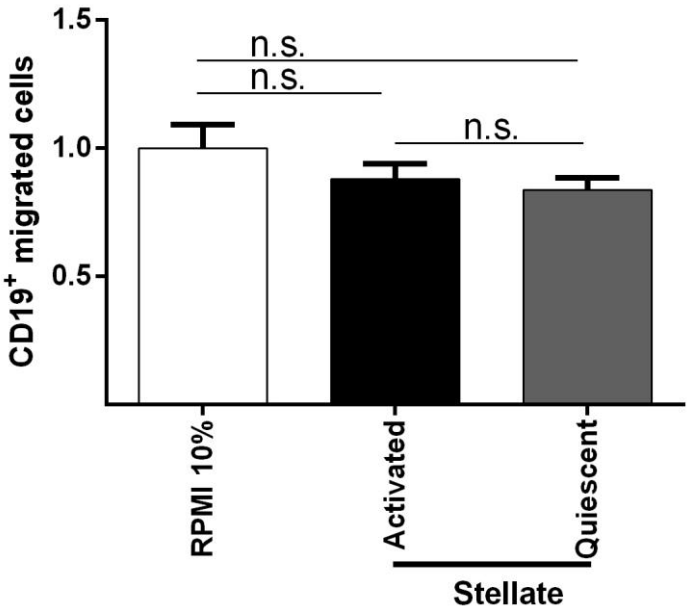

Figure 4.24 *In vitro* B-cell ($CD19^+$) migration assays

Transwell migration assay of B-cells from healthy donors towards conditioned media of activated and quiescent pancreatic stellate cells. Migration to 10% RPMI (RPMI with 10% FBS) was considered as basal serum-directed migration of Natural killer cells. Values were counted with Casy counter (Roche Diagnostics) and were normalised to the basal serum directed migration (Y axis).

B-cell migration to activated and quiescent pancreatic stellate cells was not significant over basal serum-directed migration (RPMI 10%).

Comparisons were conducted with ANOVA with comparisons between columns using Bonferroni's Multiple Comparison Test.

4.9 Effector T-cells in patient peripheral polymorphonuclear cells (PBMC) are not increased and are of a similar level with Donor PBMC

It is an established fact that naïve T-cells decrease in number as a result of age associated thymic involution, while memory cells increase as a result of pathogen encounter (Koch, Larbi et al. 2008). As I carried out migration assays with donor PBMCs, I sought to investigate the proportion of T-cell subsets in patient PBMCs and to compare with the donor sample as similarity between both samples will give clinical significance to our migration and adhesion experiments. I performed flow cytometry analysis on PBMCs from two PDAC patients and divided viable $CD4^+$ and $CD8^+$ T-cells into their subsets based on previously established gating criteria (Koch, Larbi et al. 2008; Riches, Davies et al. 2012). I compared this with data with flow cytometry data of donors.

T-cells may be divided on the basis of their expressions of the common leukocyte antigen isoform, CD45RA, and the chemokine receptor CCR7, into 4 subsets: naïve ($CD45RA^+$ $CCR7^+$), central memory (CM; $CD45RA^-$ $CCR7^+$), effector memory (EM; $CD45RA^-$ $CCR7^-$) and terminally differentiated effector memory (TEMRA; $CD45RA^+$ $CCR7^-$) cells (Sallusto, Lenig et al. 1999). CCR7 expression mediates homing to secondary lymphoid organs and lack immediate effector functions while $CCR7^-$ memory cells have low proliferative capabilities, display immediate effector functions and express receptors for migration to inflamed tissues (Sallusto, Lenig et al. 1999; D'Asaro, Dieli et al. 2006). TEMRA cells are the most differentiated of the memory cells. They express high levels of the cytotoxic molecules perforin and Fas ligand, and they are susceptible to apoptosis (D'Asaro, Dieli et al. 2006).

I observed similarities in the distribution of the $CD4^+$ and $CD8^+$ T-cell subsets among donor PBMC and PBMC of PDAC patients (Figures 4.25 and 4.26, respectively). However this was not the case in a PDAC patient with bacterial infection who had an increased TEMRA subset which suggests a shift from a naive phenotype to an effector phenotype (Figures 4.25 and 4.26).

However, to test that the T-cells of PDAC patient were not functionally impaired, I performed migration assays with patient $CD4^+$ and $CD8^+$ T-cells to activated and quiescent pancreatic stellate cell conditioned media and to the recombinant form of CXCL12 antibody. Similar to donor T-cells, patient $CD4^+$ and $CD8^+$ T-cells preferentially migrated to conditioned media of activated pancreatic stellate cell over quiescent pancreatic stellate cells. Migration of both $CD4^+$ and $CD8^+$ T-cells to recombinant CXCL12 was also significantly higher than the migration to basal media control (RPMI 10%) and quiescent pancreatic stellate cell conditioned media giving further proof to the role of CXCL12 in T-cell migration in pancreatic ductal adenocarcinoma (Figures 4.27 and 4.28). I then measured CXCR4 (receptor for CXCL12) expression on $CD4^+$ and $CD8^+$ T-cells on both donor and patient PBMCs. Interestingly, CXCR4 was significantly upregulated in PDAC patient PBMCs than in donor PBMCs (Figure 4.29).

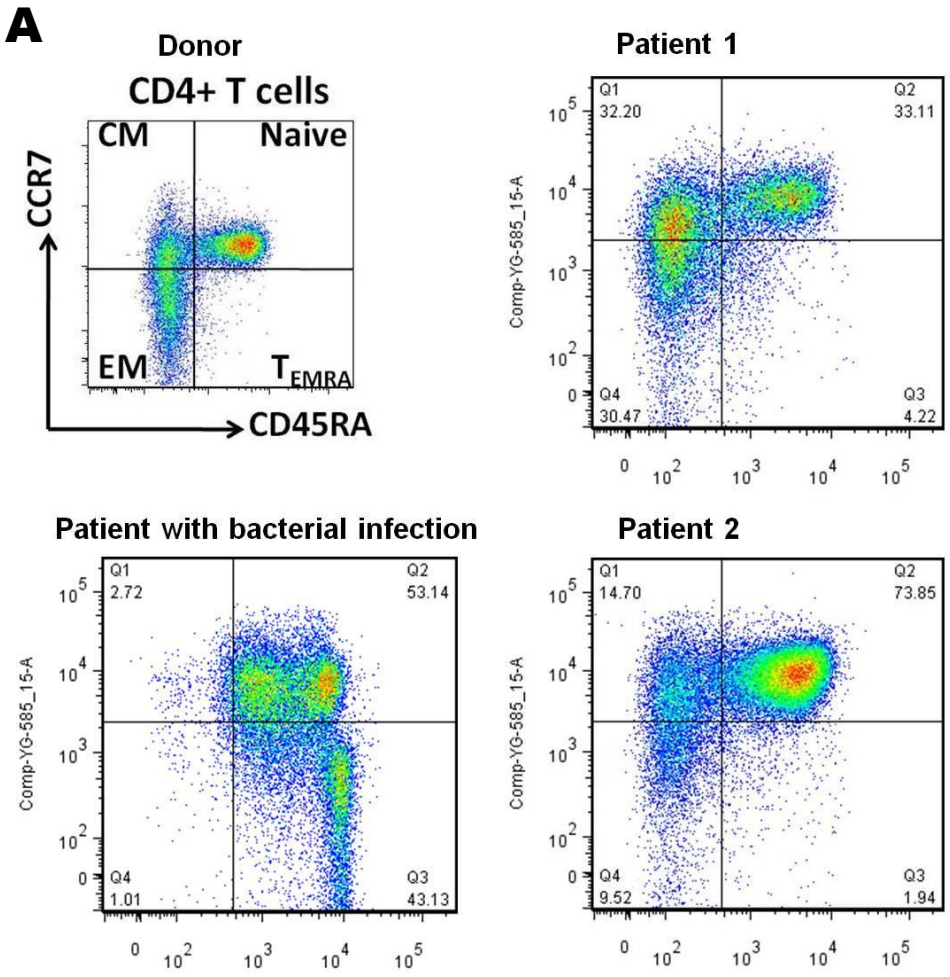
A
Donor
CD4+ T cells
CM
Naive
EM
T_{EMRA}
CCR7
CD45RA
Patient 1
Q1 32.20
Q2 33.11
Q4 30.47
Q3 4.22
Comp-YG-585_15-A
Patient with bacterial infection
Q1 2.72
Q2 53.14
Q4 1.01
Q3 43.13
Patient 2
Q1 14.70
Q2 73.85
Q4 9.52
Q3 1.94

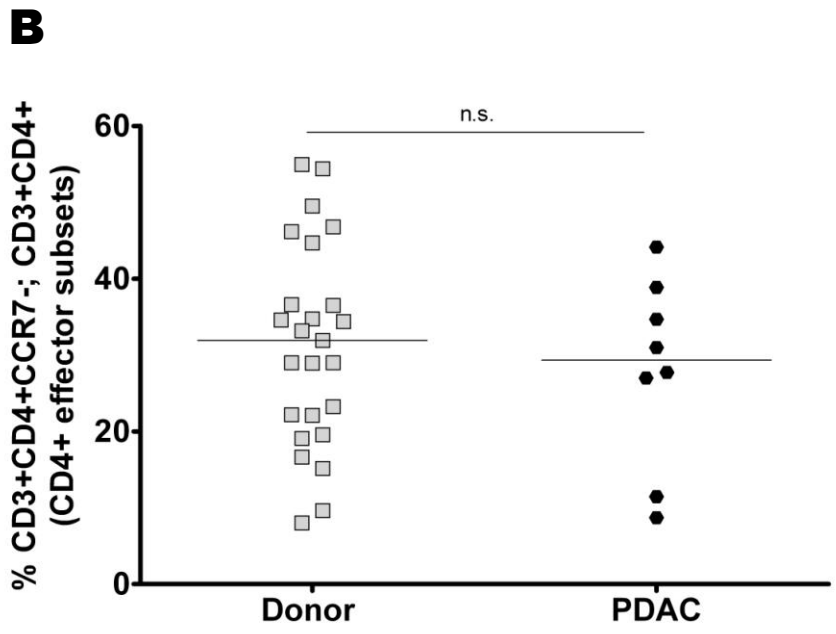
B
n.s.
% CD3+CD4+CCR7-; CD3+CD4+ (CD4+ effector subsets)
60
40
20
0
Donor
PDAC

Figure 4.25: Comparison of $CD4^+$ T-cell subsets between donor and patient PBMC

Flow cytometry analysis of $CD4^+$ T-cell subsets on donor PBMCs (n=25) and PDAC patient PBMC (n=8) (representative picture shown; (A)). Viable lymphocytes were gated and selected for $CD4^+$ T-cell (not shown). $CD4^+$ T-cells were subdivided into the four T-cell subsets using CD45RA and CCR7 markers. Distribution of the subsets were similar, particularly of note were TEMRA cells which were few. This was not the case in a patient who presented with bacterial infection and had increased levels of TEMRA. Expression of effector subsets ($CCR7^-$) was compared between the two groups without any significant differences (B).

Mann Whitney U test; p values are 2 tailed

n.s. = not significant

A

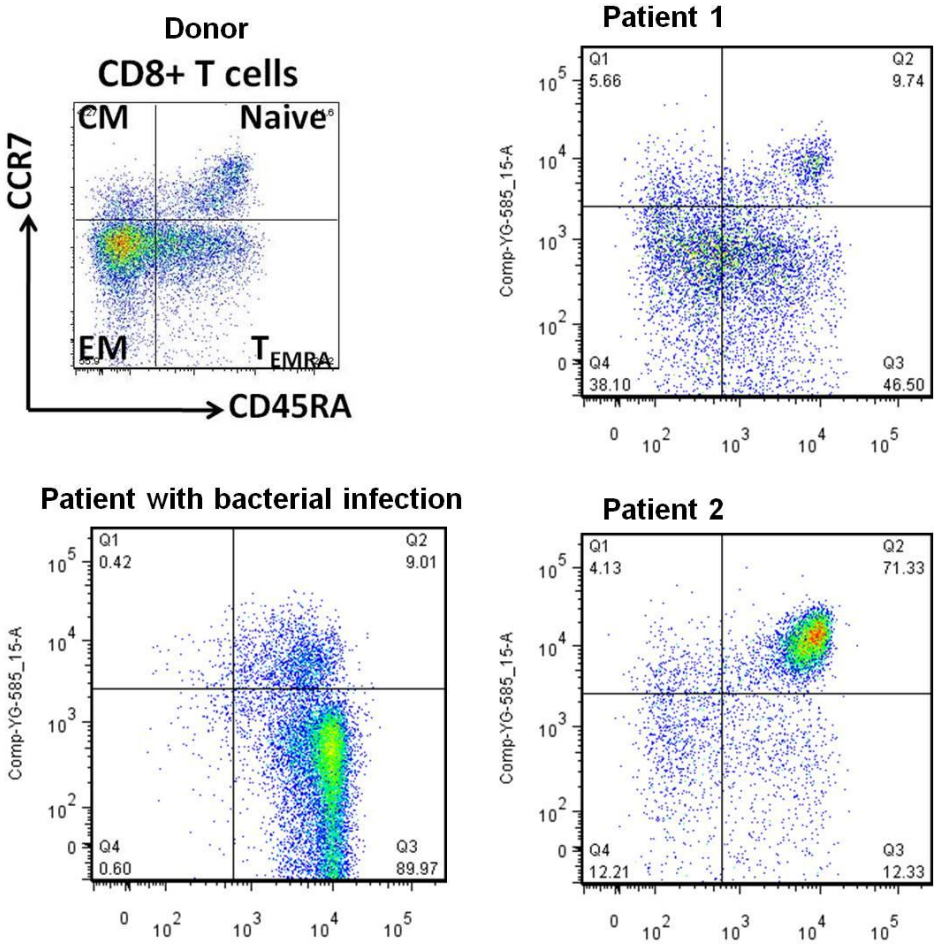
Donor
CD8+ T cells
CM
Naive
EM
T_{EMRA}
CCR7
CD45RA
Patient 1
Q1 5.66
Q2 9.74
Q4 38.10
Q3 46.50
Patient with bacterial infection
Q1 0.42
Q2 9.01
Q4 0.60
Q3 89.97
Patient 2
Q1 4.13
Q2 71.33
Q4 12.21
Q3 12.33
Comp-YG-585_15-A

B

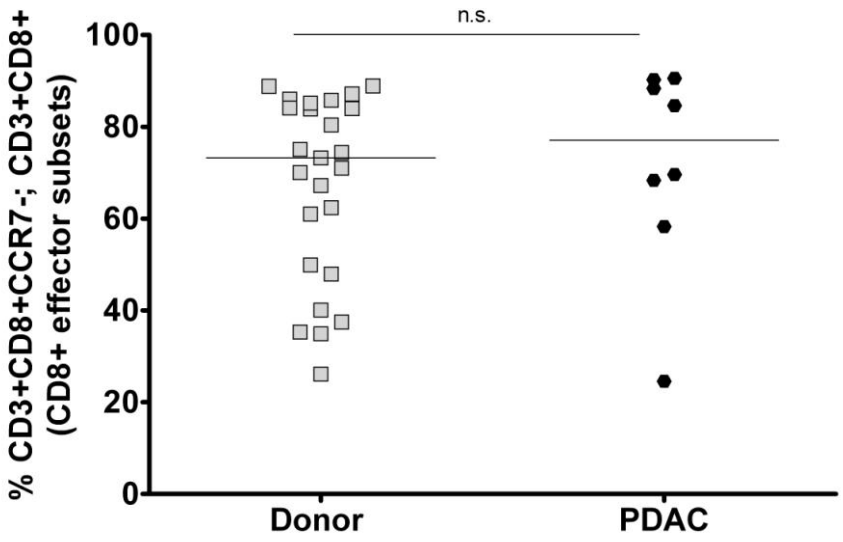
n.s.
% CD3+CD8+CCR7-; CD3+CD8+ (CD8+ effector subsets)
100
80
60
40
20
0
Donor
PDAC

Figure 4.26 Comparison of $CD8^+$ T-cell subsets between donor and patient PBMC

Flow cytometry analysis of $CD8^+$ T-cell subsets on donor PBMCs (n=25) and PDAC patient PBMC (n=8) (representative picture shown (A)). Viable lymphocytes were gated and selected for $CD8^+$ T-cell (not shown). $CD8^+$ T-cells were subdivided into the four T-cell subsets using CD45RA and CCR7. Distribution of the subsets was similar between PDAC patients and normal donors. However, this was not the case in a PDAC patient who presented with bacterial infection with an observable increase in TEMRA subsets. Expression of effector subsets ($CCR7^-$) was compared between the two groups without any significant differences (B).

Mann Whitney U test; p values are 2 tailed

n.s. = not significant

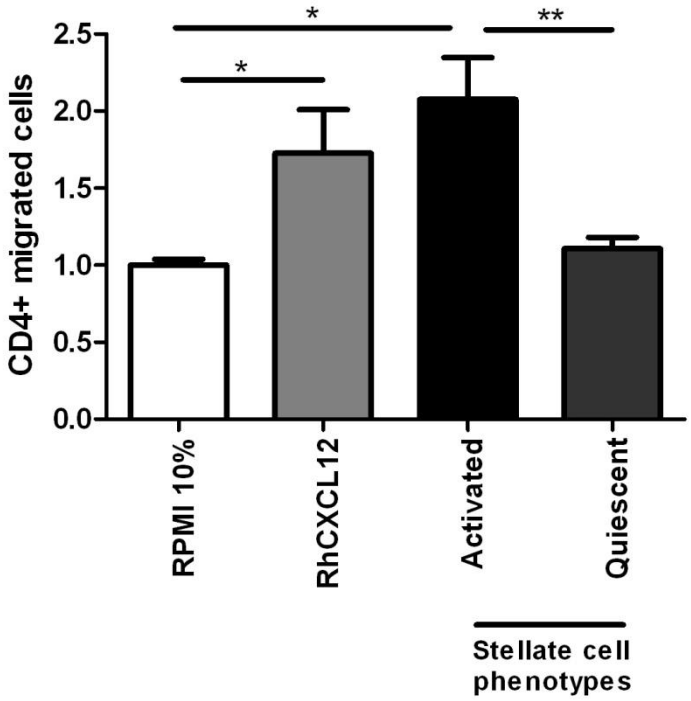

Figure 4.27 Patient CD4$^+$ T-cell migration to pancreatic stellate cell Phenotypes

Transwell migration assay of CD4$^+$ T-cells from PDAC patients (n=2) towards conditioned media (CM) from activated and quiescent pancreatic stellate cells and recombinant CXCL12 (100ng) in 10% RPMI (10% FBS). 10% RPMI was considered as basal serum-directed migration of T-cells and served as an internal control. Values were normalised to RMPI 10% (Y axis).

We demonstrated a significant reduction of migration of patient CD4$^+$ T-cells to quiescent pancreatic stellate cell CM in comparison to activated pancreatic stellate cell CM. Patient CD4$^+$ T-cells also migrated to RhCXCL12 over control (RPMI 10%) and quiescent pancreatic stellate cell.

Bar chart represents mean ± SEM. ** p= 0.001 to 0.01; * p= 0.01 to 0.05, Comparisons were conducted with ANOVA with comparisons between columns using Bonferroni's Multiple Comparison Test.

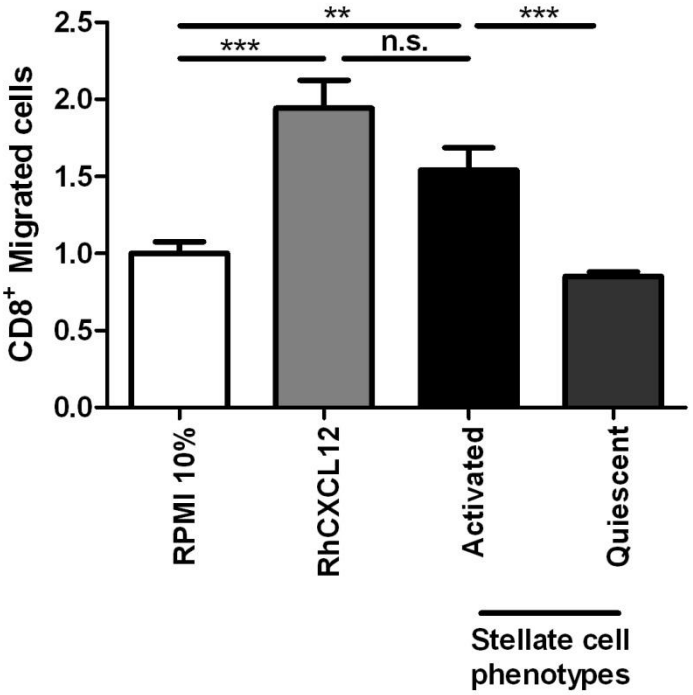

Figure 4.28 Patient C8+ T-cell migration to pancreatic stellate cell phenotypes

Transwell migration assay of $CD8^+$ T-cells from PDAC patients (n=2) towards conditioned media (CM) from activated and quiescent pancreatic stellate cells and recombinant CXCL12 (100ng) in 10% RPMI (10% FBS). 10% RPMI was considered as basal serum-directed migration of T-cells and served as an internal control. Values were normalised to RMPI 10% (Y axis).

We demonstrated a significant reduction of migration of patient $CD8^+$ T-cells to quiescent pancreatic stellate cell CM in comparison to activated pancreatic stellate cell CM. Patient $CD8^+$ T-cells also migrated to RhCXCL12 over control (RPMI 10%) and quiescent pancreatic stellate cell. Migration to RhCXCL12 was not significant from that of activated stellate cell CM.

Bar chart represents mean ± SEM. ** p= 0.001 to 0.01; * p= 0.01 to 0.05, Comparisons were conducted with ANOVA with comparisons between columns using Bonferroni's Multiple Comparison Test.

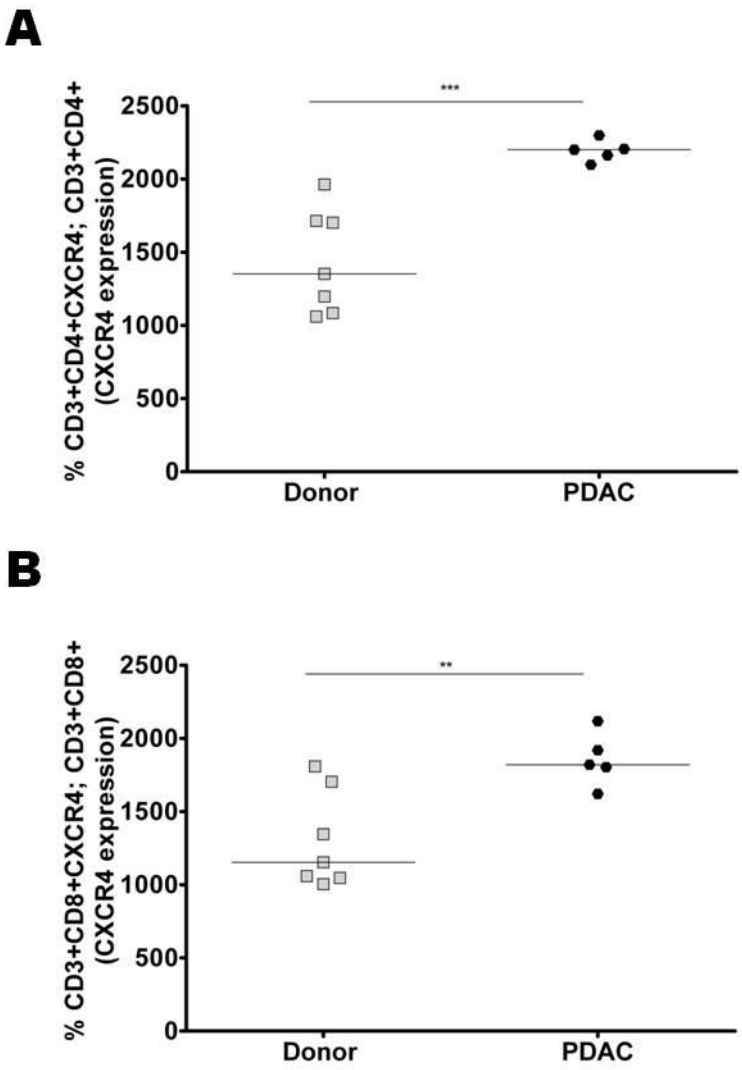

Figure 4.29 CXCR4 is upregulated in PDAC patient $CD4^+$ and $CD8^+$ T-cells

Flow cytometry analysis of CXCR4 expression on $CD4^+$ (A) and $CD8^+$ (B) T-cells of PDAC patients (n=5) and normal donors (n=7). CXCR4 was upregulated in the T-cells of PDAC patients.

Mann Whitney U test; p values are 2 tailed

***p<0.001; ** p= 0.001 to 0.01

5.0 Discussion

Using immunohistochemistry, sophisticated imaging systems and analyses on both whole tissue sections and tissue microarrays, I demonstrate for the first time, a comparison of immune cell infiltration in human PDAC and other pancreatico-biliary disease tissues. I found immune cells' infiltrate increased in PDAC tissues over normal tissues; this has been observed previously in genetic mouse models of PDAC (Clark, Hingorani et al. 2007). This fact confirms an immunological reaction in PDAC. In addition, I observed immune cell infiltration that increased from normal to inflammatory disease (chronic pancreatitis) to borderline malignant disease (mucinous cystic neoplasm) and to malignant carcinomas (ampullary carcinoma, pancreatic ductal adenocarcinoma and cholangiocarcinoma). Interestingly, patient overall survival of the above diseases has been shown to worsen in the same order as immune cell infiltration increased (Coupland, Kocher et al. 2012). This may suggest that either the immune cells are detrimental to patient prognosis, or that the immune response is equivalent to the severity of the pancreatico-biliary disease. Either of these explanations may have clinical significance; in the case of the former as potential therapeutic targets and in the case of the latter as diagnostic and prognostic markers.

Much is not known about the immune response in chronic pancreatitis (CP). Macrophages were observed in stage I of alcoholic chronic pancreatitis in association with myofibroblasts and both were found to surround areas of necrosis (Detlefsen, Sipos et al. 2006). These macrophages were also positive for latency associated protein (LAP) and TGFβ-RII particularly in early stage more than late

stage. LAP, macrophages and PDGFβ reduced in the late stages of alcoholic pancreatitis with a corresponding decrease in the number of myofibroblast activity and a waning of the fibrogenic process. Thus, the study authors hypothesize that myofibroblasts and macrophages initiate the fibrogenic process (Detlefsen, Sipos et al. 2006). In a separate study involving aetiologically different chronic pancreatitis; alcoholic CP (n=10), idiopathic CP (n=12) and tropical CP (n=21), the immune cell markers $CD45^+$, $CD4^+$, $CD8^+$ and $CD68^+$ were significantly increased in all CP compared to control (organ donors; n= 10) but did not differ amongst the aetiological types (Shrikhande, Martignoni et al. 2003). The authors, thus, concluded that different aetiological types of CP have similar histological features and immune cell reaction and that regardless of aetiology the disease reaches a certain stage from which it seemingly progresses to "a single distinctive entity" (Shrikhande, Martignoni et al. 2003). In an immune cell study performed on intraheptic cholangiocarcinoma (ICC), surgically resected ICC tissues (n=31) and corresponding cancer adjacent tissues were labelled by immunohistochemistry for the markers B7-H1, PD-1, CD8 and CD4. Expression of B7-H1 and PD-1 was upregulated in ICC compared to the adjacent tissues. B7-H1 expression on tumour correlated with TNM staging and tumour differentiation while inversely correlating with $CD8^+$ infiltration (Ye, Zhou et al. 2009)

As there is not much literature published on immune cell response in mucinous cystic neoplasm, cholangiocarcinoma and ampullary carcinoma, I can speculate based on the data I show that $CD3^+$, $CD4^+$, $CD8^+$, $FoxP3^+$ and $CD20^+$ cell density in the pancreas of MCN patients was of a level similar to normal pancreas and pancreas of CP patients except for $CD68^+$ macrophages which was significantly

more than CP. Increased tissue infiltrate of $CD4^+$, $CD8^+$, $CD68^+$ and $CD20^+$ but not $FoxP3^+$ were observed in the pancreas of AC patients. $CD4^+$, $CD68^+$, $FoxP3^+$ and $CD20^+$ in the pancreas of CC patients was of a level similar to PDAC patients with $CD8^+$ being the exception with CC having significantly more $CD8^+$ tissue infiltrate. The explanations of these findings are unclear requiring further functional assays.

Pancreatic cancer is hypovascular in contrast to most other tumours especially ampullary cancers and cholangiocarcinoma (Olive, Jacobetz et al. 2009). Furthermore the distribution of vasculature in pancreatic cancer is distinct, as it is seen mostly further away from the tumour ((Olive, Jacobetz et al. 2009) and DiMaggio, Kocher; unpublished observations). Furthermore, in pancreatic cancer, two distinct stromal compartments have been identified based on the differential gene expression (Iacobuzio-Donahue, Ryu et al. 2002; Ricci, Kern et al. 2005) Therefore, I next interrogated the pancreatico-biliary diseases to observe migration of immune cells from the panstromal region, rich with blood vessels for pancreatic cancer, to the juxtatumoural stromal region, deficient in blood vessels for pancreatic cancer(Ricci, Kern et al. 2005; Olive, Jacobetz et al. 2009). We observed distinct differential immune cell infiltration that was unique to PDAC. The hallmarks of this unique infiltration pattern were that cytotoxic immune cells such as cytotoxic T-cells ($CD8^+$) and natural killer cells ($CD56^+$) and B-cells ($CD20^+$)) were sequestrated by the panstromal compartment whereas macrophages ($CD68^+$) and neutrophils ($myeloperoxidase^+$) infiltrated the juxtatumoural compartment. The stromal environment of PDAC consists of activated fibroblasts, myofibroblasts, extracellular matrix such as collagen and fibronectin, blood vessels and inflammatory cells (Neesse, Michl et al. 2010). Furthermore stromal cell subsets that express ICAM-1,

VCAM-1and MAdCAM-1 have also been identified (Roozendaal and Mebius 2011). These coupled with chemokines secreted by stromal cells, which my data shows, make for stellate cell-immune cell interactions that are not yet fully understood and perhaps results in the formation of tertiary lymphoid aggregates in the pancreas as a result of persistent immune response (Carragher, Rangel-Moreno et al. 2008).

Patients with $CD8^+$ T-cells infiltrating the juxtatumoural compartment have a longer overall survival indicating a role of $CD8^+$ in tumour immunoclearance. Supporting our data are findings in colorectal carcinoma which showed, using *In situ* analysis, that patients with high density of $CD8^+$ had longer overall survival (Galon, Costes et al. 2006; Tosolini, Kirilovsky et al. 2011). Also recently, two studies in a mouse model of PDAC suggest the requirement of $CD8^+$ cells for immuno-editing in PDAC (Bayne, Beatty et al. 2012; Pylayeva-Gupta, Lee et al. 2012). Together, these authors presented a mechanism whereby Granulocyte Macrophage Colony Stimulating Factor (GM-CSF) production is induced by K-ras within the neoplastic cells. GM-CSF then recruits myeloid progenitor cells which differentiate into Myeloid Derived Suppressor Cells (MDSC). The MDSC's secrete arginase and inducible nitric oxide synthase which inhibit $CD8^+$ T-cells from immunoclearance of tumours (Bayne, Beatty et al. 2012; Pylayeva-Gupta, Lee et al. 2012).

Natural killer cells were also seen to increase patient overall survival when they infiltrated the tumour and along with PDAC did not influence patient survival in the panstromal compartment indicating that the proximity of these $CD8^+$ T-cells and natural killer cells are perhaps necessary for tumour clearance. Interestingly, a

subset of $CD8^+$ T-cells with a differentiated effector or memory phenotype has been found to express the natural killer associated receptor CD56 (Sallusto, Lenig et al. 1999; Tarazona, DelaRosa et al. 2001; Tarazona, DelaRosa et al. 2002). These $CD8^+$ T-cells with CD56 expression are mature cytolytic effector T-cells (Pittet, Speiser et al. 2000). These findings may highlight the use of CD56 as a marker of immune cytotoxicity in PDAC.

Although T regulatory cells ($FoxP3^+$) did not infiltrate the tumour in relatively early PDAC cases (tissue collected at resection), they were seen to reduce patient overall survival in patients with high densities of $FoxP3^+$ in both the juxtatumoural and panstromal compartments. T_{reg} cells, thus, may have a direct inhibitory effect to other cells of the immune system. The combination of stellate cells and T_{reg} cells in the PDAC tumour microenvironment therefore may serve as an entrapping barrier through which other immune cells cannot pass through. $FoxP3^+$ infiltrate should be investigated further as a prognostic marker of poor outcome in PDAC patients.

The stromal microenvironment of PDAC is certainly rich with immune cells, as many others and I have shown, some of which are thought to be immunosuppressive such as T_{regs} and MDSCs (Campbell and Koch 2011; Mace, Ameen et al. 2013). Mace et al, studied the effects activated pancreatic stellate cells have on the differentiation of the immunosuppressive MDSCs. “MDSCs are a heterogeneous population of immature myeloid cells” that when activated, inhibit T-cell and NK cell tumour specific response by the production of oxidative stress and the depletion of nutrients required by lymphocytes (Mace, Ameen et al. 2013). Using Luminex

cytokine kits they observed elevated IL-4, macrophage colony-stimulating factor (M-CSF) and vascular epidermal growth factor (VEGF), all of which regulate MDSCs, as well as monocyte chemotactic protein 1 (MCP-1) and SDF-1 chemokines which are known to be chemotactic to MDSCs (Lechner, Liebertz et al. 2010; Mundy-Bosse, Young et al. 2011; Mace, Ameen et al. 2013). They then cultured PBMCs from normal human donors with PSC conditioned media or with IL-6 and GM-CSF which served as positive control. After 7 days, they observed that PBMCs cultured with PSC conditioned media has differentiated into the MDSC markers $CD11b^+$ $CD33^+$ and a subpopulation of $CD11b^+$ $CD33^+$ $CD15^+$ polymorphonuclear cells. PBMCs cultured with human fetal primary pancreatic fibroblast (HPF; which served as control) were not differentiated (Mace, Ameen et al. 2013). To ascertain that the $CD11b^+$ $CD33^+$ cells were in fact suppressive, $CD33^+$ was isolated via magnetic bead sorting and cultured with “donor matched and autologous CFSE-labelled” $CD4^+$ and $CD8^+$ T-cells and stimulated with CD3/CD28 beads for 3 days. T-cell proliferation as measured by CFSE dilution, was significantly decreased (Mace, Ameen et al. 2013) suggesting an interaction between PSC, T-cells and MDSCs.

MDSCs can directly suppress T helper and cytotoxic T-cell function (Nagaraj and Gabrilovich 2010; Greten, Manns et al. 2011; Pylayeva-Gupta, Lee et al. 2012). In mice MDSCs are defined as $CD11b^+$ $Gr1^+$ cells, however the absence of the Gr1 analogue in humans has necessitated that a permutation of markers be used in the definition of this immune cell types and in their isolation (Nagaraj and Gabrilovich 2010). Human MDSCs are characterised as $CD11b^+$, $CD33^+$, HLA-DR $^{neg/low}$ and they can be divided into granulocytic $CD14^-$ and monocytic $CD14^+$ MDSCs (Greten, Manns et al. 2011). Other markers that are used in the classification of these

immune cells are CD15, CD16, CD66b and CD124 (Nagaraj and Gabrilovich 2010). MDSCs inhibit T-cell function via a variety of mechanisms; one of which is in the depletion of cysteine and cystine. Cysteine is required for T-cell activation and function, however, MDSCs have been found to deplete the tumour microenvironment of cystine while not secreting cysteine back into the tumour microenvironment (Nagaraj and Gabrilovich 2010; Srivastava, Sinha et al. 2010). Other ways MDSCs inhibit T-cell function are by the production of inducible nitric oxide synthase (iNOS) and arginase as a result of its ability to metabolise L-arginase; its production or reactive oxygen species (ROS); and its ability to secrete TGFβ; all of which are immunosuppressive against T-cells (Filipazzi, Valenti et al. 2007; Rodríguez and Ochoa 2008; Corzo, Cotter et al. 2009; Nagaraj and Gabrilovich 2010). MDSCs have also been seen to suppress cytotoxic NK cells. NK cells act as a first defence against infection and also regulate adaptive immunity (Greten, Manns et al. 2011). *In vitro* these NK cell functions were impaired by MDSC from patients with hepatocellular carcinoma, however when MDSCs were depleted from PBMCs, NK cell mediated lysis improved (Hoechst, Voigtlaender et al. 2009). Surprisingly, Hoechst and colleagues found that in this case immunosuppression was a result of cell-cell contact and did not involve iNOS, Arginase 1 or ROS (Hoechst, Voigtlaender et al. 2009). Targeting human MDSCs with ATRA systemically resulted in maturation of these cells, halting their immunosuppressive function. Treatment with the receptor tyrosine kinase inhibitor Sunitinib also reverses “MDSC-mediated tumour-induced immunosuppression” (Kusmartsev, Su et al. 2008; Ko, Zea et al. 2009; Greten, Manns et al. 2011).

In another study, Tjomsland et al observed significantly increased levels of the cytokines IL-6, TGFβ, COX-2, IDO, CCL20 and CCL2 in human PDAC (n=30) tissues compared to normal pancreas tissue (from individuals diseased from hypothermia (n=7)) and benign disease (n=3). CCL2 and COX-2 were expressed specifically by the fibrotic stroma; all of the above were observed by immunohistochemical studies (Tjomsland, Niklasson et al. 2011). They also observed an corresponding significant increase of the immune cells $CD8^+$ T-cells, $CD163^+$ macrophages and $CD83^+$ dendritic cells in PDAC patients over controls, where $CD8^+$ T-cells were found to be localised in the fibrotic stroma surrounding the "tumour nests" (Tjomsland, Niklasson et al. 2011). These results are similar to my observations. This led to their conclusion that the desmoplastic stroma encourages the "accumulation and modulation" of infiltrated immune cells in PDAC as a result of the cytokines produced in the tumour microenvironment (Tjomsland, Niklasson et al. 2011). To determine that ischemia was not responsible for the immune cell infiltration they observed, tissue from patients that had undergone Whipple resection on cystic tumours (where tumour is adjacent to normal histology pancreas) were compared with the normal pancreas of individuals deceased as a result of hypothermia and they found that there was no difference in immune cell infiltration (Tjomsland, Niklasson et al. 2011). Also to investigate the role of jaundice as the cause for increased immune cell infiltrate, blood bilirubin levels were compared with immune cell marker levels however this resulted in no correlation. TGFβ produced by PDAC may expand Tregs (Campbell and Koch 2011; Tjomsland, Niklasson et al. 2011) which may contribute to the immunosuppressive nature of the tumour microenvironment. A school of thought is that the seeming inability of immune cell mediated tumour clearance in PDAC may lie in the transcriptional differences

between cancer and normal PBMCs (Baine, Chakraborty et al. 2011). In a study involving 26 PDAC patients and 33 matched healthy donors analysed by whole genome cDNA microarrays, 383 genes were significantly different and 65 genes had at least a 1.5 fold change in expression between PDAC and normal PBMCs (Baine, Chakraborty et al. 2011). Of the 65 genes Baine and colleagues identified: 18 genes had the "potential to directly decrease T-cell proliferation, T-cell receptor signalling and cytotoxic T lymphocyte (CTL) cytotoxicity", 4 genes could directly decrease the activation and signalling of B-cells, 3 genes could decrease the cytotoxicity of NK cells and 2 genes could decrease the response of macrophages (Baine, Chakraborty et al. 2011). The gene ARG1, which is associated with MDSC increase (Talmadge 2007) was also upregulated more than 2 fold in PDAC PBMCs (Baine, Chakraborty et al. 2011). While the differential gene expression was validated using qRT-PCR, the lack of mechanistic experimental proof suggests a weakness that could question the conclusions of the above work.

Among the constituents of immune infiltrates in the PDAC microenvironment are mast cells and macrophages (Esposito, Menicagli et al. 2004). The presence of mast cell in the PDAC microenvironment has been found to be directly correlated with the presence of lymph node metastases (Esposito, Menicagli et al. 2004). Mast cells and macrophages in the pancreas also express VEGF-A, VEGF-C and bFGF, thus making them integral contributors of angiogenesis in PDAC(Esposito, Menicagli et al. 2004). I did not study mast cells in PDAC microenvironment. Tumour associated macrophages (TAMs) may polarise from an M1 phenotype that expresses high levels of pro-inflammatory cytokines, produces reactive oxygen and nitrogen intermediates and promotes T_H1 response to a tumour promoting M2

phenotype capable of suppressing other immune cells as a result of their expression of the genes: Arginase 1, IL-10 and TGFβ (Mantovani, Porta et al. 2006; Biswas and Mantovani 2010; Sica and Mantovani 2012). TAMs may suppress $CD8^+$ T-cells via the B7 family of co-signalling molecules: B7-H1 and B7-H4 (Kryczek, Zou et al. 2006; Kuang, Zhao et al. 2009). In a recent human PDAC study involving 483 patients, Sanford et al performed survival analysis to investigate if the prevalence of preoperative blood monocytes correlated with patient survival following tumour resection. They also compared the prevalence of monocytes in the blood and bone marrow of patients and controls and compared CCL2 expression between PDAC patients and normal donors (Sanford, Belt et al. 2013). They observed an association between decreased monocytes in the peripheral blood and better survival in PDAC patients. PDAC patients with high TAM/ CD8 ratio had poor prognosis, this was also the case when patients had high CCL2 and low $CD8^+$ T-cells. In a murine model of PDAC with pronounced desmoplastic stroma, KCKO, they observed that by inhibiting CCR7, $CD8^+$ T-cells increased while T_{regs} decreased (Sanford, Belt et al. 2013). Monocytes express CCR7 (Gordon and Taylor 2005).

The role of pancreatic stromal cells in immune cell suppression has recently been elucidated. Kraman and colleagues labelled stromal cells expressing fibroblast activating protein alpha (FAP-α) with Diphtheria toxin receptor (DTR) in a transgenic mouse model of LL2 Lewis lung carcinoma and targeted them with Diphtheria toxin. They observed a “rapid hypoxic necrosis” of stroma and tumour upon ablation of FAP-α expressing stromal cells by Diphtheria toxin that was mediated by interferon-γ and tumour necrosis factor-α (Kraman, Bambrough et al. 2010). They also depleted FAP-α expressing stromal cells in a subcutaneous mouse model of PDAC and

observed immunological control of growth; this however was not the case in the B and T-cell incompetent mouse model, the Rag2- deficient mice (Shinkai, Rathbun et al. 1992; Kraman, Bambrough et al. 2010).

In a separate study involving incurable PDAC patients and a genetically engineered mouse model of PDAC, Beatty and colleagues combined gemcitabine therapy with an agonist CD40 antibody. They observed a regression of tumours in some patients with similar results in the genetically engineered mouse models. They found however that CD40 activated macrophages infiltrated the tumours and facilitated the depletion of the stroma and performed tumour clearance (Beatty, Chiorean et al. 2011). While our patient data suggest the possibility that the $CD8^+$ T-cells rather than macrophages are involved in tumour immunoclearance, our data also points to the role of the stroma in immunosuppresion. These observations point to a putative role of the stroma in the suppression of immune cells infiltrate in PDAC.

PDAC stellate cells may be heterogeneous with markers such as $CD10^+$ and FAP-α identifying sub-population (Ikenaga, Ohuchida et al. 2010; Kraman, Bambrough et al. 2010). Therapy that involves targeting stellate cell markers may be beneficial and of clinical relevance. All-trans Retinoic acid (ATRA) is a fat soluble, vitamin A metabolite that regulates hundreds of genes by binding to nuclear transcription factors such as the retinoic acid receptors (RAR) and the retinoid X receptors (RXR) (Blomhoff and Blomhoff 2006; Kluwe, Wongsiriroj et al. 2011). Vitamin A is involved in an array of functions that include vision, apoptosis, differentiation and development of the central nervous system (Spinella, Kerley et al.

2003; Jimenez-Lara, Clarke et al. 2004; Vergara, Arsenijevic et al. 2005; Blomhoff and Blomhoff 2006), and as early as 1925 deficiency or excess vitamin A was shown to dramatically impact epithelial cell differentiation (Wolbach and Howe 1925). Vitamin A cannot be synthesized by any animal species and has to either be consumed as carotenoids and then physiologically converted to retinoids or as retinoids previously converted in tissue from food (Blomhoff and Blomhoff 2006) from whence they are stored in stellate cells as retinyl esters packaged within lipid droplets (Blomhoff and Blomhoff 2006). Inability to restore vitamin A stores in the pancreas as a result of a loss of fat soluble vitamins leads to a cycle of pancreatic stellate cell activation (Froeling, Feig et al. 2011). However, the restoration of quiescence in pancreatic stellate cells was made possible by treatment with ATRA resulting in significant increase and decrease in proliferation and apoptosis respectively of adjacent tumour cells and a reduction in tumour infiltration (Froeling, Feig et al. 2011). Also treatment with ATRA of 3D co-cultured pancreatic stellate cell and cancer cell line reduced “total, membranous and nuclear β-catenin” in cancers affecting Wnt- β-catenin signalling which has been implicated in gastro-intestinal cancers. In addition, when cancer cells were treated with conditioned media of activated pancreatic stellate cells, an increase in β-catenin activity was observed (Froeling, Feig et al. 2011).

By rendering stromal cells of the pancreas quiescent with ATRA treatment, I was able to abrogate immune cell sequestration in KPC mice. These mice were given an oral dose of ATRA dissolved in sesame oil and the control group were given sesame oil only for a period of five days, (the method has been described earlier (Froeling, Feig et al. 2011)). In the ATRA treated group I observed a stromal

collapse; an increase in the density of $CD8^+$ T-cells and no defect in $CD8^+$ T-cell infiltration of the juxtatumoural compartment. This was not the case for the control group which exhibited similar $CD8^+$ T-cell infiltration as humans. This gives further evidence to the role of pancreatic stellate cells as immunosuppressors and combined with earlier findings by other research groups (Kraman, Bambrough et al. 2010; Beatty, Chiorean et al. 2011) suggests the targeting of pancreatic stroma as a new therapeutic approach to the treatment of pancreatic ductal adenocarcinoma. There was no change however in $CD19^+$ B-cell, $CD4^+$ T-cell, $CD11b^+$ MDSC and $F4/80^+$ macrophages in KPC mice after treatment with ATRA. My observation of immune cell densities in stromal compartments of control KPC mice was in line with my observation in human PDAC tissue. Also interestingly, KPC control mice were positive for fibronectin, much like in human PDAC tissues, however after ATRA treatment there was a significant decrease in positivity.

To further investigate the role of stellate cell activation on immune cell migration and adhesion, I treated a pancreatic stellate cell line, PS1, with ATRA and vehicle (method has been described previously). The conditioned media from quiescent (treated with ATRA) and activated (treated with vehicle only) stellate cells were harvested at the end of treatment and I performed migration assays to these media. The rationale was that secreted factors such as cytokines and chemokines may vary significantly between these two pancreatic stellate cell states and might affect migration of T-cells which may account for the differential migration of T-cells we observed in our human tissue analyses. Because this experiment had not previously been performed I had to optimise for various conditions such as pore size, duration, cell culture media, etc. (these have all been discussed previously). My data

suggests a role of activated pancreatic stellate cells in inhibiting $CD8^+$ T-cell migration to the pancreatic cancer cells. I observed that activated pancreatic stellate cells *in vitro* elicited preferential migration of $CD8^+$ T-cells to themselves over pancreatic cancer cells. When activated pancreatic stellate cells were rendered quiescent, migration towards pancreatic stellate cells was significantly reduced. This preferential migration to activated pancreatic stellate cell over quiescent pancreatic stellate cell was also observed for $CD56^+$ Natural Killer cells but not for $CD20^+$ B-cells. As these assays were performed with donor PBMCs and immortalized stellate cell lines, I validated my findings by isolating PBMCs and primary pancreatic stellate cells from PDAC patients. These are used to perform transwell migration experiments with similar results.

Similarly, T-cells adhered preferentially to activated pancreatic stellate cells over quiescent pancreatic stellate cells in an adhesion assay which I developed. My adhesion results indicate an interaction between T-cells and activated pancreatic stellate cells that are increased over interactions between T-cells and quiescent pancreatic stellate cells. Leukocytes interact with cell surface molecules as they migrate to points of inflammation (Vicente-Manzanares and Sánchez-Madrid 2004). This process in Neutrophils involves the activation of the adhesion molecules, selectins, on the vascular endothelium and upregulation of integrins in leukocytes that promote rolling along the endothelium. Tighter adhesion of Neutrophils occurs through VCAM1 binding to α4β1 and α4β7 on the neutrophils with transmigration hypothetically facilitated by matrix metalloproteinases (von Andrian and Mackay 2000; Coussens and Werb 2002). The juxtatumoural stromal compartment and panstroma compartment differ from each other in their expression of MMP2 and

MMP11 (Iacobuzio-Donahue, Ryu et al. 2002). We also show that VCAM1 is upregulated in activated pancreatic stellate cells and Fibronectin which has been shown to interact with integrins on white blood cells (Johansson, Svineng et al. 1997), is upregulated particularly in the panstromal compartment. The exact nature of leukocyte interaction with pancreatic stellate cells has not been fully investigated but may suggest that T-cell inhibition, in addition to being cytokine mediated may also result from physical interactions between the immune cells and activated pancreatic stellate cells.

It has been established that treatment of human pancreatic stellate cell lines results in gene expression and protein changes (Froeling, Feig et al. 2011). With the aid of a sophisticated web-based bioinformatics tools, candidate genes from gene expression microarray data were identified (Froeling, Feig et al. 2011) that might have an effect on migration and adhesion of immune cells as the immune cells undergo extravasation and subsequently migration to the tumour. The genes involved in immune cell migration were validated by ELISA. While the majority where either upregulated in quiescent pancreatic stellate cells or were not different between stellate cell states, CXCL12 was downregulated in quiescent pancreatic stellate cells and secreted in larger amounts in activated pancreatic stellate cells. Our data is supported by the finding that activated stroma fibroblasts in breast cancer also produce CXCL12. (Orimo, Gupta et al. 2005). CXCL12 disruption brought on lethality (Nagasawa, Hirota et al. 1996). Some functions for which CXCL12 has been involved include, induction of endothelial expression of VEGF-A (Coussens and Werb 2002) which may explain the deficiency of blood vessels in the juxtatumoural region (Olive, Jacobetz et al. 2009); regulation of the expression of sonic hedgehog

for which CXCL12 /CXCR4 (ligand and receptor respectively) signalling has recently been implicated in (Singh, Arora et al. 2012); CXCL12 also induces actin polymerization in leukocytes which is necessary for chemotaxis. CXCL12 acts on lymphocytes and monocytes but not neutrophils and was suggested to have a role in immune surveillance (Bleul, Fuhlbrigge et al. 1996).

Using two different siRNA constructs for CXCL12, I silenced CXCL12 expression in activated pancreatic stellate cells. This was confirmed by ELISA performed with conditioned media of cells. I then performed migration assays as done previously. I observed a reduction of $CD8^+$ T-cells to the conditioned media of the CXCL12 silenced activated pancreatic stellate cell that was similar to the level of quiescent pancreatic stellate cell. By using two different siRNA constructs I confirmed specificity of gene silencing. On primary pancreatic stellate cells, I confirmed preferential migration of $CD8^+$ T-cells to the activated pancreatic stellate cell over its quiescent state. When CXCL12 was silenced in activated pancreatic stellate cells of primary cells, a reduction of $CD8^+$ T-cell migration to activated stellate cells was observed. Therapy that includes the reduction of CXCL12 in stroma of PDAC patients or that induces a transformation to a quiescent stroma may reduce the affinity of cytotoxic T-cells to the activated pancreatic stroma thereby allowing T-cells to reach tumours.

As donor PBMCs are not normally antigen experienced we hypothesised that to gain clinical significance with our migration assays, distribution of T-cell subsets in donors should be similar to those of patient. $CD4^+$ and $CD8^+$ T-cells each may be

distributed into the following subsets: naïve (N), central memory (CM), effector memory (EM) and terminally differentiated effector memory (TEMRA) (Sallusto, Lenig et al. 1999); with the later two characterised by their lack of CCR7 and their abilities to perform cytotoxic functions with the molecules perforin and fas ligand (Sallusto, Lenig et al. 1999; D'Asaro, Dieli et al. 2006). While recruitment, isolation and use of patient PBMCs in migration experiments were met with considerable difficulties I was able to show that in PDAC patients the distribution of effector and naïve subsets of both $CD4^+$ and $CD8^+$ T-cells was similar to those of donors. In an isolated patient who had a bacterial infection, I found that the distribution of T-cell subsets differed from donors and PDAC patient T-cells with a majority of cells present being TEMRAs and very few naïve and central memory cells (data not shown). The observation of increased TEMRAs in infected patients has also been observed by others (Riches, Davies et al. 2012).

The role of CD40 in $CD8^+$ T-cell stimulation is relatively unclear. CD40 is a 50kDa member of the tumour necrosis receptor (TNF R) family and its expression is found on all antigen presenting cell types; these include B-cells, dendritic cells, and macrophages, and on stromal cells such as fibroblasts and keratinocytes. While the expression of CD40 on B-cells is adequate, lower expression levels on macrophages etc., can be upregulated using cytokines such as IFN-γ and GM-CSF (Mackey, Barth et al. 1998). The CD40 Ligand, CD154, is a 39kDa member of the TNF family with expression predominantly on $CD4^+$ T-cells and only a weak expression on $CD8^+$ T-cells (Roy, Waldschmidt et al. 1993; Sad, Krishnan et al. 1997; Mackey, Barth et al. 1998). CD154 expression on T-cells is essential for priming, expansion and maturation into effector cells (Mackey, Barth et al. 1998). 2 groups observed

impaired helper cytokine production and cytotoxic T-cell activity in CD154-deficient and anti-CD154 treated mice (Yang and Wilson 1996; Scaria, St George et al. 1997). The role of CD40 on $CD8^+$ T-cells may be an indirect one that relies on $CD8^+$ T-cells dependence on $CD4^+$ T-cells such as the reliance on $CD4^+$ T-cells to produce T_H1 cytokines which are required for $CD8^+$ priming (Mackey, Barth et al. 1998).

Like PDAC, breast cancers have an active stroma consisting of vascular cell, myofibroblasts and innate and adaptive immune cells (DeNardo and Coussens 2007). An increase in leukocytic infiltrates in breast cancer corresponds with tumourigenesis and in rapidly proliferating tumours of the breast, the presence of T-cells is a positive prognostic factor (DeNardo and Coussens 2007). Chin et al, observed that high $CD4^+$ helper T-cells at sites of tumour in breast cancer correlates positively with tumour progression (Chin, Janseens et al. 1991), much like I observed in PDAC tissues. $CD4^+$ helper T-cells can be classified into subsets of T_H1, T_H2, T_H17 and Tregs which taken together have anti-tumour and tumour promoting effects (Zhu and Paul 2008). In their work, $CD4^+$ helper T-cell subsets were not identified. This too remains a criticism of my work. FoxP3 increase have been found to correspond with disease stage in breast cancer, from normal to ductal carcinoma *in situ* (DCIS) and to invasive carcinoma with the presence of high FoxP3 densities predicting reduced overall patient survival and reduced relapse free survival (Bates, Fox et al. 2006). In a study involving 28 chemotherapy and radiotherapy naive breast cancer patients and 14 age and sex matched donors, $CCR6^+$ T_{regs}, a newly characterised subset of T_{regs} (Kleinewietfeld, Puentes et al. 2005), was found to be increased in patients along with tumour progression. A reverse correlation was observed between $CCR6^+$ T_{regs} and IFN-γ^+ $CD8^+$ T-cells and between $CCR6^+$ T_{regs}

and patient survival (Xu, Xu et al. 2010). This again is similar to my findings in PDAC where PDAC patients with high FoxP3 densities have decreased overall survival. While breast cancers are similar to PDACs, they differ in their multiple molecular classifications such as HER2 etc. The capability to diagnose breast cancers early via physical and molecular screening methods leading to early detection and the ability to perform mastectomies may further explain the better outcome experienced by breast cancer patients compared to PDAC patients.

Also, like PDAC and breast cancers, colorectal cancer (CRC) is an adenocarcinoma, and like the pancreas, the colon is involved in digestion. CRC share the same driver genes as PDAC: KRAS, TP53 and SMAD4 (Markowitz and Bertagnolli 2009). Stroma is present in CRCs, however, in a study by Ueno et al, of a population consisting of 862 CRC patients, they observed that 53% had mature fibrotic cancer stroma, 33% had intermediate stroma and 15% had immature stroma. Characterisation of stromal types was based on histology observed after H&E staining. They also observed by immunohistochemistry that myofibroblasts were distributed “extensively” in the immature fibrotic stroma compared with mature and intermediate fibrotic stroma and those stromal T-cells became “sparser” as maturation decreased. Patients with immature stroma had a 5 year survival of 27% which was significantly lower than patients with mature (80%) and intermediate (55%) stroma (Ueno, Jones et al. 2004). Similar to my finding in PDACs, $CD8^+$ T-cells infiltrating around CRC tumour stroma contribute to better prognosis (Ropponen, Eskelinen et al. 1997; Galon, Costes et al. 2006). Again, similar to the data I show, Galon et al showed that the type, density and location of immune cells in CRC had a prognostic benefit, and in the case of CRC, superior to the TNM

classification (Galon, Costes et al. 2006). The density of peritumoural tumour associated macrophages (TAMs) in CRC were shown to prevent tumourigenesis (Öberg, Samii et al. 2002; Khorana, Ryan et al. 2003), whereas the density of intratumoural TAMs were shown to correlate with “depth of invasion, lymph node metastasis and staging of CRC” (Pancione, Forte et al. 2009; Kang, Chen et al. 2010; Deschoolmeester, Baay et al. 2011) suggesting a polarization towards the M1 and M2 macrophage phenotypes respectively. Survival effect of Tregs on CRC remains relatively unknown, however, Tregs have been associated with poor outcomes in breast, ovarian, hepato-cellular carcinomas and gastric carcinoma (Deschoolmeester, Baay et al. 2011). This is the same for PDAC.

T_{regs} have also been found to be increased in hepato-cellular carcinoma (HCC) compared to the non-tumourous liver, where a high T_{reg} infiltrate led to lower patient survival and was an independent prognostic factor. $CD8^+$ T-cells were also found to decrease during hepato-cellular carcinogenesis (Kobayashi, Hiraoka et al. 2007). Along with CRC and PDAC, higher frequencies of $CD8^+$ T-cells demonstrated improved patient survival in 117 ovarian cancer patients. As well, a high $CD8^+/FoxP3^+$ ratio demonstrated improved patient survival (Sato, Olson et al. 2005).

The tumour microenvironment of Non-small cell lung cancer (NSCLC) is made up of fibroblasts, mesenchymal stem cells and immune cell infiltrate (El-Nikhely, Larzabal et al. 2012). In a study involving the retrospective analysis of 128 NSCLC patients, the large cell or squamous cell carcinoma had more $CD8^+$ T-cell infiltrate than adenocarcinoma, however, $CD8^+$ T-cells had no effect on patient survival (Mori,

Ohtani et al. 2000). This finding was corroborated in another study involving 178 NSCLC patients in which patients having higher $CD8^+$ T-cells within cancer cell nests had shorter survival compared with patients having lower $CD8^+$ T-cell numbers (Wakabayashi, Yamazaki et al. 2003). Interestingly, NSCLC patients with higher $CD4^+$ T-cells in the stroma, but not within cancer cell nests, had longer overall survival (Wakabayashi, Yamazaki et al. 2003). These observations in NSCLC are different from what I have shown in PDAC and what others have shown in breast, ovarian, colorectal and hepatocellular cancers (all discussed above).

My work, although robust and insightful might have benefited more from further classification of immune cell markers such as the helper T-cell subsets (T_H1, T_H2, etc) and the M1 and M2 macrophage phenotypes; and immune cell markers for MDSCs and Dendritic cells (DC) in human tissues. The markers for some of these immune cells have not yet been fully developed for pathological use. Survival analysis of the advanced disease cohorts might also have proved useful. In addition, it might have proved useful to study immune cell-stellate cell interaction. I might have done this by employing immunohistochemistry and immunofluorescence in studying cell adhesion markers between these cell types both in human tissue and *in vitro*. It might also have been of consequence to identify if the use of ATRA (*in vitro* and *in vivo*) alters adhesion properties of these cells. These have not yet been looked into and may hold yet important therapeutic clinical significance.

In summary, I found that total tissue infiltrate of the immune cells ($CD3^+$, $CD4^+$, $CD8^+$, $FoxP3^+$, $CD20^+$ and $CD68^+$) increased in accordance with severity from normal to malignancy of the Pancreatico-biliary diseases with infiltration of $CD8^+$ T-

cells to PDAC tissue being significantly less than other malignant diseases. I also observed that $CD8^+$ T-cells were sequestrated in the panstroma compartment along with $CD20^+$ (B-cells) in both resected and advanced PDAC cases. This was not the case for $CD68^+$ (macrophages) and $myeloperoxidase^+$ (neutrophils). These differences in immune cell infiltration of stromal compartments were not present in other Pancreatico-biliary diseases with the exception of the $CD8^+$ marker in ampullary carcinoma. Survival analysis showed that while many of the markers studied (particularly $FoxP3^+$ (T regulatory cells)) had an anti-survival effect, patients with increased $CD8^+$ (cytotoxic T-cells) and $CD56^+$ (Natural killer cells) in the pancreas tissue or infiltrating the juxtatumoural compartment had better overall survival.

$CD3^+$ T-cells, $CD4^+$ T-cells, $CD8^+$ T-cells and $CD56^+$ NK cells significantly migrated to conditioned media from aPSC over qPSC. This was not the case for $CD19^+$ B-cells. $CD3^+$ T-cells adhered to activated pancreatic stellate cells over their quiescent phenotype. I confirmed by ELISA that CXCL12 was secreted by aPSC significantly more than qPSC; CXCL12 silencing in activated aPSC resulted in a significant reduction in $CD8^+$ T-cell migration to a level similar to basal media control. As these *in vitro* assays were performed on immortalised pancreatic stellate cell lines, I confirmed with identical results on primary pancreatic stellate cells. Also using flow cytometry I showed that donor T-cell effector and memory subsets do not differ from those of PDAC patients and patient T-cells migrated preferentially to activated pancreatic stellate cells over the quiescent phenotype. CXCR4, receptor for CXCL12, was also upregulated in $CD4^+$ and $CD8^+$ T-cells from PBMC of PDAC patients.

6.0 Conclusion

The mode by which pancreatic stellate cells may hinder immune cell, specifically T-cell, immunoclearance is not fully understood however a possible mechanism may involve modulation of the immunosuppressant myeloid derived suppressor cells (MDSC) (Mace, Ameen et al. 2013). Hepatic stellate cells which share the same modes of activation and quiescence, retinoid storage and markers for activation and quiescence (Friedman 2008) pancreatic stellate cells also express CD40 (Schwabe, Schnabl et al. 2001; Merika, Syrigos et al. 2012). CD40 is a member of the Tumour necrosis factor receptor (TNFR) super family (van Kooten and Banchereau 2000; Schwabe, Schnabl et al. 2001) and $CD40^{+}$ stellate cells may serves as a bridge to immune cells that express CD40L (Friedman 2008). This too has previously been discussed.

The nucleoside analogue Gemcitabine has been used as the standard in first line chemotherapy for metastatic pancreatic ductal adenocarcinoma since 1997 (Michl and Gress 2013) with “modest survival benefits” of a median 5.65 months. Prior to this 5-FU (5- fluorouracil) was used with a median increased survival of 4.41 months (Michl and Gress 2013). Other cytotoxic agents that are being used include: oxaliplatin, cisplatin, irinotecan, exatecan and capecitabine. Although these agents have been used in combination with gemcitabine there have been no significant increased overall survival (Stathis and Moore 2010).

Recently, a combination chemotherapy excluding gemcitabine but including oxaliplatin, irinotecan, fluorouracil and leucovorin, FOLFIRINOX, was demonstrated to increase overall survival in patients with metastatic disease and good performance status to a median of 11.1 months versus a median of 6.8 months for gemcitabine only treated controls (Conroy, Desseigne et al. 2011). This highlighted the possibility of non-gemcitabine based treatment. However, novel chemotherapeutic approaches involving gemcitabine in combination with agents targeting other components of carcinomas such as immune cells, stromal cells and blood vessels, and agents that help to deliver the chemotherapy past the surrounding stroma to the cancer cells are being researched into. Few studies have shown that ablation of stroma leads to pancreatic tumour regression (Kraman, Bambrough et al. 2010; Beatty, Chiorean et al. 2011). Also recently, the United States Food and Drug administration (FDA) approved the Nanoparticle albumin-bound (nab)-paclitaxel in the treatment of metastatic breast cancer and showed promise in phase I/ II PDAC trials (Von Hoff, Ramanathan et al. 2011). Only recently, with phase III trials in which (nab)-paclitaxel was combined with gemcitabine in advanced pancreatic cancer patients now complete, "statistically significant and clinically meaningful" results were observed (Von Hoff 2013). They observes an increase in median overall survival of patients with combination therapy which was 8.5 months compared to a median survival of 6.5 months for patients treated with gemcitabine alone. At 12 months survival for combination therapy treated PDAC patients was 35% compared to 22% for gemcitabine alone treated patients and survival at 2 years increase 2 fold from 4% in gemcitabine alone to 9% in combination therapy treated patients (Von Hoff 2013). The hypothesis of this treatment is that secreted protein acidic and rich in cysteine (SPARC) is overexpressed in PDAC tumour samples and is albumin-binding thus

sequestering nab-paclitaxel intratumourally (Von Hoff, Ramanathan et al. 2011; Michl and Gress 2013). A gemcitabine based treatment regimen that targets the pancreatic cancer stroma may hold promise. In our model, we suggest reversing the activated phenotype of pancreatic stellate cells to quiescence by treatment with ATRA. Froeling et al previously showed that when KPC mice is treated with ATRA a stromal collapse occurs (Froeling, Feig et al. 2011) and our data shows that in addition to stromal collapse, $CD8^+$ T-cells are increased in the pancreas and infiltrate the tumours.

Immune based cancer therapies may also hold many promises. Cancers co-opt checkpoint pathways such as Cytotoxic T-lymphocyte-associated antigen 4 (CTLA4) that regulate and limit immune response, specifically against T-cells. CTLA4 can be blocked by specific antibodies such as ipilimumab which leads to a sustained immune response upon binding of the antibody to CTLA4. Ipilimumab has been approved in melanoma after successful clinical trials and is now undergoing clinical trials in PDAC (Michl and Gress 2013). In considering an anti-tumour immune based therapy immune cell subtypes and functional analyses are needed (Zheng, Xue et al. 2013). This may prove extremely difficult in PDAC as the tumour microenvironment is rich with immune cell subtypes that interact with the surrounding stroma and each other. I have defined some immune cell subtypes in PDAC and their [functional] position in the PDAC architecture. I have also given a global picture of how these immune cells affect patient survival thus giving the possibility of defining these subtypes into anti-tumour and tumour supporting immune cells. Detailed functional analyses of each immune cell, including their agonist and antagonist have to be defined.

Further work might include studying more robustly the interaction [or cross talk] between pancreatic stellate cells and immune cells and why some immune cells are hindered at the surrounding panstroma while others migrate past the panstroma to the juxtatumoural stroma and further to the tumour. This further study should include staining for various potential markers of adhesion such as the weak adhesion molecules P- and L- selectin, and the firmer adhesion molecules involved in leukocyte migration arrest; ICAM-1 and VCAM-1. Other potential molecules may include Fibronectin and the matrix metalloproteinases (MMPs). It may also be interesting to study the presence (or absence) of immune cell synapses with pancreatic stellate cells; will this include F-actin or α-SMA and might there be polarization of actin? (Ramsay, Johnson et al. 2008).

Few markers have been proposed for pancreatic stellate cells such as CD10 and Fibroblast activating protein (FAP) (Ikenaga, Ohuchida et al. 2010; Kraman, Bambrough et al. 2010). A possibility might exist of pancreatic stellate cells being of various subtypes and a study to identify these subtypes might prove essential. Perhaps the different subtypes might correlate with the juxtatumoural stroma and panstroma and might play a role in immune cell migration and adhesion. Identifying markers for pancreatic stellate cells subtypes might aid in target specificity. It may also be of interest to investigate immune cell interaction with stellate cells of other desmoplastic cancers such as breast and colorectal cancers (Hewitt, Powe et al. 1993; Walker 2001) and if any differences may account for the differences in patient overall survival.

7.0 References

Abcam. (2013). "Flow cytometry guide." Retrieved 26 March, 2013, from http://docs.abcam.com/pdf/protocols/Introduction_to_flow_cytometry_May_10.pdf)

Albores-Saavedra, J., A. Angeles-Angeles, et al. (1987). "Mucinous cystadenocarcinoma of the pancreas. Morphologic and immunocytochemical observations." The American journal of surgical pathology **11**(1): 11-20.

Altman, D. G., B. Lausen, et al. (1994). "Dangers of Using "Optimal" Cutpoints in the Evaluation of Prognostic Factors." Journal of the National Cancer Institute **86**(11): 829-835.

Alugupalli, K. R., J. M. Leong, et al. (2004). "B1b Lymphocytes Confer T Cell-Independent Long-Lasting Immunity." Immunity **21**(3): 379-390.

Anfossi, N., P. André, et al. (2006). "Human NK Cell Education by Inhibitory Receptors for MHC Class I." Immunity **25**(2): 331-342.

Anne, O. G. (1998). "Cytokines Induce the Development of Functionally Heterogeneous T Helper Cell Subsets." Immunity **8**(3): 275-283.

Asseman, C., S. Mauze, et al. (1999). "An Essential Role for Interleukin 10 in the Function of Regulatory T Cells That Inhibit Intestinal Inflammation." The Journal of Experimental Medicine **190**(7): 995-1004.

Bachem, M. G., M. Schünemann, et al. (2005). "Pancreatic carcinoma cells induce fibrosis by stimulating proliferation and matrix synthesis of stellate cells." Gastroenterology **128**(4): 907-921.

Baine, M. J., S. Chakraborty, et al. (2011). "Transcriptional profiling of peripheral blood mononuclear cells in pancreatic cancer patients identifies novel genes with potential diagnostic utility." PLoS ONE **6**(2): e17014.

Baker, M. L., E. S. Seeley, et al. (2012). "Invasive mucinous cystic neoplasms of the pancreas." Experimental and Molecular Pathology **93**(3): 345-349.

Barreiro, O. (2002). "Dynamic interaction of VCAM-1 and ICAM-1 with moesin and ezrin in a novel endothelial docking structure for adherent leukocytes." The Journal of Cell Biology **157**(7): 1233-1245.

Bates, G. J., S. B. Fox, et al. (2006). "Quantification of regulatory T cells enables the identification of high-risk breast cancer patients and those at risk of late relapse." Journal of Clinical Oncology **24**(34): 5373-5380.

Bayne, Lauren J., Gregory L. Beatty, et al. (2012). "Tumor-Derived Granulocyte-Macrophage Colony-Stimulating Factor Regulates Myeloid Inflammation and T Cell Immunity in Pancreatic Cancer." Cancer Cell **21**(6): 822-835.

Beatty, G. L., E. G. Chiorean, et al. (2011). "CD40 Agonists Alter Tumor Stroma and Show Efficacy Against Pancreatic Carcinoma in Mice and Humans." Science **331**(6024): 1612-1616.

Bekkers, R. L. M., J. Bulten, et al. (2003). "Coexisting high-grade glandular and squamous cervical lesions and human papillomavirus infections." British Journal of Cancer **89**(5): 886-890.

Belkaid, Y. (2007). "Regulatory T cells and infection: a dangerous necessity." Nat Rev Immunol **7**(11): 875-888.

BENDALL, L. (2005). "Chemokines and their receptors in disease." Histology and histopathology **20**(3): 907-926.

Bendall, L. (2005). "Chemokines and their receptors in disease."

Beyer, M. (2006). "Regulatory T cells in cancer." Blood **108**(3): 804-811.

Bingle, L., N. J. Brown, et al. (2002). "The role of tumour-associated macrophages in tumour progression: implications for new anticancer therapies." The Journal of Pathology **196**(3): 254-265.
Bioconductor. (2013). Retrieved 26 March, 2013, from http://www.bioconductor.org/.
Biogenex. (2013). Retrieved 26 March 2013, from http://www.biogenex.com/index.php?option=com_virtuemart&page=shop.browse&category_id=76&Itemid=25.
Biswas, S. K. and A. Mantovani (2010). "Macrophage plasticity and interaction with lymphocyte subsets: cancer as a paradigm." Nature Immunology **11**(10): 889-896.
Bleul, C. C., R. C. Fuhlbrigge, et al. (1996). "A highly efficacious lymphocyte chemoattractant, stromal cell-derived factor 1 (SDF-1)." The Journal of Experimental Medicine **184**(3): 1101-1109.
Blomhoff, R. and H. K. Blomhoff (2006). "Overview of retinoid metabolism and function." Journal of Neurobiology **66**(7): 606-630.
Bolton, K. L., M. Garcia-Closas, et al. (2010). "Assessment of Automated Image Analysis of Breast Cancer Tissue Microarrays for Epidemiologic Studies." Cancer Epidemiology Biomarkers & Prevention **19**(4): 992-999.
Borge, M., P. R. Nannini, et al. (2010). "CXCL12-induced chemotaxis is impaired in T cells from patients with ZAP-70-negative chronic lymphocytic leukemia." Haematologica **95**(5): 768-775.
Borge, M., P. R. Nannini, et al. (2010). "CXCL12-induced chemotaxis is impaired in T cells from patients with ZAP-70-negative chronic lymphocytic leukemia." Haematologica **95**(5): 768-775.
Bosetti, C., E. Lucenteforte, et al. (2012). "Cigarette smoking and pancreatic cancer: an analysis from the International Pancreatic Cancer Case-Control Consortium (Panc4)." Annals of Oncology **23**(7): 1880-1888.
Buchwalow, I. B. and W. Böcker (2010). Immunohistochemistry: basics and methods, Springer.
Camp, R. L., M. Dolled-Filhart, et al. (2004). "X-Tile: A New Bio-Informatics Tool for Biomarker Assessment and Outcome-Based Cut-Point Optimization." Clinical Cancer Research **10**(21): 7252-7259.
Campbell, D. J., C. H. Kim, et al. (2003). "Chemokines in the systemic organization of immunity." Immunological Reviews **195**(1): 58-71.
Campbell, D. J. and M. A. Koch (2011). "Phenotypical and functional specialization of FOXP3+ regulatory T cells." Nature Reviews Immunology **11**(2): 119-130.
Carragher, D. M., J. Rangel-Moreno, et al. (2008). Ectopic lymphoid tissues and local immunity. Seminars in immunology, Elsevier.
Chesnut, R. and H. Grey (1981). "Studies on the capacity of B cells to serve as antigen-presenting cells." The Journal of Immunology **126**(3): 1075-1079.
Chin, Y., J. Janseens, et al. (1991). "Phenotypic analysis of tumor-infiltrating lymphocytes from human breast cancer." Anticancer research **12**(5): 1463-1466.
Clark, C. E., S. R. Hingorani, et al. (2007). "Dynamics of the Immune Reaction to Pancreatic Cancer from Inception to Invasion." Cancer Research **67**(19): 9518-9527.
Clark, C. E., S. R. Hingorani, et al. (2007). "Dynamics of the immune reaction to pancreatic cancer from inception to invasion." Cancer Res **67**(19): 9518-9527.

Clear, A. J., A. M. Lee, et al. (2010). "Increased angiogenic sprouting in poor prognosis FL is associated with elevated numbers of CD163+ macrophages within the immediate sprouting microenvironment." Blood **115**(24): 5053-5056.
Clemens, G., K. R. Flower, et al. (2013). "The action of all-trans-retinoic acid (ATRA) and synthetic retinoid analogues (EC19 and EC23) on human pluripotent stem cells differentiation investigated using single cell infrared microspectroscopy." Molecular BioSystems.
Clemente, C. G., M. C. Mihm, et al. (1996). "Prognostic value of tumor infiltrating lymphocytes in the vertical growth phase of primary cutaneous melanoma." Cancer **77**(7): 1303-1310.
Cohen, P. E., O. Chisholm, et al. (1996). "Absence of colony-stimulating factor-1 in osteopetrotic (csfmop/csfmop) mice results in male fertility defects." Biology of Reproduction **55**(2): 310-317.
Conroy, T., F. Desseigne, et al. (2011). "FOLFIRINOX versus gemcitabine for metastatic pancreatic cancer." New England Journal of Medicine **364**(19): 1817-1825.
Cooper, M. A., T. A. Fehniger, et al. (2001). "The biology of human natural killer-cell subsets." Trends in Immunology **22**(11): 633-640.
Corporation, P. (2013). "Monte Carlo simulation." Retrieved 26 March, 2013, from http://www.palisade.com/risk/monte_carlo_simulation.asp.
Corzo, C. A., M. J. Cotter, et al. (2009). "Mechanism regulating reactive oxygen species in tumor-induced myeloid-derived suppressor cells." The Journal of Immunology **182**(9): 5693-5701.
Coupland, V. H., H. M. Kocher, et al. (2012). "Incidence and survival for hepatic, pancreatic and biliary cancers in England between 1998 and 2007." Cancer Epidemiol.
Coupland, V. H., H. M. Kocher, et al. "Incidence and survival for hepatic, pancreatic and biliary cancers in England between 1998 and 2007." Cancer Epidemiology(0).
Coupland, V. H., H. M. Kocher, et al. (2012). "Incidence and survival for hepatic, pancreatic and biliary cancers in England between 1998 and 2007." Cancer Epidemiology.
Coussens, L. M. and Z. Werb (2002). "Inflammation and cancer." Nature **420**(6917): 860-867.
D'Asaro, M., F. Dieli, et al. (2006). "Increase of CCR7- CD45RA+ CD8 T cells (TEMRA) in chronic graft-versus-host disease." Leukemia **20**(3): 545-547.
de Groen, P. C., G. J. Gores, et al. (1999). "Biliary Tract Cancers." New England Journal of Medicine **341**(18): 1368-1378.
DeNardo, D. G. and L. M. Coussens (2007). "Inflammation and breast cancer. Balancing immune response: crosstalk between adaptive and innate immune cells during breast cancer progression." Breast Cancer Research **9**(4): 212.
Deschoolmeester, V., M. Baay, et al. (2011). "Immune cells in colorectal cancer: Prognostic relevance and role of MSI." Cancer Microenvironment **4**(3): 377-392.
Detlefsen, S., B. Sipos, et al. (2006). "Fibrogenesis in alcoholic chronic pancreatitis: the role of tissue necrosis, macrophages, myofibroblasts and cytokines." Modern pathology **19**(8): 1019-1026.
Dong, C. (2006). "Diversification of T-helper-cell lineages: finding the family root of IL-17-producing cells." Nat Rev Immunol **6**(4): 329-334.

Dong, C. (2008). "TH17 cells in development: an updated view of their molecular identity and genetic programming." Nature Reviews Immunology **8**(5): 337-348.
Dudda, J. C., N. Perdue, et al. (2008). "Foxp3+ regulatory T cells maintain immune homeostasis in the skin." Journal of Experimental Medicine **205**(7): 1559-1565.
Eckmann, K. R., D. K. Patel, et al. (2011). "Chemotherapy outcomes for the treatment of unresectable intrahepatic and hilar cholangiocarcinoma: a retrospective analysis." Gastrointestinal cancer research : GCR **4**(5-6): 155-160.
Ehrenstein, M. R. (2004). "Compromised Function of Regulatory T Cells in Rheumatoid Arthritis and Reversal by Anti-TNF Therapy." Journal of Experimental Medicine **200**(3): 277-285.
El-Nikhely, N., L. Larzabal, et al. (2012). "Tumor-stromal interactions in lung cancer: novel candidate targets for therapeutic intervention." Expert Opinion on Investigational Drugs **21**(8): 1107-1122.
Esposito, I., M. Menicagli, et al. (2004). "Inflammatory cells contribute to the generation of an angiogenic phenotype in pancreatic ductal adenocarcinoma." Journal of Clinical Pathology **57**(6): 630-636.
Fasanella, S., E. Leonardi, et al. (2011). "Proliferative activity in human breast cancer: Ki-67 automated evaluation and the influence of different Ki-67 equivalent antibodies." Diagnostic Pathology **6**(Suppl 1): S7.
Ferlazzo, G. and C. Münz (2004). "NK Cell Compartments and Their Activation by Dendritic Cells." The Journal of Immunology **172**(3): 1333-1339.
Filipazzi, P., R. Valenti, et al. (2007). "Identification of a new subset of myeloid suppressor cells in peripheral blood of melanoma patients with modulation by a granulocyte-macrophage colony-stimulation factor–based antitumor vaccine." Journal of Clinical Oncology **25**(18): 2546-2553.
Fischer, H.-P. and H. Zhou (2004). "Pathogenesis of carcinoma of the papilla of Vater." Journal of Hepato-Biliary-Pancreatic Surgery **11**(5): 301-309.
Fitch, F. W., M. D. McKisic, et al. (1993). "Differential Regulation of Murine T Lymphocyte Subsets." Annual Review of Immunology **11**(1): 29-48.
Freyschmidt, E.-J., C. B. Mathias, et al. (2010). "Skin Inflammation Arising from Cutaneous Regulatory T Cell Deficiency Leads to Impaired Viral Immune Responses." The Journal of Immunology **185**(2): 1295-1302.
Friedman, S. L. (2008). "Hepatic Stellate Cells: Protean, Multifunctional, and Enigmatic Cells of the Liver." Physiological Reviews **88**(1): 125-172.
Froeling, F. E., C. Feig, et al. (2011). "Retinoic Acid-Induced Pancreatic Stellate Cell Quiescence Reduces Paracrine Wnt-beta-Catenin Signaling to Slow Tumor Progression." Gastroenterology **141**(4): 1486-1497.
Froeling, F. E. M., C. Feig, et al. (2011). "Retinoic Acid–Induced Pancreatic Stellate Cell Quiescence Reduces Paracrine Wnt–β-Catenin Signaling to Slow Tumor Progression." Gastroenterology **141**(4): 1486-1497.e1414.
Froeling, F. E. M., T. A. Mirza, et al. (2009). "Organotypic Culture Model of Pancreatic Cancer Demonstrates that Stromal Cells Modulate E-Cadherin, β-Catenin, and Ezrin Expression in Tumor Cells." The American Journal of Pathology **175**(2): 636-648.
Fukushima, N., K. Mukai, et al. (1997). "Intraductal papillary tumors and mucinous cystic tumors of the pancreas: Clinicopathologic study of 38 cases." Human Pathology **28**(9): 1010-1017.

Galon, J., A. Costes, et al. (2006). "Type, Density, and Location of Immune Cells Within Human Colorectal Tumors Predict Clinical Outcome." Science **313**(5795): 1960-1964.
Garside, P. (1998). "Visualization of Specific B and T Lymphocyte Interactions in the Lymph Node." Science **281**(5373): 96-99.
Genecards. (2013). Retrieved 26 March, 2013.
Gokhale, S., D. Rosen, et al. (2007). "Assessment of Two Automated Imaging Systems in Evaluating Estrogen Receptor Status in Breast Carcinoma." Applied Immunohistochemistry & Molecular Morphology **15**(4): 451-455 410.1097/PAI.1090b1013e31802ee31998.
Gordon, S. and P. R. Taylor (2005). "Monocyte and macrophage heterogeneity." Nat Rev Immunol **5**(12): 953-964.
Gouon-Evans, V., E. Lin, et al. (2002). "Requirement of macrophages and eosinophils and their cytokines/chemokines for mammary gland development." Breast Cancer Res **4**(4): 155 - 164.
Gouon-Evans, V., M. E. Rothenberg, et al. (2000). "Postnatal mammary gland development requires macrophages and eosinophils." Development **127**(11): 2269-2282.
Grégoire, C., L. Chasson, et al. (2007). "The trafficking of natural killer cells." Immunological Reviews **220**(1): 169-182.
Greten, T. F., M. P. Manns, et al. (2011). "Myeloid derived suppressor cells in human diseases." International immunopharmacology **11**(7): 802-807.
Hadi, A. M., K. T. B. Mouchaers, et al. (2011). "Rapid quantification of myocardial fibrosis: a new macro-based automated analysis." Cellular Oncology.
Hamasaki, T., H. Suzuki, et al. (2012). "Efficacy of a Novel Class of RNA Interference Therapeutic Agents." PLoS ONE **7**(8): e42655.
Hanley, K. Z., M. T. Siddiqui, et al. (2009). "Evaluation of new monoclonal antibodies in detection of estrogen receptor, progesterone receptor, and Her2 protein expression in breast carcinoma cell block sections using conventional microscopy and quantitative image analysis." Diagnostic Cytopathology **37**(4): 251-257.
Harty, J. T., A. R. Tvinnereim, et al. (2000). "CD8+ T Cell Effector Mechanisms in Resistance to Infection." Annual Review of Immunology **18**(1): 275-308.
Harwood, N. E. and F. D. Batista (2010). "Early Events in B Cell Activation." Annual Review of Immunology **28**(1): 185-210.
Hayakawa, Y. and M. J. Smyth (2006). "CD27 Dissects Mature NK Cells into Two Subsets with Distinct Responsiveness and Migratory Capacity." The Journal of Immunology **176**(3): 1517-1524.
Hewitt, R. E., D. G. Powe, et al. (1993). "Desmoplasia and its relevance to colorectal tumour invasion." International Journal of Cancer **53**(1): 62-69.
Hezel, A. F., A. C. Kimmelman, et al. (2006). "Genetics and biology of pancreatic ductal adenocarcinoma." Genes & Development **20**(10): 1218-1249.
Hoechst, B., T. Voigtlaender, et al. (2009). "Myeloid derived suppressor cells inhibit natural killer cells in patients with hepatocellular carcinoma via the NKp30 receptor." Hepatology **50**(3): 799-807.
Holzheimer, R. G. and J. A. Mannick (2001). Surgical treatment: evidence-based and problem-oriented, Zuckschwerdt.
Holzheimer, R. G., J. A. Mannick, et al. (2001). "Cystic tumors of the pancreas."
Hori, S. (2003). "Control of Regulatory T Cell Development by the Transcription Factor Foxp3." Science **299**(5609): 1057-1061.

Horwitz, D. A. (2008). "Regulatory T cells in systemic lupus erythematosus: past, present and future." Arthritis Research & Therapy **10**(6): 227.
Howe, J. R., D. S. Klimstra, et al. (1998). "Factors Predictive of Survival in Ampullary Carcinoma." Annals of Surgery **228**(1): 87-94.
Hruban, R. H., A. Maitra, et al. (2007). "Precursors to pancreatic cancer." Gastroenterology clinics of North America **36**(4): 831-849, vi.
Hsu, S. M., L. Raine, et al. (1981). "Use of avidin-biotin-peroxidase complex (ABC) in immunoperoxidase techniques: a comparison between ABC and unlabeled antibody (PAP) procedures." Journal of Histochemistry & Cytochemistry **29**(4): 577-580.
Hwang, R. F., T. Moore, et al. (2008). "Cancer-Associated Stromal Fibroblasts Promote Pancreatic Tumor Progression." Cancer Research **68**(3): 918-926.
Iacobuzio-Donahue, C. A., P. Argani, et al. (2002). "The Desmoplastic Response to Infiltrating Breast Carcinoma: Gene Expression at the Site of Primary Invasion and Implications for Comparisons between Tumor Types." Cancer Research **62**(18): 5351-5357.
Iacobuzio-Donahue, C. A., B. Ryu, et al. (2002). "Exploring the host desmoplastic response to pancreatic carcinoma: gene expression of stromal and neoplastic cells at the site of primary invasion." Am J Pathol **160**(1): 91-99.
Iacobuzio-Donahue, C. A., B. Ryu, et al. (2002). "Exploring the Host Desmoplastic Response to Pancreatic Carcinoma: Gene Expression of Stromal and Neoplastic Cells at the Site of Primary Invasion." The American Journal of Pathology **160**(1): 91-99.
Iida, N. and G. R. Grotendorst (1990). "Cloning and sequencing of a new gro transcript from activated human monocytes: expression in leukocytes and wound tissue." Molecular and Cellular Biology **10**(10): 5596-5599.
Ikenaga, N., K. Ohuchida, et al. (2010). "CD10+ Pancreatic Stellate Cells Enhance the Progression of Pancreatic Cancer." Gastroenterology **139**(3): 1041-1051.e1048.
Incorporated, C. (2010). "Transwell Permeable Supports Selection and Use Guide." Retrieved 26 March, 2013, from http://catalog2.corning.com/Lifesciences/media/pdf/transwell_guide.pdf.
Infante-Duarte, C., H. F. Horton, et al. (2000). "Microbial Lipopeptides Induce the Production of IL-17 in Th Cells." The Journal of Immunology **165**(11): 6107-6115.
Jiang, H., Z. Ju, et al. (2007). "Telomere shortening and ageing." Zeitschrift für Gerontologie und Geriatrie **40**(5): 314-324.
Jimenez-Lara, A., N. Clarke, et al. (2004). "Retinoic-acid-induced apoptosis in leukemia cells." Trends in molecular medicine **10**(10): 508-515.
Johansson, S., G. Svineng, et al. (1997). "Fibronectin-integrin interactions." Front. Biosci **2**: d126-d146.
Jung, Y.-J., J. S. Isaacs, et al. (2003). "IL-1β mediated up-regulation of HIF-1α via an NFkB/COX-2 pathway identifies HIF-1 as a critical link between inflammation and oncogenesis." The FASEB Journal.
Kang, J. C., J. S. Chen, et al. (2010). "Intratumoral macrophage counts correlate with tumor progression in colorectal cancer." Journal of surgical oncology **102**(3): 242-248.
Khalid, A. and W. Brugge (2007). "ACG practice guidelines for the diagnosis and management of neoplastic pancreatic cysts." The American journal of gastroenterology **102**(10): 2339-2349.

Khan, S. A., B. R. Davidson, et al. (2002). "Guidelines for the diagnosis and treatment of cholangiocarcinoma: consensus document." Gut **51**(suppl 6): vi1-vi9.
Khorana, A. A., C. K. Ryan, et al. (2003). "Vascular endothelial growth factor, CD68, and epidermal growth factor receptor expression and survival in patients with stage II and stage III colon carcinoma." Cancer **97**(4): 960-968.
Kirby, B. J., A. R. Wheeler, et al. (2003). "Programmable modification of cell adhesion and zeta potential in silica microchips." Lab on a Chip **3**(1): 5-10.
Kirkegaard, T., J. Edwards, et al. (2006). "Observer variation in immunohistochemical analysis of protein expression, time for a change?" Histopathology **48**(7): 787-794.
Kleinewietfeld, M., F. Puentes, et al. (2005). "CCR6 expression defines regulatory effector/memory-like cells within the CD25+ CD4+ T-cell subset." Blood **105**(7): 2877-2886.
Klöppel, G. and N. V. Adsay (2009). "Chronic Pancreatitis and the Differential Diagnosis Versus Pancreatic Cancer." Archives of Pathology & Laboratory Medicine **133**(3): 382-387.
Kluwe, J., N. Wongsiriroj, et al. (2011). "Absence of hepatic stellate cell retinoid lipid droplets does not enhance hepatic fibrosis but decreases hepatic carcinogenesis." Gut.
Ko, J. S., A. H. Zea, et al. (2009). "Sunitinib mediates reversal of myeloid-derived suppressor cell accumulation in renal cell carcinoma patients." Clinical Cancer Research **15**(6): 2148-2157.
Kobayashi, N., N. Hiraoka, et al. (2007). "FOXP3+ regulatory T cells affect the development and progression of hepatocarcinogenesis." Clinical Cancer Research **13**(3): 902-911.
Koch, S., A. Larbi, et al. (2008). "Multiparameter flow cytometric analysis of CD4 and CD8 T cell subsets in young and old people." Immunity & Ageing **5**(1): 6.
Kraman, M., P. J. Bambrough, et al. (2010). "Suppression of Antitumor Immunity by Stromal Cells Expressing Fibroblast Activation Protein- " Science **330**(6005): 827-830.
Kryczek, I., L. Zou, et al. (2006). "B7-H4 expression identifies a novel suppressive macrophage population in human ovarian carcinoma." The Journal of Experimental Medicine **203**(4): 871-881.
Kuang, D.-M., Q. Zhao, et al. (2009). "Activated monocytes in peritumoral stroma of hepatocellular carcinoma foster immune privilege and disease progression through PD-L1." The Journal of Experimental Medicine **206**(6): 1327-1337.
Kusmartsev, S., Z. Su, et al. (2008). "Reversal of myeloid cell–mediated immunosuppression in patients with metastatic renal cell carcinoma." Clinical Cancer Research **14**(24): 8270-8278.
Lanier, L. L. (2005). "NK CELL RECOGNITION." Annual Review of Immunology **23**(1): 225-274.
Lechner, M. G., D. J. Liebertz, et al. (2010). "Characterization of cytokine-induced myeloid-derived suppressor cells from normal human peripheral blood mononuclear cells." The Journal of Immunology **185**(4): 2273-2284.
Lee, J. H., S. G. Kang, et al. (2007). "FoxP3+ T Cells Undergo Conventional First Switch to Lymphoid Tissue Homing Receptors in Thymus but Accelerated Second Switch to Nonlymphoid Tissue Homing Receptors in Secondary Lymphoid Tissues." The Journal of Immunology **178**(1): 301-311.

Leek, R. D. and A. L. Harris (2002). "Tumor-Associated Macrophages in Breast Cancer." Journal of Mammary Gland Biology and Neoplasia **7**(2): 177-189.
Leek, R. D., C. E. Lewis, et al. (1996). "Association of Macrophage Infiltration with Angiogenesis and Prognosis in Invasive Breast Carcinoma." Cancer Research **56**(20): 4625-4629.
Levi, E., D. S. Klimstra, et al. (2004). "MUC1 and MUC2 in pancreatic neoplasia." J Clin Pathol **57**(5): 456-462.
Lin, E. Y., V. Gouon-Evans, et al. (2002). "The Macrophage Growth Factor CSF-1 in Mammary Gland Development and Tumor Progression." Journal of Mammary Gland Biology and Neoplasia **7**(2): 147-162.
Lin, E. Y., A. V. Nguyen, et al. (2001). "Colony-Stimulating Factor 1 Promotes Progression of Mammary Tumors to Malignancy." The Journal of Experimental Medicine **193**(6): 727-740.
Lopes-Carvalho, T. and J. F. Kearney (2004). "Development and selection of marginal zone B cells." Immunological Reviews **197**(1): 192-205.
Lu, B. and O. J. Finn (2007). "T-cell death and cancer immune tolerance." Cell Death and Differentiation **15**(1): 70-79.
Lund, J. M., L. Hsing, et al. (2008). "Coordination of Early Protective Immunity to Viral Infection by Regulatory T Cells." Science **320**(5880): 1220-1224.
Mace, T. A., Z. Ameen, et al. (2013). "Pancreatic Cancer-Associated Stellate Cells Promote Differentiation of Myeloid-Derived Suppressor Cells in a STAT3-Dependent Manner." Cancer Research **73**(10): 3007-3018.
Mace, T. A., Z. Ameen, et al. (2013). "Pancreatic Cancer-Associated Stellate Cells Promote Differentiation of Myeloid-Derived Suppressor Cells in a STAT3-Dependent Manner." Cancer Research **73**(10): 3007-3018.
Mackey, M. F., R. Barth, et al. (1998). "The role of CD40/CD154 interactions in the priming, differentiation, and effector function of helper and cytotoxic T cells." Journal of Leukocyte Biology **63**(4): 418-428.
Maden, M. (2007). "Retinoic acid in the development, regeneration and maintenance of the nervous system." Nat Rev Neurosci **8**(10): 755-765.
Maitra, A., N. Fukushima, et al. (2005). "Precursors to Invasive Pancreatic Cancer." Advances in Anatomic Pathology **12**(2): 81-91.
Maitra, A. and R. H. Hruban (2008). "Pancreatic Cancer." Annual Review of Pathology: Mechanisms of Disease **3**(1): 157-188.
Mantovani, A., C. Porta, et al. (2006). "Tumor-associated macrophages (TAMs) as new target in anticancer therapy." Drug Discovery Today: Therapeutic Strategies **3**(3): 361-366.
Mantovani, A., A. Sica, et al. (2004). "The chemokine system in diverse forms of macrophage activation and polarization." Trends in Immunology **25**(12): 677-686.
Markowitz, S. D. and M. M. Bertagnolli (2009). "Molecular Basis of Colorectal Cancer." New England Journal of Medicine **361**(25): 2449-2460.
Marrogi, A. J., A. Munshi, et al. (1997). "Study of tumor infiltrating lymphocytes and transforming growth factor-β as prognostic factors in breast carcinoma." International Journal of Cancer **74**(5): 492-501.
Martin, I., P. Hammond, et al. (1998). "Cystic tumours of the pancreas." British Journal of Surgery **85**(11): 1484-1486.
Mazur, P. K. and J. T. Siveke (2011). "Genetically engineered mouse models of pancreatic cancer: unravelling tumour biology and progressing translational oncology." Gut.

McEver, R. P. (2002). "Selectins: lectins that initiate cell adhesion under flow." Current Opinion in Cell Biology **14**(5): 581-586.
McEver, R. P. and R. D. Cummings (1997). "Perspectives series: cell adhesion in vascular biology. Role of PSGL-1 binding to selectins in leukocyte recruitment." The Journal of Clinical Investigation **100**(3): 485-491.
McHeyzer-Williams, L. J., M. Cool, et al. (2000). "Antigen-Specific B Cell Memory." The Journal of Experimental Medicine **191**(7): 1149-1166.
Meiron, M., Y. Zohar, et al. (2008). "CXCL12 (SDF-1) suppresses ongoing experimental autoimmune encephalomyelitis by selecting antigen-specific regulatory T cells." Journal of Experimental Medicine **205**(11): 2643-2655.
Merika, E., K. Syrigos, et al. (2012). "Desmoplasia in pancreatic cancer. Can we fight it?" Gastroenterology research and practice **2012**.
Metz, B., G. F. A. Kersten, et al. (2004). "Identification of Formaldehyde-induced Modifications in Proteins: REACTIONS WITH MODEL PEPTIDES." Journal of Biological Chemistry **279**(8): 6235-6243.
Michl, P. and T. M. Gress (2013). "Current concepts and novel targets in advanced pancreatic cancer." Gut **62**(2): 317-326.
Microsystems, L. (2011). "Ariol." Retrieved 26 March, 2013, from http://www.leica-microsystems.com/fileadmin/downloads/Ariol/Intended%20Use/Ariol_Intended-Use.pdf.
Miles, D. W., L. C. Happerfield, et al. (1994). "Expression of tumour necrosis factor (TNFα) and its receptors in benign and malignant breast tissue." International Journal of Cancer **56**(6): 777-782.
Miller, M. J. (2003). "Autonomous T cell trafficking examined in vivo with intravital two-photon microscopy." Proceedings of the National Academy of Sciences **100**(5): 2604-2609.
Minges Wols, H. A. (2006). "Plasma Cells."
Minot, D. M., B. R. Kipp, et al. (2009). "Automated Cellular Imaging System III for Assessing HER2 Status in Breast Cancer Specimens: Development of a Standardized Scoring Method That Correlates With FISH." American Journal of Clinical Pathology **132**(1): 133-138.
Moore, K. W., A. O'Garra, et al. (1993). "Interleukin-10." Annual Review of Immunology **11**(1): 165-190.
Mori, M., H. Ohtani, et al. (2000). "Infiltration of CD8+ T cells in non-small cell lung cancer is associated with dedifferentiation of cancer cells, but not with prognosis." The Tohoku journal of experimental medicine **191**(2): 113-118.
Mosmann, T. R. and R. L. Coffman (1989). "TH1 and TH2 Cells: Different Patterns of Lymphokine Secretion Lead to Different Functional Properties." Annual Review of Immunology **7**(1): 145-173.
Mundy-Bosse, B. L., G. S. Young, et al. (2011). "Distinct myeloid suppressor cell subsets correlate with plasma IL-6 and IL-10 and reduced interferon-alpha signaling in CD4+ T cells from patients with GI malignancy." Cancer Immunology, Immunotherapy **60**(9): 1269-1279.
Murphy, K. M. and S. L. Reiner (2002). "Decision making in the immune system: The lineage decisions of helper T cells." Nature Reviews Immunology **2**(12): 933-944.
Nagaraj, S. and D. I. Gabrilovich (2010). "Myeloid-derived suppressor cells in human cancer." The Cancer Journal **16**(4): 348-353.

Nagasawa, T., S. Hirota, et al. (1996). "Defects of B-cell lymphopoiesis and bone-marrow myelopoiesis in mice lacking the CXC chemokine PBSF/SDF-1." Nature **382**(6592): 635-638.
Naito, Y., K. Saito, et al. (1998). "CD8+ T Cells Infiltrated within Cancer Cell Nests as a Prognostic Factor in Human Colorectal Cancer." Cancer Research **58**(16): 3491-3494.
Neesse, A., P. Michl, et al. (2010). "Stromal biology and therapy in pancreatic cancer." Gut **60**(6): 861-868.
Neesse, A., P. Michl, et al. (2011). "Stromal biology and therapy in pancreatic cancer." Gut **60**(6): 861-868.
Neesse, A., P. Michl, et al. (2011). "Stromal biology and therapy in pancreatic cancer." Gut **60**(6): 861-868.
Nexcelom. (2013). "Counting Cells for Immunology Using CellometerTM Auto T4 Cell Counter." Retrieved 26 March, 2013, from http://www.nexcelom.com/Literature/App%20Note%2006005%20Immunology.pdf.
Nielsen, P. S., J. Lindebjerg, et al. (2010). "Virtual microscopy: an evaluation of its validity and diagnostic performance in routine histologic diagnosis of skin tumors." Human Pathology **41**(12): 1770-1776.
Nishikawa, H. and S. Sakaguchi (2010). "Regulatory T cells in tumor immunity." International Journal of Cancer **127**(4): 759-767.
Nummer, D., E. Suri-Payer, et al. (2007). "Role of Tumor Endothelium in CD4+CD25+ Regulatory T Cell Infiltration of Human Pancreatic Carcinoma." JNCI Journal of the National Cancer Institute **99**(15): 1188-1199.
O'Connor, B. P., M. Cascalho, et al. (2002). "Short-lived and Long-lived Bone Marrow Plasma Cells Are Derived from a Novel Precursor Population." The Journal of Experimental Medicine **195**(6): 737-745.
Öberg, Å., S. Samii, et al. (2002). "Different occurrence of CD8+, CD45R0+, and CD68+ immune cells in regional lymph node metastases from colorectal cancer as potential prognostic predictors." International journal of colorectal disease **17**(1): 25-29.
Olive, K. P., M. A. Jacobetz, et al. (2009). "Inhibition of Hedgehog Signaling Enhances Delivery of Chemotherapy in a Mouse Model of Pancreatic Cancer." Science **324**(5933): 1457-1461.
Olive, K. P., M. A. Jacobetz, et al. (2009). "Inhibition of Hedgehog Signaling Enhances Delivery of Chemotherapy in a Mouse Model of Pancreatic Cancer." Science **324**(5933): 1457-1461.
Ong, C. W., L. G. Kim, et al. (2010). "Computer-assisted pathological immunohistochemistry scoring is more time-effective than conventional scoring, but provides no analytical advantage." Histopathology **56**(4): 523-529.
Ono, S. J., T. Nakamura, et al. (2003). "Chemokines: Roles in leukocyte development, trafficking, and effector function." The Journal of allergy and clinical immunology **111**(6): 1185-1199.
Onodera, T., M. H. Jang, et al. (2009). "Constitutive Expression of IDO by Dendritic Cells of Mesenteric Lymph Nodes: Functional Involvement of the CTLA-4/B7 and CCL22/CCR4 Interactions." The Journal of Immunology **183**(9): 5608-5614.
Oo, Y. H. and D. H. Adams (2010). "The role of chemokines in the recruitment of lymphocytes to the liver." Journal of autoimmunity **34**(1): 45-54.

Orimo, A., P. B. Gupta, et al. (2005). "Stromal Fibroblasts Present in Invasive Human Breast Carcinomas Promote Tumor Growth and Angiogenesis through Elevated SDF-1/CXCL12 Secretion." Cell **121**(3): 335-348.
Ottenhof, N. A., R. F. de Wilde, et al. (2011). "Molecular Characteristics of Pancreatic Ductal Adenocarcinoma." Pathology Research International **2011**: 1-16.
Pamer, E. and P. Cresswell (1998). "MECHANISMS OF MHC CLASS I–RESTRICTED ANTIGEN PROCESSING." Annual Review of Immunology **16**(1): 323-358.
Pancione, M., N. Forte, et al. (2009). "Reduced< i> β</i>-catenin and peroxisome proliferator–activated receptor–< i> γ</i> expression levels are associated with colorectal cancer metastatic progression: correlation with tumor-associated macrophages, cyclooxygenase 2, and patient outcome." Human Pathology **40**(5): 714-725.
Pankov, R. and K. M. Yamada (2002). "Fibronectin at a glance." Journal of Cell Science **115**(20): 3861-3863.
Parsons, M. and H. Grabsch (2009). "How to make tissue microarrays." Diagnostic histopathology **15**(3): 142-150.
Picca, C. C., J. Larkin, et al. (2006). "Role of TCR specificity in CD4+CD25+ regulatory T-cell selection." Immunological Reviews **212**(1): 74-85.
Pittet, M. J., D. E. Speiser, et al. (2000). "Cutting Edge: Cytolytic Effector Function in Human Circulating CD8+ T Cells Closely Correlates with CD56 Surface Expression." The Journal of Immunology **164**(3): 1148-1152.
Pollard, J. W. (2004). "Tumour-educated macrophages promote tumour progression and metastasis." Nat Rev Cancer **4**(1): 71-78.
Prasad, K. and G. K. Prabhu (2011). "Image Analysis Tools for Evaluation of Microscopic Views of Immunohistochemically Stained Specimen in Medical Research–a Review." Journal of Medical Systems.
Pylayeva-Gupta, Y., Kyoung E. Lee, et al. (2012). "Oncogenic Kras-Induced GM-CSF Production Promotes the Development of Pancreatic Neoplasia." Cancer Cell **21**(6): 836-847.
Qian, B.-Z. and J. W. Pollard (2010). "Macrophage Diversity Enhances Tumor Progression and Metastasis." Cell **141**(1): 39-51.
R-Project. (2013). Retrieved 26 March, 2013, from www.r-project.org.
Rahman, M. (2006). "Introduction to flow cytometry." Retrieved 26 March, 2013, from http://static.abdserotec.com/uploads/Flow-Cytometry.pdf.
Ramsay, A. G., A. J. Johnson, et al. (2008). "Chronic lymphocytic leukemia T cells show impaired immunological synapse formation that can be reversed with an immunomodulating drug." Journal of Clinical Investigation.
Reeves, M. E. and R. P. DeMatteo (2000). "Genes and viruses in hepatobiliary neoplasia." Seminars in Surgical Oncology **19**(2): 84-93.
Ricci, F., S. E. Kern, et al. (2005). "Stromal responses to carcinomas of the pancreas: juxtatumoral gene expression conforms to the infiltrating pattern and not the biologic subtype." Cancer Biol Ther **4**(3): 302-307.
Ricci, F., S. E. Kern, et al. (2005). "Stromal responses to carcinomas of the pancreas: Juxtatumoral gene expression conforms to the infiltrating pattern and not the biologic subtype." Cancer Biology & Therapy **4**(3): 302-307.
Riches, J. C., J. K. Davies, et al. (2012). "T cells from CLL patients exhibit features of T-cell exhaustion but retain capacity for cytokine production." Blood **121**(9): 1612-1621.

Rodríguez, P. C. and A. C. Ochoa (2008). "Arginine regulation by myeloid derived suppressor cells and tolerance in cancer: mechanisms and therapeutic perspectives." Immunological Reviews **222**(1): 180-191.
Rojo, M. G. a., G. Bueno, et al. (2010). Review of imaging solutions for integrated quantitative immunohistochemistry in the Pathology daily practice.
Roozendaal, R. and R. E. Mebius (2011). "Stromal Cell–Immune Cell Interactions." Annual Review of Immunology **29**(1): 23-43.
Ropponen, K. M., M. J. Eskelinen, et al. (1997). "Prognostic value of tumour-infiltrating lymphocytes (TILs) in colorectal cancer." The Journal of Pathology **182**(3): 318-324.
Roy, M., T. Waldschmidt, et al. (1993). "The regulation of the expression of gp39, the CD40 ligand, on normal and cloned CD4+ T cells." The Journal of Immunology **151**(5): 2497-2510.
Rubtsov, Y. P., J. P. Rasmussen, et al. (2008). "Regulatory T Cell-Derived Interleukin-10 Limits Inflammation at Environmental Interfaces." Immunity **28**(4): 546-558.
Ryu, B., J. Jones, et al. (2001). "Invasion-specific Genes in Malignancy: Serial Analysis of Gene Expression Comparisons of Primary and Passaged Cancers." Cancer Res **61**(5): 1833-1838.
Sad, S., L. Krishnan, et al. (1997). "Cytotoxicity and weak CD40 ligand expression of CD8+ type 2 cytotoxic T cells restricts their potential B cell helper activity." European Journal of Immunology **27**(4): 914-922.
Sahani, D. V., R. Kadavigere, et al. (2005). "Cystic Pancreatic Lesions: A Simple Imaging-based Classification System for Guiding Management1." Radiographics **25**(6): 1471-1484.
Sakaguchi, S. (2005). "Naturally arising Foxp3-expressing CD25+CD4+ regulatory T cells in immunological tolerance to self and non-self." Nature Immunology **6**(4): 345-352.
Sakaguchi, S., T. Yamaguchi, et al. (2008). "Regulatory T Cells and Immune Tolerance." Cell **133**(5): 775-787.
Sallusto, F., D. Lenig, et al. (1999). "Two subsets of memory T lymphocytes with distinct homing potentials and effector functions." Nature **401**(6754): 708-712.
Sanford, D. E., B. A. Belt, et al. (2013). "Inflammatory Monocyte Mobilization Decreases Patient Survival in Pancreatic Cancer: A Role for Targeting the CCL2/CCR2 Axis." Clinical Cancer Research **19**(13): 3404-3415.
Sather, B. D., P. Treuting, et al. (2007). "Altering the distribution of Foxp3+ regulatory T cells results in tissue-specific inflammatory disease." Journal of Experimental Medicine **204**(6): 1335-1347.
Sato, E., S. H. Olson, et al. (2005). "Intraepithelial CD8+ tumor-infiltrating lymphocytes and a high CD8+/regulatory T cell ratio are associated with favorable prognosis in ovarian cancer." Proceedings of the National Academy of Sciences of the United States of America **102**(51): 18538-18543.
Scaria, A., J. St George, et al. (1997). "Antibody to CD40 ligand inhibits both humoral and cellular immune responses to adenoviral vectors and facilitates repeated administration to mouse airway." Gene therapy **4**(6): 611-617.
Schwabe, R. F., B. Schnabl, et al. (2001). "CD40 activates NF-κB and c-Jun N-terminal kinase and enhances chemokine secretion on activated human hepatic stellate cells." The Journal of Immunology **166**(11): 6812-6819.
Sergio, R. (1994). "Regulation of the development of type 2 T-helper cells in allergy." Current Opinion in Immunology **6**(6): 838-846.

Shapiro-Shelef, M. and K. Calame (2005). "Regulation of plasma-cell development." Nat Rev Immunol **5**(3): 230-242.
Sharma, S. and K. B. Green (2004). "The Pancreatic Duct and Its Arteriovenous Relationship: An Underutilized Aid in the Diagnosis and Distinction of Pancreatic Adenocarcinoma From Pancreatic Intraepithelial Neoplasia. A Study of 126 Pancreatectomy Specimens." The American journal of surgical pathology **28**(5): 613-620.
Sher, A. and R. L. Coffman (1992). "Regulation of Immunity to Parasites by T Cells and T Cell-Derived Cytokines." Annual Review of Immunology **10**(1): 385-409.
Shi, S.-R., Y. Shi, et al. (2011). "Antigen Retrieval Immunohistochemistry: Review and Future Prospects in Research and Diagnosis over Two Decades." Journal of Histochemistry & Cytochemistry **59**(1): 13-32.
Shinkai, Y., G. Rathbun, et al. (1992). "RAG-2-deficient mice lack mature lymphocytes owing to inability to initiate V(D)J rearrangement." Cell **68**(5): 855-867.
Shrikhande, S., M. Martignoni, et al. (2003). "Comparison of histological features and inflammatory cell reaction in alcoholic, idiopathic and tropical chronic pancreatitis." British Journal of Surgery **90**(12): 1565-1572.
Sica, A. and A. Mantovani (2012). "Macrophage plasticity and polarization: in vivo veritas." The Journal of Clinical Investigation **122**(3): 787-795.
Singh, A. P., S. Arora, et al. (2012). "CXCL12/CXCR4 signaling axis induces SHH expression in pancreatic cancer cells via ERK- and Akt- mediated activation of NF-κB: implications for bidirectional tumor-stromal interactions." Journal of Biological Chemistry.
Sivori, S., M. Falco, et al. (2004). "CpG and double-stranded RNA trigger human NK cells by Toll-like receptors: Induction of cytokine release and cytotoxicity against tumors and dendritic cells." Proceedings of the National Academy of Sciences of the United States of America **101**(27): 10116-10121.
Skipworth, J. R. A., S. W. M. Olde Damink, et al. (2011). "Review article: surgical, neo-adjuvant and adjuvant management strategies in biliary tract cancer." Alimentary Pharmacology & Therapeutics **34**(9): 1063-1078.
Słodkowska, J., T. Markiewicz, et al. (2011). "Accuracy of a remote quantitative image analysis in the whole slide images." Diagnostic Pathology **6**(Suppl 1): S20.
Smith, A. (2003). "LFA-1-induced T cell migration on ICAM-1 involves regulation of MLCK-mediated attachment and ROCK-dependent detachment." Journal of Cell Science **116**(15): 3123-3133.
Spinella, M. J., J. S. Kerley, et al. (2003). "Retinoid target gene activation during induced tumor cell differentiation: human embryonal carcinoma as a model." The Journal of nutrition **133**(1): 273S-276S.
Srivastava, M. K., P. Sinha, et al. (2010). "Myeloid-derived suppressor cells inhibit T-cell activation by depleting cystine and cysteine." Cancer Research **70**(1): 68-77.
Stathis, A. and M. J. Moore (2010). "Advanced pancreatic carcinoma: current treatment and future challenges." Nature Reviews Clinical Oncology **7**(3): 163-172.
Suffia*, I., S. K. Reckling*, et al. (2005). "A Role for CD103 in the Retention of CD4+CD25+ Treg and Control of Leishmania major Infection." The Journal of Immunology **174**(9): 5444-5455.

Talmadge, J. E. (2007). "Pathways mediating the expansion and immunosuppressive activity of myeloid-derived suppressor cells and their relevance to cancer therapy." Clinical Cancer Research **13**(18): 5243-5248.
Tanaka, M., S. Chari, et al. (2006). "International Consensus Guidelines for Management of Intraductal Papillary Mucinous Neoplasms and Mucinous Cystic Neoplasms of the Pancreas." Pancreatology **6**(1–2): 17-32.
Tangye, S. G., Y.-J. Liu, et al. (1998). "Identification of Functional Human Splenic Memory B Cells by Expression of CD148 and CD27." The Journal of Experimental Medicine **188**(9): 1691-1703.
Tarazona, R., O. DelaRosa, et al. (2001). "Increased expression of NK cell markers on T lymphocytes in aging and chronic activation of the immune system reflects the accumulation of effector/senescent T cells." Mechanisms of Ageing and Development **121**(1–3): 77-88.
Tarazona, R., O. DelaRosa, et al. (2002). "NK-associated receptors on CD8 T cells from treatment-naive HIV-infected individuals: defective expression of CD56." Aids **16**(2): 197-200.
Tarlinton, D. (2006). "B-cell memory: are subsets necessary?" Nat Rev Immunol **6**(10): 785-790.
Ticchioni, M., C. Charvet, et al. (2002). "Signaling through ZAP-70 is required for CXCL12-mediated T-cell transendothelial migration." Blood **99**(9): 3111-3118.
Tjomsland, V., L. Niklasson, et al. (2011). "The desmoplastic stroma plays an essential role in the accumulation and modulation of infiltrated immune cells in pancreatic adenocarcinoma." Clinical and Developmental Immunology **2011**.
Tosolini, M., A. Kirilovsky, et al. (2011). "Clinical Impact of Different Classes of Infiltrating T Cytotoxic and Helper Cells (Th1, Th2, Treg, Th17) in Patients with Colorectal Cancer." Cancer Research **71**(4): 1263-1271.
Tosolini, M., A. Kirilovsky, et al. (2011). "Clinical Impact of Different Classes of Infiltrating T Cytotoxic and Helper Cells (Th1, Th2, Treg, Th17) in Patients with Colorectal Cancer." Cancer Research **71**(4): 1263-1271.
Trinchieri, G. (1989). Biology of Natural Killer Cells. Advances in Immunology. J. D. Frank, Academic Press. **Volume 47:** 187-376.
Turashvili, G., S. Leung, et al. (2009). "Inter-observer reproducibility of HER2 immunohistochemical assessment and concordance with fluorescent in situ hybridization (FISH): pathologist assessment compared to quantitative image analysis." BMC Cancer **9**(1): 165.
Ueno, H., A. M. Jones, et al. (2004). "Histological categorisation of fibrotic cancer stroma in advanced rectal cancer." Gut **53**(4): 581-586.
Valenick, L. V., H. C. Hsia, et al. (2005). "Fibronectin fragmentation promotes α4β1 integrin-mediated contraction of a fibrin–fibronectin provisional matrix." Experimental Cell Research **309**(1): 48-55.
Van den Eynde, B. J. and P. van der Bruggen (1997). "T cell defined tumor antigens." Current Opinion in Immunology **9**(5): 684-693.
van Kooten, C. and J. Banchereau (2000). "CD40-CD40 ligand." Journal of Leukocyte Biology **67**(1): 2-17.
Varga, V. S. n., L. Ficsor, et al. (2009). "Automated multichannel fluorescent whole slide imaging and its application for cytometry." Cytometry Part A **75A**(12): 1020-1030.
Vectorlabs. (2011). Retrieved 26 March, 2013, from (http://www.vectorlabs.com/data/protocols/PK-6100.pdf). .

Vergara, M. N., Y. Arsenijevic, et al. (2005). "CNS regeneration: a morphogen's tale." Journal of Neurobiology **64**(4): 491-507.
Vicente-Manzanares, M. and F. Sánchez-Madrid (2004). "Role of the cytoskeleton during leukocyte responses." Nature Reviews Immunology **4**(2): 110-122.
Viglietta, V. (2004). "Loss of Functional Suppression by CD4+CD25+ Regulatory T Cells in Patients with Multiple Sclerosis." Journal of Experimental Medicine **199**(7): 971-979.
Vivier, E., E. Tomasello, et al. (2008). "Functions of natural killer cells." Nature Immunology **9**(5): 503-510.
von Andrian, U. H. and C. R. Mackay (2000). "T-Cell Function and Migration — Two Sides of the Same Coin." New England Journal of Medicine **343**(14): 1020-1034.
von Andrian, U. H. and T. R. Mempel (2003). "Homing and cellular traffic in lymph nodes." Nature Reviews Immunology **3**(11): 867-878.
Von Hoff, D. D. (2013). 2013, from http://gicasym.asco.org/nab-paclitaxel-plus-gemcitabine-new-standard-care-first-line-metastatic-pancreatic-cancer.
Von Hoff, D. D., R. K. Ramanathan, et al. (2011). "Gemcitabine Plus nab-Paclitaxel Is an Active Regimen in Patients With Advanced Pancreatic Cancer: A Phase I/II Trial." Journal of Clinical Oncology **29**(34): 4548-4554.
Vonlaufen, A., S. Joshi, et al. (2008). "Pancreatic Stellate Cells: Partners in Crime with Pancreatic Cancer Cells." Cancer Res **68**(7): 2085-2093.
Wakabayashi, O., K. Yamazaki, et al. (2003). "CD4+ T cells in cancer stroma, not CD8+ T cells in cancer cell nests, are associated with favorable prognosis in human non-small cell lung cancers." Cancer science **94**(11): 1003-1009.
Walker, R. A. (2001). "The complexities of breast cancer desmoplasia." Breast Cancer Research **3**(3): 143-145.
Wing, K., Y. Onishi, et al. (2008). "CTLA-4 Control over Foxp3+ Regulatory T Cell Function." Science **322**(5899): 271-275.
Wolbach, S. B. and P. R. Howe (1925). "Tissue changes following deprivation of fat-soluble A vitamin." The Journal of Experimental Medicine **42**(6): 753-777.
Wong, P. and E. G. Pamer (2003). "Cd8 Tcellresponses Toinfectiouspathogens." Annual Review of Immunology **21**(1): 29-70.
Xu, L., W. Xu, et al. (2010). "Enrichment of CCR6Foxp3 regulatory T cells in the tumor mass correlates with impaired CD8 T cell function and poor prognosis of breast cancer." Clin. Immunol **135**: 466-475.
Yang, Y. and J. M. Wilson (1996). "CD40 ligand-dependent T cell activation: requirement of B7-CD28 signaling through CD40." Science **273**(5283): 1862-1864.
Ye, Y., L. Zhou, et al. (2009). "Interaction of B7-H1 on intrahepatic cholangiocarcinoma cells with PD-1 on tumor-infiltrating T cells as a mechanism of immune evasion." Journal of surgical oncology **100**(6): 500-504.
Yokoyama, W. M. and B. F. M. Plougastel (2003). "Immune functions encoded by the natural killer gene complex." Nat Rev Immunol **3**(4): 304-316.
Zabaglo, L., J. Salter, et al. (2010). "Comparative validation of the SP6 antibody to Ki67 in breast cancer." Journal of Clinical Pathology **63**(9): 800-804.
Zhang, L., J. R. Conejo-Garcia, et al. (2003). "Intratumoral T Cells, Recurrence, and Survival in Epithelial Ovarian Cancer." New England Journal of Medicine **348**(3): 203-213.

Zhang, N. and Michael J. Bevan (2011). "CD8+ T Cells: Foot Soldiers of the Immune System." Immunity **35**(2): 161-168.
Zhang, Y., D. L. Wallace, et al. (2007). "In vivo kinetics of human natural killer cells: the effects of ageing and acute and chronic viral infection." Immunology **121**(2): 258-265.
Zheng, L., J. Xue, et al. (2013). "Role of Immune Cells and Immune-Based Therapies in Pancreatitis and Pancreatic Ductal Adenocarcinoma." Gastroenterology **144**(6): 1230-1240.
Zhu, J. and W. E. Paul (2008). "CD4 T cells: fates, functions, and faults." Blood **112**(5): 1557-1569.

8.0 Appendix

Appendix 1: Patient diagnosis and TMA construction

Pathology number	DIAGNOSIS	Tumour	Stroma	Normal	AA TMA NUMBER
A1	biopsy	y	y		3
A1	biopsy	y		y-LN	3
A1	biopsy	Y	Y		3
B1	biopsy	Y	Y		3
a1	biopsy	Y	Y	Y-NAD	3
A1	biopsy	Y	Y	Y-NAD	3
d1	biopsy	Y	Y		3
b1	biopsy	Y	Y		3
A1	biopsy	Y	Y		3
b1	biopsy	Y	Y	Y-NAD	3
A1	biopsy	Y	Y	Y-NAD	3
b1	biopsy	Y	Y		3
b1	biopsy	Y	Y		3
a1	biopsy	Y	Y		2
c1	biopsy	Y	Y	Y-NAD	3
a1	biopsy	Y	Y		3
b1	biopsy	Y	Y		3
b5, b10	PDAC	Y	Y	Y-NAD	2
D7	PDAC	Y	Y		2
d6	PDAC	Y	Y	Y-NAD	2
b6	PDAC	Y	Y	Y-NAD	2
c8	PDAC	Y	Y	Y-NAD	2
d2	PDAC	Y	Y		2
c8	PDAC	Y	Y	Y-NAD	2
e9	PDAC	Y	Y	Y-NAD	2
b7	PDAC	missing slide			?2
	Mucinous cystic neoplasm	Y	Y		1,2,3
	Mucinous cystic neoplasm	Y	Y		1,2,3
	ampullary carcinoma	Y	Y	Y-NAD	1,2,3
a6, a9	Neuroendocrine tumour	Y			1,2,3
c28	Neuroendocrine tumour	Y		Y-NAD	1,2,3
b2	Neuroendocrine tumour	Y			1,2,3
b16	Cholangiocarcinoma	Y	Y	Y-NAD	2
b6	Cholangiocarcinoma	Y	Y	Y-NAD	2
a6	Cholangiocarcinoma	Y	Y	Y-NAD	2
a7	Cholangiocarcinoma	Y	Y	Y-NAD	2
c14	Cholangiocarcinoma	Y	Y		2
a5	Cholangiocarcinoma	Y	Y		2
c9	Cholangiocarcinoma	Y	Y	Y-NAD	2

a15, a2	Gistoblastoma	Y		Y-NORMAL	1, 2N, 3N	
c	Gistoblastoma	Y				1
a1	Unknown					
1a	Unknown					
	Unknown					
1A	biopsy	Y	Y			3
2A	biopsy	Y	Y			3
L	PDAC	Y	Y	Y-NAD		2
1A	biopsy	Y				3
1A	biopsy	Y				3
1B	biopsy	Y				3
A2	Mucinous cystic neoplasm	Y		Y-NAD	1,2,3	
B7	PDAC	Y	Y			3
A9	Normal			Y-NORMAL	2,3	
B8	PDAC	Y	Y	Y-NAD		2
B1	biopsy	Y	Y			3
C10	PDAC	Y	Y	Y-NAD		2
a4	Insulinoma	Y		Y: NORMAL	2N, 3N, 1, 2, 3	
a2	Insulinoma	Y				1
a3	Insulinoma	Y		Y: NORMAL	2N, 3N, 1, 2, 3	
a2	insulinoma	Y	Y			1
a4	insulinoma	Y		Y: NORMAL	2N, 3N, 1, 2, 3	
a5	NE Ca(insulinoma)	Y		Y, NAD		1
a3	Insulinoma	Y		Y: NORMAL	2N, 3N, 1, 2, 3	
a4	ampullary carcinoma duodenal carcinoma	Y	Y		1,2,3	
d8		Y	Y		1,2,3	
a7	ampullary carcinoma	Y	Y		1,2,3	
b4	Cholangiocarcinoma	Y	Y	Y, NAD, LN	2LN, 3LN	
a6	chronic pancreatitis secondary to pancreas divisum	Y, NO TUMOUR CP ONLY		Y,NAD	2, 3	
a8	Cholangiocarcinoma duodenal carcinoma	Y	Y	Y, NAD	1,2,3	
a7	duodenal carcinoma	Y	Y		1,2,3	
a4	duodenal carcinoma	Y	Y		1,2,3	
b15		Y	Y	Y,NAD	1,2,3	
c6	ampullary carcinoma ampullary carcinoma	Y		Y, NAD	1,2,3	
a9	duodenal carcinoma	Y	Y	Y, NAD	1,2,3	
c6		Y	Y		1,2,3	
a8	Chronic pancreatitis	Y, NO TUMOUR CP ONLY		Y, NAD	2, 3	

b9	Cholangiocarcinoma	Y	Y	Y, NAD	1,2,3	
a2	insulinoma	Y				1
a5	insulinoma	Y		Y-NAD, PANIN		1
b10	Chronic Pancreatitis	Y, NO TUMOUR CP ONLY		Y-NAD	2, 3	
e17	duodenal carcinoma	Y	Y	Y-NAD	1,2,3	
a8	ampullary carcinoma	Y	Y	Y-NAD	1,2,3	
a6	Chronic pancreatitis and pseudocyst	Y, NO TUMOUR CP ONLY		Y-NAD	2, 3	
b11	Cholangiocarcinoma	Y	Y	Y-NAD	1,2,3	
b2	Ampullary adenoma	Y			1,2,3,	

Key

LN=LYMPH NODE
NAD=NORMAL ADJACENT TO DISEASE
N=NORMAL

Appendix 2: Other Pancreas slide 1 TMA design

Tissue type	Diagnosis	Array position
Spleen	Normal	A1
Tumour	Insulinoma	A2
Tumour	Insulinoma	A3
Tumour	Insulinoma	A4
Tumour	Insulinoma	A5
Tumour	Insulinoma	A6
Tumour	Insulinoma	A7
Stroma	Insulinoma	A8
Stroma	Insulinoma	A9
Stroma	Insulinoma	A10
Tumour	Insulinoma	A11
Tumour	Insulinoma	A12
Tumour	Insulinoma	A13
Normal	Insulinoma	A14
Normal	Insulinoma	A15
Normal	Insulinoma	B1
Tumour	Ampullary carcinoma	B2
Tumour	Ampullary carcinoma	B3
Tumour	Ampullary carcinoma	B4
Stroma	Ampullary carcinoma	B5
Stroma	Ampullary carcinoma	B6
Stroma	Ampullary carcinoma	B7
Tumour	duodenal carcinoma	B8
Tumour	duodenal carcinoma	B9
Tumour	duodenal carcinoma	B10
Stroma	duodenal carcinoma	B11
Stroma	duodenal carcinoma	B12
Stroma	duodenal carcinoma	B13
Tumour	Ampullary carcinoma	B14
Tumour	Ampullary carcinoma	B15
Tumour	Ampullary carcinoma	C1
Stroma	Ampullary carcinoma	C2
Stroma	Ampullary carcinoma	C3

Stroma	Ampullary carcinoma	C4
Tumour	Cholangiocarcinoma	C5
Tumour	Cholangiocarcinoma	C6
Tumour	Cholangiocarcinoma	C7
Stroma	Cholangiocarcinoma	C8
Stroma	Cholangiocarcinoma	C9
Stroma	Cholangiocarcinoma	C10
Normal	Cholangiocarcinoma	C11
Normal	Cholangiocarcinoma	C12
Normal	Cholangiocarcinoma	C13
Tumour	duodenal carcinoma	C14
Tumour	duodenal carcinoma	C15
Tumour	duodenal carcinoma	D1
Stroma	duodenal carcinoma	D2
Stroma	duodenal carcinoma	D3
Stroma	duodenal carcinoma	D4
Tumour	duodenal carcinoma	D5
Tumour	duodenal carcinoma	D6
Tumour	duodenal carcinoma	D7
Stroma	duodenal carcinoma	D8
Stroma	duodenal carcinoma	D9
Stroma	duodenal carcinoma	D10
Tumour	duodenal carcinoma	D11
Tumour	duodenal carcinoma	D12
Tumour	duodenal carcinoma	D13
Stroma	duodenal carcinoma	D14
Stroma	duodenal carcinoma	D15
Stroma	duodenal carcinoma	E1
Normal	duodenal carcinoma	E2
Normal	duodenal carcinoma	E3
Normal	duodenal carcinoma	E4
Tumour	Ampullary carcinoma	E5
Tumour	Ampullary carcinoma	E6
Tumour	Ampullary carcinoma	E7
Normal	Ampullary carcinoma	E8
Normal	Ampullary carcinoma	E9
Normal	Ampullary carcinoma	E10
Tumour	Ampullary carcinoma	E11
Tumour	Ampullary	E12

	carcinoma	
Tumour	Ampullary carcinoma	E13
Stroma	Ampullary carcinoma	E14
Stroma	Ampullary carcinoma	E15
Stroma	Ampullary carcinoma	F1
Normal	Ampullary carcinoma	F2
Normal	Ampullary carcinoma	F3
Normal	Ampullary carcinoma	F4
Tumour	duodenal carcinoma	F5
Tumour	duodenal carcinoma	F6
Tumour	duodenal carcinoma	F7
Stroma	duodenal carcinoma	F8
Stroma	duodenal carcinoma	F9
Stroma	duodenal carcinoma	F10
Tumour	Cholangiocarcinoma	F11
Tumour	Cholangiocarcinoma	F12
Tumour	Cholangiocarcinoma	F13
Stroma	Cholangiocarcinoma	F14
Stroma	Cholangiocarcinoma	F15
Stroma	Cholangiocarcinoma	G1
Normal	Cholangiocarcinoma	G2
Normal	Cholangiocarcinoma	G3
Normal	Cholangiocarcinoma	G4
Tumour	Insulinoma	G5
Tumour	Insulinoma	G6
Tumour	Insulinoma	G7
Tumour	Insulinoma	G8
Tumour	Insulinoma	G9
Tumour	Insulinoma	G10
Normal	Insulinoma	G11
Normal	Insulinoma	G12
Normal	Insulinoma	G13
Tumour	duodenal carcinoma	G14
Tumour	duodenal carcinoma	G15
Tumour	duodenal carcinoma	H1
Stroma	duodenal carcinoma	H2
Stroma	duodenal carcinoma	H3
Stroma	duodenal carcinoma	H4
Normal	duodenal carcinoma	H5
Normal	duodenal carcinoma	H6

Normal	duodenal carcinoma	H7
Tumour	Ampullary carcinoma	H8
Tumour	Ampullary carcinoma	H9
Tumour	Ampullary carcinoma	H10
Stroma	Ampullary carcinoma	H11
Stroma	Ampullary carcinoma	H12
Stroma	Ampullary carcinoma	H13
Normal	Ampullary carcinoma	H14
Normal	Ampullary carcinoma	H15
Normal	Ampullary carcinoma	I1

Appendix 3: Other pancreas slide 2 TMA design

Tissue type	Diagnosis	Array position
Spleen	Normal	A1
Tumour	Cholangiocarcinoma	A2
Tumour	Cholangiocarcinoma	A3
Tumour	Cholangiocarcinoma	A4
Stroma	Cholangiocarcinoma	A5
Stroma	Cholangiocarcinoma	A6
Stroma	Cholangiocarcinoma	A7
Normal	Cholangiocarcinoma	A8
Normal	Cholangiocarcinoma	A9
Normal	Cholangiocarcinoma	A10
Tumour	Ampullary adenoma	A11
Tumour	Ampullary adenoma	A12
Tumour	Ampullary adenoma	A13
Tumour	Mucinous cystic neoplasm	A14
Tumour	Mucinous cystic neoplasm	A15
Tumour	Mucinous cystic neoplasm	B1
Stroma	Mucinous cystic neoplasm	B2
Stroma	Mucinous cystic neoplasm	B3
Stroma	Mucinous cystic neoplasm	B4
Tumour	Mucinous cystic neoplasm	B5
Tumour	Mucinous cystic neoplasm	B6
Tumour	Mucinous cystic neoplasm	B7
Stroma	Mucinous cystic neoplasm	B8
Stroma	Mucinous cystic neoplasm	B9
Stroma	Mucinous cystic neoplasm	B10
Tumour	Ampullary carcinoma	B11
Tumour	Ampullary carcinoma	B12
Tumour	Ampullary carcinoma	B13
Stroma	Ampullary carcinoma	B14

Stroma	Ampullary carcinoma	B15
Stroma	Ampullary carcinoma	C1
Normal	Ampullary carcinoma	C2
Normal	Ampullary carcinoma	C3
Normal	Ampullary carcinoma	C4
Tumour	Neuroendocrine tumour	C5
Tumour	Neuroendocrine tumour	C6
Tumour	Neuroendocrine tumour	C7
Tumour	Neuroendocrine tumour	C8
Tumour	Neuroendocrine tumour	C9
Tumour	Neuroendocrine tumour	C10
Normal	Neuroendocrine tumour	C11
Normal	Neuroendocrine tumour	C12
Normal	Neuroendocrine tumour	C13
Tumour	Neuroendocrine tumour	C14
Tumour	Neuroendocrine tumour	C15
Tumour	Neuroendocrine tumour	D1
Tumour	Gistoblastoma	D2
Tumour	Gistoblastoma	D3
Tumour	Gistoblastoma	D4
Normal	Gistoblastoma	D5
Normal	Gistoblastoma	D6
Normal	Gistoblastoma	D7
Tumour	Gistoblastoma	D8
Tumour	Gistoblastoma	D9
Tumour	Gistoblastoma	D10
Tumour	Mucinous cystic neoplasm	D11
Tumour	Mucinous cystic neoplasm	D12
Tumour	Mucinous cystic neoplasm	D13

Stroma	Mucinous cystic neoplasm	D14
Stroma	Mucinous cystic neoplasm	D15
Stroma	Mucinous cystic neoplasm	E1

Appendix 4: Pancreas 2 TMA slide 1 design

Tissue type	Diagnosis	Array position
Spleen	Normal	A1
Tumour	Biopsy	A2
Tumour	Biopsy	A3
Tumour	Biopsy	A4
Stroma	Biopsy	A5
Stroma	Biopsy	A6
Stroma	Biopsy	A7
Tumour	PDAC	A8
Tumour	PDAC	A9
Tumour	PDAC	A10
Stroma	PDAC	A11
Stroma	PDAC	A12
Stroma	PDAC	A13
Normal	PDAC	A14
Normal	PDAC	A15
Normal	PDAC	B1
Tumour	PDAC	B2
Tumour	PDAC	B3
Tumour	PDAC	B4
Stroma	PDAC	B5
Stroma	PDAC	B6
Stroma	PDAC	B7
Tumour	PDAC	B8
Tumour	PDAC	B9
Tumour	PDAC	B10
Stroma	PDAC	B11
Stroma	PDAC	B12
Stroma	PDAC	B13
Normal	PDAC	B14
Normal	PDAC	B15
Normal	PDAC	C1
Tumour	PDAC	C2
Tumour	PDAC	C3
Tumour	PDAC	C4
Stroma	PDAC	C5
Stroma	PDAC	C6
Stroma	PDAC	C7
Normal	PDAC	C8
Normal	PDAC	C9
Normal	PDAC	C10
Tumour	PDAC	C11
Tumour	PDAC	C12

Tumour	PDAC	C13
Stroma	PDAC	C14
Stroma	PDAC	C15
Stroma	PDAC	D1
Normal	PDAC	D2
Normal	PDAC	D3
Normal	PDAC	D4
Tumour	PDAC	D5
Tumour	PDAC	D6
Tumour	PDAC	D7
Stroma	PDAC	D8
Stroma	PDAC	D9
Stroma	PDAC	D10
Tumour	PDAC	D11
Tumour	PDAC	D12
Tumour	PDAC	D13
Stroma	PDAC	D14
Stroma	PDAC	D15
Stroma	PDAC	E1
Normal	PDAC	E2
Normal	PDAC	E3
Normal	PDAC	E4
Tumour	PDAC	E5
Tumour	PDAC	E6
Tumour	PDAC	E7
Stroma	PDAC	E8
Stroma	PDAC	E9
Stroma	PDAC	E10
Normal	PDAC	E11
Normal	PDAC	E12
Normal	PDAC	E13
Tumour	Mucinous cystic neoplasm	E14
Tumour	Mucinous cystic neoplasm	E15
Tumour	Mucinous cystic neoplasm	F1
Stroma	Mucinous cystic neoplasm	F2
Stroma	Mucinous cystic neoplasm	F3
Stroma	Mucinous cystic neoplasm	F4
Tumour	Mucinous cystic neoplasm	F5
Tumour	Mucinous cystic	F6

	neoplasm	
Tumour	Mucinous cystic neoplasm	F7
Stroma	Mucinous cystic neoplasm	F8
Stroma	Mucinous cystic neoplasm	F9
Stroma	Mucinous cystic neoplasm	F10
Tumour	Ampullary carcinoma	F11
Tumour	Ampullary carcinoma	F12
Tumour	Ampullary carcinoma	F13
Stroma	Ampullary carcinoma	F14
Stroma	Ampullary carcinoma	F15
Stroma	Ampullary carcinoma	G1
Normal	Ampullary carcinoma	G2
Normal	Ampullary carcinoma	G3
Normal	Ampullary carcinoma	G4
Tumour	Neuroendocrine tumour	G5
Tumour	Neuroendocrine tumour	G6
Tumour	Neuroendocrine tumour	G7
Tumour	Neuroendocrine tumour	G8
Tumour	Neuroendocrine tumour	G9
Tumour	Neuroendocrine tumour	G10
Normal	Neuroendocrine tumour	G11
Normal	Neuroendocrine tumour	G12
Normal	Neuroendocrine tumour	G13
Tumour	Neuroendocrine tumour	G14
Tumour	Neuroendocrine tumour	G15
Tumour	Neuroendocrine tumour	H1
Tumour	Cholangiocarcinoma	H2
Tumour	Cholangiocarcinoma	H3
Tumour	Cholangiocarcinoma	H4
Stroma	Cholangiocarcinoma	H5
Stroma	Cholangiocarcinoma	H6
Stroma	Cholangiocarcinoma	H7
Normal	Cholangiocarcinoma	H8
Normal	Cholangiocarcinoma	H9
Normal	Cholangiocarcinoma	H10
Tumour	Cholangiocarcinoma	H11
Tumour	Cholangiocarcinoma	H12
Tumour	Cholangiocarcinoma	H13
Stroma	Cholangiocarcinoma	H14
Stroma	Cholangiocarcinoma	H15
Stroma	Cholangiocarcinoma	I1

Normal	Cholangiocarcinoma	I2
Normal	Cholangiocarcinoma	I3
Normal	Cholangiocarcinoma	I4

Appendix 5: Pancreas 2 TMA slide 2 design

Tissue type	**Diagnosis**	**Array position**

Spleen	Normal	A1
Tumour	Cholangiocarcinoma	A2
Tumour	Cholangiocarcinoma	A3
Tumour	Cholangiocarcinoma	A4
Stroma	Cholangiocarcinoma	A5
Stroma	Cholangiocarcinoma	A6
Stroma	Cholangiocarcinoma	A7
Normal	Cholangiocarcinoma	A8
Normal	Cholangiocarcinoma	A9
Normal	Cholangiocarcinoma	A10
Tumour	Cholangiocarcinoma	A11
Tumour	Cholangiocarcinoma	A12
Tumour	Cholangiocarcinoma	A13
Stroma	Cholangiocarcinoma	A14
Stroma	Cholangiocarcinoma	A15
Stroma	Cholangiocarcinoma	B1
Normal	Cholangiocarcinoma	B2
Normal	Cholangiocarcinoma	B3
Normal	Cholangiocarcinoma	B4
Tumour	Cholangiocarcinoma	B5
Tumour	Cholangiocarcinoma	B6
Tumour	Cholangiocarcinoma	B7
Stroma	Cholangiocarcinoma	B8
Stroma	Cholangiocarcinoma	B9
Stroma	Cholangiocarcinoma	B10
Tumour	Cholangiocarcinoma	B11
Tumour	Cholangiocarcinoma	B12
Tumour	Cholangiocarcinoma	B13
Stroma	Cholangiocarcinoma	B14
Stroma	Cholangiocarcinoma	B15
Stroma	Cholangiocarcinoma	C1
Tumour	Cholangiocarcinoma	C2
Tumour	Cholangiocarcinoma	C3
Tumour	Cholangiocarcinoma	C4
Stroma	Cholangiocarcinoma	C5
Stroma	Cholangiocarcinoma	C6
Stroma	Cholangiocarcinoma	C7
Normal	Cholangiocarcinoma	C8
Normal	Cholangiocarcinoma	C9
Normal	Cholangiocarcinoma	C10
Tumour	Gistoblastoma	C11
Tumour	Gistoblastoma	C12
Tumour	Gistoblastoma	C13
Normal	Gistoblastoma	C14

Normal	Gistoblastoma	C15
Normal	Gistoblastoma	D1
Tumour	PDAC	D2
Tumour	PDAC	D3
Tumour	PDAC	D4
Stroma	PDAC	D5
Stroma	PDAC	D6
Stroma	PDAC	D7
Normal	PDAC	D8
Normal	PDAC	D9
Normal	PDAC	D10
Tumour	Mucinous cystic neoplasm	D11
Tumour	Mucinous cystic neoplasm	D12
Tumour	Mucinous cystic neoplasm	D13
Normal	Mucinous cystic neoplasm	D14
Normal	Mucinous cystic neoplasm	D15
Normal	Mucinous cystic neoplasm	E1
Normal	Normal	E2
Normal	Normal	E3
Normal	Normal	E4
Tumour	PDAC	E5
Tumour	PDAC	E6
Tumour	PDAC	E7
Stroma	PDAC	E8
Stroma	PDAC	E9
Stroma	PDAC	E10
Normal	PDAC	E11
Normal	PDAC	E12
Normal	PDAC	E13
Tumour	PDAC	E14
Tumour	PDAC	E15
Tumour	PDAC	F1
Stroma	PDAC	F2
Stroma	PDAC	F3
Stroma	PDAC	F4
Normal	PDAC	F5
Normal	PDAC	F6
Normal	PDAC	F7
Tumour	Insulinoma	F8

Tumour	Insulinoma	F9
Tumour	Insulinoma	F10
Normal	Insulinoma	F11
Normal	Insulinoma	F12
Normal	Insulinoma	F13
Tumour	Insulinoma	F14
Tumour	Insulinoma	F15
Tumour	Insulinoma	G1
Normal	Insulinoma	G2
Normal	Insulinoma	G3
Normal	Insulinoma	G4
Tumour	Insulinoma	G5
Tumour	Insulinoma	G6
Tumour	Insulinoma	G7
Normal	Insulinoma	G8
Normal	Insulinoma	G9
Normal	Insulinoma	G10
Tumour	Insulinoma	G11
Tumour	Insulinoma	G12
Tumour	Insulinoma	G13
Normal	Insulinoma	G14
Normal	Insulinoma	G15
Normal	Insulinoma	H1
Tumour	Ampullary carcinoma	H2
Tumour	Ampullary carcinoma	H3
Tumour	Ampullary carcinoma	H4
Stroma	Ampullary carcinoma	H5
Stroma	Ampullary carcinoma	H6
Stroma	Ampullary carcinoma	H7
Tumour	Duodenal carcinoma	H8
Tumour	Duodenal carcinoma	H9
Tumour	Duodenal carcinoma	H10
Stroma	Duodenal carcinoma	H11
Stroma	Duodenal carcinoma	H12
Stroma	Duodenal carcinoma	H13
Tumour	Ampullary carcinoma	H14
Tumour	Ampullary carcinoma	H15
Tumour	Ampullary carcinoma	I1
Stroma	Ampullary carcinoma	I2
Stroma	Ampullary carcinoma	I3
Stroma	Ampullary carcinoma	I4

Appendix 6: Pancreas 2 TMA slide 3 design

Tissue types	Diagnosis	Array position
Spleen	Normal	A1

Tumour	Cholangiocarcinoma	A2
Tumour	Cholangiocarcinoma	A3
Tumour	Cholangiocarcinoma	A4
Stroma	Cholangiocarcinoma	A5
Stroma	Cholangiocarcinoma	A6
Stroma	Cholangiocarcinoma	A7
Normal	Cholangiocarcinoma	A8
Normal	Cholangiocarcinoma	A9
Normal	Cholangiocarcinoma	A10
Tumour	Chronic pancreatitis	A11
Tumour	Chronic pancreatitis	A12
Tumour	Chronic pancreatitis	A13
Normal	Chronic pancreatitis	A14
Normal	Chronic pancreatitis	A15
Normal	Chronic pancreatitis	B1
Tumour	Cholangiocarcinoma	B2
Tumour	Cholangiocarcinoma	B3
Tumour	Cholangiocarcinoma	B4
Stroma	Cholangiocarcinoma	B5
Stroma	Cholangiocarcinoma	B6
Stroma	Cholangiocarcinoma	B7
Normal	Cholangiocarcinoma	B8
Normal	Cholangiocarcinoma	B9
Normal	Cholangiocarcinoma	B10
Tumour	Duodenal carcinoma	B11
Tumour	Duodenal carcinoma	B12
Tumour	Duodenal carcinoma	B13
Stroma	Duodenal carcinoma	B14
Stroma	Duodenal carcinoma	B15
Stroma	Duodenal carcinoma	C1
Tumour	Duodenal carcinoma	C2
Tumour	Duodenal carcinoma	C3
Tumour	Duodenal carcinoma	C4
Stroma	Duodenal carcinoma	C5
Stroma	Duodenal carcinoma	C6
Stroma	Duodenal	C7

	carcinoma	
Tumour	Duodenal carcinoma	C8
Tumour	Duodenal carcinoma	C9
Tumour	Duodenal carcinoma	C10
Stroma	Duodenal carcinoma	C11
Stroma	Duodenal carcinoma	C12
Stroma	Duodenal carcinoma	C13
Normal	Duodenal carcinoma	C14
Normal	Duodenal carcinoma	C15
Normal	Duodenal carcinoma	D1
Tumour	Ampullary carcinoma	D2
Tumour	Ampullary carcinoma	D3
Tumour	Ampullary carcinoma	D4
Normal	Ampullary carcinoma	D5
Normal	Ampullary carcinoma	D6
Normal	Ampullary carcinoma	D7
Tumour	Ampullary carcinoma	D8
Tumour	Ampullary carcinoma	D9
Tumour	Ampullary carcinoma	D10
Stroma	Ampullary carcinoma	D11
Stroma	Ampullary carcinoma	D12
Stroma	Ampullary carcinoma	D13
Normal	Ampullary carcinoma	D14
Normal	Ampullary carcinoma	D15
Normal	Ampullary carcinoma	E1
Tumour	Duodenal	E2

	carcinoma	
Tumour	Duodenal carcinoma	E3
Tumour	Duodenal carcinoma	E4
Stroma	Duodenal carcinoma	E5
Stroma	Duodenal carcinoma	E6
Stroma	Duodenal carcinoma	E7
Tumour	Chronic pancreatitis	E8
Tumour	Chronic pancreatitis	E9
Tumour	Chronic pancreatitis	E10
Normal	Chronic pancreatitis	E11
Normal	Chronic pancreatitis	E12
Normal	Chronic pancreatitis	E13
Tumour	Cholangiocarcinoma	E14
Tumour	Cholangiocarcinoma	E15
Tumour	Cholangiocarcinoma	F1
Stroma	Cholangiocarcinoma	F2
Stroma	Cholangiocarcinoma	F3
Stroma	Cholangiocarcinoma	F4
Normal	Cholangiocarcinoma	F5
Normal	Cholangiocarcinoma	F6
Normal	Cholangiocarcinoma	F7
Tumour	Chronic pancreatitis	F8
Tumour	Chronic pancreatitis	F9
Tumour	Chronic pancreatitis	F10
Normal	Chronic pancreatitis	F11
Normal	Chronic pancreatitis	F12
Normal	Chronic pancreatitis	F13
Tumour	Duodenal carcinoma	F14
Tumour	Duodenal carcinoma	F15
Tumour	Duodenal carcinoma	G1
Stroma	Duodenal carcinoma	G2
Stroma	Duodenal carcinoma	G3
Stroma	Duodenal carcinoma	G4
Normal	Duodenal carcinoma	G5
Normal	Duodenal	G6

	carcinoma	
Normal	Duodenal carcinoma	G7
Tumour	Ampullary carcinoma	G8
Tumour	Ampullary carcinoma	G9
Tumour	Ampullary carcinoma	G10
Stroma	Ampullary carcinoma	G11
Stroma	Ampullary carcinoma	G12
Stroma	Ampullary carcinoma	G13
Normal	Ampullary carcinoma	G14
Normal	Ampullary carcinoma	G15
Normal	Ampullary carcinoma	H1
Tumour	Chronic pancreatitis	H2
Tumour	Chronic pancreatitis	H3
Tumour	Chronic pancreatitis	H4
Normal	Chronic pancreatitis	H5
Normal	Chronic pancreatitis	H6
Normal	Chronic pancreatitis	H7
Tumour	Cholangiocarcinoma	H8
Tumour	Cholangiocarcinoma	H9
Tumour	Cholangiocarcinoma	H10
Stroma	Cholangiocarcinoma	H11
Stroma	Cholangiocarcinoma	H12
Stroma	Cholangiocarcinoma	H13
Normal	Cholangiocarcinoma	H14
Normal	Cholangiocarcinoma	H15
Normal	Cholangiocarcinoma	I1
Tumour	Ampullary carcinoma	I2
Tumour	Ampullary carcinoma	I3
Tumour	Ampullary carcinoma	I4

Appendix 7: Pancreas 3 TMA slide 1 design

Tissue type	**Diagnosis**	**Array position**

Spleen	Normal	A1
Tumour	Biopsy	A2
Tumour	Biopsy	A3
Tumour	Biopsy	A4
Stroma	Biopsy	A5
Stroma	Biopsy	A6
Stroma	Biopsy	A7
Tumour	Biopsy	A8
Tumour	Biopsy	A9
Tumour	Biopsy	A10
Normal	Biopsy	A11
Normal	Biopsy	A12
Normal	Biopsy	A13
Tumour	Biopsy	A14
Tumour	Biopsy	A15
Tumour	Biopsy	B1
Stroma	Biopsy	B2
Stroma	Biopsy	B3
Stroma	Biopsy	B4
Tumour	Biopsy	B5
Tumour	Biopsy	B6
Tumour	Biopsy	B7
Stroma	Biopsy	B8
Stroma	Biopsy	B9
Stroma	Biopsy	B10
Tumour	Biopsy	B11
Tumour	Biopsy	B12
Tumour	Biopsy	B13
Stroma	Biopsy	B14
Stroma	Biopsy	B15
Stroma	Biopsy	C1
Normal	Biopsy	C2
Normal	Biopsy	C3
Normal	Biopsy	C4
Tumour	Biopsy	C5
Tumour	Biopsy	C6
Tumour	Biopsy	C7
Stroma	Biopsy	C8
Stroma	Biopsy	C9
Stroma	Biopsy	C10
Normal	Biopsy	C11
Normal	Biopsy	C12
Normal	Biopsy	C13
Tumour	Biopsy	C14

Tumour	Biopsy	C15
Tumour	Biopsy	D1
Stroma	Biopsy	D2
Stroma	Biopsy	D3
Stroma	Biopsy	D4
Tumour	Biopsy	D5
Tumour	Biopsy	D6
Tumour	Biopsy	D7
Stroma	Biopsy	D8
Stroma	Biopsy	D9
Stroma	Biopsy	D10
Tumour	Biopsy	D11
Tumour	Biopsy	D12
Tumour	Biopsy	D13
Stroma	Biopsy	D14
Stroma	Biopsy	D15
Stroma	Biopsy	E1
Tumour	Biopsy	E2
Tumour	Biopsy	E3
Tumour	Biopsy	E4
Stroma	Biopsy	E5
Stroma	Biopsy	E6
Stroma	Biopsy	E7
Normal	Biopsy	E8
Normal	Biopsy	E9
Normal	Biopsy	E10
Tumour	Biopsy	E11
Tumour	Biopsy	E12
Tumour	Biopsy	E13
Stroma	Biopsy	E14
Stroma	Biopsy	E15
Stroma	Biopsy	F1
Normal	Biopsy	F2
Normal	Biopsy	F3
Normal	Biopsy	F4
Tumour	Biopsy	F5
Tumour	Biopsy	F6
Tumour	Biopsy	F7
Stroma	Biopsy	F8
Stroma	Biopsy	F9
Stroma	Biopsy	F10
Tumour	Biopsy	F11
Tumour	Biopsy	F12
Tumour	Biopsy	F13

Stroma	Biopsy	F14
Stroma	Biopsy	F15
Stroma	Biopsy	G1
Tumour	Biopsy	G2
Tumour	Biopsy	G3
Tumour	Biopsy	G4
Stroma	Biopsy	G5
Stroma	Biopsy	G6
Stroma	Biopsy	G7
Normal	Biopsy	G8
Normal	Biopsy	G9
Normal	Biopsy	G10
Tumour	Biopsy	G11
Tumour	Biopsy	G12
Tumour	Biopsy	G13
Stroma	Biopsy	G14
Stroma	Biopsy	G15
Stroma	Biopsy	H1
Tumour	Biopsy	H2
Tumour	Biopsy	H3
Tumour	Biopsy	H4
Stroma	Biopsy	H5
Stroma	Biopsy	H6
Stroma	Biopsy	H7
Tumour	MCN	H8
Tumour	Mucinous cystic neoplasm	H9
Tumour	Mucinous cystic neoplasm	H10
Stroma	Mucinous cystic neoplasm	H11
Stroma	Mucinous cystic neoplasm	H12
Stroma	Mucinous cystic neoplasm	H13
Tumour	Mucinous cystic neoplasm	H14
Tumour	Mucinous cystic neoplasm	H15
Tumour	Mucinous cystic neoplasm	I1
Stroma	Mucinous cystic neoplasm	I2
Stroma	Mucinous cystic neoplasm	I3
Stroma	Mucinous cystic neoplasm	I4

Appendix 8: Pancreas 3 TMA slide 2 design

Tissue type	Diagnosis	Array position
Spleen	Normal	A1

Tumour	Ampullary carcinoma	A2
Tumour	Ampullary carcinoma	A3
Tumour	Ampullary carcinoma	A4
Stroma	Ampullary carcinoma	A5
Stroma	Ampullary carcinoma	A6
Stroma	Ampullary carcinoma	A7
Normal	Ampullary carcinoma	A8
Normal	Ampullary carcinoma	A9
Normal	Ampullary carcinoma	A10
Tumour	Neuroendocrine tumour	A11
Tumour	Neuroendocrine tumour	A12
Tumour	Neuroendocrine tumour	A13
Tumour	Neuroendocrine tumour	A14
Tumour	Neuroendocrine tumour	A15
Tumour	Neuroendocrine tumour	B1
Normal	Neuroendocrine tumour	B2
Normal	Neuroendocrine tumour	B3
Normal	Neuroendocrine tumour	B4
Tumour	Neuroendocrine tumour	B5
Tumour	Neuroendocrine tumour	B6
Tumour	Neuroendocrine tumour	B7
Tumour	Gistoblastoma	B8
Tumour	Gistoblastoma	B9
Tumour	Gistoblastoma	B10
Normal	Gistoblastoma	B11
Normal	Gistoblastoma	B12
Normal	Gistoblastoma	B13
Tumour	Biopsy	B14
Tumour	Biopsy	B15
Tumour	Biopsy	C1
Stroma	Biopsy	C2
Stroma	Biopsy	C3
Stroma	Biopsy	C4
Tumour	Biopsy	C5
Tumour	Biopsy	C6
Tumour	Biopsy	C7
Stroma	Biopsy	C8
Stroma	Biopsy	C9
Stroma	Biopsy	C10
Tumour	Biopsy	C11
Tumour	Biopsy	C12
Tumour	Biopsy	C13
Tumour	Biopsy	C14
Tumour	Biopsy	C15

Tumour	Biopsy	D1
Tumour	Biopsy	D2
Tumour	Biopsy	D3
Tumour	Biopsy	D4
Tumour	Mucinous cystic neoplasm	D5
Tumour	Mucinous cystic neoplasm	D6
Tumour	Mucinous cystic neoplasm	D7
Normal	Mucinous cystic neoplasm	D8
Normal	Mucinous cystic neoplasm	D9
Normal	Mucinous cystic neoplasm	D10
Tumour	PDAC	D11
Tumour	PDAC	D12
Tumour	PDAC	D13
Stroma	PDAC	D14
Stroma	PDAC	D15
Stroma	PDAC	E1
Normal	Normal	E2
Normal	Normal	E3
Normal	Normal	E4
Tumour	Biopsy	E5
Tumour	Biopsy	E6
Tumour	Biopsy	E7
Stroma	Biopsy	E8
Stroma	Biopsy	E9
Stroma	Biopsy	E10
Tumour	Insulinoma	E11
Tumour	Insulinoma	E12
Tumour	Insulinoma	E13
Normal	Insulinoma	E14
Normal	Insulinoma	E15
Normal	Insulinoma	F1
Tumour	Insulinoma	F2
Tumour	Insulinoma	F3
Tumour	Insulinoma	F4
Normal	Insulinoma	F5
Normal	Insulinoma	F6
Normal	Insulinoma	F7
Tumour	Insulinoma	F8
Tumour	Insulinoma	F9

Tumour	Insulinoma	F10
Normal	Insulinoma	F11
Normal	Insulinoma	F12
Normal	Insulinoma	F13
Tumour	Insulinoma	F14
Tumour	Insulinoma	F15
Tumour	Insulinoma	G1
Normal	Insulinoma	G2
Normal	Insulinoma	G3
Normal	Insulinoma	G4
Tumour	Ampullary carcinoma	G5
Tumour	Ampullary carcinoma	G6
Tumour	Ampullary carcinoma	G7
Stroma	Ampullary carcinoma	G8
Stroma	Ampullary carcinoma	G9
Stroma	Ampullary carcinoma	G10
Tumour	Duodenal carcinoma	G11
Tumour	Duodenal carcinoma	G12
Tumour	Duodenal carcinoma	G13
Stroma	Duodenal carcinoma	G14
Stroma	Duodenal carcinoma	G15
Stroma	Duodenal carcinoma	H1
Tumour	Ampullary carcinoma	H2
Tumour	Ampullary carcinoma	H3
Tumour	Ampullary carcinoma	H4
Stroma	Ampullary carcinoma	H5
Stroma	Ampullary carcinoma	H6
Stroma	Ampullary carcinoma	H7
Tumour	Cholangiocarcinoma	H8
Tumour	Cholangiocarcinoma	H9
Tumour	Cholangiocarcinoma	H10
Stroma	Cholangiocarcinoma	H11
Stroma	Cholangiocarcinoma	H12
Stroma	Cholangiocarcinoma	H13
Normal	Cholangiocarcinoma	H14
Normal	Cholangiocarcinoma	H15
Normal	Cholangiocarcinoma	I1

Appendix 9: Pancreas 3 TMA slide 3 design

Tissue type	**Diagnosis**	**Array position**
Spleen	Normal	A1
Tumour	Chronic	A2

	pancreatitis	
Tumour	Chronic pancreatitis	A3
Tumour	Chronic pancreatitis	A4
Normal	Chronic pancreatitis	A5
Normal	Chronic pancreatitis	A6
Normal	Chronic pancreatitis	A7
Tumour	cholangio carcinoma	A8
Tumour	cholangio carcinoma	A9
Tumour	cholangio carcinoma	A10
Stroma	cholangio carcinoma	A11
Stroma	cholangio carcinoma	A12
Stroma	cholangio carcinoma	A13
Normal	cholangio carcinoma	A14
Normal	cholangio carcinoma	A15
Normal	cholangio carcinoma	B1
Tumour	duodenal carcinoma	B2
Tumour	duodenal carcinoma	B3
Tumour	duodenal carcinoma	B4
Stroma	duodenal carcinoma	B5
Stroma	duodenal carcinoma	B6
Stroma	duodenal carcinoma	B7
Tumour	duodenal carcinoma	B8
Tumour	duodenal carcinoma	B9
Tumour	duodenal carcinoma	B10
Stroma	duodenal carcinoma	B11
Stroma	duodenal	B12

	carcinoma	
Stroma	duodenal carcinoma	B13
Tumour	duodenal carcinoma	B14
Tumour	duodenal carcinoma	B15
Tumour	duodenal carcinoma	C1
Stroma	duodenal carcinoma	C2
Stroma	duodenal carcinoma	C3
Stroma	duodenal carcinoma	C4
Normal	duodenal carcinoma	C5
Normal	duodenal carcinoma	C6
Normal	duodenal carcinoma	C7
Tumour	ampullary carcinoma	C8
Tumour	ampullary carcinoma	C9
Tumour	ampullary carcinoma	C10
Normal	ampullary carcinoma	C11
Normal	ampullary carcinoma	C12
Normal	ampullary carcinoma	C13
Tumour	ampullary carcinoma	C14
Tumour	ampullary carcinoma	C15
Tumour	ampullary carcinoma	D1
Stroma	ampullary carcinoma	D2
Stroma	ampullary carcinoma	D3
Stroma	ampullary carcinoma	D4
Normal	ampullary carcinoma	D5
Normal	ampullary carcinoma	D6
Normal	ampullary	D7

	carcinoma	
Tumour	duodenal carcinoma	D8
Tumour	duodenal carcinoma	D9
Tumour	duodenal carcinoma	D10
Stroma	duodenal carcinoma	D11
Stroma	duodenal carcinoma	D12
Stroma	duodenal carcinoma	D13
Tumour	Chronic pancreatitis	D14
Tumour	Chronic pancreatitis	D15
Tumour	Chronic pancreatitis	E1
Normal	Chronic pancreatitis	E2
Normal	Chronic pancreatitis	E3
Normal	Chronic pancreatitis	E4
Tumour	cholangio carcinoma	E5
Tumour	cholangio carcinoma	E6
Tumour	cholangio carcinoma	E7
Stroma	cholangio carcinoma	E8
Stroma	cholangio carcinoma	E9
Stroma	cholangio carcinoma	E10
Normal	cholangio carcinoma	E11
Normal	cholangio carcinoma	E12
Normal	cholangio carcinoma	E13
Tumour	Chronic pancreatitis	E14
Tumour	Chronic pancreatitis	E15
Tumour	Chronic pancreatitis	F1
Normal	Chronic	F2

	pancreatitis	
Normal	Chronic pancreatitis	F3
Normal	Chronic pancreatitis	F4
Tumour	duodenal carcinoma	F5
Tumour	duodenal carcinoma	F6
Tumour	duodenal carcinoma	F7
Stroma	duodenal carcinoma	F8
Stroma	duodenal carcinoma	F9
Stroma	duodenal carcinoma	F10
Normal	duodenal carcinoma	F11
Normal	duodenal carcinoma	F12
Normal	duodenal carcinoma	F13
Tumour	ampullary carcinoma	F14
Tumour	ampullary carcinoma	F15
Tumour	ampullary carcinoma	G1
Stroma	ampullary carcinoma	G2
Stroma	ampullary carcinoma	G3
Stroma	ampullary carcinoma	G4
Normal	ampullary carcinoma	G5
Normal	ampullary carcinoma	G6
Normal	ampullary carcinoma	G7
Tumour	Chronic pancreatitis	G8
Tumour	Chronic pancreatitis	G9
Tumour	Chronic pancreatitis	G10
Normal	Chronic pancreatitis	G11
Normal	Chronic	G12

	pancreatitis	
Normal	Chronic pancreatitis	G13
Tumour	cholangio carcinoma	G14
Tumour	cholangio carcinoma	G15
Tumour	cholangio carcinoma	H1
Stroma	cholangio carcinoma	H2
Stroma	cholangio carcinoma	H3
Stroma	cholangio carcinoma	H4
Normal	cholangio carcinoma	H5
Normal	cholangio carcinoma	H6
Normal	cholangio carcinoma	H7
Tumour	Ampullary adenoma	H8
Tumour	Ampullary adenoma	H9
Tumour	Ampullary adenoma	H10